Absolute Configuration by Circular Dichroism: Quantum Chemical CD Calculations

DISSERTATION ZUR ERLANGUNG DES
NATURWISSENSCHAFTLICHEN DOKTORGRADES
DER JULIUS-MAXIMILIANS-UNIVERSITÄT WÜRZBURG

vorgelegt von

Katja Maksimenka

aus
Minsk, Weiβrussland

Würzburg 2010

Eingereicht am: _____

bei der Fakultät für Chemie und Pharmazie.

1. Gutachter: _____

2. Gutachter: _____

der Dissertation.

1. Prüfer: _____

2. Prüfer: _____

3. Prüfer: _____

des öffentlichen Promotionskolloquiums.

Datum des öffentlichen Promotionskolloquiums: _____

Doktorurkunde ausgehändigt am: _____

Die vorliegende Arbeit wurde in der Zeit von Juli 2002 bis April 2007
am Institut für Organische Chemie
der Bayerischen Julius-Maximilians-Universität Würzburg angefertigt.

Ich danke herzlich Herrn Prof. Dr. Dr. h.c. G. Bringmann für
die Möglichkeit an diesem faszinierenden Thema zu arbeiten,
die umfassende Unterstützung und
die Geduld und Verständnis

Teile der im Rahmen dieser Arbeit erzielten Ergebnisse waren bereits Gegenstand von Publikationen[18, 30–41, 44] sowie von Postern und Vorträgen.

To my boys,

Roma, Matvei and Stepane

Contents

Chapter 1

Introduction

Discoveries are often made by not following instructions,
by going off the main road, by trying the untried.
FRANK TYGER

The term "chirality", which simply speaking means "handedness", i.e., the existence of left/right oppositions was introduced by LORD KELVIN in 1904. In his Baltimore Lectures on Molecular Dynamics and the Wave Theory of Light[1] he stated: "*… I call any geometrical figure, or group of points, chiral, and say it has chirality, if its image in a plane mirror, ideally realized, cannot be brought to coincide with itself.*"

However, the concepts of "chirality", "asymmetry" and "enantiomerism" have already been known from the 1870's, the time of fundamental statements by J. H. VAN'T HOFF and J.-A. LE BEL, and even earlier, when the first experimental evidences were obtained by J.-B. BIOT and L. PASTEUR.[2] Jean-Baptiste Biot observed a phenomenon of optical activity first in quartz (1812) and then in several liquids (1815), such as turpentine and solutions of sucrose, camphor and tartaric acid. In 1848 L. PASTEUR manually separated two types of crystals (due to their dissymmetric facets inclined to the right or left) of the sodium ammonium salts of (+)- and (–)-

tartaric acid out of their racemic (non-rotating) mixture. He recognized that solution of one type of crystals – (+)-tartaric acid –rotated linearly polarized light to the right, whereas the other form – the (–)-enantiomer – rotated to the left. Actually, L. PASTEUR was the first who proposed that the source of natural optical activity is the molecular asymmetry.

In early days, for differentiation of isomers, trivial names were used, and enantiomers were indicated with d- (*dextrorotary*) and l- (*levorotary*) depending on which direction molecules polarized light. Nowadays, a description system based on the proposals of CAHN, INGOLD and PRELOG[3] is in use (later completed by Prelog & Helmchen),[4] specifying chiral elements of a molecule by *R* (for *rectus*, Latin for right) and *S* (for *sinister*, Latin for left), and by *P* (for *plus*) and *M* (for *minus*) for helical-like structures.

Knowledge of the absolute stereostructure has become important in understanding phenomena not only in organic, but also in physical, inorganic, analytical, supramolecular, and particularly, in biological chemistry. Thus, no biochemical or pharmaceutical studies of any kind can be complete without three-dimensional information on the relationships between the molecules concerned, and this can not be achieved until the absolute configurations of all compounds are known. This requirement is obvious, since two enantiomeric forms can possess substantially different (since diastereomeric!) properties in a chiral environment, like, e.g., diverse bioactivities, which may affect the life processes in completely different ways. Thus, more than 285 enantiomeric pairs are known in perfume industry that, due to their various 3D fit on an odor receptor (or receptors), differ either in odor quality or in fragrance intensity.[5] For example, (*S*)-(+)-2-hephyl acetate [(S)-**1**] smells of mushrooms, while its mirror image, (*R*)-(–)-2-hephyl acetate [(*R*)-**1**], has a fruity, banana-like fragrance (Figure 1a).[6] By the same principle, enantiomeric molecules can also be distinguished by taste: Amino acids of the L-series are usually bitter, while those of the D-series are sweet [e.g., asparagine (**2**), Figure 1b].[7] In the world of insects, the chirality of pheromones plays an extremely important role. An example is

olean (**3**): The *R*-enantiomer of this sex pheromone of the olive fruit fly (*Bactrocera oleae*) is active on male insects, whereas (*S*)-**3** attracts only females (Figure 1c).[8]

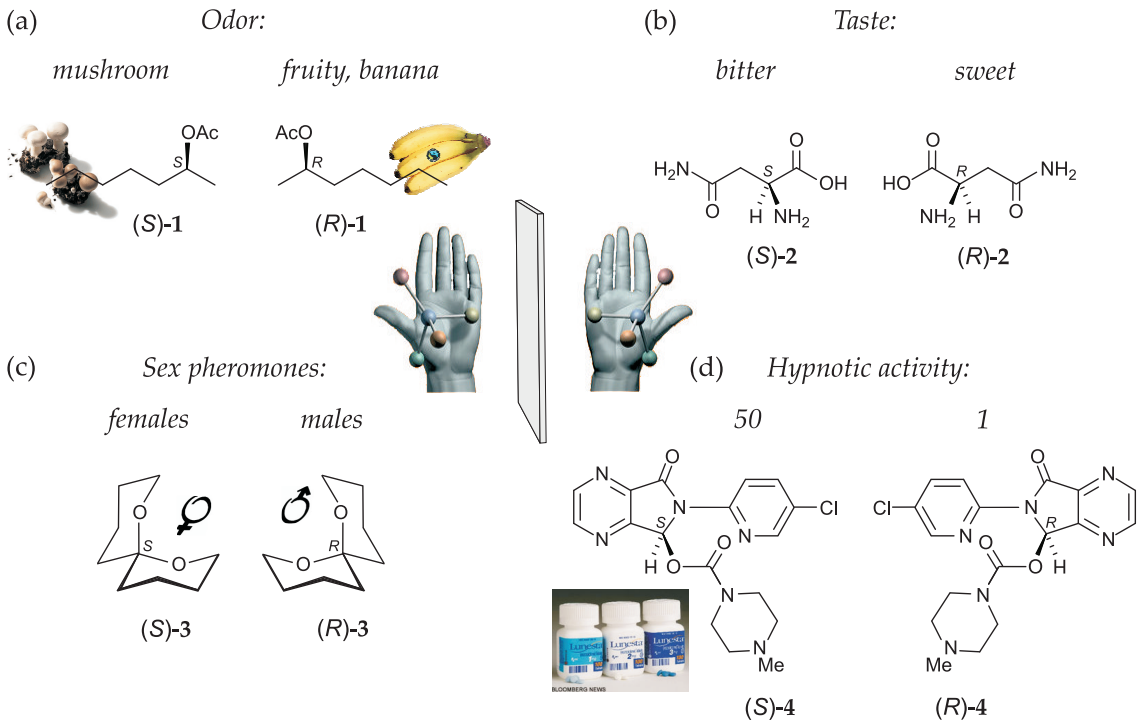

Figure 1. Enantiomeric pairs possessing different (a) aroma characteristics [(*S*)- versus (*R*)-2-hephyl acetate (**1**)], (b) taste [(*S*)- versus (*R*)-asparagine (**2**)], (c) pheromone activities [(*S*)- versus (*R*)-olean (**3**)], and (d) pharmacological activities [(*S*)- versus (*R*)-zopiclone (**4**)].

In pharmacology, stereochemistry appears an essential factor in the sense of drug efficacy. Most of the currently applied drugs, containing chiral compounds, are used therapeutically as racemates. In many of them only one enantiomeric form is active and the other one is inactive. For example, only one of the two enantiomers of zopiclone (**4**) (distributed as Imovane®), which is a hypnotic agent used in the treatment of insomnia, is pharmacologically active [relative activity *S* : *R* = 50 : 1, Figure 1d].[9] In 2005, the pharmaceutical company Seprecor started the marketing of the active stereoisomer of zopiclone [i.e., (*S*)-**4**] under the name Lunesta®. The change to the production of one-enantiomer chemicals and drugs is a general tendency in the chemical and pharmaceutical industries in the past years, thereby

stimulating the development of new efficient methods for the determination of the absolute configurations of chiral compounds.

Remarkable advances in computer technologies and computational chemistry made possible reasonably fast and accurate investigations of three-dimensional structures (i.e., absolute configurations and conformations) of most different molecules, with regard to their size or chirality type. Quantum chemical calculations of chiroptical properties,[10] such as optical rotation ($[\alpha]_D$),[11] optical rotatory dispersion (ORD),[12] electronic circular dichroism (ECD or CD),[13,14,15,16,17,18] and vibrational circular dichroism (VCD),[19] represent a valuable alternative to the traditional methods of assigning the absolute stereostructure, such as X-ray structure analysis,[20] partial or total enantioselective synthesis,[21] NMR analysis of Mosher esters and related derivatives,[22] and chemical degradation.[21,23]

In our research group, which is specialized on isolation and synthesis of novel biologically relevant agents, theoretical prediction of circular dichroism (CD) spectra has become a general procedure for the attribution of the absolute configurations of optically active compounds.[13,17,24,25,26] This appears important particularly for those cases in which none of the conventional experimental methods can be applied, or their use seems unfavorable. Moreover, the increased computational resources in our group during the past few years have permitted application of highly advanced quantum chemical methods, which afforded a more accurate simulation of CD spectra.

During this work, the CD behavior of various chiral molecules of natural or synthetic origin was investigated by using the semiempirical CNDO/S[27] and OM2[28] methods, by applying *ab initio* approaches based on a time-dependent density functional theory (TDDFT),[29] and a multireference configuration interaction procedure (DFT/MRCI),[30] the latter two being employed wherever they seemed applicable and/or reasonable. The scope and limitations of the CD calculations for an assignment of the absolute configuration are discussed in the context of the assayed

compounds, which were classified with respect to the ability of the different methods used to predict the molecular CD.

- Compounds studied only by the semiempirical methods are described in Chapter 4.1. These are the naturally occurring axially chiral biaryls ancistrotanzanine A (**5**)[31] and isoplagiochin D (**6**),[32] the synthetically produced biaryl amide **7**[33] and bi[10]paracyclophane **8**,[34] and additionally, the centrally chiral natural product sorbicillactone B (**9**),[35] and the synthetic benz[e]indole derivative **10**[36] (Figure2a).

- In Chapter 4.2., all those substances are reported for which both, semiempirical and TDDFT methods were used, yielding almost identical CD spectra. These are the synthetically produced compounds, the axially chiral bisisonigerone (**11**),[37] nigerone (**12**),[37] and the 'leuco' phenylanthracene derivative **13**,[38] as well as the centrally chiral hydroxyoxosorbicillinol (**14**) and resistoflavin (**15**),[39] both isolated from natural sources (Figure 2b).

- In Chapter 4.3., those compounds are summarized for which again both types of CD calculations were performed, but for which only TDDFT computations were capable of unambiguous assigning the absolute configurations. These are the synthetically obtained centrally chiral harman derivative TaClo (**16**),[40] and the naturally occurring gephyromycin (**17**)[41] and neoechinulin A (**18**) (Figure 2c). Furthermore, in this chapter, two other compounds are reported, knipholone (**19**)[38] and knipholone anthrone (**20**),[38] whose absolute configurations were revised due to the use of higher-level methods as compared to earlier investigations, viz.TDDFT and DFT/MRCI.

- In Chapter 4.4., problematic cases of theoretical predictions of molecular CD are discussed, covering the natural products joziknipholones A (**21**) and B (**22**),[42] which are dimeric phenylanthraquinones possessing both, central and axial

chirality, and petrosifungin A (**23**) with its multicentered chiral system, whose absolute configurations could not be assigned by quantum chemical CD calculations (Figure 2d).

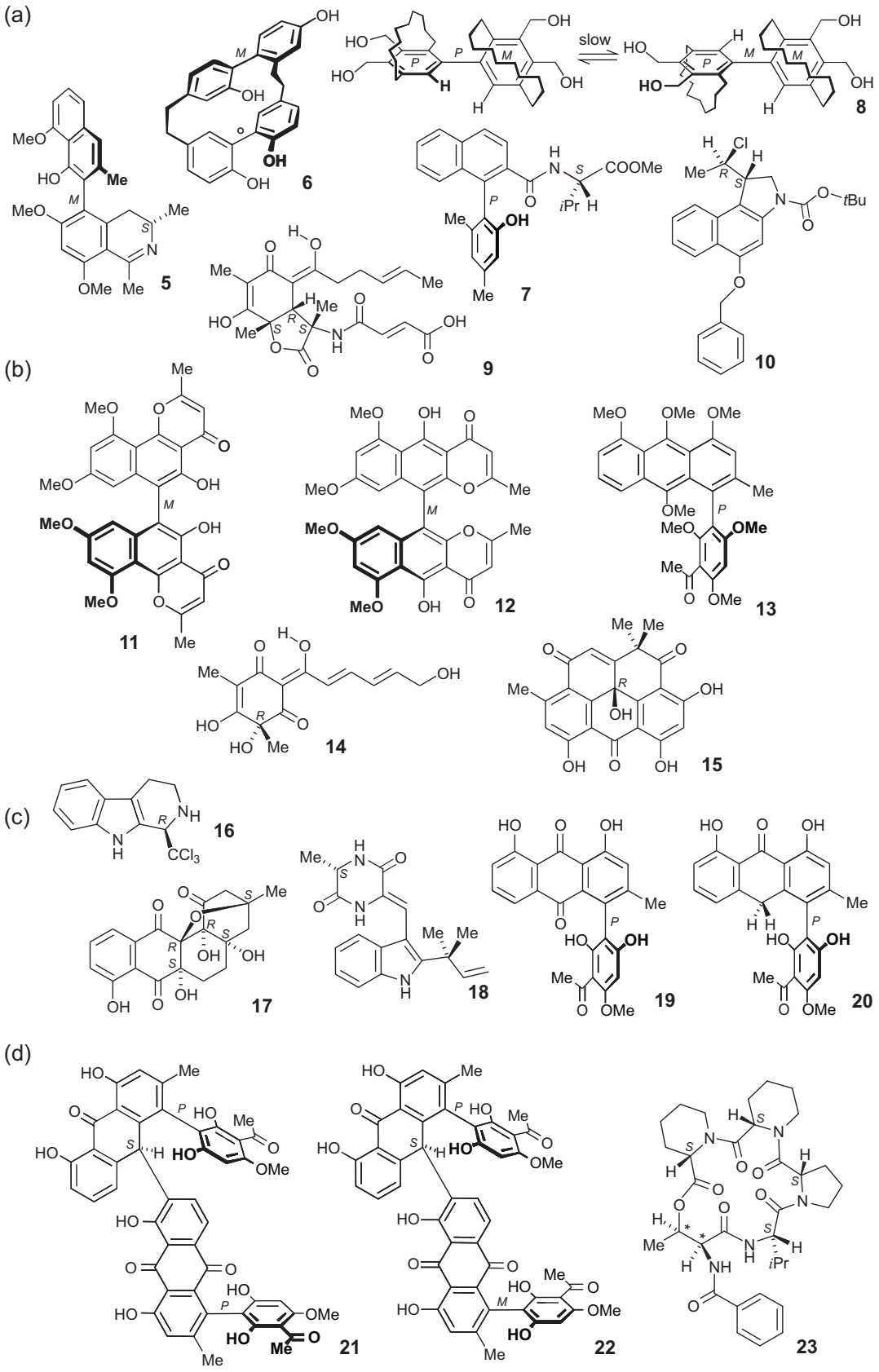

Figure 2. Overview of the compounds that have been investigated during this work by quantum chemical CD calculations.

Within a second project of this work, a novel methodology of determining an absolute configuration, based on the combination of the solid-state CD spectroscopy and quantum chemical CD calculations,[43,44] was tested on the axially chiral naphthylisoquinoline alkaloid dioncophylline A (**24**) (Figure 3), which, although configurationally stable at the biaryl axis, is characterized by a large degree of rotational flexibility around the chiral axis. In addition to a 'usual' prediction of the CD spectrum for the single conformer of **24** found in the crystal, an influence of the neighboring molecules of **24** in the solid state on its CD behavior has been investigated for the first time (Chapter 5).[45]

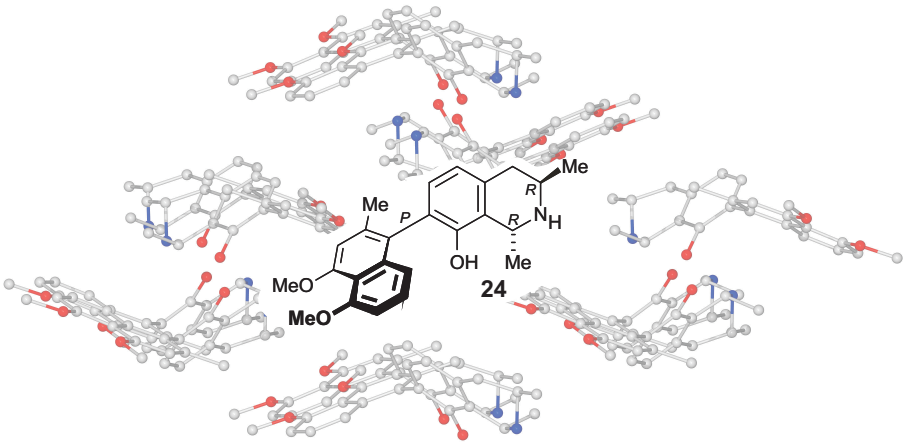

Figure 3. Dioncophylline A (**24**) and a fragment of its crystal structure.

Chapter 2

Elucidation of the absolute configuration

Knowledge is of no value unless you put it into practice.

ANTON CHEKHOV

Determination of the absolute configuration of chiral molecules of natural or synthetic origin is one of the central topics of modern organic chemistry. Thus, the stereochemical outcome of an asymmetric synthesis can be used as a proof or disproof for a postulated reaction mechanism. The attribution of the absolute configuration of a product obtained by an enzymatic transformation is important for obtaining more precise knowledge about the three-dimensional relationship between a given enzyme and its substrate. There are generally two groups of methods for elucidation of the absolute stereostructure: non-chiroptical, so-called "chemical" methods (Chapter 2.1.) and spectroscopic, in particular chiroptical techniques. The latter ones permit to distinguish between stereoisomers in even sub-µg amounts without requiring great experimental efforts (Chapter 2.2).

2.1. Non-chiroptical methods

- **X-ray structure analysis** is often used to determine the relative configuration of all chiral centers in the molecule, whereas it does not normally yield the absolute stereostructure as a whole. Nevertheless, if the absolute configuration of one stereocenter present in the molecule or introduced by an enantiopure reagent is known, the attribution of all other chiral centers follows straightforwardly.[20] Alternatively, the BIJVOET anomalous scattering method[46] can be applied, if a chiral molecule contains a heavy atom ($Z \geq 15$).[47] An essential precondition of using X-ray crystallography for the determination of the absolute configuration, however, still is the availability of crystals of suitable quality,[48] which sometimes appears to be a non-trivial task.

- **One- and two-dimensional NMR spectroscopies**, which are most frequently used techniques for structural elucidation, may also be applicable for the assignment of absolute stereostructures in some cases. Thus, by using enantiomerically pure derivatizing agents, such as Mosher acid [α-methoxy-α-(trifluoromethyl)phenyl acetic acid],[22] *O*-methylatrolactic acid,[49] ADPD (5-amino-2,2-dimethyl-4-phenyl-1,3-dioxan),[50] or phosphorus-containing reagents,[51] an enantiomeric mixture can be converted to a pair of diastereomers, which can easily be distinguished by conventional ^{1}H NMR or ^{31}P NMR measurements due to the induced non-equivalence of certain chemical shifts. Alternatively, such NMR spectral non-identity of enantiomers can be initiated by chiral solvents, e.g., aryltrifluoromethylcarbinols,[52] allowing the determination of enantiomeric purity and absolute configuration without additional derivatization work. On the other hand, two-dimensional NMR-spectroscopic methods, such as NOE and ROE techniques (NOESY and ROESY), which provide information on the "through-space" interactions between protons, may also be used to determine the relative and – if a stereocenter of reference in the molecule – the absolute configuration.[53] In particular, it has been demonstrated for a number of biarylic compounds possessing both, axial and central chirality[54] that the absolute configuration at the biaryl axis can be

deduced from the relative axial vs. central configuration by measuring the long-range NOE interactions between protons of the two ring systems. However, this method is restricted to those systems in which at least one stereogenic center is known, and, furthermore, in which the distances between the respective protons are sufficiently small.[55]

- **Partial or total syntheses.** The absolute stereostructure of a chiral compound can be deduced from partial or total enantioselective synthesis.[56] This is a very effective and reliable, but sometimes also expensive and time-consuming method. By this way, the elucidation of the absolute configuration can be attained when starting from a chiral precursor of known configuration, and all chemical interconversions proceed without affecting bonds to the stereogenic center. A second possibility is the use of synthetic methods that modify the chiral center, but in a stereoselective way. In both cases, the verification of the obtained intermediates for their relative configuration by some other analytic methods is desirable at each stage of the synthesis.

- **Chemical degradation.** Alternatively to the above mentioned constructive, since total-synthestic approach, the configurational assignment of the centrally chiral compound can also be done by chemical degradation to optically active products suited for further comparison with reference material of known configuration.[57]

2.2. Chiroptical approaches

Spectroscopic measurements of chiroptical properties, such as optical rotation, optical rotatory dispersion (ORD), and circular dichroism (CD) represent an excellent tool for the elucidation of absolute configurations of chiral compounds. The main advantage of these methods is that they allow the rapid and unambiguous differentiation between stereoisomers without major experimental efforts and dissipating only small amounts of substance.

2.2.1. Optical rotation and optical rotatory dispersion (ORD)

When passing linearly polarized light (Lpl) of a given wavelength through a chiral sample, the phenomenon of optical rotation (i.e., the rotation of the plane of polarization of the Lpl beam) can be observed. Two enantiomers generate rotations of equal magnitude but of opposite sign and, therefore, can be easily distinguished. To comprehend the origin of the optical rotation, one has to keep in mind that the linearly polarized light can be mathematically and graphically represented as a superposition of left and right coherent rotating beams of circularly polarized light (Cpl), which are enantiomeric to each other. In an optically inactive medium, e.g., in a racemate, the two light components migrate at the same velocity c ($c_{lCpl} = c_{rCpl} \Rightarrow n_{lCpl} = n_{rCpl}$; n is a refractive index), so that the resultant vector sum, which exhibits the properties of the Lpl, does not change its orientation, that is, no rotation occurs (Figure 4a). If, however, the linearly polarized light passes through a chiral sample, both circular components, lCpl and rCpl, are slowed down relative to their prior velocities, but to a different extent (e.g., $c_{lCpl} < c_{rCpl} \Rightarrow n_{lCpl} > n_{rCpl}$), which can be explained by an unequal, diastereomorphous interaction between the two chiral rays and the chiral molecules. Consequently, the resulting linearly polarized light appears rotated relative to the incident beam by a certain angle α, which is called optical rotation (Figure 4b).

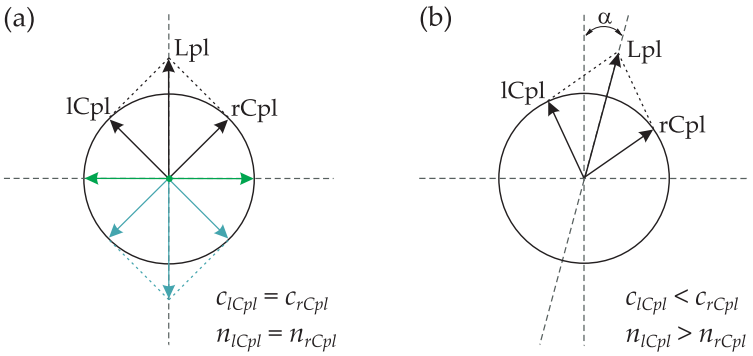

Figure 4. Superposition of left- (lCpl) and right- (rCpl) circularly polarized light (a) in the isotropic medium, and (b) in the optically active, anisotropic environment. c_{lCpl}/c_{rCpl} and n_{lCpl}/n_{rCpl} are the respective velocities and refractive indices of the lCpl and rCpl components.

The measured optical rotation angle α depends on the concentration of the chiral compound *c* and on the path length *l* (or sample cell thickness) (1).

$$\alpha = [\alpha]_{\lambda}^{T} cl \tag{1}$$

The proportionality factor $[\alpha]_{\lambda}^{T}$ is defined as a specific rotatory power or specific rotation, which is a function of the temperature T and the wavelength λ of the measurement, and represents a characteristic quantity of a chiral molecule. The correction for the molecular weight M of an optically active compound gives the molecular rotation $[\phi]_{\lambda}^{T}$ (2).

$$[\phi]_{\lambda}^{T} = \frac{M}{100}[\alpha]_{\lambda}^{T} \tag{2}$$

In former times, the prediction of the absolute configuration from specific rotation was mostly based on empirical approaches, such as WHIFFEN's method[58] or BREWSTER's rules,[59] which are derived from the assumption that the specific rotation of a chiral compound can be considered as a sum of the contributions from the individual chiral centers and dihedral segments in the molecule. However, none of these methods have found a broad practical application. Nowadays, high-level quantum mechanical calculations are in use, allowing the prediction of a magnitude and a sign of specific or molecular rotation with a reasonable accuracy.[11,60]

The measurement of the specific rotation $[\alpha]^{T}$ in dependence on the wavelength of the UV/Vis light gives the so-called optical rotatory dispersion (ORD). There are generally two types of ORD spectra: the normal, plain curves (also called "background rotation"), which are characterized by a monotonic increase of $[\alpha]^{T}$ while the wavelength is decreased; and the anomalous spectra of dispersion, which are defined by reversal of direction and inflection in the curves around a maximum of an absorption band (Figure 5). The ORD curves of the first type are normally obtained if no selective absorption by the sample has appeared. The anomalous behavior can be observed if molecule possesses a chiral element in the vicinity of a

chromophore that has a maximum in the UV/Vis region. The anomalous ORD is also described as a COTTON effect (CE) curve. In particular, a CE is called positive if the rotation magnitude first increases with a decreasing λ; conversely, the curve corresponds to a negative CE if the rotation value first decreases while going towards shorter wavelengths. It is remarkable that, e.g., for an originally positive specific rotation $[\alpha]^T$ two principal types of anomalous ORD spectra are possible (Figure 5).

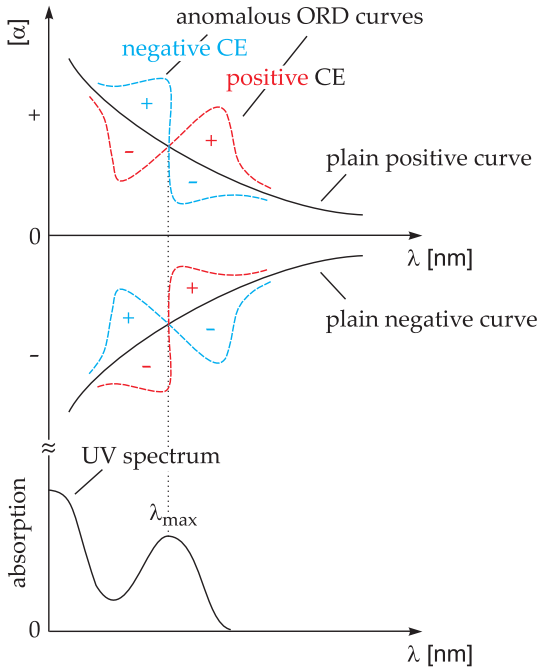

Figure 5. Typical ORD spectra: normal, plain curves (black) and anomalous ORD spectra, defined as positive (red) and negative (blue) COTTON effects (CE), whose crossover point closely corresponds to the wavelength of the respective UV maximum, λ_{max}.

Elucidation of the absolute stereostructure by using ORD spectroscopy is mainly based on the comparison of the ORD spectra of the examined molecule with the ORD curves of closely related compounds of known configurations.[61] Furthermore, analogous to optical rotation, the ORD spectra can be predicted by quantum chemical calculations.[12]

2.2.2. Circular dichroism

Circular dichroism (CD) is a second chiroptical phenomenon, most frequently applied for the assignment of the absolute stereostructure. When the linearly polarized light passes an optically active medium in a spectral region where absorption takes place, left- and right-circularly polarized rays do not only propagate with different velocities, but they are also absorbed by a chiral sample to a different extent (i.e., $A_{lCpl} \neq A_{rCpl}$). Thereupon, the incident Lpl is converted into elliptically polarized light (Epl), and, consequently, the resulting electric field vector sum traces an ellipse (Figure 6a), which is characterized by the major and minor axes, a and b, respectively, and by the angle ψ, defined as the ellipticity (Figure 6b).

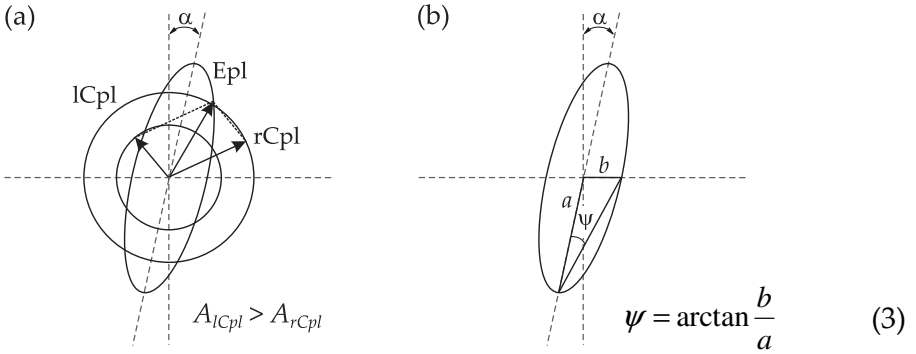

Figure 6. Source of the elliptically polarized light (Epl) (a), and definition of ellipticity ψ (b).

As seen in Figure 6, elliptically polarized light (i.e., if $a \neq b$) is the most general form of polarized light, whereas linear (if a or b = 0) and circular (if $a = b$) polarizations are special cases of the elliptical polarization.

In analogy with the quantities related to optical rotation (1 and 2), a specific ellipticity $[\psi]_\lambda^T$ (4) and a molar ellipticity $[\theta]_\lambda^T$ (5) can be defined for characterization of CD.

$$[\psi]_\lambda^T = \frac{\psi}{cl} \tag{4}$$

$$[\theta]_\lambda^T = \frac{M}{100}[\psi]_\lambda^T \tag{5}$$

Nowadays, however, circular dichroism is usually obtained by measuring the difference in the molar extinction coefficients of left- ε_{lCpl} and right- ε_{rCpl} circularly polarized components of light (6).

$$\Delta\varepsilon = \varepsilon_{lCpl} - \varepsilon_{rCpl} \tag{6}$$

Δε is also called molar CD, and it directly correlates with the molar ellipticity $[\theta]_\lambda^T$ (7).

$$[\theta]_\lambda^T = 3298\Delta\varepsilon \tag{7}$$

Similarly as the ORD curve can be obtained, the measurement of the Δε value as a function of the wavelength λ leads to a CD spectrum. In general, the measured CD effect is directly associated with the ORD anomaly, since they both reflect the interaction of the polarized light with the same chiroptical chromophore. The maximum of the CD curve coincides with the wavelength of anomalous ORD crossover, and the sign of COTTON effect in ORD spectrum corresponds to that of CD (Figure 7). Furthermore, if one of the two curves is known over the entire spectral range, the other can be calculated by using the KRONIG-KRAMERS equations.[62,63]

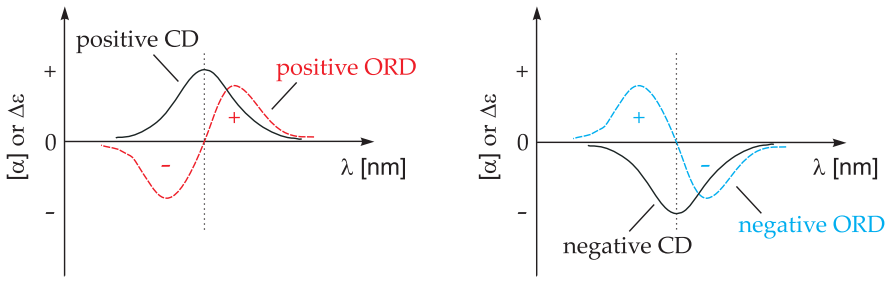

Figure 7. CD and ORD spectra describing (a) the positive and (b) negative CEs of a single electronic transition.

Although both phenomena afford complementary information, CD spectroscopy has now completely replaced the ORD technique, because it provides better discrimination between overlapping bands, whereas the ORD curves often possess a

fine structure due to molecular vibrations, which complicates the interpretation of the spectra.

2.2.2.1. Methods for the interpretation of CD spectra

Since the topic of the present work is directly related to CD spectroscopy, the different methods for the interpretation of CD spectra for the elucidation of the absolute stereostructure will be discussed in more detail. In general, the measured CD spectrum can be analyzed by using either empirical or semiempirical relations (Chapter 2.2.2.1), or it can be simulated by means of quantum chemical CD calculations (Chapter 3).

- **Empirical comparison of experimental CD spectra.** The absolute configuration of a new molecule from nature or from chemical synthesis can be easily deduced from a simple empirical comparison of the respective measured CD spectrum with the CD data of a previously obtained compound for which the absolute stereostructure has been already defined. Furthermore, the comparison with the CD spectra of closely related substances of known configurations may also give hints at the configuration of the investigated molecule.[64] Thus, for example, the axial configuration of the natural product ancistrobenomine A (**25**)[65] was elucidated by CD comparison with the *P*-configured structurally similar compound ancistrocladeine (**26**)[66] (Figure 8), whose stereochemistry has been clearly defined from the synthetic work as well as from theoretical studies.[67]

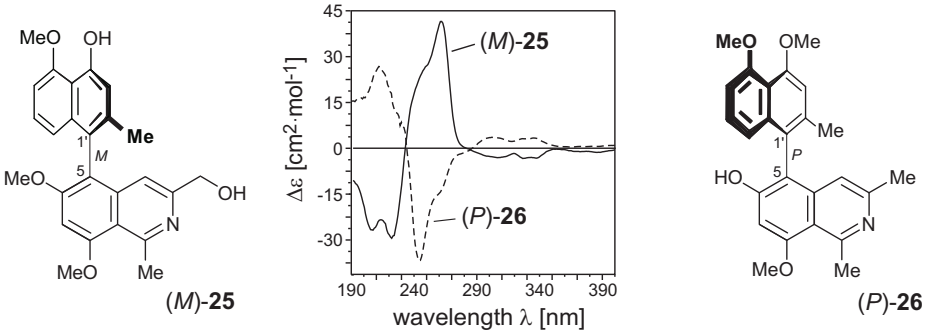

Figure 8. The assignment of the absolute axial configuration of ancistrobenomine A (**25**) by CD comparison with the known *P*-configured ancistrocladeine (**26**).

It has to be emphasized that in this case an unambiguous attribution of the absolute stereostructure is possible only if a reference compound possesses an identical chromophoric framework and differs only in a substitution pattern not affecting the chromophor or conformation, since small modifications in the structure of the chromophore or even minor conformational alterations may cause substantial changes in the CD spectrum.[24b] This has impressively been demonstrated on an example of rocaglamide (**27**)[24b] and its cyclic derivative cyclorocaglamide (**28**),[68] which showed an almost opposite CD spectra while having a near-identical constitution and the same absolute configuration at each stereogenic center (Figure 9). Such a mirrored-like CD behavior has been proven to be a result of the essentially different conformational distribution found for **27** and **28**.[69]

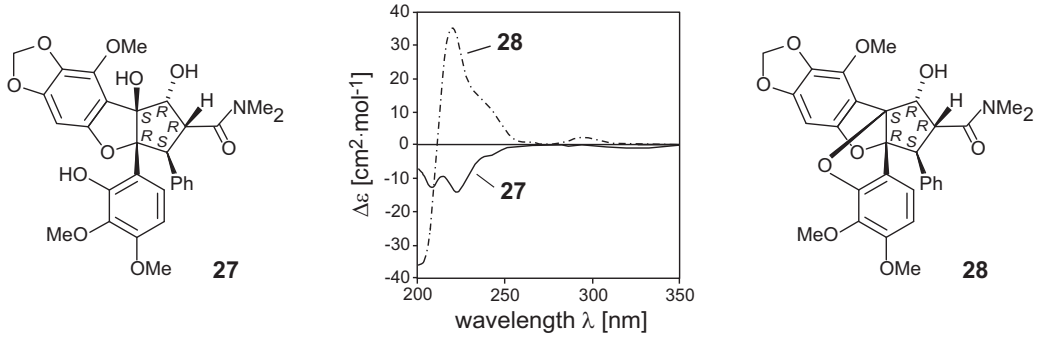

Figure 9. Stereostructures of rocaglamide (**27**) and cyclorocaglamide (**28**), and their experimental CD spectra.

- **Empirical rules.** A number of *Sector Rules* has been postulated to elucidate the absolute stereostructure of various chiral molecules possessing an inherently achiral chromophore, such as alkene, carbonyl, or benzene.[70] The basic idea of these rules is that the sign of a CE associated with a specific transition is considered to be very sensitive to contributions from all substituents ("perturbers") in a chromophore surrounding. These contributions are assessed by dividing the 3D space around the chromophore into sectors characterized by empirically attributed signs. As an example, the *Four-Sector Rule (Quadrant Rule)* for the benzene chromophore as applied for the elucidation of the absolute configuration of (+)-1-phenylethanol (**29**)[71] is demonstrated in Figure 10.

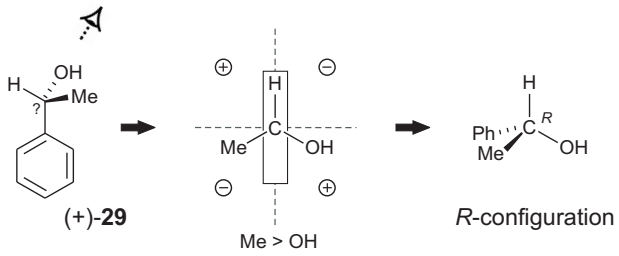

Figure 10. The *Quadrant Rule* applied for the assignment of the absolute configuration of (+)-1-phenylethanol (**29**).

The measured CD spectrum of compound (+)-**29** exhibits a negative CE at 268 nm ($\Delta\varepsilon$ –0.17 in CH_3OH),[71] corresponding to the characteristic ^1L_b transition of the benzene chromophore. Based on a sequence of contributions (SH, CO_2^- , $C(CH_3)_3$ > CH_3 > NH_2, OH, OCH_3, Cl) developed particularly for compounds of this type (C_6H_5CHRR'), the methyl group of **29** causes a larger contribution to the ^1L_b transition than does the hydroxy substituent, and hence the observed negative CE of (+)-**29** can be only obtained if the respective phenylcarbinol is *R*-configured. Analogous sector rules have been also designed for chiral alkenes,[72] allenes,[73] carboxylic acids,[74] primary amines,[75] and also for cyclic secondary alcohols.[76] The most popular and extensively studied one is the *Octant Rule* postulated for centrochiral saturated ketones and aldehydes.

The *Octant Rule* correlates the sign of the CE of the carbonyl chromophore, as measured at about 300 nm (n-π* transition) in saturated cyclic ketones, to the configuration of the chiral center in the vicinity of the chromophore.[77] According to this rule, the whole space surrounding the carbonyl group is divided by two nodal planes of the corresponding MOs and one extra-surface into eight sectors or octants. For a known conformation, any atom or group of atoms anywhere in the vicinity of the chromophore makes a certain contribution to the n-π* CE according to their location in the octant. The simplest example of applying the *Octant Rule* for the determination of the absolute configuration is (+)-3-methylcyclohexanone (**30**), which shows a positive n-π* CE at 290 nm (Δε +0.6).[78] In compound **30**, whose energetically preferred chair conformation has the equatorial methyl, the key "pertuber" (the methyl group) gives a desired positive contribution to the CD only when 3-methylcyclohexanone (**30**) is *R*-configured (Figure 11a), whereas in the case of (*S*)-**30**, the methyl group lies in a "negative" octant (Figure 11b).[78]

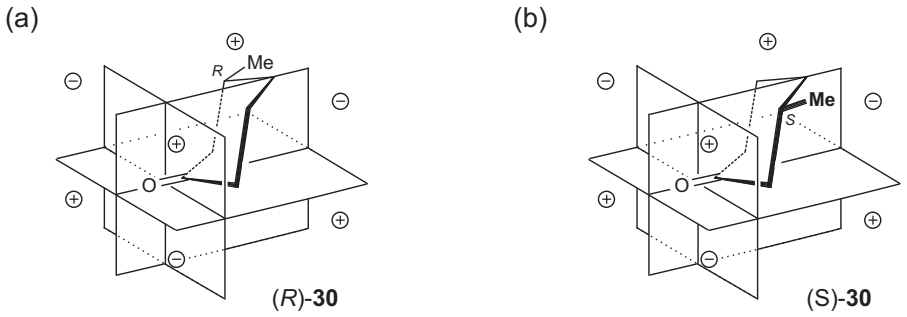

Figure 11. Elucidation of the absolute configuration of (+)-3-methylcyclohexanone (**30**) by applying the *Octant Rule*.

Although the interpretation of the CD spectra by means of *Octant Rule* seems to be a rapid and simple procedure, its application is rigorously restricted to the centrochiral saturated carbonyl compounds owing a rigid skeleton with the well-defined conformational behavior. The presence of several chromophores in the molecule can also affect the result. Furthermore, for β-axial substituted cyclohexanones and fluorine-containing compounds, which reveal an antioctant

behavior,[79,80] the utilization of this rule for determining the absolute stereostructure has proven to be particularly troublesome.

Finally, for compounds possessing inherently chiral chromophores, such as distorted β,γ-unsaturated ketones,[81] dienes,[82] disulfides,[83] and helicenes, various *Helicity Rules* have been designed, which are based on the determination of the direction of a helical path corresponding to the specific electronic transition.

- **The semiempirical *Exciton Chirality Method*.** Another important approach for establishing absolute stereostructures is the *Exciton Chirality Method*.[84] Although this method has been frequently applied in an empirical manner, it is actually based on a non-empirical coupled oscillator[85,86] and on group polarizability[87] theories. These declare that in a molecule containing two or more well-separated, strongly absorbing chromophores, the oscillating transition dipoles localized on each chromophore can spatially interact by dipole–dipole coupling in a symmetric and antisymmetric fashion. This gives rise to a split of the energy level of the excited state (Δλ, Davydov splitting[88]), resulting in a broadening of the respective UV absorption band. The CD band corresponding to this transition becomes bisignate (Figure 12a). The intensity of such a CD split is inversely proportional to the square of the inter-chromophoric distance.[89]

When viewing the CD spectrum from the longer to the shorter wavelengths the first band of the CD couplet shows a positive CE followed by a negative one, the CD is said to represent a positive chirality. In this case, a mutual orientation of the two chromophores corresponds to a clockwise twist between the respective transition moments (Figure 12b). And, *vice versa*, the CD spectrum with the first negative CE indicates a negative chirality, and hence an anticlockwise twist for the two chromophores. Thus, analysis of the CD spectrum with respect to the chiral spatial arrangement of the chromophoric units permits elucidation of the absolute stereostructure (for an example, see Figure 12b).

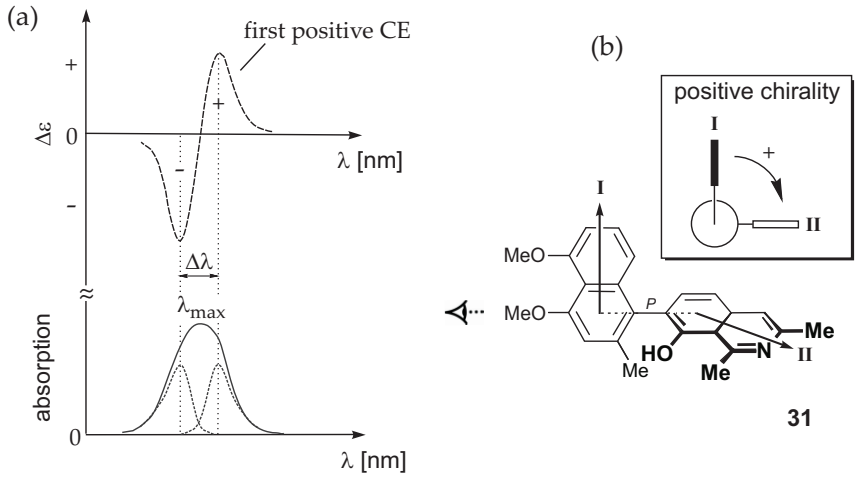

Figure 12. CD and UV spectra resulting from the Exciton Splitting Effect (a). Exemplarily, the CD spectrum with a positive CD couplet is shown. Application of the *Exciton Chirality Method* to the dehydrogenated, still axially chiral derivative **31** of dioncophylline A (**24**) possessing a strong positive first CE at 224 nm, which represents a case of positive chirality, here corresponding to a *P*-configuration (b).[90,13]

There are three general preconditions for the application of the *Exciton Chirality Method* for the assignment of the absolute configuration. The first is the presence of two identical or at least structurally and electronically similar chromophores. However, a fulfilment of only this requirement has been verified to be not sufficient.[20b,91] Thus, the simple qualitative prediction of the absolute axial configuration of the 1,1'-biphenanthryl compounds by using the *Exciton Chirality Method* has proven to be impossible due to the complexity of the electronic transitions involved into the CD splitting.[91] Therefore, according to the second precondition, the analyzed CD couplet should be isolated from other strong CD bands in order to avoid misinterpretations.[63,92] Furthermore, as it is defined within the *Exciton Chirality Method*, the exact knowledge of the directions of the electric transition moments of the individual chromophores appears to be a third essential requirement, since CD analysis based on incorrect assumptions of the polarization directions may likewise lead to the wrong configurational assignment. The information about the orientations of the transition dipoles can be achieved either from linear dichroism measurements[93] or from theoretical studies.

Although the *Exciton Chirality Method* has found a broad application for a great variety of chiral compounds,[94] the aforementioned preconditions substantially restrict the use of this method for the attribution of the absolute configuration, thereby leaving numerous cases where only quantum chemical CD calculations will successfully be applied (Chapter 3).

2.2.2.2. Circular dichroism in the solid state

Up to now all chiroptical properties, $[\alpha]^T$, ORD, and CD, have always been discussed as observables in solution. Although it usually requires more intricate techniques, these effects can also be measured in both, gas[95] and solid states.[96] Moreover, historically, a phenomenon of optical activity has been first discovered by BIOT in the solid sample, viz in a quartz crystal,[2] and only three years later these observations have been expanded to liquids. Evidently, the study of chiral compounds in the solid state has a substantial advantage over that in the gas phase or in solution, namely that the relative orientations and conformations of the molecules in the crystal can be easily and unambiguously revealed by X-ray crystallography. Furthermore, those conformations that are unstable in solution can be frozen in the crystalline state and then investigated, also with regard to the "solvent effect", by means of solid-state CD spectroscopy.[97] In light of the aforementioned properties and potentials, solid-state CD seems also to be useful in solving the stereochemical problems, particularly for compounds possessing high conformational flexibility. While the consideration of such molecules in solution requires a detailed analysis of all possibly occurring conformers, which may become a very difficult task, the crystalline state provides one or only few 'known' conformers for the CD study. The CD spectrum predicted for these well-defined, X-ray derived structures by using, e.g., quantum chemical calculations, can be compared with the experimental solid-state CD curve, thereby allowing an assignment of the absolute configuration.[43,44,98] This is a rather new and not much investigated field of application of solid-state CD spectroscopy. A reason for this

might be experimental difficulties associated with the acquirement of the true CD spectrum. In particular, the CD effect measured in the crystalline sample can be induced either by chiral molecules themselves or by a chiral helical arrangement of the molecules in the crystal, or by a combination of both factors, which are quite difficult to separate. However, it is possible to account for the influence of the second factor, i.e., a crystal lattice effect, by estimating a chirality index r (8),[99] which equals 1 for a quartz crystal ($\rho_s = 0$).

$$r = \frac{\rho_c - \rho_s}{\rho_c} \tag{8}$$

The parameters ρ_c and ρ_s are rotatory powers per molecule in a randomly oriented crystal aggregate and in solution, respectively. They can be determined by using the high-accuracy universal polarimeter (HAUP).[100]

The other difficulties of attaining the correct solid-state CD spectrum are related to the presence of the artificial CD signals induced by side-effects such as birefringence, dispersion at grain boundaries, linear dichroism, and linear birefringence, whose magnitudes are much larger than that of the molecule-induced CD.[96] Therefore, great care and advanced techniques[101] are needed to obtain spectra of high quality. Experimentally, the solid-state CD spectra can be measured for a chiral substance being either in the form of a single crystal, which is a rare case for organic compounds, or as microcrystals dispersed in a KBr matrix or in a nujol mull. The KBr matrix method, however, requires the preparation of dense pellets, as for IR measurements, applying high pressure, which may affect the CD spectrum, while the experiments with using a nujol mull often suffer from large dispersion effects, and furthermore, hydrophobic compounds may dissolve in nujol losing the unique property of the crystalline state.[97,102] Alternatively, the solid-state CD spectra can be measured in a diffuse reflectance mode, i.e., DRCD.[101,102,103] While in 'ordinary' CD spectroscopy the transmitted light is analyzed, the DRCD method deals with the back reflected, diffusely scattered light, which carries the sample information

through preferential absorption of either left- or right-circularly polarized incident light. The DRCD spectrophotometer built by Kuroda *et al.*[101,103] permits the measurements of the solid-state CD spectra on a powdered sample from pure microcrystalles or as a mixed with KBr, thus almost excluding negative effects of pressure and dilution.

In the course of this PhD work the solid-state CD behavior of one of the naphthylisoquinoline alkaloids, dioncophylline A (**24**), as a model compound, was investigated in cooperation with Prof. Reiko Kuroda from the University of Tokyo.[104] The results of this project are presented in Chapter 5.[45]

2.2.3. Other chiroptical techniques: VCD and ROA

Among the above mentioned traditional chiroptical methods, other spectroscopic techniques, such as vibrational circular dichroism (VCD)[105] and RAMAN optical activity (ROA),[106] play an increasingly important role in modern stereochemical analysis. In combination with high-level *ab initio* quantum chemical calculations, these methods likewise permit to determine the absolute configuration.[19,107] In contrast to the conventional electronic optical activity effects, ORD and CD, which are associated with transitions between the electronic states of the molecule, both, VCD and ROA phenomena are related to the vibrational transitions within the same electronic ground state. However, these are two essentially different techniques. Thus, VCD deals with a differential *absorption* of left- and right-circularly polarized infrared radiation, by analogy with ECD, whereas ROA is defined as a differential *scattering* for left and right circularly polarized components of visible light. Furthermore, the ROA technique provides a broader range of experimental variability than VCD. Thus, in dependence on the type of circular polarization modulation, four distinct types of ROA spectra can be obtained, viz. incident circular polarization ICP-ROA,[106a] scattered circular polarization SCP-ROA,[108] and two forms of dual polarization modulation (in-phase and out-of-phase) giving DCP_I and DCP_{II}-ROA spectra.[109] The main advantage of the vibrational chiroptical techniques

is their ability to distinguish equally good between the enantiomers possessing or lacking a chromophoric unit, whereas in electronic CD, the presence of a chromophore is a fundamental precondition. Furthermore, in comparison with ECD curves, vibrational optical activity spectra contain much more transitions, through which the absolute stereochemistry can be determined. Also from the theoretical point of view, VCD spectra are easier to accurately calculate than ECD curves, since only ground electronic state properties have to be considered. However, the prediction of the full ROA spectra for the "normal", medium-sized molecules is still a computational challenge. Despite these obvious advantages of VCD and ROA techniques, the standard electronic CD, due to its easier availability and handling, still remains the leading spectroscopic method.

Chapter 3

Theoretical background

It is the theory that decides what can be observed.

ALBERT EINSTEIN

As mentioned in the previous chapter, quantum mechanical calculations of molecular chiroptical properties, followed by a comparison with the experimental data, represent a powerful tool for the unambiguous determination of the absolute stereostructure of chiral molecules.[11–19,24,60,107] In our research group, calculations of the electronic CD spectra have become an indispensable procedure in structure elucidation processes. Therefore, the basic fundamentals and conceptions of calculating the CD spectra are thoroughly discussed in this chapter.

3.1. CD and UV spectra by quantum chemical calculations

3.1.1. Rotatory strength

While a magnitude of the experimentally observed CD effect is usually characterized by the Δε value, in quantum mechanical theory of circular dichroism this function performs a rotatory strength *R*, which directly correlates with the measured quantity as follows,[110]

$$R = \frac{3(2303)\hbar c}{16\pi^2 N_A}\int \frac{\Delta\varepsilon(\lambda)}{\beta\lambda}d\lambda \;=\; 2.297\times10^{-39}\int \frac{\Delta\varepsilon(\lambda)}{\beta\lambda}d\lambda. \qquad (9)$$

In this equation, $\hbar$ stands for the DIRACK's constant, c for the speed of light, and N_A for the AVOGADRO number. Parameter β is defined as the LORENTZ correction, which accounts for a local field on the chromophore, and normally is equated to unity, while the wavelength λ is often replaced by λ_{max}. Quantum mechanically, rotatory strength is calculated in accordance with the ROSENFELD equation[111] as the imaginary part of the product of the electric dipole $\boldsymbol{\mu}$ and the magnetic dipole transition moments $\boldsymbol{m}$ between the ground state and an excited electronic state (10).[112]

$$R_{0k} = \Im\left\{\langle\Psi_0|\boldsymbol{\mu}|\Psi_k\rangle\cdot\langle\Psi_k|\boldsymbol{m}|\Psi_0\rangle\right\} \qquad (10)$$

Here, Ψ_0 and Ψ_k are the wavefunctions of the ground state and the kth excited state, respectively. Substitution of the electric and magnetic moments in (10), which are defined as

$$\boldsymbol{\mu} = e\sum_{i=1}^{N_{el}} r_i \qquad (11)$$

$$\boldsymbol{m} = \frac{e\hbar}{2m_{el}c\Im}\sum_{i=1}^{N_{el}}(r_i \times \nabla_i), \tag{12}$$

leads to the expression for the rotatory strength in the dipole length formalism[113] form R_{0k}^{r} (13). Thus the derived rotatory strength obeys the *Rotatory Strength Sum Rule*,[114] but it appears origin-dependent.[113,115]

$$R_{0k}^{r} = \frac{e^2\hbar}{2m_{el}c}\left\{\langle\Psi_0|\sum_{i=1}^{N_{el}} r_i|\Psi_k\rangle \cdot \langle\Psi_k|\sum_{i=1}^{N_{el}} r_i \times \nabla_i|\Psi_0\rangle\right\} \tag{13}$$

In the above terms, e is the elementary charge, N_{el} is the number of all electrons in the molecule, and m_{el} is the mass of an electron, while r_i and ∇_i are position and gradient operators of the ith electron, respectively. By applying some transformation to the position operator r_i (14),[116] the rotatory strength can be rewritten in the gradient or dipole velocity form (15).[113]

$$r_i = \frac{\hbar^2}{m_{el}} \cdot \frac{1}{E_k - E_0}\nabla_i \tag{14}$$

$$R_{0k}^{\nabla} = \frac{e^2\hbar^3}{2m_{el}^2c} \cdot \frac{1}{E_k - E_0}\left\{\langle\Psi_0|\sum_{i=1}^{N_{el}} \nabla_i|\Psi_k\rangle \cdot \langle\Psi_k|\sum_{i=1}^{N_{el}} r_i \times \nabla_i|\Psi_0\rangle\right\} \tag{15}$$

The obtained rotatory strength R_{0k}^{∇} is origin-invariant,[115] but on the other hand, turns out relatively sensitive to the quality of the wavefunctions used, and furthermore violates the above mentioned *Rotatoty Strength Sum Rule*.[114] Some of the computational chemistry programs, e.g., TURBOMOLE[117] or GAUSSIAN[118] provide both types of the rotatory strength, permitting a direct comparison between R_{0k}^{r} and R_{0k}^{∇} in each particular case.

3.1.2. Oscillator strength

The quantum chemical predictions of CD spectra are frequently or nearly always accompanied by the calculations of the absorption UV/Vis spectra. Although the UV spectrum is a one-dimensional probe of the molecule, which is unsuitable for checking the chirality, the comparison of the measured UV spectrum with the theoretically predicted one may provide information on the accuracy of the calculations, and hence may serve as a tool for correction of the compared experimental and calculated CD spectra (for details, see Chapter 3.3.2).

In analogy to the rotatory strength for CD spectrum, a UV band is characterized by the dipole strength *D*, which can either be evaluated from the experimental UV data according to equation (16),[110] or might be calculated as the square of the electric dipole transition moment $\boldsymbol{\mu}$ (17).

$$D = \frac{3(2303)\hbar c}{4\pi^2 N_A}\int \frac{\varepsilon(\lambda)}{(\beta^2/n)\lambda}d\lambda \;=\; 9.18\times10^{-39}\int \frac{\varepsilon(\lambda)}{(\beta^2/n)\lambda}d\lambda \tag{16}$$

$$D_{0k} = \left|\boldsymbol{\mu}_{0k}\right|^2 = \left|\left\langle \Psi_0 \left| \boldsymbol{\mu} \right| \Psi_k \right\rangle\right|^2 \tag{17}$$

In theoretical chemistry it is, however, customary to use an analogous dimensionless quantity, which is called oscillator strength f_{0k} (18).

$$f_{0k} = \frac{4\pi m_{el} c}{3\hbar e^2 \lambda}\left|\boldsymbol{\mu}_{0k}\right|^2 \tag{18}$$

3.2. Theoretical approaches used for computation of the electronic excitations

For the calculation of such molecular characteristics as the electronic spectra, it is indispensable to take account of the electron correlation. By definition, the energy error associated with neglect of the electron correlation (which is called the total

correlation energy) is defined as the difference between the true energy of the system E and the energy predicted by the *ab initio* HARTREE-FOCK quantum chemical method E_{HF} in a complete basis ("HF limit") (19).

$$E_{corr} = E - E_{HF} \tag{19}$$

Electron correlation implicates its dynamic and static components. Dynamic electron correlation describes the pairwise interactions between each electron with every other electron of the system. The non-dynamic component refers to the cases when the HF single-determinantal representation of the wave function appears not sufficient (e.g., due to near-degeneracy of the states). There are several different quantum mechanical methods for taking into account the electron correlation, but this sub-chapter will concentrate only on those approaches that were used in this work. These are the *Configuration Interaction* (CI) method, the *Time-Dependent Density Functional Theory* (TDDFT) approach, and the combined *Density Functional Theory/Multireference Configuration Interaction* (DFT/MRCI) method.

3.2.1. Configuration Interaction (CI) methods

Essentially, the purpose of all quantum chemical approaches is the finding of the wave function Ψ of the investigated molecular system, since this, when operated upon an appropriate operator, provides the molecular properties (e.g., energy, spectroscopic or thermodynamic quantities) that one is interested in. The fundamental HARTREE-FOCK method[119] describes the complete wave function of the system as a single SLATER determinant, which is not adequate for the accurate description of the system, as it does not include the electron correlation effects. Within the post-HF approach, viz. the *Configuration Interaction* (CI) method, the wave function is expressed as a linear combination of multiple determinants (20) with the HF one (Ψ_{HF} in 20) as a reference:

$$\Psi_{CI} = a_0\Psi_{HF} + \sum_S a_S\Psi_S + \sum_D a_D\Psi_D + \sum_T a_T\Psi_T + ..., \qquad (20)$$

where wave functions Ψ_i with subscripts S, D, and T are the configuration state functions (CSFs) describing all single, double, and triple electronic excitations, respectively. Some examples of such excitations are depicted in Figure 13. An increase of the number of configuration terms in the expansion (20) recovers more and more of the electron correlation, making the method more and more exact.

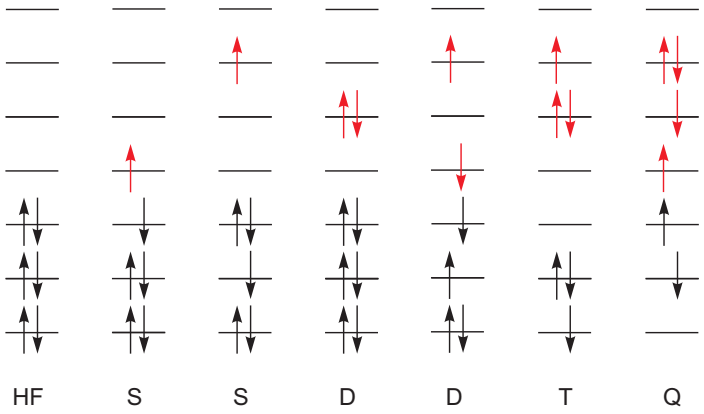

Figure 13. Excited configurations formed from the HF determinant as the reference (single-reference CI).

The coefficients a_i in (20) reflect the weight of each particular CSF in the wave function expansion. Although a_0 has the largest contribution (up to 99%), the impact of the other configurations still might be very important for describing some chemical processes. Evaluation of these coefficients is performed from the CI secular equation (21) according to the variational principle.

$$\begin{vmatrix} H_{00}-E & H_{01} & \cdots & H_{0N} \\ H_{10} & H_{11}-E & \cdots & H_{1N} \\ \vdots & \vdots & \ddots & \vdots \\ H_{N0} & H_{N1} & \cdots & H_{NN}-E \end{vmatrix} = 0 \qquad (21)$$

Here, each energy value E corresponds to a particular set of coefficients, and H_{mn} are the CI matrix elements determined as

$$H_{mn} = \langle \Psi_m | H | \Psi_n \rangle, \tag{22}$$

where H is the Hamiltonian operator, including one- and two-electron components. Such integrals containing two determinants, Ψ_m and Ψ_n, differing by more than two orbitals are equated to zero, while for the remaining cases, the CI matrix elements are established in accordance with the CONDON-SLATER rules and BRILLOUIN's theorem. The problem of the CI method is the rapidly growing size of the CI matrix (i.e., the number of the matrix elements H_{mn}) with the number of electrons and orbitals. Therefore, the consideration of all electrons and all orbitals of the system, and of all possible excitations, which forms the so-called *full CI* method, is practically possible only for atoms or very small molecules with few electrons, and only when using a small basis set. Consequently, although the *full CI* approach is the most accurate method, which gives an exact solution of the non-relativistic, time-independent Schrödinger equation within the chosen basis set, it finds only application as the reference method for estimation of the quality of other, more approximate approaches in including the electron correlation. Computationally more feasible methods are derived from truncating the expansion 20: Thus, taking into account only single or double excitations results in CIS (CI with Singles) and CID (CI with Doubles) methods, respectively; CISD calculations consider both, singly and doubly excited configurations; and consequently, an additional inclusion of triple and quadruple excitations yields the respective CISDT and CISDTQ approaches. According to BRILLOUIN's theorem, CI matrix elements (22) between the HF wave function and the singly excited determinants are zero, and therefore the CIS method does not provide any improvement in the calculation of the ground state over the HF approach. However, it remains important for the excited-states calculations. The higher-roots methods CISDT and CISDTQ are very accurate and verge towards the

full CI results, but they are still computationally very costly. Furthermore, it has been shown[120] that the higher-order excitations (like triple, quadruple, etc) are usually insignificant in the low-energy excited states, which are normally the most interesting ones for chemists. Thus, the only CI models that remain computationally reasonable are CIS and CISD methods. Moreover, the combination of these approaches with the semiempirical approximations, which drastically reduce the number of the costly four-index integrals when calculating the molecular orbitals and the CI matrix elements, permits the use of the CI technique for systems with an extremely large number of electrons. During this work, the semiempirical CNDO/S[27] and INDO/S[121] methods, and the MNDO-based OM2[28] approach were used in conjunction with CIS and CISD calculations, the latter one being available only for the OM2 method. Another way to reduce the computational time during the CI calculations is the restriction of the active molecular orbitals space, i.e., the number of the lowest occupied and highest unoccupied MOs between which electronic excitations are set to be allowed. Usually, the maximum number of configurations admitted within the software used, were treated during this work.

Reverting to *ab initio* level, the CI methods mentioned so far refer to the single-reference approaches, as they consider the CSFs generated only from the single-determinantal HF wave function as the reference. Taking the multiconfigurational wave function – analogous to (20) – as a basis for constructing the CSFs yields *Multireference Configuration Interaction* (MRCI) methods. Evidently, the MRCI calculations are computationally even more demanding than the respective single-reference CI ones, although the former methods provide significantly improved virtual orbitals, which make the CI calculations more rapidly converged. An additional efficiency with regard to the computational costs of the MRCI computations can be achieved by considering the reduced number of single and/or double excitations, by limitation of the size of the multiconfigurational wave function, and by employing the restricted active MOs space, thus giving rise to a number of different MRCI methods.

3.2.2. Time-Dependent Density Functional Theory (TDDFT) and DFT/MRCI

The *Density Functional Theory* (DFT)[122] method is an alternative quantum chemical approach. It uses the electron density ρ instead of the wave function Ψ for describing the molecular system. The DFT methodology is based on three principles: The electron density uniquely determines the ground-state electronic energy, as it defines the external potential, the wave function and the Hamiltonian of the system (HOHENBERG-KOHN existence theorem).[123] According to the second HOHENBERG-KOHN theorem,[123] electron density obeys the variational principle, and as a consequence, an analogous to the MO theory mathematical instrumentation can be applied for finding the most optimal electron density, which will provide the lowest energy. The last and very important issue is that the overall ground-state density of the real system of interest (with interacting electrons) can be derived as the density of some fictitious system of non-interacting electrons moving in an effective local one-particle potential (KOHN-SHAM potential).[124] The energy of the real system (as a functional of the electron density, $E[\rho]$) is then expressed as a sum of the kinetic energy of the non-interacting electrons T_{ni}, the nuclear–electron interaction V_{ne}, the classical electron–electron repulsion V_{ee}, and the exchange-correlation energy E_{xc}, which comprises all corrections to T_{ni} and V_{ee}, i.e., all those that account for the interacting nature of electrons (23).

$$E_{DFT}[\rho] = T_{ni}[\rho] + V_{ne}[\rho] + V_{ee}[\rho] + E_{xc}[\rho] = \tag{23}$$

$$= \sum_{i}^{N}\left(\langle \chi_i | -\frac{1}{2}\nabla_i^2 | \chi_i \rangle - \langle \chi_i | \sum_{k}^{Nuclei} \frac{Z_k}{|r_i - r_k|} | \chi_i \rangle \right) + \sum_{i}^{N} \langle \chi_i | \frac{1}{2} \int \frac{\rho(r')}{r_i - r'} dr' | \chi_i \rangle + E_{xc}[\rho(r)]$$

The orbitals χ_i are the KOHN-SHAM one-electron orbitals, which are obtained iteratively just in a fashion developed for the HF approach, but solving now the one-electron KOHN-SHAM equations (24) in which V_{xc} is an exchange-correlation potential (25).

$$\left(-\frac{1}{2}\nabla_i^2 - \sum_k^{Nuclei}\frac{Z_k}{|r_i - r_k|} + \int\frac{\rho(r')}{|r_i - r'|}dr' + V_{xc}\right)\chi_i = \varepsilon_i\chi_i \tag{24}$$

$$V_{xc} = \frac{\delta E_{xc}[\rho(r)]}{\delta\rho(r)} \tag{25}$$

DFT is posed as an exact theory due to its all-embracing exchange-correlation energy term E_{xc}, which considers all 'problematic' many-body interactions and furthermore, includes the difference between kinetic energies of the real system and the auxiliary one. On the other hand, a view of this density functional is unknown, and therefore, it has to be used in an approximate form. The simplest one provides a Local Density Approximation (LDA) or the spin-polarization adopted Local Spin Density Approximation (LSDA), for which the electron density is locally treated as a uniform electron gas (*ueg*), or in other words, the density is a very slowly varying function (26). In this equation, the term $\varepsilon_{x/c}$ is an energy density, which is usually approximated for its two individual components, the exchange ε_x and correlation portion ε_c, separately.

$$E_{xc}^{LDA}[\rho] = \int\rho(r)\cdot\varepsilon_{x/c}^{ueg}[\rho_{local}(r)]dr \tag{26}$$

The LDA is, however, not sufficiently accurate for chemical applications, as the electron density in the molecule is not homogenously distributed. Therefore, it is necessary to include terms that explicitly take into account the spatial variation of the density, i.e., the gradient of the density (27). Such a construction of the functionals

refers to a Generalized Gradient Approximation (GGA), which yields a substantial increase in the accuracy of DFT calculations.

$$\varepsilon_{x/c}^{GGA}[\rho] = \varepsilon_{x/c}^{LSDA}\left[\rho_{local}(r)\right] + \Delta\varepsilon_{x/c}\left[\frac{\left|\nabla\rho(r)\right|}{\rho^{4/3}(r)}\right] \qquad (27)$$

Additional improvements offer the so-called hybrid functionals, which incorporate certain fractions of both, LSDA and GGA based exchange and correlation components, as well as the HF exchange energy, following the *Adiabatic Connection Method* (ACM).[125] Among different hybrid functionals, B3LYP[126] and BHLYP[127] are the most popular and the most effective ones to date.

For calculation of the electronic excited states, a time-dependent extension to the DFT method (TDDFT)[29] has to be applied, as this permits to describe the system under time-dependent perturbation induced by a fluctuating external electric field. The main ideas of this approach are the same as in DFT. Thus, for any interacting many-particle system subject to a given time-dependent potential, all physical observables are uniquely determined by knowledge of the time-dependent electron density and the state of the system at an arbitrary, single instant in time.[128] Such time-dependent density is determined by solving a set of non-interacting SCHRÖDINGER-like equations, viz. the time-dependent KOHN-SHAM equations (28,29), in which, analogously, the time-dependent exchange-correlation term A_{xc} has to be approximated. Most calculations, however, use an Adiabatic Approximation (29) where the function $\rho(r,t)$ is replaced with the electron density $\rho^t(r)$ defined at the fixed time t, which thus permits the application of the known time-independent functionals E_{xc}.

$$\Im \frac{\partial}{\partial t}\chi_i(r,t) = \left(-\frac{1}{2}\nabla_i^2 - \sum_k^{Nuclei} \frac{Z_k}{|r_i - r_k(t)|} + \int \frac{\rho(r',t)}{|r_i - r'|} dr' + V_{xc}(r,t) \right) \chi_i(r,t) \qquad (28)$$

$$V_{xc}(r,t) = \frac{\delta A_{xc}[\rho(r,t)]}{\delta \rho(r,t)} \cong \frac{\delta E_{xc}[\rho^t(r)]}{\delta \rho^t(r)} \qquad (29)$$

As to the calculation of the excited states, it has been shown that solving of the time-dependent equations (28) is equivalent to finding the poles of the frequency-dependent polarizability $\alpha(\omega)$ of the molecule in the basis of the KOHN-SHAM orbitals. Polarizability is well approximated by

$$\alpha(\omega) = \sum_{k>0} \frac{\left| \langle \Psi_0 | \hat{\mu}_{0k} | \Psi_k \rangle \right|^2}{(E_k - E_0)^2 - \omega^2}, \qquad (30)$$

where the numerator corresponds to the electric transition dipole moments, while the denominator consists of the frequency of the incident electric field ω and the energies of the ground E_0 and the excited E_k states. Consequently, the pole of the polarizability function, i.e., if E_k-E_0 corresponds to ω, provides the excitation energy of the system. Application of this approach, a so-called propagator method, has a substantial advantage with respect to the computational costs, as the poles are determined without the need to compute all excited-state wave functions and the respective energies.

TDDFT calculations, in particular when using hybrid functionals (like B3LYP[126]) and sufficiently large AO basis (at least double-ζ basis set), provide very accurate results for excitation energies, electric and magnetic dipole moments for well-localized states involving mainly single excitations. This guarantees a wide application of TDDFT for calculation of chiroptical properties of many different chiral compounds.[14,129,130,131] However, the method fails in describing more complex

situations as e.g., the states implying charge-transfer,[132] RYDBERG,[133] double or higher order excitations. The use of advanced functionals, viz. with an asymptotically corrected behavior[134] or with a substantial inclusion of the HF exchange (like in the hybrid BHLYP[127] and M06-HF[135] functionals), or recently developed double-hybrid B2PLYP[136] density functional, may solve the problems of charge-transfer and RYDBERG states to a great extent.

In cases when multiple excitations are substantially involved into the excited state, a multireference description appears more appropriate. The combined *Density Functional Theory/Multireference Configuration Interaction* (DFT/MRCI) method developed by Grimme and Waletzke[30] provides an effective compromise between the highly accurate but expensive MRCI method, and the easy-to-perform and yet sufficiently reliable DFT approach. By this way, a major part of dynamic electron correlation is covered by DFT, while the non-dynamical contributions are considered by MRCI calculations. The DFT/MRCI method has been shown to give good results for excited states of numerous organic molecules.[14,129,137] Within this approach, a multireference-based CI expansion covers single and double excitations. The spin- and space-symmetry adapted CSFs for the CI wave function are now built from KOHN-SHAM orbitals. The matrix elements between two CSFs (31) of the CI matrix (32) are calculated as following: the diagonal elements are computed by using the exact Hartree-Fock expression, including KOHN-SHAM orbital energies and a DFT-specific correction term, while for the off-diagonal elements, an empirical, energy-dependent scaling is used, which additionally permits to avoid a double counting of the correlation effects. In summary, five empirical parameters are involved.

$$H_{mn}^{DFT} = \left\langle \Psi_m^{fromKS} \middle| H^{(DFT)} \middle| \Psi_n^{fromKS} \right\rangle \tag{31}$$

$$\begin{pmatrix} H_{00}^{DFT} & H_{01}^{DFT} & \cdots & H_{0N}^{DFT} \\ H_{10}^{DFT} & H_{11}^{DFT} & \cdots & H_{0N}^{DFT} \\ \vdots & \vdots & \ddots & \vdots \\ H_{N0}^{DFT} & H_{N1}^{DFT} & \cdots & H_{NN}^{DFT} \end{pmatrix} \tag{32}$$

At present, DFT/MRCI calculations are adopted only for the hybrid BHLYP[127] functional. As to the basis set, it has recently been shown[138] that the use of the small SVP basis, which drastically reduces the computational time, has a negligible effect on the excitation energies and oscillator strengths as compared to the larger TZVP basis. The Resolution-of-Identity (RI)[139] method is applied to evaluate the computationally costly four-index integrals, which are approximated as products of RI integrals that are less expensive to compute. Thus, DFT/MRCI calculations are applicable for rather large molecules having more than 200 electrons. Additional efficiency is gained by using a selection procedure for the iteratively obtained reference CSFs. This is based on an energy gap criterion of δE_{sel} = 1.0 Hartrees,[30] which permits to choose only the most important configurations, and thus to save computational time. For larger molecules, a selection threshold of 0.08 Hartrees has appeared also reasonable,[14] and, therefore, this value was used for the compounds described in this work.

3.3. General proceedings of simulating CD and UV spectra

From a practical point of view, the concept of "CD calculations" implies three general steps: 1) Investigation of the conformational preferences of a chiral molecule; 2) Calculation of the rotatory and oscillator strengths, and finally, 3) Treatment of the obtained values, leading to the simulation of the CD and UV curves, which are then compared with the experimental data.

3.3.1. Investigation of the conformational behavior

Since circular dichroism strongly depends on the orientation of the chromophores to each other and, thus, on the conformational behavior, the detailed study of the conformers equilibrium is a crucial procedure in CD calculations.[24,140,141] This can be achieved by means of two different procedures, viz. by using a conformational analysis[13] or via molecular dynamics (MD) simulations.[142] Furthermore, there is a

third alternative, which combines features of both above methods, and can be referred to as a hybrid approach.[143]

- **Conformational analysis – the BOLTZMANN method.** Within this approach, the potential-energy surface of a given molecule is "manually scanned" in order to locate all possible minimum structures which are sufficiently populated at the room temperature, and hence can influence on the overall molecular CD. It can be shown that conformers lying in the range of 3 kcal·mol^{-1} above the presumably global minimum represent almost 100% of the population according to the BOLTZMANN distribution. Therefore, it is justified to take into account the structures within this energy cut-off only. Practically, the conformational search is started with one or few initial structures, which are at first preoptimized by force field[144] calculations within the molecular modelling package SYBYL,[145] and then further optimized at the semiempirical AM1[146] or PM3[147] levels by using, e.g., the GAUSSIAN software.[118] As a next step, the flexibility of the molecule is investigated by calculating the internal rotation energy profiles for the characteristic dihedral angles of each flexible part of the molecule, and determining their energetically preferential orientations (i.e., minima in the energy profiles). Then, a systematic tree-like hierarchical 'permutation' procedure is performed to generate all possible conformations. Thus, for example, if a molecule contains three rotating groups each leading to two preferred orientations, the overall number of the geometries resulted from the permutation is defined as 2 × 2 × 2 = 8. The subsequent semiempirical optimization and discarding of the duplicate and energetically unprofitable conformers provide the final minima structures. These can be further improved by DFT calculations employing e.g., the BLYP[148,126b] or the B3LYP[126] functionals, in combination with the RI approximation, which drastically saves computational costs. To sum up, the BOLTZMANN method results in well-optimized conformers and their relative energies.
- **The Molecular Dynamics (MD) method** is another conformational searching technique, based on classical molecular mechanics. The MD approach permits to

study molecules in motion, which represents, actually, the calculated 'jumps' in conformational changes on a very short time scale (in nano-, pico- or femto-seconds), thereby coming nearer to the reality. At the first step of the simulation cycle, the given starting kinetic energy, defined by the chosen temperature, supplies all atoms with initial velocities. The potentials for each degree of freedom are then calculated within the TRIPOS[145] or MM3[149] force fields. As next, the forces affecting each atom are derived, followed by solution of NEWTON's equation, which results in new atom velocities. The latter have to be additionally scaled because of the dependence of the particular system on the chosen temperature. The last step is the calculation of the new molecular structure, which serves further as a new starting point for the next cycle. This procedure takes place until the MD simulation time is finished. Consequently, the result of MD simulations is a series of snapshots of new, fixed conformations. To properly describe the molecular motion as a continuous process, NEWTON's equation is solved every 0.2 fs within a time period of 500 ps, whereas the single structures are extracted from the MD trajectory every 0.5 ps, thus providing 1000 conformers for further CD calculations. The most complete sampling of the conformational space of the molecule can be achieved either by increasing the duration of an MD run, or by variation of the temperature. Therefore, MD calculations are usually carried out at several temperatures to select the most appropriate, i.e., the most realistic MD simulation. A choice of the particular MD run is normally based on a comparative analysis of the MD trajectories recorded for each flexible part of the molecule with the respective reaction coordinate calculated during the conformational analysis. Evidently, the MD approach appears to be an advantageous and undemanding alternative for the characterization of the conformational behavior. This has particular importance for highly flexible molecules, with a great number of degrees of freedom to be considered, which makes the application of the BOLTZMANN method very difficult or even impossible. On the other hand, MD simulations provide the single conformers that are optimized by

force fields only, which may cause difficulties for the following quantum chemical CD calculations.

- **The Hybrid method**, which comprises elements of both of the above techniques, may solve this problem. Within this approach, a comprehensive conformational sampling is performed by means of MD simulations, while further procedures, namely, the semiempirical pre-optimization of the collected 1000 structures, the selection of the relevant conformers, and their higher-level optimization, are carried out in a way analogous to the BOLTZMANN approach.[143] Evidently, a weak point of this method is the pre-optimization step, which is very time consuming. In any case, a choice of one or another conformational searching method depends on the particular molecular system, i.e., on its size and flexibility.

3.3.2. Steps towards CD and UV spectra

As soon as the conformational distribution is defined by one of the above procedures, the excited-state energy calculations will be performed for each single conformer by using either the configuration interaction (CI) technique, involving the semiempirical CNDO/S,[27] INDO/S[121] or OM2[28] Hamiltonians, or by using advanced time-dependent DFT (TDDFT)[29] or DFT/MRCI approaches.[30] Evidently, the CD spectra for the MD simulated conformers can only be calculated at the semiempirical level, as the application of the TDDFT or DFT/MRCI methods is a computationally too demanding process. Going into detail, the semiempirical CI calculations were carried out within the BDZDO/MCDSPD[150] (for CNDO/S or INDO/S) and MNDO99[151] (for OM2) program packages, which permitted to consider up to 784 and 900 singly excited electronic configurations, respectively. The TDDFT calculations usually involved the BLYP[148,126b] or B3LYP[126] functionals and the TZVP (triple-ζ valence polarized)[152] basis set, as implemented in the TURBOMOLE[117] program. In this case, the number of the excited states required for reproducing the entire experimental CD and UV spectra, depended on the particular molecular system, and varied from 30 to 100 for the molecules investigated during this work.

The DFT/MRCI method, using Grimme's program packages,[127] permitted the calculation of the molecules with up to 250 electrons,[a] by using the standard BHLYP hybrid functional and the SVP (slit-valence polarized)[153] atomic orbitals basis. The application of a larger basis set, e.g., TZVP, was not possible in most of the cases because of too high computational costs. Furthermore, to reduce the calculations time without significant loss of accuracy, the configuration selection cut-off of 0.8 E_h[14] was used.

Finally, the series of the rotatory and oscillator strengths calculated for each conformer were extracted by appropriate scripts[154] and plotted against the wavelengths resulting in so-called bar or stick CD and UV spectra.

- **Acquirement of the overall spectra.** The next step is the summing up of the single spectra of the individual conformers to provide the overall CD or UV spectrum. For the conformers obtained from the conformational analysis, adding up is carried out in accordance with the BOLTZMANN statistics. Thus, the contribution of the particular single spectrum to the overall one is estimated by calculating the weighting factor f_i for each ith conformer in the dependence on its relative energy ΔE_i with respect to the global minimum structure (33).

$$f_i = \frac{e^{-\frac{\Delta E_i}{k_B T}}}{\sum_i^{N_{conf}} e^{-\frac{\Delta E_i}{k_B T}}} \tag{33}$$

Here, k_B is the BOLTZMANN's constant, T is the absolute temperature, and N_{conf} is the number of all conformers considered. The overall CD or UV spectrum is then obtained as the weighted average of the single spectra (34).

$$CD_{overall} = \sum_i^{N_{conf}} f_i CD_i \quad \text{and} \qquad UV_{overall} = \sum_i^{N_{conf}} f_i UV_i \tag{34}$$

[a] Recently, even larger systems became accessible for DFT/MRCI calculations.

In the case of the MD approach, the single spectra are arithmetically averaged (35), disregarding the conformational energies, that is, all MD generated conformers equally contribute to the overall spectrum.

$$CD_{overall} = \frac{\sum_{i}^{N_{conf}} CD_i}{N_{conf}} \quad \text{and} \quad UV_{overall} = \frac{\sum_{i}^{N_{conf}} UV_i}{N_{conf}} \tag{35}$$

In practice, it is convenient to perform these procedures on the bar spectra, before converting them into the band-shape form.

- **Simulation of the band-shape curves Δε(λ) and ε(λ)** from the bar spectra is performed by utilizing a Gaussian distribution.[110] Thus, for each *k*th electronic excitation centered at the wavelength λ_k the Gaussian shape function is constructed according to expression (36), followed by the addition of these Gausses over the whole wavelength range λ to provide the final CD curve $\Delta\varepsilon(\lambda)$, or the UV spectrum $\varepsilon(\lambda)$ when pursuing equation (37).

$$\Delta\varepsilon(\lambda) = \frac{16\pi^2 N_A \lambda R_{0k}}{6909\hbar c} \cdot \frac{1}{\sigma\sqrt{2\pi}} \exp\left[-\frac{(\lambda-\lambda_k)^2}{2\sigma^2}\right] \tag{36}$$

$$\varepsilon(\lambda) = \frac{4\pi^2 N_A \lambda D_{0k}}{6909\hbar c} \cdot \frac{1}{\sigma\sqrt{2\pi}} \exp\left[-\frac{(\lambda-\lambda_k)^2}{2\sigma^2}\right] \tag{37}$$

In these equations, σ is the exponential half-width, i.e., half the width of the CD or UV band at 1/*e* height, which is used as an adjustable parameter for reproducing the experimental CD or UV features. An influence of the σ value on the shape of the theoretically predicted spectrum is exemplarily demonstrated for the CD curve in Figure 14. At small σ the "detailed", structured CD spectrum is obtained, whereas

larger σ values make the spectrum smoother and broader. For compounds presented here, the half width ranged from 0.08 eV to 0.2 eV.

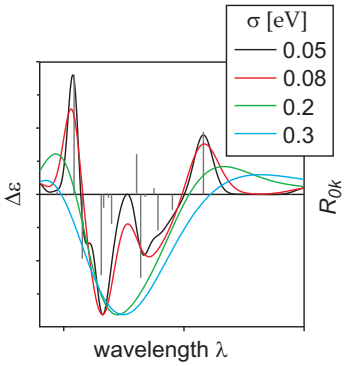

Figure 14. Dependence of the shape of the simulated "Gauss" CD curve on the empirical parameter σ.

- **Comparison of the experimental spectra.** First, the calculated UV spectrum is compared with the experimental UV curve in order to estimate the accuracy of the calculations and to take into account systematic errors of the methods used. Thus, it is common that the semiempirical CIS methods provide overestimated excitation energies due to the lack of the dynamic electron correlation, and the calculated spectrum has to be red-shifted to reproduce the measured curve, whereas the TDDFT calculations often underestimate the transition energies,[132b] so that a correcting blue-shift is required to match the experimental UV spectrum. Such correction of the computed UV spectrum is given by a so-called UV-shift,[14] which is further applied to the calculated CD spectrum (Figure 15). Finally, the comparison of thus corrected theoretical CD spectrum with the measured curve provides the assignment of the absolute configuration.

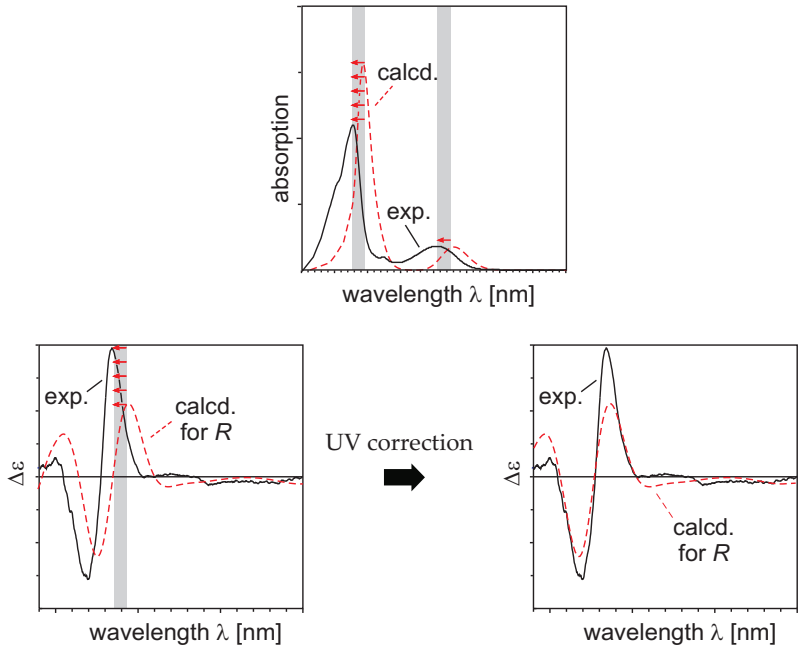

Figure 15. Principle of a UV correction.[14]

Chapter 4

Configurational assignment by CD calculations

If you want to find out anything from the theoretical physicists about the methods they use, I advise you to stick closely to one principle: Don't listen to their words, fix your attention on their deeds.

ALBERT EINSTEIN

4.1. Application of semiempirical methods

4.1.1. Ancistrotanzanine A (5)

Naphthylisoquinoline alkaloids, exclusively occurring in tropical lianas of the Dioncophyllaceae and Ancistrocladaceae plant families, represent an important class

of structurally, pharmacologically, and biogenetically intriguing biarylic compounds, which are of great interest due to their wide range of vitally important biological activities, e.g., antiplasmodial,[155] antileishmanial,[65,156] antitrypanosomal,[157] as well as fungicidal and molluscicidal properties.[158] Furthermore, these molecules are interesting stereochemically due to the presence of one or two stereocenters in the isoquinoline part, and, in particular, biaryl axis between the naphthalene and isoquinoline portions which is usually rotationally hindered. This makes the compounds attractive to researchers, because the exact knowledge of the absolute configuration, especially at the axis, is an essential requirement for directed structure-activity relationship investigations.[159] While the absolute configurations at the stereogenic centers can be established by oxidative degradation[57] in combination with NMR measurements, quantum chemical CD calculations have proven as a very efficient and reliable method[13,24] for the determination of the absolute axial configuration.

Ancistrotanzanine A (**5**) is the first and up to now only 5,3′-coupled naphthylisoquinoline alkaloid. It has been isolated in our group by M. Dreyer from East African liana *Ancistrocladus tanzaniensis* (Figure 16).[31,65b] Its constitution and its relative configuration have been determined by extensive spectroscopic and chemical investigations.

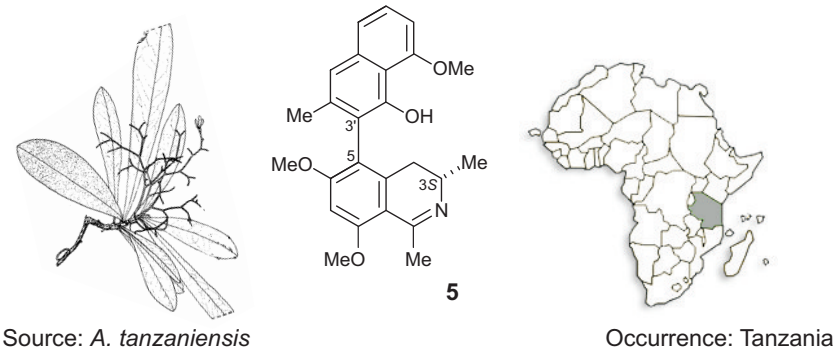

Figure 16. Structure of ancistrotanzanine A (**5**) (in the middle), its source, viz. leaves of *Ancistrocladus tanzaniensis* (on the left), collected in Tanzania in the Uzungwa mountains. The plant picture has been taken from Frimodt-Møller[160] and modified.

The absolute configuration at C-3 was determined by a ruthenium-mediated oxidative degradation procedure.[31] The stereochemical assignment of the 5,3′-coupled-biaryl axis by determining the configuration relative to the known *S*-configured center at C-3 by specific long-range NOESY interactions (Chapter 2.1) appeared impossible because of the overlap of the two diastereotopic, but largely isochronous protons at C-4. Therefore, to establish the axial configuration of ancistrotanzanine A (**5**), CD investigations were carried out. Due to a novel 5,3′-coupling type in **5**, its measured CD spectrum could not be correlated with that of any configurationally known naphthylisoquinoline alkaloid. The *Exciton Chirality Method*[84] seemed also inapplicable due to the presence of two inherently different chromophores in the molecule of **5**, which do not provide a classical CD couplet for the configurational analysis. Therefore, the experimental CD spectrum of ancistrotanzanine A (**5**) was interpreted by quantum chemical CD calculations.

The computations were arbitrarily performed for the (*M*,*S)*-atropo-diastereomer of ancistrotanzanine A (**5**). To locate all possible conformers that should contribute to the overall CD of **5**, the molecular dynamics approach was applied. For an analysis of the molecular flexibility, the MD simulations were carried out by using the MM3[149] force field at virtual temperatures of 300–1100 K in 200-K steps. Within each MD run the single trajectories were recorded for all flexible parts of the molecule, viz. for the three methoxy groups, the hydroxy function at C-4′, the 1,3-dimethyldihydro-isoquinoline ring, and for the biaryl axis (Figure 17, top). It was found that all methoxy groups and the hydroxyl revealed a high flexibility already at 300 K. Therefore, the choice of an appropriate MD run for further CD calculations was based only on the analysis of the trajectories for the axis and for the dihydroisoquinoline ring. As seen in Figure 17a, the biaryl linkage appeared rotationally stable up to 900 K, whereas the simulation at 1100 K resulted in a mixture of both atropo-diastereomers. On the other hand, a virtual temperature of 300 K seemed to be too low, since only an equatorial alignment for the methyl substituent at C-3 of the 1,3-dimethyldihydroisoquinoline ring was realized. The

remaining MD runs, corresponding to the temperatures of 500, 700, and 900 K, provided a similar conformational behavior: a significant predominance of the conformers with the methyl at C-3 in an equatorial position, and the presence of two conformational species differing in the dihedral angle at the biaryl axis, with averaged values of 60° and 120°, the latter one being more favorable. Finally, the simulation at 500 K (Figure 17b) was chosen as a basis for CD calculations, since higher temperatures lead to increasingly equal populations regarding the axis and the methoxy substituent.

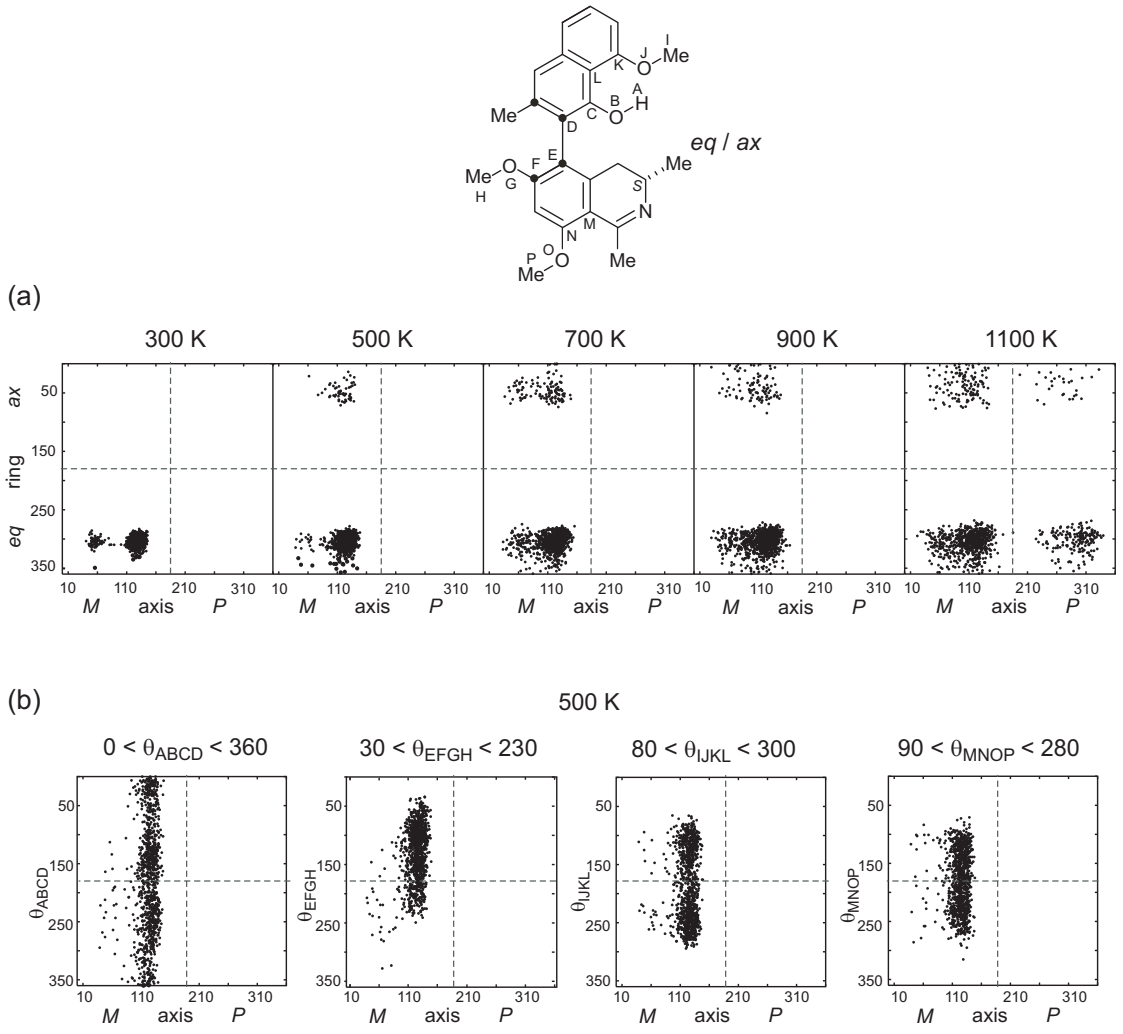

Figure 17. Definition of the dihedral angles analyzed; (a) MD trajectories recorded for the biaryl axis and the 1,3-dimethyldihydroisoquinoline ring, simulated at different virtual temperatures; (b) MD trajectories for the hydroxy and methoxy groups at 500 K.

CD and UV spectra were calculated for 1000 extracted conformers of (*M*,*S*)-**5** by using the semiempirical CNDO/S-CIS[27] method. The overall bar CD spectrum, resulting from the arithmetical averaging of the single spectra, considerably resembled the experimental CD spectrum of **5** (Figures 18a and b). Thus, a broad set of positive rotatory strengths in the range of 260–290 nm were attributed to the experimentally observed band around 310–360 nm, and the arrays of signals of the negative sign located about 250 and 230 nm were correlated to the experimental peaks at 245 and 215 nm, respectively. Two positive bands at 235 and 200 nm in the measured CD spectrum of **5** were also reproduced by the calculations (at 240 and 210 nm, respectively), although the first one was predicted with a too low intensity. For an easier comparison of the experimental and theoretical CD curves, the bar spectrum was overlayed with a Gaussian shape function by using an exponential half-width of 0.08 eV. Despite the fact that such an MD based overall bar spectrum itself covers a statistical Gaussian conformational distribution, this "additional" overlay did not misrepresent the calculated bars (Figure 18a). The signs of all calculated CD peaks were in a total agreement with the experimentally observed features, although the respective excitation energies were somewhat underestimated, particularly in a range of 180–260 nm, so that a blue-shift of approximately 10 nm was required for the UV correction.

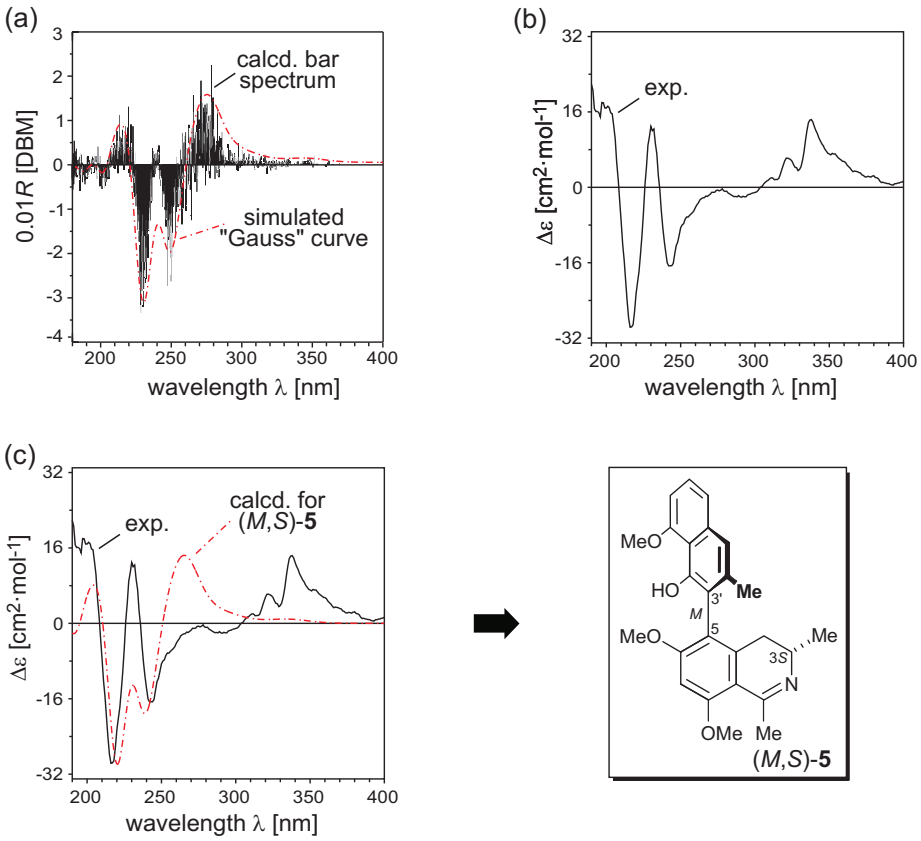

Figure 18. (a) Simulation of the "Gauss" CD curve over the MD based overall bar spectrum. (b) The measured CD spectrum of **5** in methanol. (c) Attribution of the absolute axial configuration of ancistrotanzanine A (**5**).

The final comparison of the CD curve thus simulated for the *M*,*S*-atropo-diastereomer of **5** with the CD spectrum measured in methanol showed a good agreement in a decisive region of 190–260 nm, thus allowing the attribution of the absolute axial configuration of **5** as *M*. The observed difference in the position of the first positive band between the experimental and the theoretically predicted curves might be related to errors of the CNDO/S method in describing of n-π* transitions lying in this spectral region.

The configurational assignment of ancistrotanzanine A (**5**) thus achieved was also confirmed by semiempirical CD calculations based on the BOLTZMANN method, which were performed by M. Reichert for both atropo-diastereomers of **5**, i.e., (*M*,*S*)- and (*P*,*S*)-**5**.[31,161]

4.1.2. Isoplagiochin D (6)

Another example of a successful determination of the absolute axial configuration by the molecular dynamics approach is a liverwort-produced metabolite, isoplagiochin D (**6**), which was isolated from various *Plagiochila*,[162] *Herbertus*,[163] and *Bazzania*[32] species. Structurally, isoplagiochin D (**6**) is a macrocyclic bisbibenzyl possessing two biaryl axes, which seemed at first sight configurationally unstable due to the presence of only two small *ortho*-substituents next to each axis. However, just as most isoplagiochin-like compounds, isoplagiochin D (**6**), is optically active and its atropo-enantiomers can be resolved by HPLC on a chiral phase.[32] Furthermore, for the most prominent representative of this class, namely for isoplagiochin C (**32**), extensive experimental and theoretical studies on the stereostructure and on the atropoisomerization were performed in our group by M. Dreyer, J. Mühlbacher, and M. Reichert,[24c] revealing that one of the two biaryl axes, viz. the 'northern' one, is stable at room temperature and thus determines the overall chiroptical behavior. Despite the close structural similarity of the two compounds, **6** and **32**, a direct configurational assignment of the two enantiomers of isoplagiochin D (**6**) by comparison of its CD spectra with the curves of the known isoplagiochin C (**32**) appeared difficult. Thus, the more rapidly eluting enantiomer of isoplagiochin C (**32**), which had been attributed to have the *M*-configuration, showed a classical bisignated positive CD couplet with an intersection at 225 nm (Figure 19a), whereas the CD spectrum of the faster atropo-enantiomer of isoplagiochin D (**6**) exhibited a rather complex CD behavior, revealing a first negative CE at 280 nm, followed by three positive signals at 250, 230, and 215 nm without pronounced minima, and displaying a strong negative band below 210 nm (Figure 19b). Consequently, for an independent configurational assignment of the two peaks of isoplagiochin D (**6**) to the respective enantiomers, quantum chemical CD calculations were carried out.

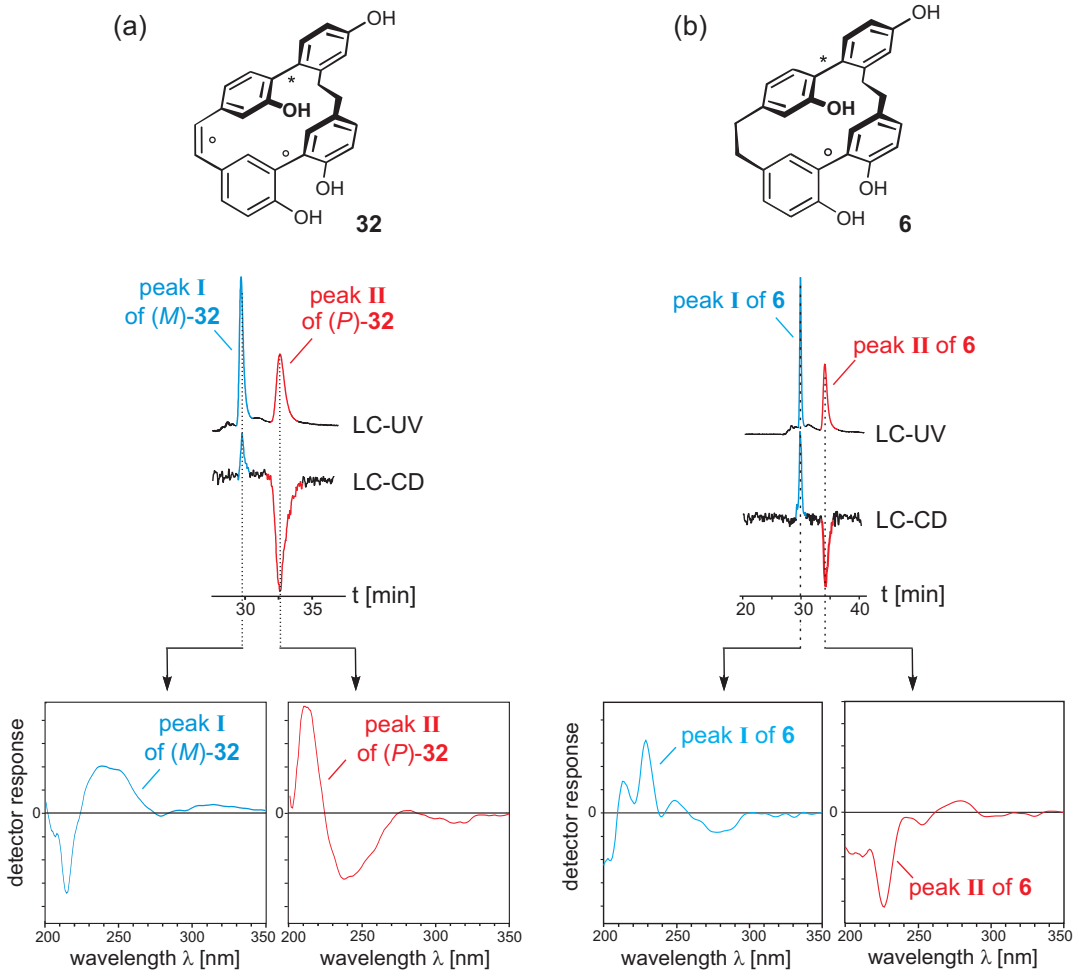

Figure 19. Isoplagiochins C (**32**) (a) and D (**6**) (b) with their LC-UV and LC-CD chromatograms and full online CD spectra of the respective enantiomers.

As had already been shown in the case of the related bisbibenzyl isoplagiochin C (**32**),[24c] the molecular dynamics approach is the most appropriate method for the investigation of the conformational behavior of such flexible molecules. Arbitrarily starting with the M_A,M_B-stereoisomer of isoplagiochin D (**6**), the molecular motion was simulated within 500 ps by means of the TRIPOS force field, applying a virtual heating in a temperature range of 500–2000 K with an interval of 100 K. To select the most appropriate MD run, the flexibilities of all hydroxy functions and of two biaryl axes were analyzed, whereas the two highly flexible ethylene bridges were not taken into consideration because of their negligible impact to the molecular chromophore. A high conformational lability of the hydroxy functions of **6** was realized already at a virtual temperature of 700 K, giving all possible orientations, so that only the

trajectories of the two axes remained important. In analogy to isoplagiochin C (**32**), the most stable axis in isoplagiochin D (**6**) is the 'upper' ('northern') one (**A**, joining C-12' and C-14), which stayed configurationally invariable over all MD simulations up to 2000 K (Figure 20), whereas the 'bottom' biaryl linkage (**B**, connecting C-2' and C-6) revealed a flexibility at 1000 K resulting in two sets of interconverting diastereomers, (M_A,M_B)-**6** and (M_A,P_B)-**6**, with averaged dihedral angles at the axis of 110° and 250° (Figure 20).

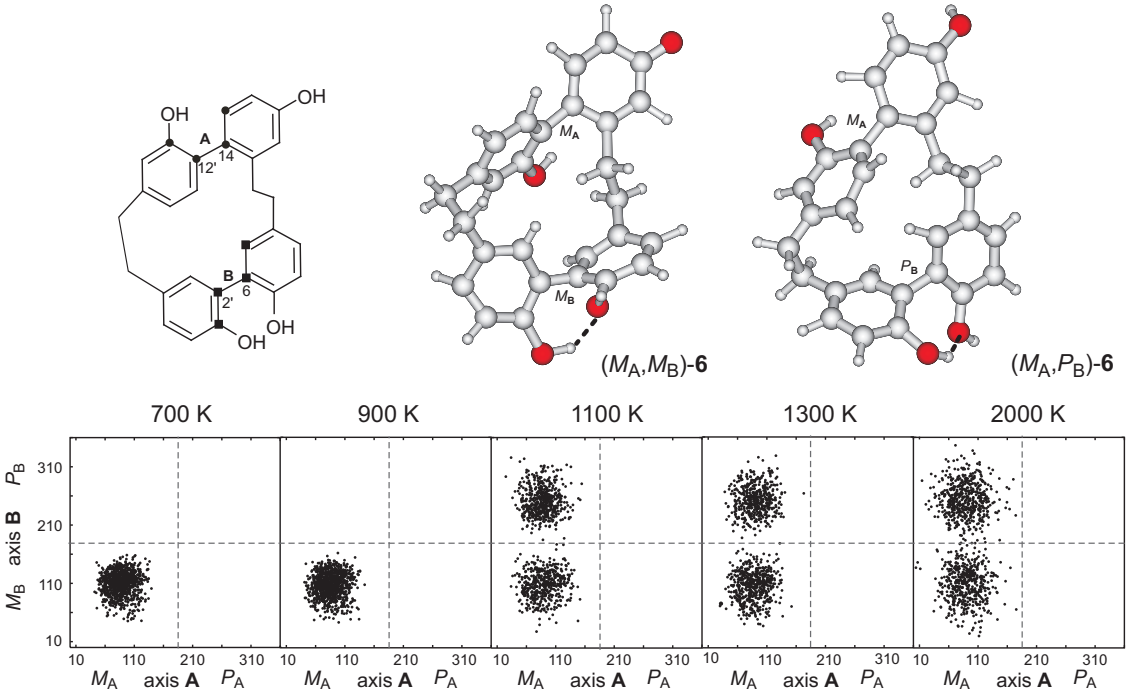

Figure 20. MD trajectories of the two biaryl axes of isoplagiochin D (**6**) simulated at different virtual temperatures, and two averaged conformers of **6** corresponding to the easily interconverting diastereomeric structures, (M_A,M_B)-**6** and (M_A,P_B)-**6**.

CD computations were performed for 1000 structures collected from the MD run at 1300 K, which seemed to correspond to the real situation at ambient temperature. The single CD and UV spectra for each of the conformer of **6** were calculated at the CNDO/S level, taking into account 784 singly occupied configurations. The resulting arithmetically averaged spectra of (M_A)- and (P_A)-**6** were correlated with the experimental data. UV comparison revealed only a small blue-shift of 9 nm, which was subsequently applied to the CD spectra.

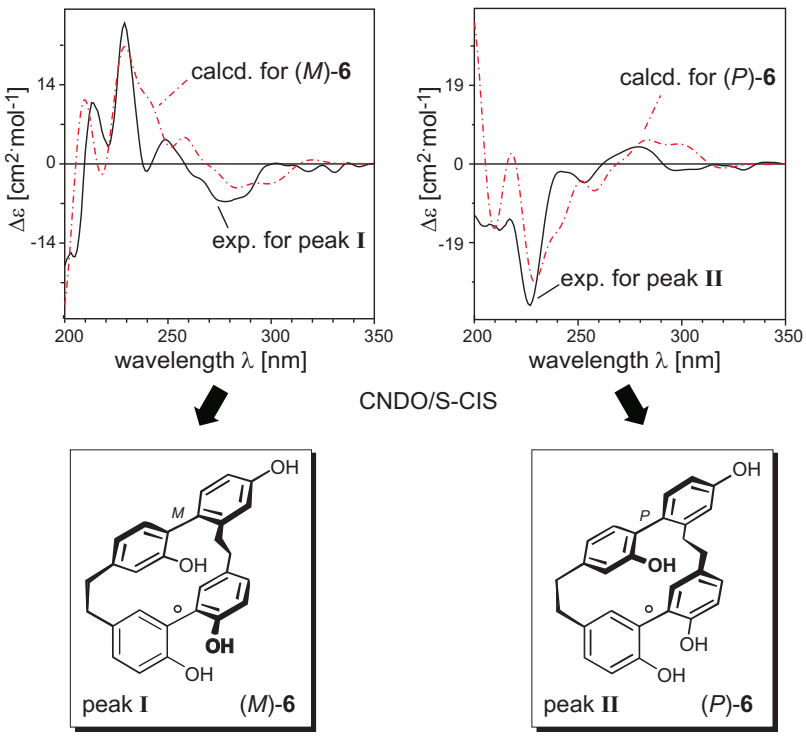

Figure 21. Assignment of the absolute configuration of isoplagiochin D (**6**) by comparison of the theoretical MD-based CD spectra calculated for both (*M*)- and (*P*)-**6** with the experimental online curves.

As seen in Figure 21, the CD spectrum calculated for the M_A-configured stable axis of **6** matches very well with the experimental curve of the first eluting peak **I**, accurately reproducing all CD features, while the experimental CD curve of the second peak **II** is in a good agreement with the spectrum predicted for P_A, clearly indicating peak **I** to correspond to (*M*)-**6** and peak **II** to (*P*)-**6** (Figure 21).[32] Thus, it was proven that although the CD pattern of the closely related isoplagiochins C (**32**) and D (**6**) are substantially different, their HPLC behavior–absolute configuration relations remain identical, i.e., the more rapidly eluting peak correlates with the *M*-enantiomer and the more slowly eluting one is *P*-configured. This stereochemical correlation was furthermore confirmed experimentally by hydrogenolysis of enantiopure samples of (*M*)- and (*P*)-**32** to give (*M*)- and (*P*)-**6**, respectively.[32]

4.1.3. The biaryl amide 7

Biaryls are fascinating building blocks in many kinds of organic systems: compounds of biological significance, such as pharmaceuticals,[164] herbicides,[165] and natural products,[166] as well as engineering materials, such as conducting polymers, molecular wires,[167] and liquid crystals.[168] Moreover, they display unique properties as chiral elements in supramolecular chemistry[169] and enantioselective catalysis.[170] The importance of these compounds has stimulated great interest to their directed, stereospecific synthesis. Among different methods for constructing configurationally stable biaryl axes,[171] the "lactone" method,[172] developed in our group, has proven to be particularly effective, as regarding the chemical yields and the enantiomeric purities of the products. A key step of this method is the atropo-diastereoselective cleavage of the configurationally unstable biaryl lactone **32** by using for example chiral *N*- or *O*-nucleophiles to give rotationally hindered biaryls with given axial chirality (Figure 22). Configurational attribution of the obtained products can be rapidly achieved by means of CD calculations, as these can be performed with computationally inexpensive semiempirical methods, which usually provide reasonably accurate results for such biaryl systems.[13,24] Thus, the absolute configuration of the axially chiral biaryl amide **7**, obtained from the stereoselective amidolysis of lactone **33** with L-valine methyl ester (**34**) (Figure 22), was unambiguously determined by using the CNDO/S-CIS method without the necessity of an implication of higher-level computations.[33]

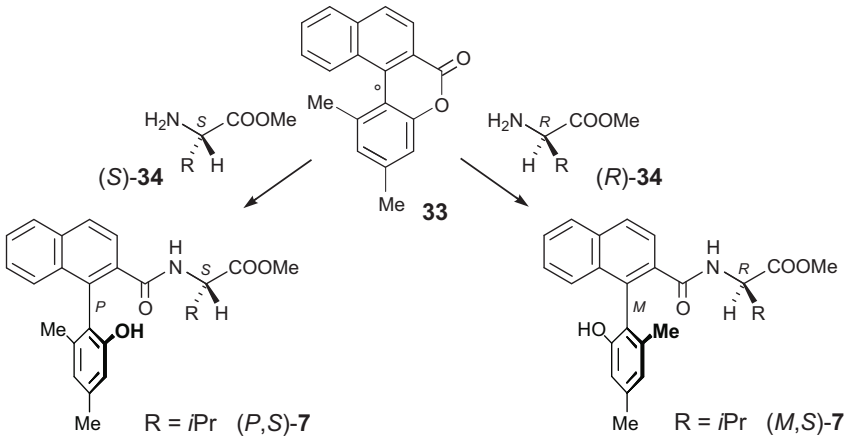

Figure 22. Method of stereoselective synthesis of axially chiral biaryl systems, such as **7**, by atropo-diastereoselective ring cleavage of configurationally unstable lactone-bridged biaryl **33** with amino acid ester like **34**.

The measured CD spectra of the two synthesized atropo-diastereomers of **7** showed an almost opposite, nearly enantiomer-like behavior, hinting at a dominating influence of the axial chirality on the CD spectrum of **7** in comparison to the stereogenic center. In order to prove this prevailing role of the biaryl chromophore, theoretical stereochemical investigations were carried out for both atropo-diastereomers, (*P*,*S*)-**7** and (*M*,*S*)-**7**, independently.

The conformational space of biaryl amide **7** is spanned by five internal coordinates: one characterizing the flexibility of the hydroxy function at C-2′ (θ_{ABCD}) and four corresponding to the amide rest at C-2 (θ_{EFGH}, θ_{IJKL}, θ_{MNOP}, θ_{QRST}; Table 1). The dihedral angle at the stereogenic axis varied from 92° to 103° in case of the *M*,*S*-diastereomer of **7** and adopted values from -76 to -102° for the *P*,*S*-configured isomer, as calculated by the AM1 method. Screening of the reaction coordinate for the rotation around the C-O bond of the ester group, i.e., θ_{QRST}, showed a preference of the *s-trans* conformation over *s-cis* by 6.7 kcal·mol^{-1} for both diastereomers (Table 1). One favorable orientation was also found for the N-C_{sp3} bond, i.e., θ_{MNOP}, which provided a maximal distance between the two carbonyl groups (COULOMB repulsion) and the adopted values of -114° for (*M*,*S*)- and -105° for (*P*,*S*)-**7**. The AM1-based analysis of the remaining coordinates resulted in seven minimum conformers within

an energetic range of 3 kcal·mol^{-1} above the global minimum for the *P*-atropisomer of **7**, while in the case of the *M*-diastereomer, only five geometries besides the global minimum were located (Table 1). For both stereostructures, the global minimum conformers, (*P*,*S*)-**7**$_{conf1}$ and (*M*,*S*)-**7**$_{conf1}$, showed strong hydrogen bonds ($d_{O\text{-}H}$ 2.0 Å) between the amide proton and the oxygen atom of the hydroxy function (Table 1).

Table 1. Definition of the reaction coordinates calculated for biaryl amide **7** and the AM1 optimized conformers of two atropo-diastereomeric structures, (*P*,*S*)- and (*M*,*S*)-**7**, with their relative energies and characteristic dihedral angles, and the respective global minimum conformers.

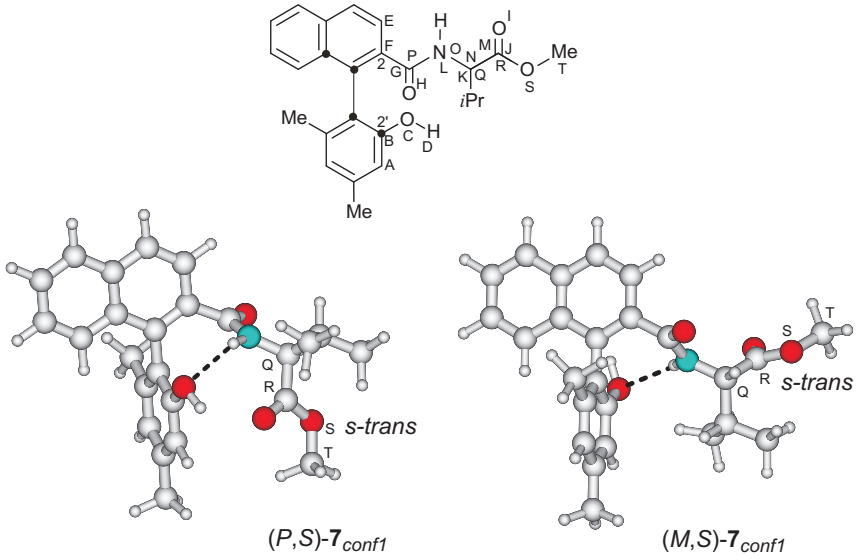

Conformer	ΔΔH*f* [kcal·mol^{-1}]	axis [°]	θ_{ABCD} [°]	θ_{EFGH} [°]	θ_{IJKL} [°]
(*P*,*S*)-**7**$_{conf1}$	0.00	-102	-163	-79	-34
(*P*,*S*)-**7**$_{conf2}$	0.76	-102	-29	100	-43
(*P*,*S*)-**7**$_{conf3}$	1.08	-94	-6	53	-43
(*P*,*S*)-**7**$_{conf4}$	1.34	-102	-29	99	139
(*P*,*S*)-**7**$_{conf5}$	1.61	-87	20	-52	-50
(*P*,*S*)-**7**$_{conf6}$	1.67	-94	-6	52	142
(*P*,*S*)-**7**$_{conf7}$	1.96	-101	-162	-77	145
(*P*,*S*)-**7**$_{conf8}$	2.18	-76	15	-62	136

Conformer	$\Delta\Delta Hf$ [kcal·mol^{-1}]	axis [°]	θ_{ABCD} [°]	θ_{EFGH} [°]	θ_{IJKL} [°]
(*M*,*S*)-**7**$_{conf1}$	0.00	92	162	63	-42
(*M*,*S*)-**7**$_{conf2}$	0.46	92	162	62	142
(*M*,*S*)-**7**$_{conf3}$	0.53	102	-152	-102	-40
(*M*,*S*)-**7**$_{conf4}$	1.10	94	6	64	-46
(*M*,*S*)-**7**$_{conf5}$	1.11	103	-152	-103	145
(*M*,*S*)-**7**$_{conf6}$	1.62	93	7	64	140

The single CD and UV spectra for each conformer of **7** were semiempirically calculated using the CNDO/S-CIS approach and then added up according to the BOLTZMANN statistics, as based on the AM1 energies, to give the overall CD and UV curves for (*P*,*S*)- and (*M*,*S*)-**7**. The comparison of the measured UV spectrum with the spectra predicted for the two atropo-diastereomers revealed that the calculated transition energies were somewhat underestimated, particularly those that correspond to the first UV band at 285 nm, and thus, the theoretical UV and CD spectra were blue-shifted by 10 nm. The resulting overall CD spectrum predicted for (*P*,*S*)-**7** showed a weak negative CD signal around 285 nm, followed by an exciton CD splitting with the first positive CE at 225 nm and the second negative one at 205 nm arising from the dipole-dipole interaction between the naphthylamide and benzene chromophores, which matched very well with the CD curve measured for the main cleavage product. The experimental CD spectrum of the minor product showed a good agreement with the curve calculated for (*M*,*S*)-**7** (Figure 23). The fact that the theoretical CD spectra predicted for two atropo-diastereomers of **7** were entirely opposite as would be expected for atropo-enantiomers, confirmed the aforementioned dominating influence of the axial chirality, and hence of the biaryl chromophore, on the CD spectrum of **7** and the relatively negligible effect of the amide substituent. The configurational assignments thus obtained by the semiempirical CNDO/S CD computations were furthermore corroborated by X-ray crystallographic experiments and by chemical transformations.[33]

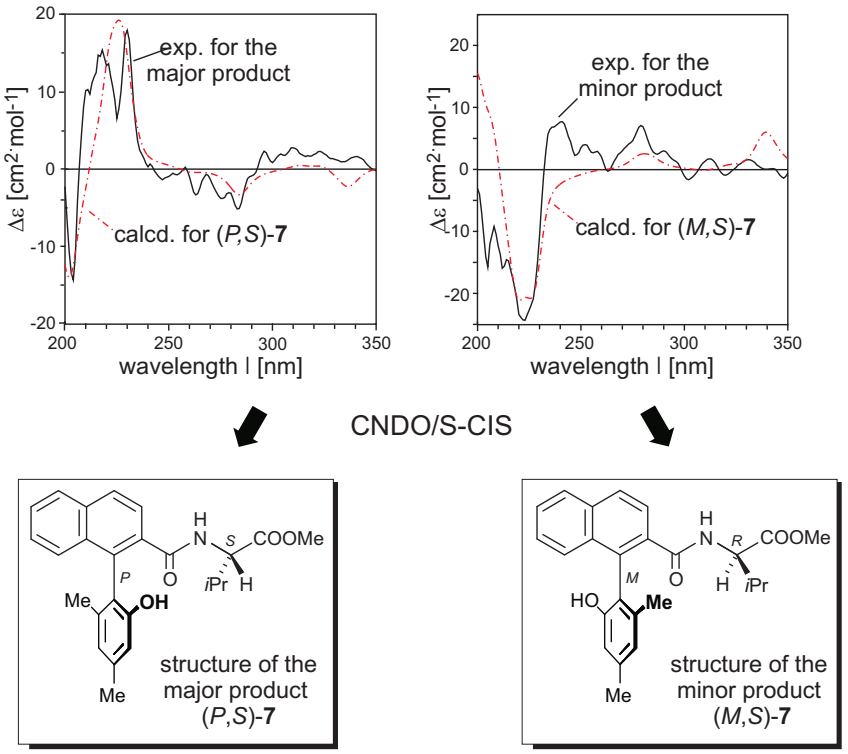

Figure 23. Assignment of the absolute axial configuration of the major and minor ring cleavage products **7** by means of CNDO/S-based CD calculations.

4.1.4. The bi[10]paracyclophane 8

Another interesting biaryl, or more exactly biphenyl, whose absolute axial configuration was elucidated by semiempirical CD calculations, is the bi[10]paracyclophane **8** (Figure 24a), synthesized by Prof. Tochtermann and co-workers from the University of Kiel.[34] This compound is remarkable from a stereochemical point of view: possessing two constitutionally identical, but oppositely configured planar-chiral paracyclophane portions, its biaryl axis with only two medium-sized *ortho*-substituents (the alkylidene chains) is configurationally semi-stable, which made bi[10]paracyclophane **8** to be a borderline case between an achiral *meso*-configured molecule (with the central C,C-bond rotating) and a chiral, C_1-symmetric compound (with discrete, separable atropo-enantiomers). Indeed, the separation of the two atropo-enantiomers at room temperature was most

unsatisfactory, making it necessary to perform the resolution at lower temperature (5 °C) (Figure 24a).[34] The stereochemical attribution of the two peaks of **8** was achieved by direct CD correlation with the known configurationally stable bi[10]paracyclophane **35**, whose absolute configuration had previously been investigated by J. Kraus in our group.[173] Interesting was the fact that the HPLC behavior of these two structurally very similar compounds was inverse, viz. the enantiomer with the positive CD couplet, which was the faster peak in the case of **35**, now eluted as the second peak (Figure 24). Thus, for a robust configurational assignment of the two atropo-enantiomers of bi[10]paracyclophane **8**, quantum chemical CD calculations were performed.

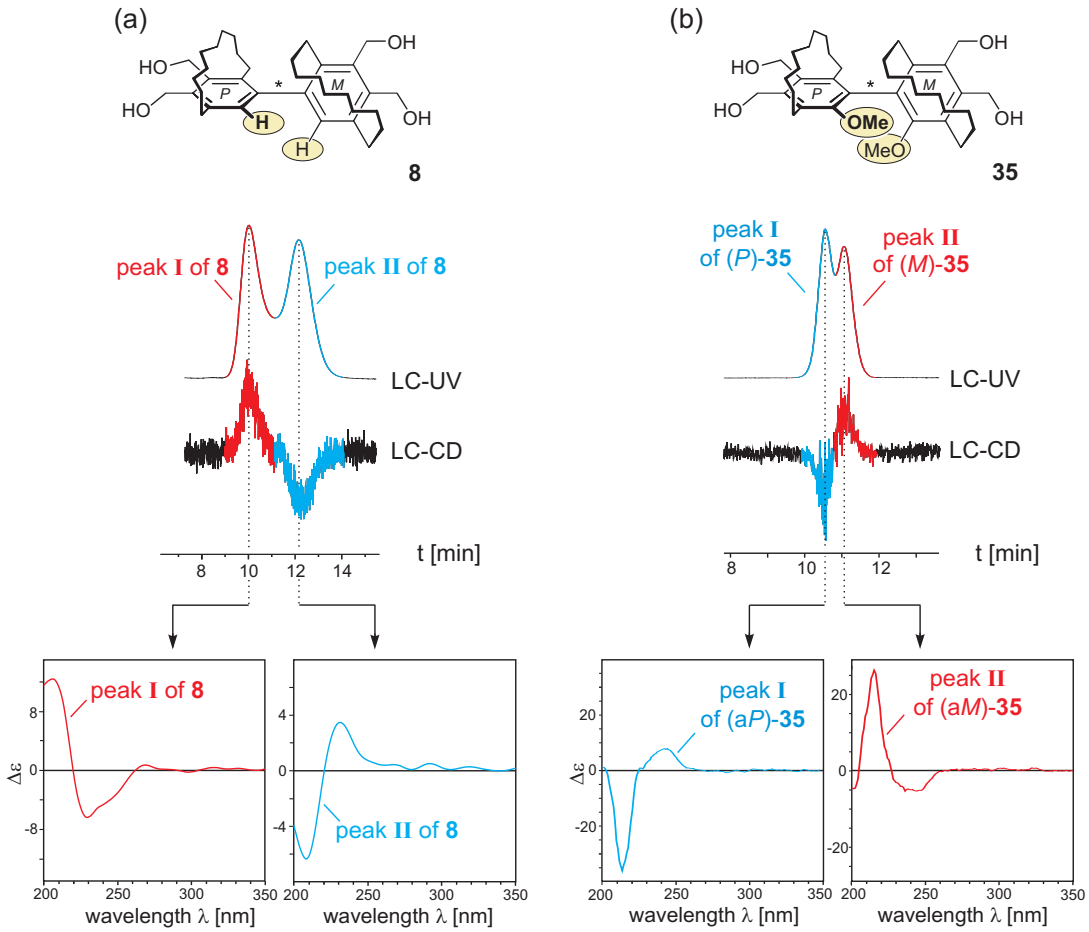

Figure 24. Structures of bi[10]paracyclophanes, **8** and **35**, and their enantiomeric resolution by HPLC on a chiral reversed phase, as well as the online CD spectra of the respective atropo-enantiomers.

In view of the high flexibility of **8**, its conformational behavior was first analyzed by means of the MD approach, which was done starting with the p*P*,a*P*,p*M*-enantiomer. MD simulations were carried out at different temperatures (from 200 K to 800 K) by using the TRIPOS force field to imitate the conformational changes of the hydroxymethyl substituents and the alkylidene bridges, while avoiding the rotation of the biaryl axis to the other respective atropo-enantiomer. The subsequent CNDO/S CD calculations for thus produced structures provided the overall CD spectrum that was, strikingly, in contradiction to the results earlier obtained for bi[10]paracyclophane **35**, and which also disagreed with the expectations from the *Exciton Chirality* theory, i.e., that the a*P*-configured biphenyl should give a positive CD couplet around 220 nm due to the dipole-dipole interactions between the ^1B_b transitions of the substituted benzene chromophores.[174]

When looking more closely at the MD-simulated conformers of **8**, it was found that the two phenyl rings, which actually constitute the chromophore, were not entirely planar, which might cause an error in the exited states calculations. To confirm this assumption, one arbitrarily chosen TRIPOS FF-based conformer of **8** was further optimized at the AM1 level, thus improving the geometries of the phenyl rings, and then again submitted to the CNDO/S CD calculations. As a result, only a minor change was observed for the stereogenic biaryl axis (dihedral angle altered from 98.1 to 99.0), while the CD spectra of the initial MD derived structure and the AM1 optimized one were substantially different (Figure 25), showing the expected first positive and second negative COTTON effects in the case of the better optimized geometry.

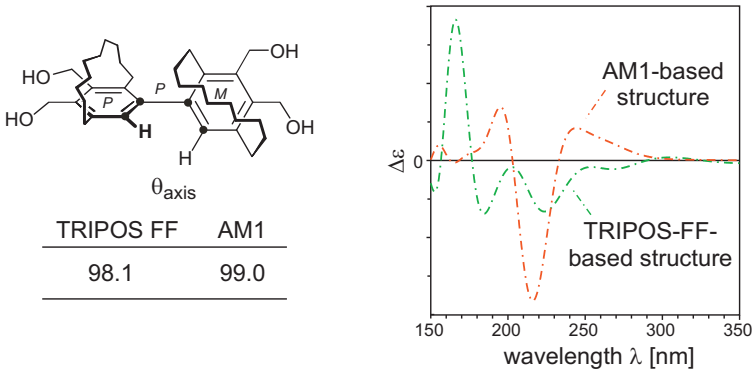

Figure 25. Comparison of the CD spectra calculated (CNDO/S) for the MD simulated structure of (a*P*)-**8** and the respective AM1 optimized one.

Consequently, to obtain better optimized conformers, bi[10]paracyclophane **8** was subjected to the standard conformational analysis using the AM1 method. Assuming that the highly flexible -CH_2- bridges do not have a significant influence on the overall CD spectrum, the analysis of the conformational space was concentrated on the hydroxymethyl substituents (θ_{ABCD} – $\theta_{E'F'G'H'}$), which revealed strong hydrogen bondings (*d*H–O ca. 2.15 Å) to each other in the global minimum conformer (Figure 26). The oxygen atoms were preferably located above or below the plane of the corresponding phenyl rings. For the biaryl axis, the dihedral angle varied from 94 to 104°, demonstrating a higher flexibility as compared to the related bi[10]paracyclophane **35** (in **35**: from 88 to 94°).[173]

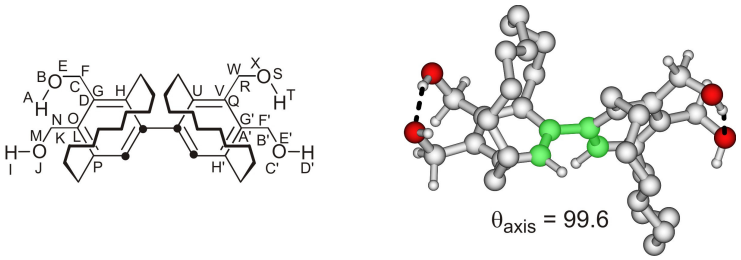

Figure 26. The reaction coordinates analyzed for bi[10]paracyclophane **8** (left), and the global minimum conformer, as found by the AM1 method (right).

Finally, 240 structures were located within an energetic cut-off of 3 kcal·mol^{-1}, for which the single CD and UV spectra were computed again using the CNDO/S method (with a CI expansion including 784 singly occupied configurations), and then added up in the BOLTZMANN-weighted manner to give overall curves for the

(p*P*,a*P*,p*M*)-enantiomer of **8**. Comparison of the resulting theoretical UV spectrum with the measured curve revealed that the excitation energies were calculated with a reasonable accuracy, so that no UV correction was required. Due to the symmetric constitution of **8**, reflection of the spectrum of (p*P*,a*P*,p*M*)-**8** at the zero line (λ) produced the CD curve for the (p*P*,a*M*,p*M*)-enantiomer of **8**. The comparison of the CD spectra thus predicted with the online measured ones allowed the attribution of the absolute configuration of the two atropo-enantiomers. As can be seen in Figure 27, the spectrum predicted for the p*P*,a*M*,p*M*-enantiomer of **8** closely reproduced the negative CD couplet observed in the experimental CD curve of the more rapidly eluting peak **I**, while the one calculated for (p*P*,a*P*,p*M*)-**8** matched well with the slower peak **II**, thus, permitting assignment of the peak **I** to correspond to (p*P*,a*M*,p*M*)-**8** and peak **II** to (p*P*,a*P*,p*M*)-**8** (Figure 27).

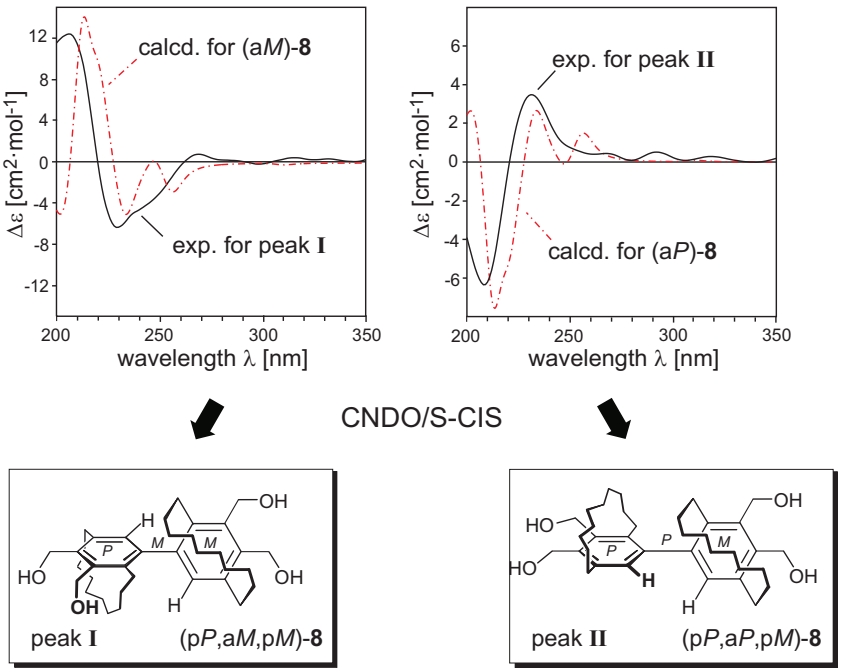

Figure 27. Assignment of the absolute configuration of the two atropo-enantiomers of **8** by comparison of the CNDO/S calculated CD spectra with the online measured ones.

Consequently, these semiempirically calculated results unambiguously confirmed that two bi[10]paracyclophanes, **8** and **35**, despite their close structural similarity, indeed exhibit an inverse HPLC behavior.

4.1.5. Sorbicillactone B (9)

While all previous examples of the beneficial application of the semiempirical CNDO/S-CIS approach for the attribution of the absolute configuration were axially chiral biaryls with the extended aromatic π-systems, compounds closing this chapter are the centrally chiral sorbicillactone B (**9**) and the benz[e]indole derivative **10** (Chapter 4.1.6), which possess substantially different structural and chromophoric frameworks.

Sorbicillactone B (**9**) and the closely related sorbicillactone A (**36**), which differ only in having or lacking a C-2′–C-3′ double bond in the sorbyl side chain (Figure 28), are the first members of a novel class of sorbicillin-derived alkaloids, which have been isolated by G. Lang and T. Gulder from a strain of *Penicillium chrysogenum* derived from the Mediterranean sponge *Ircinia fasciculata*.[35] Compound **36** has shown to exhibit highly selective antileukemic[35] activities and also antiviral and neuroprotective properties,[35] which made sorbicillactone A (**36**) to be a potential novel drug candidate, while 2′,3′-dihydrogenated sorbicillactone B (**9**) was found to be substantially less active (by a factor of 10), despite their almost identical molecular structure. The constitutions and relative configurations of these alkaloids were determined by various NMR experiments and further confirmed by X-ray structure analysis. An ascertained *cis*-array of H-6 and two methyl groups at C-5 and C-9 indicated only two possible absolute stereostructures for **9** and **36**, viz. 5*S*,6*R*,9*S* or 5*R*,6*S*,9*R* (Figure 28, bottom).

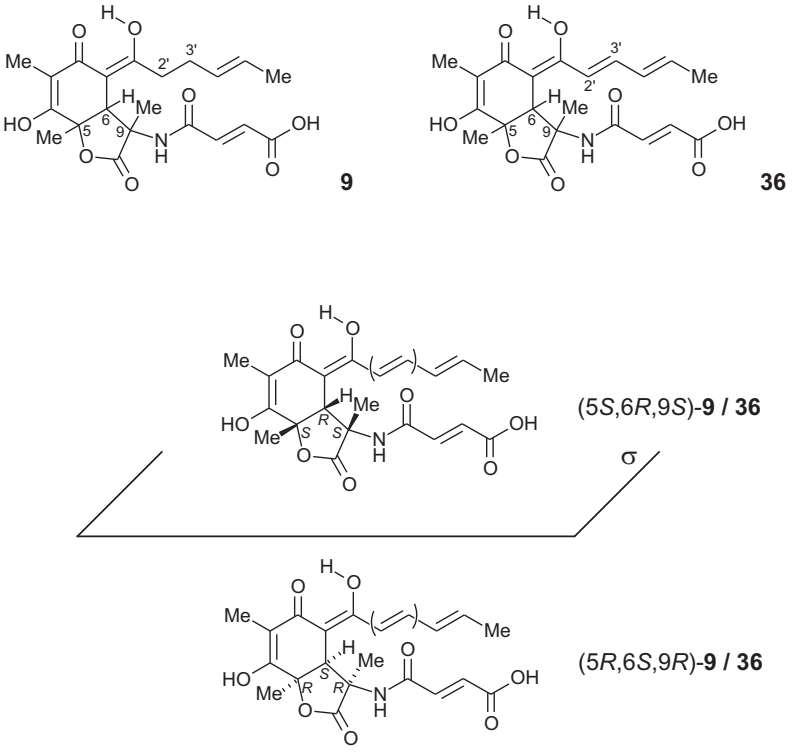

Figure 28. Sorbicillactones A (**36**) and B (**9**), and their possible absolute stereostructures.

The elucidation of the absolute configuration of sorbicillactone A (**36**) had already been done by J. Mühlbacher by applying the molecular dynamics approach.[69] For a further solid confirmation of the configurational assignment of these novel-type bicyclic lactones, independent stereochemical investigations of the 2′,3′-dihydro derivative sorbicillactone B (**9**) were performed by both, MD and BOLTZMANN methods. Taking into account the previous experience with the MD approach, which gave improper geometries for bi[10]paracyclophane **8**, the application of the more tedious conformational analysis in the case of such highly flexible compound as **9** seemed justified.

To describe the conformational diversity of the randomly chosen 5*S*,6*R*,9*S*-enantiomer of sorbicillactone B (**9**), eight internal coordinates (θ_{ABCD}-$\theta_{E'F'G'H'}$, Figure 29) were necessary. According to the AM1 calculations, the hydroxy function at C-1′ showed only one preferable orientation with a strong hydrogen bond to the adjacent carbonyl function ($d_{O\text{-}H}$ 1.98 Å), whereas the one at C-4 adopted two possible alignments, one of which was also characterized by hydrogen bond formation ($d_{O\text{-}H}$

2.23 Å) with the oxygen of the lactone ring. In analogy to the biaryl amide **7**, for the carbonyl group of **9** (i.e., $\theta_{E'F'G'H'}$, Figure 29), the *s-trans* conformation was found to be more favorable than the respective *s-cis* array, by ca. 6 kcal·mol^{-1}. The combinations of all possible orientations for the two flexible residues, the sorbyl and the fumaryl side chains, and subsequent elimination of the structures with relative energies higher than 3 kcal·mol^{-1} as compared to the global minimum conformer (**9**$_{conf1}$, Figure 29), finally resulted in 118 AM1 optimized geometries.

The TRIPOS force field based MD simulations for **9** were carried out at three different temperatures (400, 500, and 600 K). As the preliminarily performed conformational analysis provided the information about the possible conformational preferences of all flexible parts of the molecule, the choice of the most suitable MD run for CD calculations now was much easier. Thus, comparison of the MD trajectories for the eight aforementioned internal coordinates revealed that the structures simulated at 600 K mostly resembled the AM1 optimized ones, and therefore these were taken for further excited-states energy calculations.

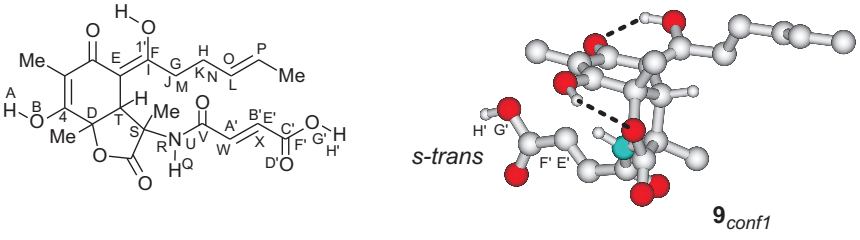

9$_{conf1}$

θ_{ABCD} [°]	θ_{EFGH} [°]	θ_{IJKL} [°]	θ_{MNOP} [°]
-15	-82	178	-135

θ_{QRST} [°]	θ_{UVWX} [°]	$\theta_{A'B'C'D'}$ [°]	$\theta_{E'F'G'H'}$ [°]
-44	49	-1	179

Figure 29. Internal coordinates defining the conformational behavior of sorbicillactone B (**9**), and the AM1 predicted global minimum structure of **9** with its characteristic dihedral angles.

All CD computations were performed at the CNDO/S level. The single UV and CD spectra calculated for 118 AM1-based conformers were added up according to the BOLTZMANN statistics, while those predicted for the MD simulated structures were arithmetically averaged to provide overall curves for (5*S*,6*R*,9*S*)-**9**. According to the comparison of the experimental UV data of **9** with the predicted UV curves, the CNDO/S calculated transition energies were substantially overestimated, and therefore, the resulting overall theoretical UV and CD spectra had to be red-shifted by 20 nm (BM) and 25 nm (MD). The experimental CD spectrum of **9** is rather complex, exhibiting five highly pronounced CD bands, three with a negative sign (330, 250, and 195 nm) and two with positive COTTON effects centered at 270 and 220 nm. For both methods (Figure 30a/b), the theoretical CD spectrum calculated for the 5*S*,6*R*,9*S*-enantiomer of **9** reasonably reproduced all experimental features, although the intensity of the second positive CD band around 270 nm was somewhat underestimated. The specularly reflected CD spectrum, corresponding to the 5*R*,6*S*,9*R*-enantiomer, consequently showed an opposite behavior as compared to the measured curve of **9** (Figure 30), clearly indicating that natural sorbicillactone B (**9**) has the 5*S*,6*R*,9*S*-configuration.[35]

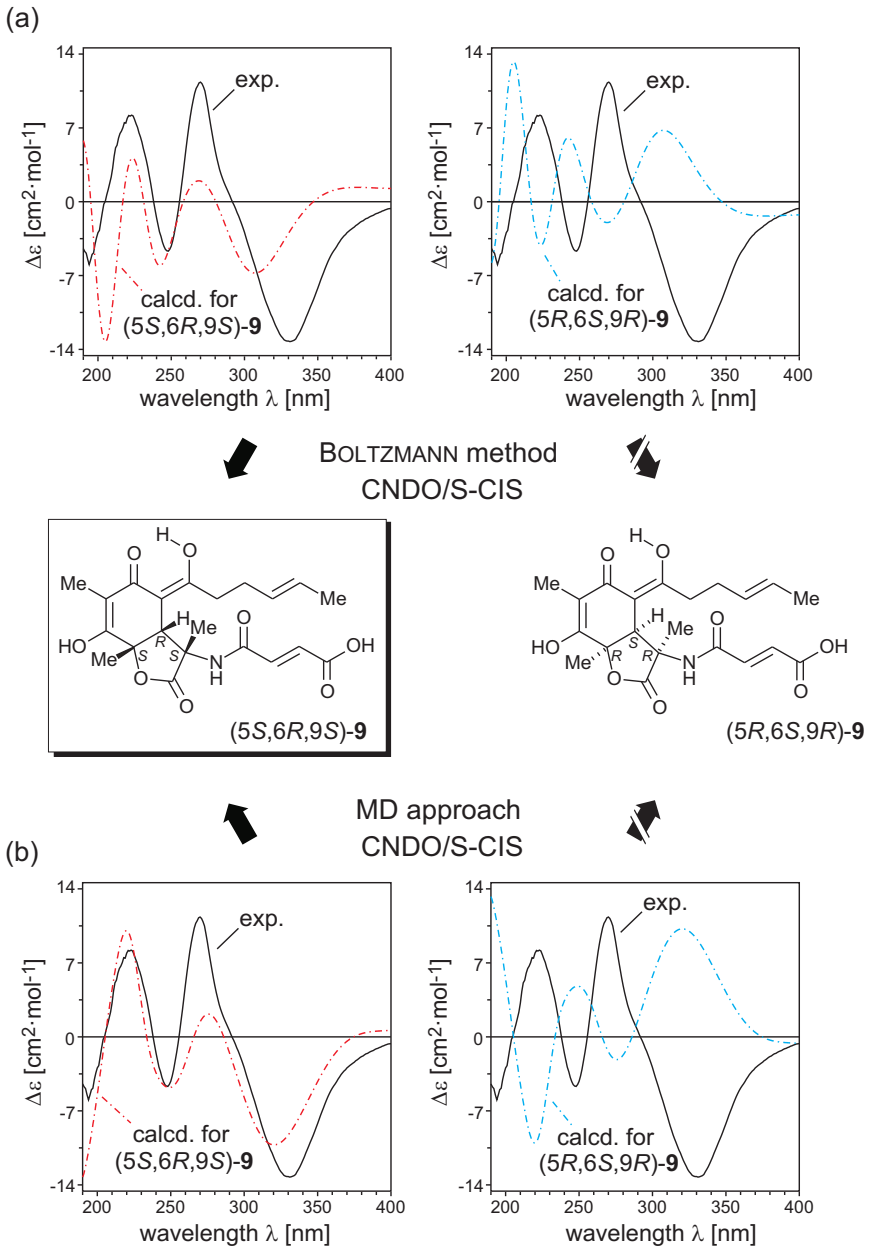

Figure 30. Determination of the absolute configuration of sorbicillactone B (**9**) by the semiempirical CNDO/S CD calculations based on the BOLTZMANN approach (a) and the MD method (b).

4.1.6. The benz[e]indole derivative 10

In the group of Prof. L. F. Tietze (University of Göttingen), who is dealing with the design and synthesis of novel cytotoxic compounds and vaccines for the selective treatment of cancer, a new type of prodrugs (like **36**, Figure 31a) for an antibody-

directed enzyme prodrug therapy (ADEPT)[175] has been developed.[36] These new compounds, bearing a 1,2-dihydro benz[e]indole core and a 2′-chloroethyl substituent as a precursor for a spirocyclopropane moiety, which is a pharmacophoric group in the most potent antitumor agents CC-1065 and duocarmycins,[176] have been proven to be superior to all other compounds known so far for the use in ADEPT.[36] A key intermediate in the synthesis of these drug predecessors is the benz[e]indole derivative **10**, containing two stereogenic centers (Figure 31a), whose absolute configurations appear critical for the biological activities. Thus, compounds with a *syn*-orientation of the two hydrogens at C-1 and C-10, viz. with 1*S*,10*S*- or 1*R*,10*R*-configurations (Figure 31b), are not suitable for the development of prodrugs due to a rather low cytotoxicity (with respect to the cancer cells) of the corresponding drugs, whereas compounds with the *anti*-orientation, i.e., 1*S*,10*R*- or 1*R*,10*S*-configured substrates (Figure 31b), show appropriate properties.[177] The *syn*- and *anti*-diastereomers could be easily separated by chromatography on silica gel, so that our task was to distinguish between the two *anti*-enantiomers of **10** [viz. between (1*S*,10*R*)-**10** and (1*R*,10*S*)-**10**] by prediction of the respective theoretical CD spectra and comparison with the experimental curves.

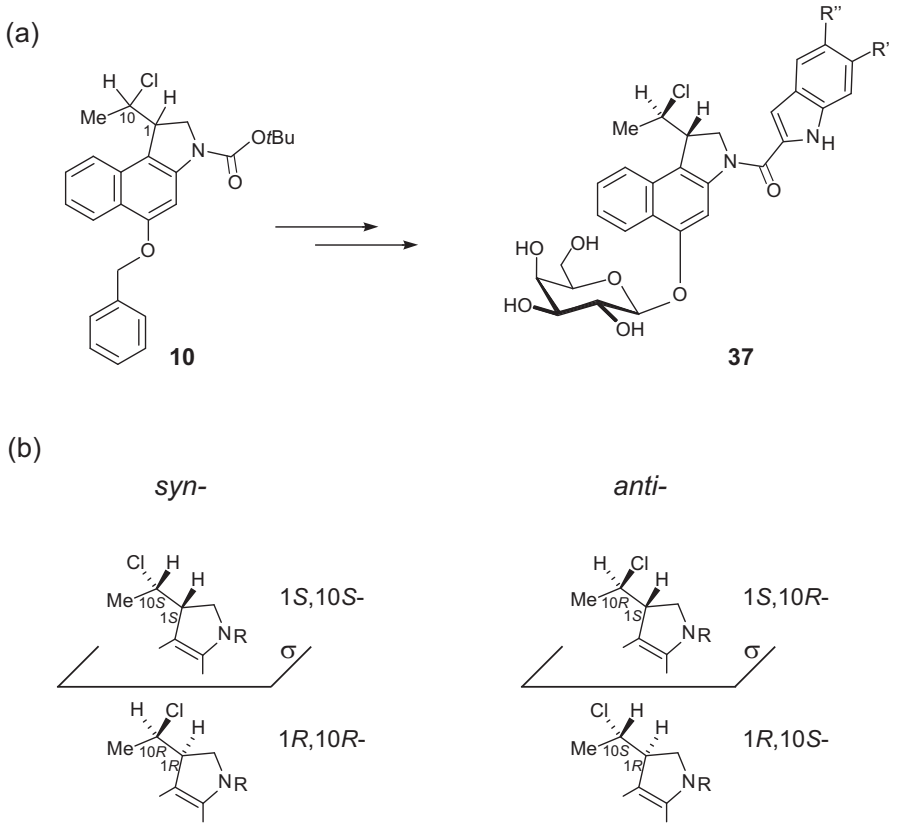

Figure 31. The centrally chiral benz[e]indole derivative **10** as a key intermediate in the synthesis of novel type antitumor prodrugs (such as **37**) (a), and four possible stereostructures with *syn*- and *anti*-orientation for the two hydrogens at C-1 and C-10 of **10**.

To consider all possible conformational species that may influence the overall CD behavior of **10**, again both approaches, viz. the BOLTZMANN method and the MD simulations, were applied. The calculations were arbitrarily started with the (1*S*,10*R*)-enantiomer of **10**. The conformational analysis was performed at the semiempirical AM1 level, taking into account six characteristic internal coordinates shown in Table 2, which finally revealed the existence of 15 conformers with energies not higher than 3.2 kcal·mol^{-1} above the global minimum **10**$_{conf1}$ (Table 2).

Table 2. Reaction coordinates analyzed for the benz[e]indole **10**, and the results of the AM1 based conformational analysis of (1*S*,10*R*)-**10**; a set of 16 low-energy conformers, with their relative energies and characteristic dihedral angles, and the global minimum conformer.

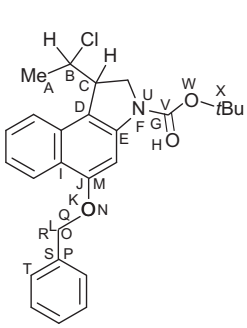

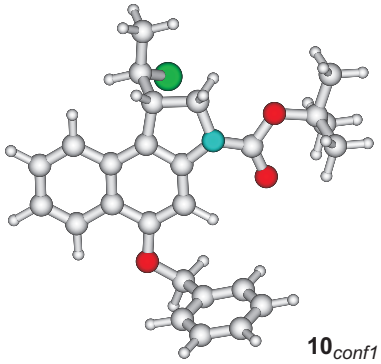

Conformer	$\Delta\Delta H_f$ [kcal·mol^{-1}]	θ_{ABCD} [°]	θ_{EFGH} [°]	θ_{IJKL} [°]	θ_{MNOP} [°]	θ_{QRST} [°]
10$_{conf1}$	0.00	172	-22	171	82	49
10$_{conf2}$	0.56	172	-23	177	-177	25
10$_{con3}$	1.00	172	159	172	83	28
10$_{conf4}$	1.44	172	160	-179	-178	30
10$_{conf5}$	1.48	172	160	178	-179	-28
10$_{conf6}$	1.72	-16	-21	172	81	50
10$_{conf7}$	2.23	-16	-21	-179	179	-23
10$_{conf8}$	2.25	-16	-21	179	-178	24
10$_{conf9}$	2.28	-164	-22	171	82	50
10$_{conf10}$	2.37	172	-23	80	83	31
10$_{conf11}$	2.68	-15	158	174	82	25
10$_{conf12}$	2.78	173	158	76	87	36
10$_{conf13}$	2.86	-164	-23	177	-177	-25
10$_{conf14}$	3.12	-15	158	-177	180	30
10$_{conf15}$	3.13	-15	159	-178	179	-29
10$_{conf16}$	3.20	-163	160	172	84	24

Since halogen atoms are not parametrized within the semiempirical CNDO/S and OM2 methods, the chlorine atom in **10** had to be replaced by other appropriate groups. On the one hand an ethyl group as the closest no lone-pair electrons containing substituent and on the other hand a hydroxy group, which does possess

an electron pair, were chosen. Based on the geometries found during the conformational analysis, the chlorine atom was replaced by an ethyl substituent (to give structure **10a**) and, in a second approach, by a hydroxy group (*i.e.*, structure **10b**). Assuming that the flexibility of the 2′-substituted ethyl moiety of **10** will not be largely affected by such a replacement, for a matter of simplification, the MD simulations were directly started with the modified structures **10a** and **10b**. The calculations were carried out with the TRIPOS force field within a temperature interval of 300–900 K in 200-K steps. Comparison of the MD trajectories, recorded for the rotation of each of the flexible part of the molecule, with the respective AM1-based reaction coordinates indicated that the MD simulation at 500 K provided the most realistic conformational behavior and thus appeared to be the most suitable for further CD computations, which were performed at the semiempirical CNDO/S level. For the 16 conformers obtained from the conformational analysis, CD calculations were performed by the CNDO/S approach, and furthermore, by the OM2 method.

An analysis of the structure–spectrum relationships revealed that for compound **10**, with its two well-separated, independent chromophoric units, viz. the benz[e]indole and benzene portions, the mutual orientation of these aromatic π-systems has a dramatic influence on the CD spectrum. Thus, despite their identical absolute configuration, those two single conformers (**A** and **B**, Figure 32) that differed only in the position of the "freely" rotating phenyl ring, provided almost opposite CD spectra. Consequently, this allowed us to expect that the molecular dynamics simulated conformational picture should more closely correspond to the real situation in solution and therefore provide better CD spectra.

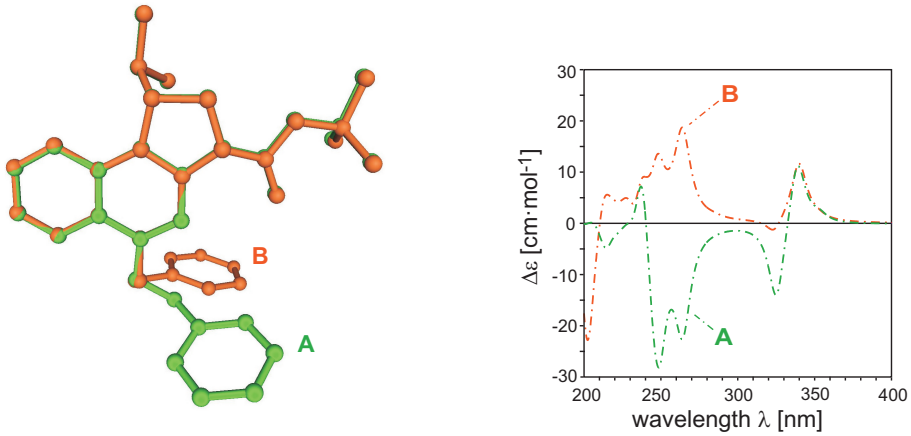

Figure 32. Two single conformers, **A** and **B**, of (1*S*,10*R*)-**10** which differ only in the orientation of the phenyl ring, and the corresponding CNDO/S based CD spectra.

In the case of the conformational analysis, the overall calculated CD curves of **10a** and **10b** were obtained by BOLTZMANN weighting of the single CD spectra, based on the AM1 predicted relative energies of the conformers (Table 2), while for the MD simulated structures the respective single spectra were just arithmetically added up. Reflection of these calculated CD spectra at the zero line generated the theoretical spectra predicted for the enantiomeric compounds, (1*R*,10*S*)-**10a** and (1*R*,10*S*)-**10b**. The CD spectra thus obtained were then UV-corrected by 15 nm in the case of the conformational analysis, and by 5 nm for the MD based approach, while the OM2-based calculations for 16 conformers resulted in a red shift of 25 nm. The experimental CD spectrum of (+)-**10**, measured in different solvents, always exhibited the same CD features, two broad low-intensity bands with positive COTTON effect around 350 and 315 nm, followed by two strong negative signals at 255 and 210 nm. The calculated CD spectra of **10a** and **10b** were very similar, showing only minor difference for the negative CE at 210 nm, which was better reproduced in the case of the compound with lone-pair electrons containing substituent, OH. Finally, the comparison of the calculated CD spectra of both, (1*S*,10*R*)-**10a** and (1*S*,10*R*)-**10b**, with the measured CD curve of (+)-**10** showed a reasonable agreement in the region of 200–290 nm, while the broad doubled band between 300 and 380 nm was not entirely reproduced (Figure 33a, left). The same behavior was found in the case of the OM2

predicted spectra (not shown here, but in the Supporting Information of Ref. 36). On the other hand, the respective MD based CD spectra reflected this region correctly (Figure 33b, left). Consequently, the CD curves obtained for (1*R*,10*S*)-**10a** and (1*R*,10*S*)-**10b** behaved almost oppositely (Figure 33a/b, right). By this way, the absolute configuration of (+)-**10** was assigned to be 1*S*,10*R*.[36] An independent confirmation of these results was obtained by anomalous X-ray scattering of the bromo derivative of (+)-(1*S*,10*R*)-**10**.[36]

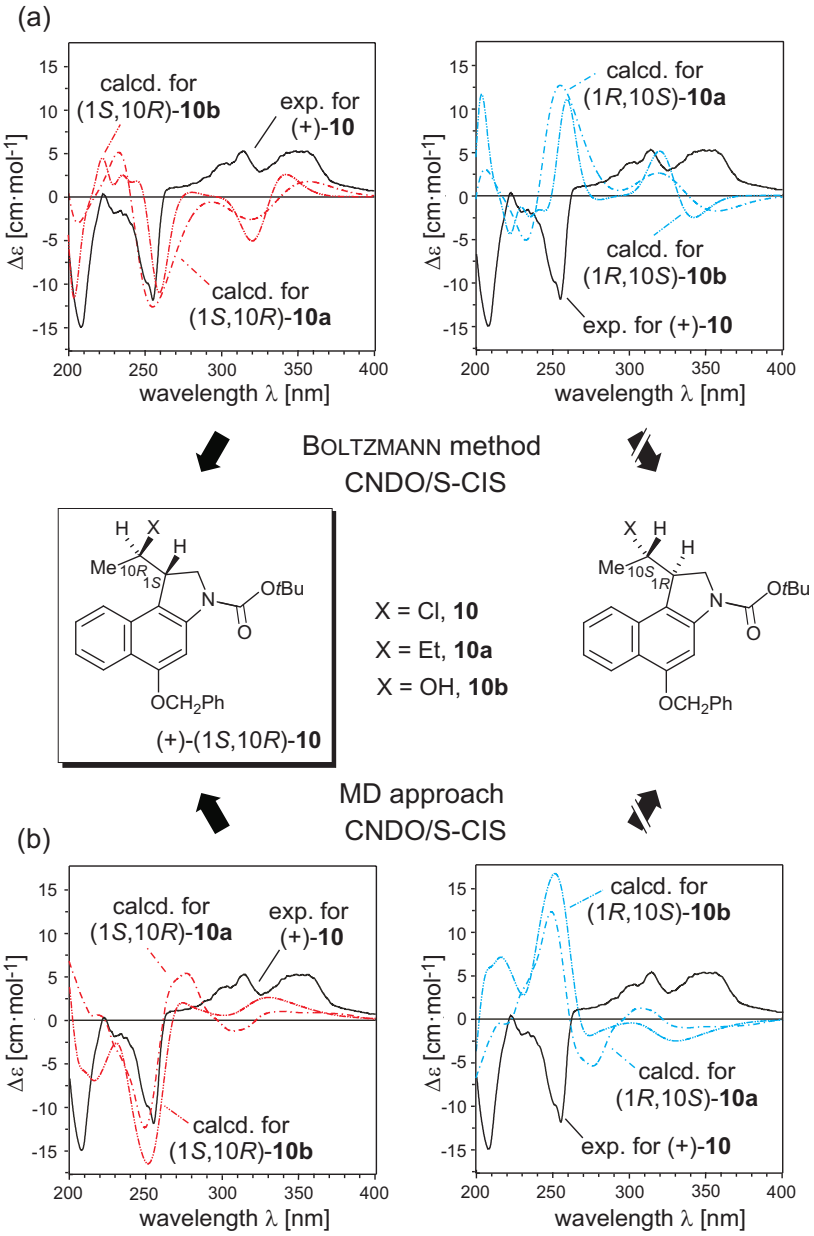

Figure 33. Determination of the absolute configuration of (+)-**10** as 1*S*,10*R*, by comparison of the experimental CD curve (in acetonitrile) with the theoretically predicted CD spectra (CNDO/S) of **10a** and **10b**; a) according to the conformational analysis; b) by using the MD method.

4.2. Semiempirical and TDDFT methods resulting in almost the same accuracy

4.2.1. Bisisonigerone (11)

The axially chiral bisisonigerone (**11**) is a key intermediate in the first enantioselective synthesis of the bisnaphthopyrone natural product nigerone (**12**) by M. C. Kozlowski *et al*.[37] This symmetric biaryl has been obtained by an efficient catalytic asymmetric oxidative coupling of 2-naphtol substrates by using 1,5-diaza-*cis*-decalin copper catalysts like **38** (Figure 34). Although this reaction is stereochemically predictable, viz. the (*S,S*)-catalyst should yield (*M*)-binaphthol and (*P,P*)-configured one should give the *P*-configuration,[178] the CD spectra of bisisonigerone (**11**) thus synthesized initially raised some doubts about the assignment of the absolute axial configuration of **11**.

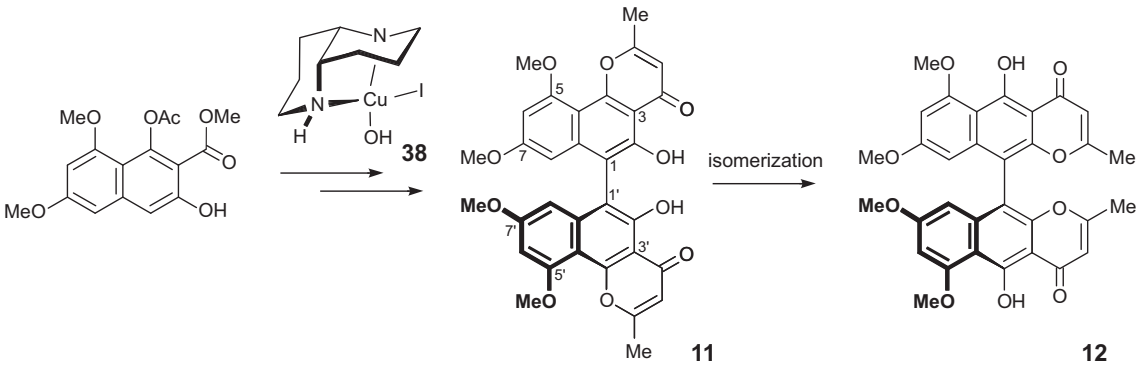

Figure 34. Schematic route to nigerone (**12**) via bisisonigerone (**11**).

Thus, due to the constitutionally symmetric structure of **11**, it should be possible to assign its configuration by the classical *Exciton Chirality Method*.[84] In bisisonigerone [(+)-**11**], with its two interacting flavasperone[179] chromophores, the UV band at 285 nm gave rise to an exciton couplet in the CD spectrum with the first, negative Cotton effect at 300 nm and the second, positive one at 280 nm (Figure 35), indicating a "negative chirality" of **11**, here corresponding to an *M*-configuration.

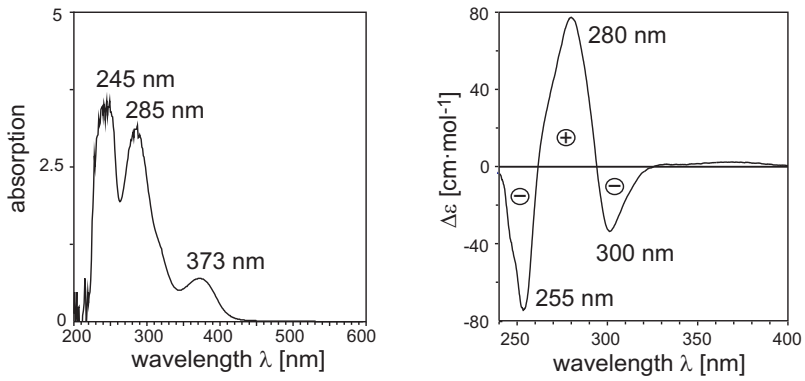

Figure 35. Experimental UV and CD spectra of (+)-bisisonigerone (**11**).

On the other hand, the presence of a third band at 255 nm with a strong negative Cotton effect, showing the same amplitude as the positive one, made a simple empirical configurational attribution impossible or at least uncertain. Therefore, the experimental CD spectrum of **11** was independently investigated by quantum chemical CD calculations.[37]

Starting with the *P*-enantiomer of **11**, the reaction coordinates for the rotations of all flexible parts of the molecule, including the axis, were calculated by using the AM1 method. This calculations revealed that the two hydroxy functions (at C-2 and C-2′) adopt only one energetically preferable array, with strong hydrogen bonds ($d_{H\text{-}O}$ *ca.* 1.60 Å) to the adjacent carbonyl groups, and that the two methoxy substituents at C-5 and C-5′, due to the steric hindrance, adopt a maximum distance from the pyrone ring. For the chiral biaryl axis of **11**, only one stable orientation was found. The other two methoxy groups at C-7 and C-7′ (θ_{ABCD} and θ_{EFGH}) showed two energetically relevant orientations each, thus resulting in four possible input structures for further DFT (RI-BLYP/SVP) optimizations (Figure 36).

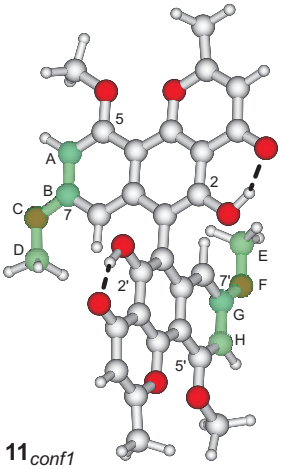

11$_{conf1}$

Conformer	$\Delta\Delta H_f$ [kcal·mol^{-1}]	θ_{ABCD} [°]	θ_{EFGH} [°]
11$_{conf1}$	0.00	-179	-179
11$_{conf2}$	2.11	-179	-1
11$_{conf3}$	2.11	-1	-179
11$_{conf4}$	4.19	-2	-2

Figure 36. The results of RI-BLYP/SVP optimization of four possible conformers of **11**, and the global minimum structure thus predicted.

Since structures **11**$_{conf2}$ and **11**$_{conf3}$ were identical, due to the symmetric constitution of **11**, excited-state energy calculations were performed only for three conformers **11**$_{conf1}$, **11**$_{conf2}$, and **11**$_{conf4}$. At first, the single CD and UV spectra were calculated with the semiempirical CNDO/S[27] and OM2[28] approaches (Figure 37), considering 784 and 900 singly occupied configurations, respectively. The resulting BOLTZMANN-weighted overall spectra were then submitted to a 'UV correction',[14] requiring red-shifts of 5 nm for the CNDO-based spectra, and of 35 nm for the OM2-based curves.

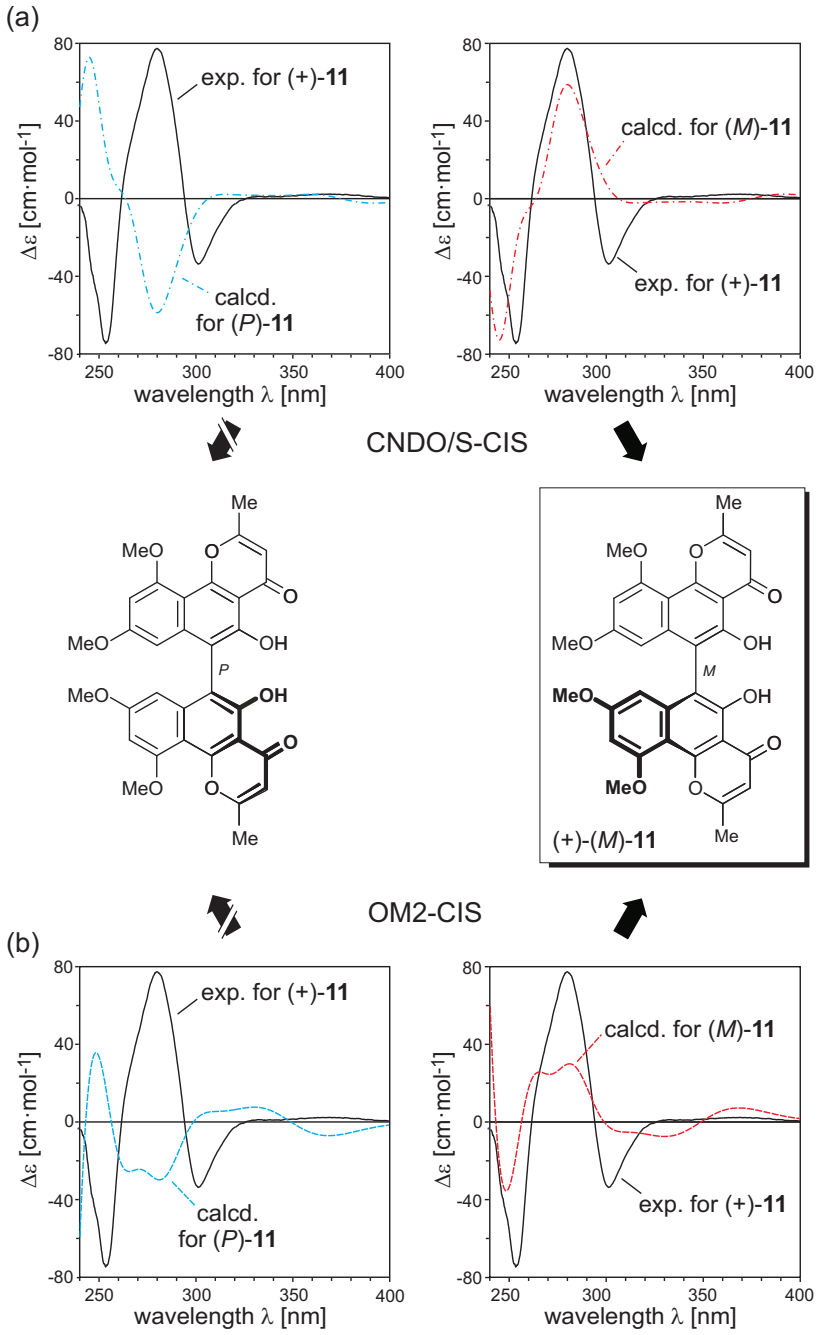

Figure 37. Assignment of the absolute axial configuration of (+)-**11** by the semiempirical approaches, CNDO/S-CIS (a) and OM2-CIS (b).

Although the rotatory strength values for the band above 300 nm were substantially underestimated by both semiempirical methods, the CD spectra calculated for the *P*-enantiomer of **11** clearly showed an opposite behavior in the

region of 240–290 nm, while the spectra predicted for *M* were in full agreement with the experimental features (Figure 37).

Higher-level time-dependent DFT calculations of the three minima of **11** were carried out with the hybrid functional B3LYP and the TZVP basis set, taking into account 50 lowest-energy excited states. In this case, a blue-shift of 20 nm was required to reproduce the experimental UV bands.[37] Final comparison of the theoretical TDDFT CD spectra with the measured curve of (+)-**11** showed that the experimental band at 255 nm was predicted with a too low intensity, and therefore this band was not considered for the attribution of the absolute configuration (Figure 38). It should be mentioned, however, that the B3LYP/TZVP-based CD spectrum of (*P*)-**11** actually possesses excitations with large positive rotatory strengths in the region below 240 nm, but their energies are too high (i.e., they are strongly blue-shifted), which complicated the attribution of these excitations to the experimental band at 255 nm. Nevertheless, the strong, characteristic band observed at 280 nm was reproduced most accurately by all of the calculation methods, the semiempirical and the TDDFT ones, predicting a negative Cotton effect for the *P*-configured atropo-enantiomer of **11** and a positive one for *M* (Figure 38). Consequently, the dextrorotatory form of bisisonigerone, (+)-**11**, was attributed the *M*-configuration.[37]

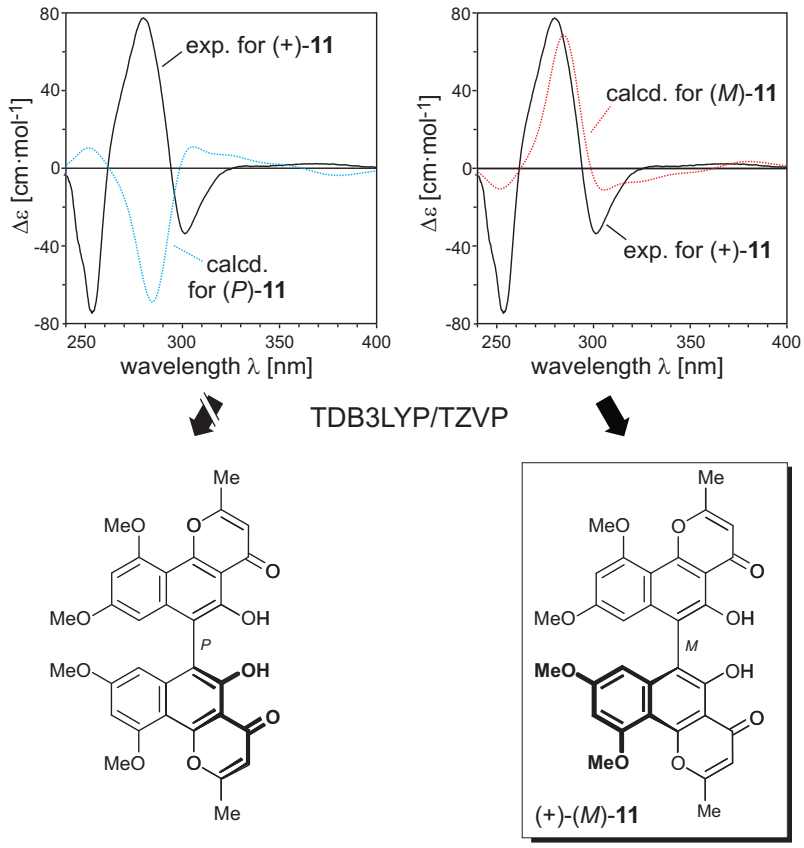

Figure 38. Assignment of the absolute configuration of (+)-bisisonigerone (**11**) by the TDDFT (B3LYP/TZVP) approach, which is in agreement with the semiempirical prediction.

4.2.2. Nigerone (12)

After having evidenced the axial configuration of the intermediate bisisonigerone (**11**), we focused on the final product nigerone (**12**) (Figure 34). This seemed highly rewarding because the direct comparison of the experimental CD spectrum of (*M*)-(+)-bisisonigerone (**11**) with the CD curve of (–)-nigerone (**12**), which was also expected to have the *M*-configuration, showed a substantial difference, revealing the first negative and the second positive Cotton effects of (*M*)-**11** to be red-shifted by 16 and 18 nm, respectively (Figure 39). Furthermore, previous attempts to attribute the absolute configuration of natural nigerone (**12**) had been contradictory: The comparison of its CD and ORD data with those of other bisnaphthopyrones of

known absolute configuration[180] led to a *P*-configuration, while the interpretation by using the *Exciton Chirality Approach* gave *M*.[181]

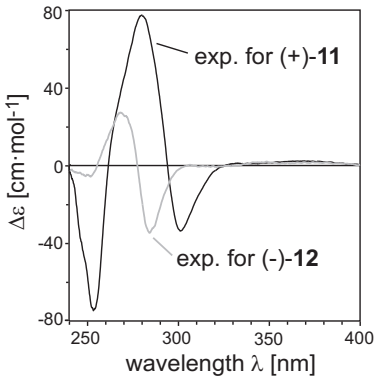

Figure 39. Comparison of the experimental CD spectra of (+)-(*M*)-bisisonigerone (**11**) and (–)-nigerone (**12**).

The conformational behavior of **12** was supposed to be similar to that of bisisonigerone (**11**). Indeed, RI-BLYP/SVP calculations of the *P*-enantiomer of **12** revealed the same respective conformers, differing only in the orientation of two methoxy substituents at C7 and C7′ (Figure 40). As before for **11**, the other flexible parts, viz. the OMe groups at C-5 and C-5′, the hydroxy functions, and the biaryl axis showed only one favorable orientation each.

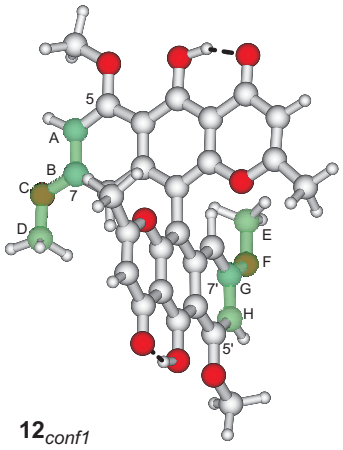

12$_{conf1}$

Conformer	$\Delta\Delta H_f$ [kcal·mol^{-1}]	θ_{ABCD} [°]	θ_{EFGH} [°]
12$_{conf1}$	0.00	180	180
12$_{conf2}$	1.81	180	-0.1
12$_{conf3}$	3.63	0.2	-2

Figure 40. Low-energy conformers of nigerone (**12**) as optimized at the RI-BLYP/SVP level, and the global minimum structure of **12**.

CD calculations were performed at the semiempirical CNDO/S and OM2 levels, and also by using the B3LYP/TZVP method. All parameters, viz. the number of the configurations and of the excited states calculated, were taken the same as for bisisonigerone (**11**). Comparison of the experimental UV spectrum of **12** with the computed ones revealed that only the OM2-based UV curve required a shift of 40 nm to higher wavelengths to reproduce the experimental bands. This UV shift, which seemed to be systematic for this approach, might probably be reduced by not only considering the single, but also the double excitations (OM2-CISD). The spectra calculated by CNDO and B3LYP/TZVP methods were compared to the experimental curve of (–)-**12** without shift.

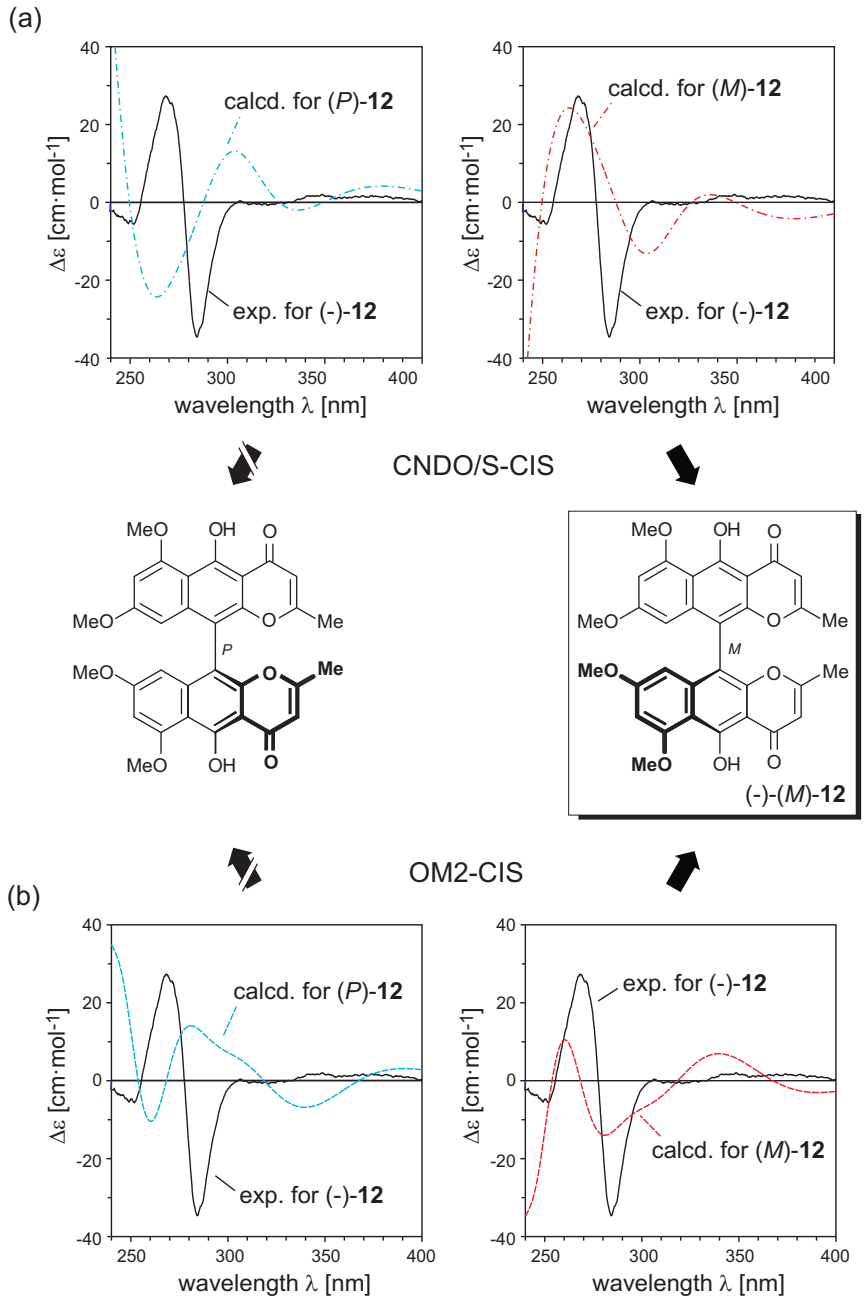

Figure 41. Assignment of the absolute axial configuration of (–)-**12** by the semiempirical approaches CNDO/S-CIS (a) and OM2-SCI (b).

The first CD band observed at 280 nm was slightly underestimated in energy (about 15 nm) by the CNDO calculations, while the second peak was predicted very accurately, revealing that the CD spectrum theoretically simulated for the *M*-enantiomer of **12** reproduced the negative CD split of the experimental curve of (-)-**12** whereas the one calculated for (*P*)-**12** behaved oppositely (Figure 41a). The

same results were obtained from the OM2 (Figure 41b) and B3LYP/TZVP calculations (Figure 42), which firmly corroborated the previous attribution based on the *Exciton Chirality Method*, thus indicating that the natural product (–)-nigerone (**12**) is *M*-configured.

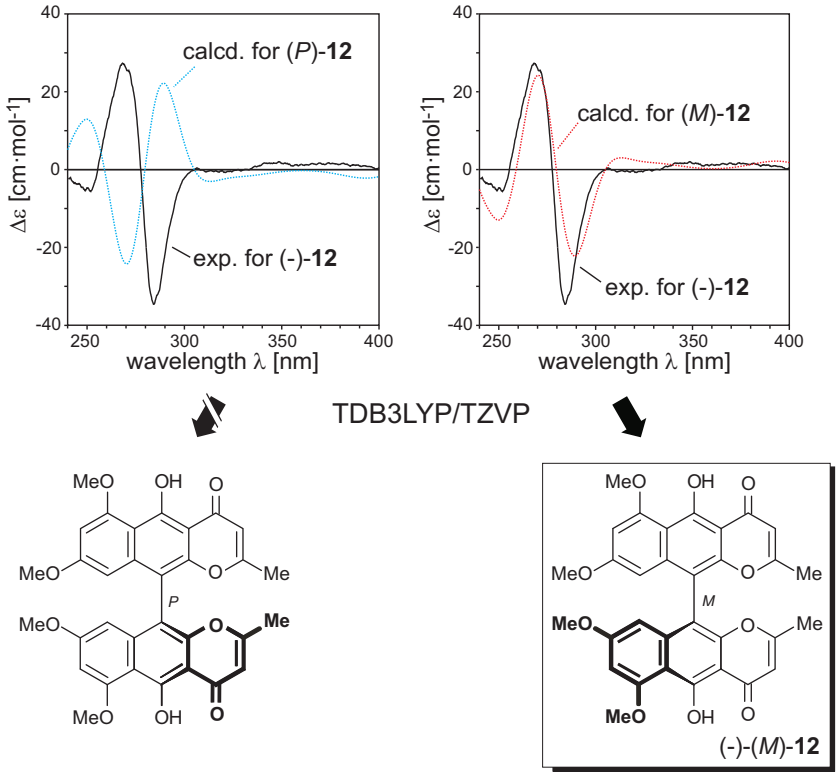

Figure 42. Determination of the absolute configuration of (–)-nigerone (**12**) by comparison of the experimental CD curve with the CD spectra theoretically (TDB3LYP/TZVP) predicted for its two possible enantiomers.

4.2.3. The 'leuco' phenylanthracene derivative 13 of knipholone

The 'leuco' phenylanthracene derivative **13** (Figure 43), synthesized in our group by M. Knauer, had a great significance in clarifying the configurational assignment of two important natural phenylanthraquinones, knipholone (**19**) and knipholone anthrone (**20**) (see Chapters 4.3.4 and 4.3.5).[38]

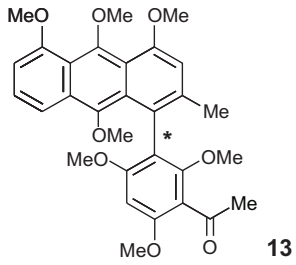

Figure 43. Structure of the semisynthetic phenylanthracene derivative **13**.

This fully conjugated anthracene derivative **13**, obtained stereochemically unambiguously from the enantiopure or enantio-enriched knipholone (**19**), was expected to have a simpler CD spectrum as compared to that of **19** and **20**, which could be interpreted more easily by quantum chemical CD calculations for an independent configurational assignment.

Thus, the enantio-enriched (+)-knipholone [(+)-**19**, *er* 89:11], with its newly determined *P*-configuration, was smoothly transformed by M. Knauer into the 'leuco' derivative **13** by subsequent *O*-methylation, reduction, and renewed *O*-methylation (Scheme 1, top), without substantial loss of enantiomerical purity (Scheme 1, bottom).[38] The online-measured CD spectra of two peaks corresponding to the atropo-enantiomers of the obtained phenylanthracene **13** indeed showed a significantly simpler chiroptical behavior as compared to that of **19**, viz. a classical positive couplet for the first-eluting peak hinting at the *P*-configuration, and a negative couplet in the case of the second-eluting peak, which is in agreement with the *M*-configuration (Scheme 1, at the right bottom). To corroborate this tentative assignment, based on the empirical application of the *Exciton Chirality Method*, extensive quantum chemical CD investigations were performed at both, semiempirical and *ab initio* levels.

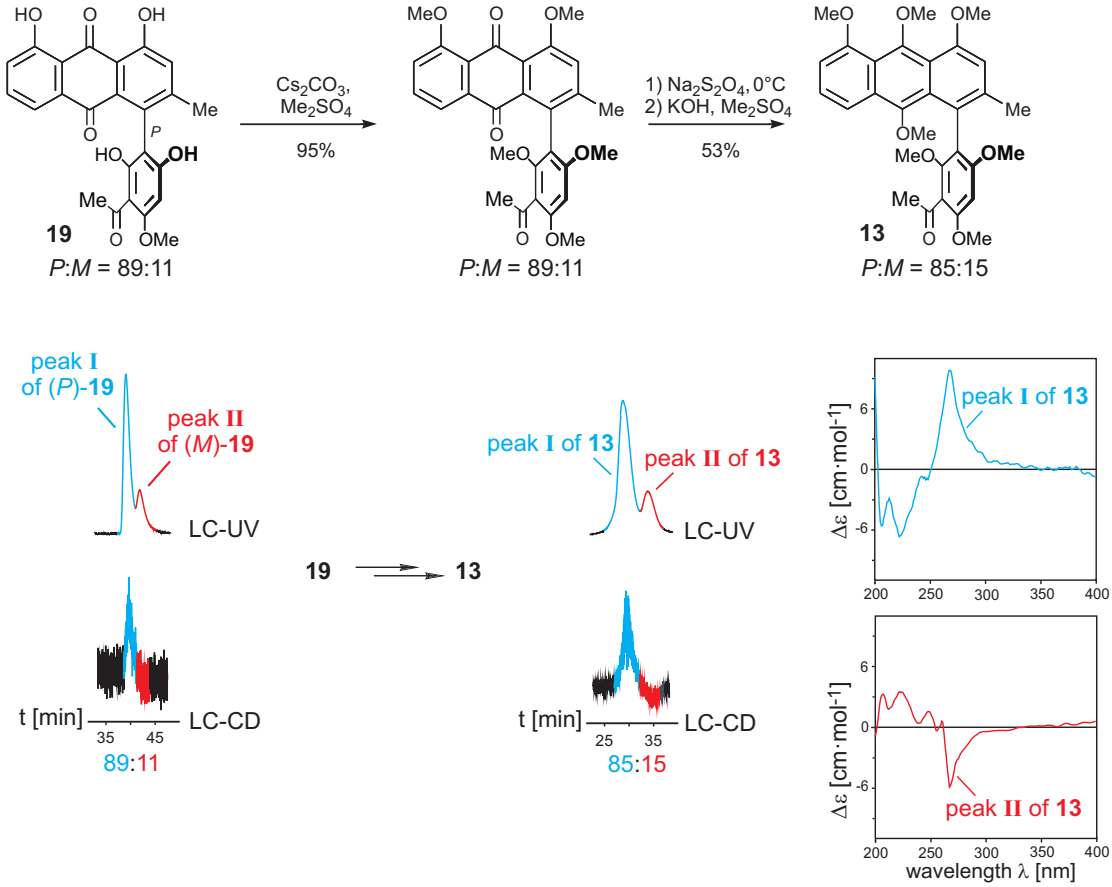

Scheme 1. Synthetic route to the 'leuco' derivative **13** of knipholone (**19**),[38] and monitoring of the enantiomeric ratio of the starting material (**19**, 89:11 *P* to *M*) and of the obtained product (**13**, 85:15 *P* to *M*) by HPLC-CD coupling on a Chiralcel OD-H column. This work was done by M. Knauer.

Starting with the *M*-atropo-enantiomer of **13**, a comprehensive conformational analysis was carried out by using the AM1 method. A preliminary screening of the reaction coordinates calculated for all methoxy substituents and for the acetyl function of **13** revealed that the three methoxy groups at C-1, C-8, and C-4' adopt only one energetically preferable array, with the *O*-methyls lying in the plane of the respective aromatic rings and with a maximum distance from the neighboring methoxy (for OMe-1 and OMe-8) and acetyl (for OMe-4') substituents. The other groups showed two to four possible orientations, which were used for further perturbation and optimization procedures. As a result, 41 conformers were found within an energetic cut-off of 3 kcal·mol^{-1} above the presumable global minimum (Table 3).

Table 3. Identification of the reaction coordinates analyzed; the AM1 optimized conformers of **13**, with their relative energies and characteristic dihedral angles, as well as the AM1 global minimum conformer.

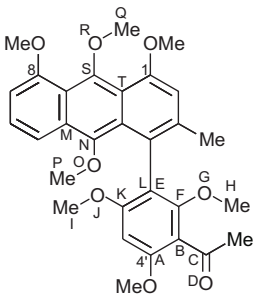

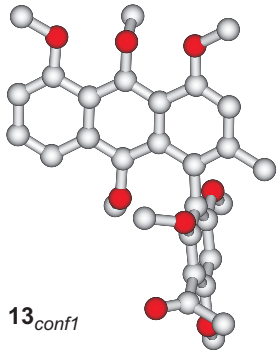

Conformer	$\Delta\Delta H_f$ [kcal·mol^{-1}]	θ_{ABCD} [°]	θ_{EFGH} [°]	θ_{IJKL} [°]	θ_{MNOP} [°]	θ_{QRST} [°]
13$_{conf1}$	0.00	-113	93	-177	78	-92
13$_{conf2}$	0.11	-112	95	-175	79	91
13$_{conf3}$	0.26	114	-95	-167	-79	91
13$_{conf4}$	0.33	-117	87	-165	-77	93
13$_{conf5}$	0.39	-117	86	-165	-77	-90
13$_{conf6}$	0.42	-116	87	-128	-78	93
13$_{conf7}$	0.44	114	-92	-95	-77	93
13$_{conf8}$	0.48	-116	87	-128	-77	-90
13$_{conf9}$	0.49	114	-96	-168	-80	-91
13$_{conf10}$	0.71	113	-95	-110	-79	-91
13$_{conf11}$	0.87	114	-93	-46	-76	94
13$_{conf12}$	1.01	113	-90	-173	81	93
13$_{conf13}$	1.07	-113	91	86	76	-94
13$_{conf14}$	1.08	113	-90	-174	82	-89
13$_{conf15}$	1.29	114	-93	-47	-76	-88
13$_{conf16}$	1.30	112	105	-176	80	-92
13$_{conf17}$	1.32	-116	91	-37	-74	94
13$_{conf18}$	1.32	-113	92	86	76	88
13$_{conf19}$	1.48	65	53	-180	78	-93
13$_{conf20}$	1.51	-116	90	-38	-73	-88
13$_{conf21}$	1.70	-113	93	21	77	-93
13$_{conf22}$	1.73	65	54	-179	78	90
13$_{conf23}$	1.74	-112	37	-167	-75	-90
13$_{conf24}$	1.76	-113	95	8	77	89
13$_{conf25}$	1.76	-112	37	-167	-76	92
13$_{conf26}$	1.78	106	42	-180	77	-93

Conformer	$\Delta\Delta H_f$ [kcal·mol^{-1}]	θ_{ABCD} [°]	θ_{EFGH} [°]	θ_{IJKL} [°]	θ_{MNOP} [°]	θ_{QRST} [°]
13$_{conf27}$	1.88	-111	98	-78	74	89
13$_{conf28}$	1.90	-111	97	-79	74	-94
13$_{conf29}$	1.99	-111	40	-122	-76	-90
13$_{conf30}$	2.00	-111	40	-121	-76	93
13$_{conf31}$	2.03	106	43	-179	77	89
13$_{conf32}$	2.05	112	-91	120	80	-90
13$_{conf33}$	2.07	112	-91	122	80	92
13$_{conf34}$	2.44	-116	88	73	-75	92
13$_{conf35}$	2.51	-116	87	74	-75	-90
13$_{conf36}$	2.51	72	12	-169	-77	-91
13$_{conf37}$	2.67	113	-90	-73	76	90
13$_{conf38}$	2.73	113	-89	-73	75	-92
13$_{conf39}$	2.83	113	-93	-21	76	91
13$_{conf40}$	2.94	71	23	-122	-78	-90
13$_{conf41}$	2.98	113	107	0	78	90
13$_{conf42}$	2.99	113	-93	-19	77	-91

The CD and UV spectra for each of thus found conformer of **13** were calculated by using the CNDO/S-CIS method, with the highest available CI expansion, including 28 occupied and unoccupied molecular orbitals. The overall spectra resulted from the BOLTZMANN weighting of the single spectra and their subsequent addition. Comparison of the experimental UV curve of **13** with the calculated one revealed the necessity for a red-shift of 5 nm. Therefore, the theoretical CD spectra predicted for (*M*)- and (*P*)-**13** were accordingly shifted to higher wavelengths. The spectrum calculated for the *P*-enantiomer of **13** reproduced very well the curve of the first-eluting peak, whereas the one predicted for (*M*)-**13** was almost identical with the spectrum of the second peak (Figure 44), thus confirming the exciton-chirality based assignment.

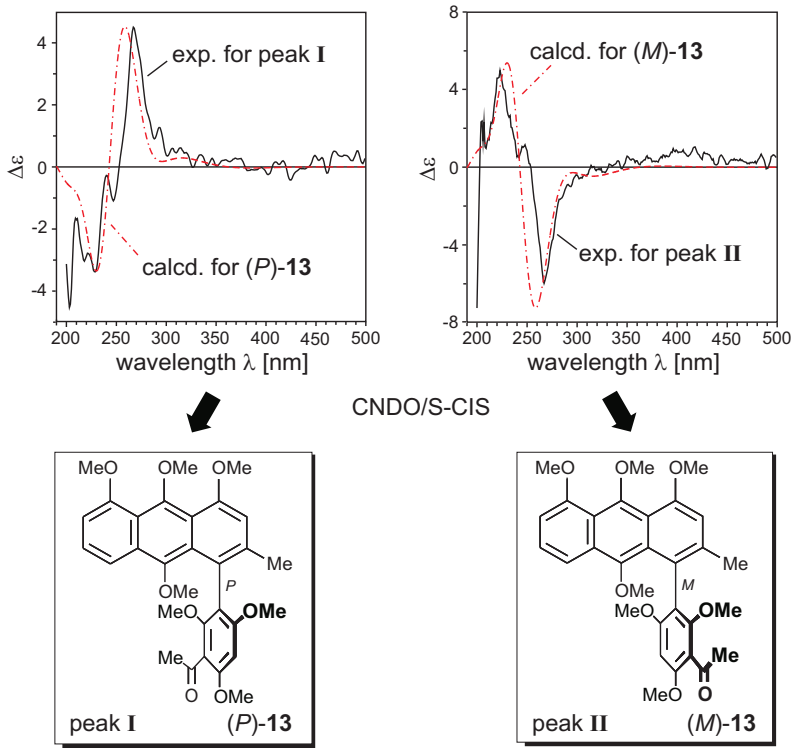

Figure 44. Configurational assignment of two peaks of phenylanthracene **13** by the semiempirical CNDO/S-CIS method.

In view of the challenging character of the semiempirical treatment of the parent compounds, knipholone (**19**) and also knipholone anthrone (**20**) (Chapter 4.3.3 and 4.3.4), the 'leuco' phenylanthracene derivative **13** of knipholone (**19**), although possessing the unambiguous configurational attribution provided by the CNDO/S calculations, was further submitted to higher-level calculations.

Because of the large number of AM1 conformers, only the most important structures were chosen for the more expensive DFT calculations. The CNDO computations showed that the conformers with a different dihedral angle θ_{ABCD} at the acetyl function gave the CD spectra diverging to the largest degree, while the structures differing in orientations of the methoxy groups gave an almost identical CD pattern. Therefore, the AM1-predicted global minimum, **13**$_{conf\ 01}$, with its orientations of all methoxy substituents (Table 3), was taken as a basis skeleton, and only the rotation of the acetyl function was considered. The validity of the choice of this basis framework was furthermore proven by the test BLYP/SVP calculations,

revealing that the alternative orientations of the methoxy substituents were energetically not favorable. The DFT-based BLYP/SVP analysis of the rotation of the acetyl function resulted in three low-energy conformers lying within an energetic cut-off of 3 kcal·mol^{-1} (Figure 45). In these minimum structures the acetyl was twisted out of the phenyl plane in either direction due to the steric hindrance by the methoxy substituent at C-2'. The structure with the carbonyl oxygen 'left down', was found to be unstable. To provide more accurate energies and geometries, these structures were further optimized at the BLYP/TZVP and B3LYP/TZVP levels (Figure 45).

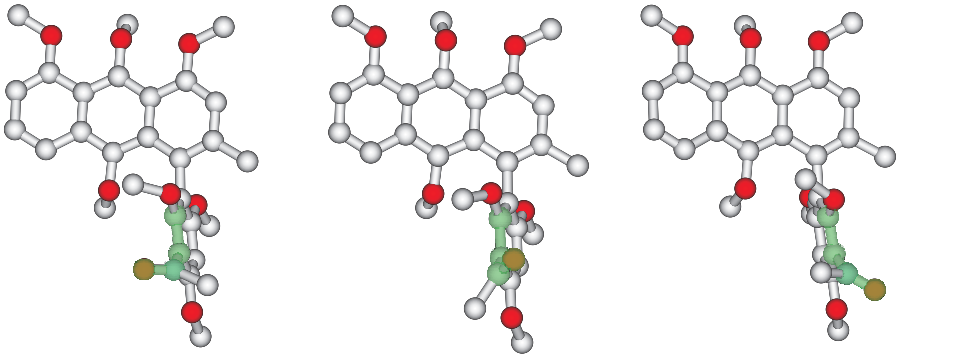

13$_{conf1}$ (O_{Ac} 'left up') **13**$_{conf2}$ (O_{Ac} 'right up') **13**$_{conf3}$ (O_{Ac} 'right down')

$\Delta\Delta H_f$ [kcal·mol^{-1}]	**13**$_{conf1}$	**13**$_{conf2}$	**13**$_{conf3}$
BLYP/SVP	0.00	-0.09	2.15
BLYP/TZVP	0.00	0.68	1.55
B3LYP/TZVP	0.00	1.09	2.09
f_i^{B3LYP}	0.72	0.25	0.02

Figure 45. The low-energy conformers of phenylanthracene **13** with their relative energies, and the weighting factors calculated from the B3LYP energies.

The excited-state energy calculations were carried with the TDDFT (B3LYP/TZVP) and DFT/MRCI (BHLYP/SVP) methods. The single UV and CD spectra calculated for each DFT-based conformer of **13** were added up according to their B3LYP/TZVP energies, following the Boltzmann statistic. The TDDFT based overall UV spectrum of **13** reproduced the experimental UV curve with a reasonable accuracy,[38] so that no UV correction was necessary. Comparison of the respective

CD spectra predicted for two enantiomers of **13**, clearly showed that the more rapidly eluting peak, corresponding to the major product, has the *P*-configuration, and the minor, more slowly eluting enantiomer is *M*-configured (Figure 47a).

For the computationally costly DFT/MRCI CD calculations, several simplifications were applied: Due to its almost negligible impact (2 %, Figure 45) in the overall CD spectrum, the third conformer (**13**$_{conf\ 3}$, O_{Ac} 'right down') was not considered; furthermore, for the remaining two minimum structures, all *O*-methyl groups in the anthracene part of the molecule and the one of the OMe group at C-6' in the acetylphloroglucinol ring were manually replaced by a hydrogen atom each (**13a**, Figure 46), since only a molecule with fewer than 250 electrons[b] could be treated by the MRCI/SVP calculations. Exemplarily for the global minimum conformer (**13**$_{conf1}$), it was proven by B3LYP/TZVP calculations that such a replacement does not change the resulting CD spectrum, and hence the overall CD spectra calculated for (*P*)- and (*M*)-**13a** can be safely compared with the experimental curves of the 'leuco' phenylanthracene derivative **13**. The excitation energies calculated by the DFT/MRCI/SVP method for **13a** were overestimated by 0.3 eV (corresponding to ca. 15 nm) as compared to the experimental UV spectrum.[38] The accordingly shifted CD spectra were compared with the experimental curves (Figure 46b), unambiguously confirming the configurational assignment of the two peaks of **13** provided by the above described semiempirical and time-dependent DFT calculations.

[b] As mentioned above, at present larger systems (i.e., with more than 250 electrons) can be treated by the DFT/MRCI method, too.

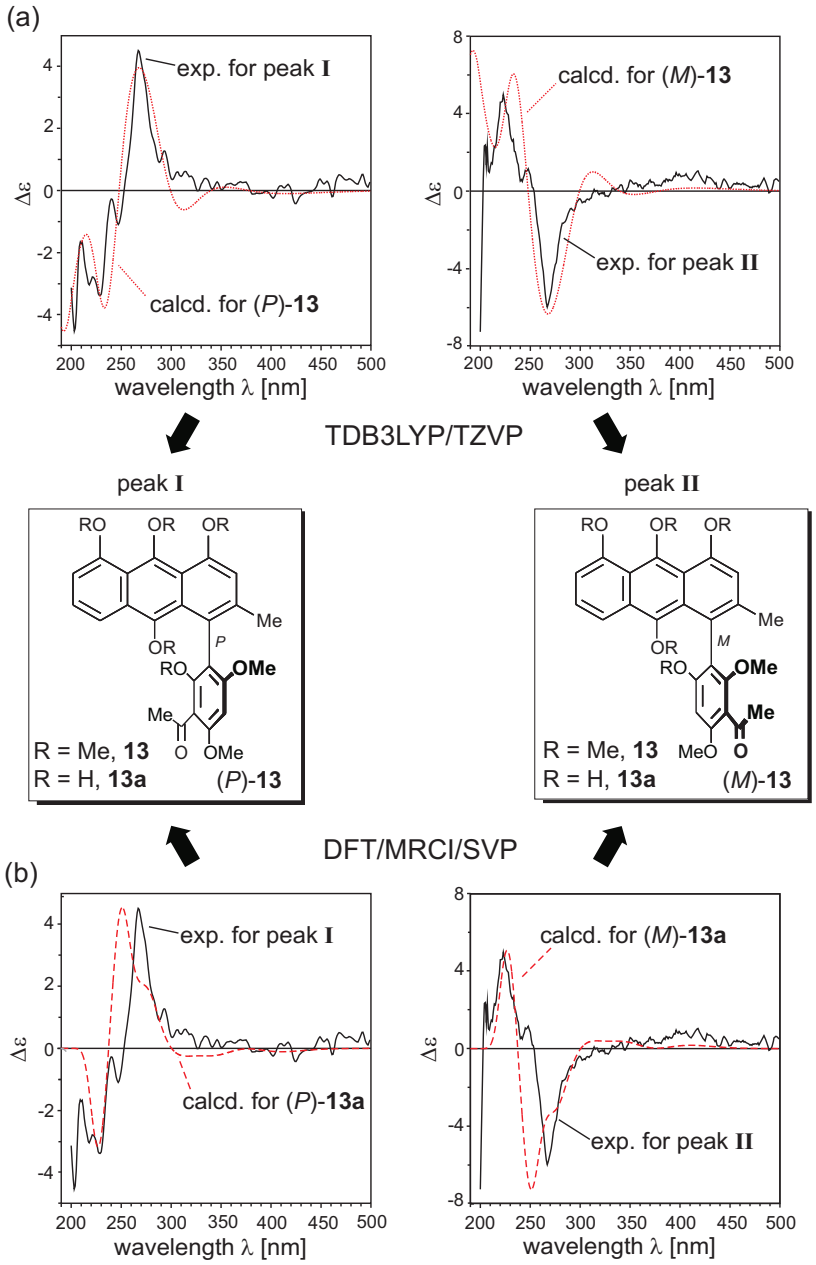

Figure 46. Assignment of the absolute axial configuration of the 'leuco' phenylanthracene derivative **13** by comparison of the online experimental CD spectra of the two peaks with the theoretically predicted CD curves, as deduced from the results of the TDDFT (a) and of the DFT/MRCI (b) calculations.

These investigations were important for a confirmation of the the new, revised configurational attribution of the naturally occurring knipholone (**19**) (Chapter 4.3.4), clearly showing that the *P*-configured 'leuco' derivative **13** does results from (*P*)-(+)-(**19**), according to its new assignment, and *vice versa*, the *M*-atropo-enantiomer of **13** is produced from (*M*)-(–)-**19**.[38]

4.2.4. Hydroxyoxosorbicillinol (14)

Fungi of both, marine and terrestrial origin are valuable resources for biologically active natural products, which find a broad use in practical medicine. Among them, antibiotic agents, such as penicillin (the earliest discovered and probably the most famous fungal-derived compound),[182] cephalosporin,[183] fusidic acid,[184] immuno-suppressant drugs like cyclosporin,[185] and a wide range of further beneficial compounds possessing antifungal, antioxidant, and antiviral activities. Sorbicillin-related compounds, such as sorbicillinol,[186] bisorbicillinol,[187] trichodimerol,[188] bisorbibetanone,[189] and sorbicillactone A (**35**)[35] belong to the class of biologically relevant fungi-derived metabolites. As was mentioned above, compound **35** was isolated in our group from a strain of *Penicillium chrysogenum* and was found to exhibit high antitumoral and antiviral activities.[35] Recently, a new substance was isolated from this fungal species by To. Gulder, viz. a highly oxygenated representative of the sorbicillin natural products with the constitution **14**, named hydroxyoxosorbicillinol (**14**). It possesses an additional hydroxy function in the side chain as compared to the known oxosorbicillinol (**39**) (Figure 47).[190] In the literature the absolute configuration at the stereogenic center at C-5 of **39** was only suggested to be *R*, in accordance with the stereoanalysis of the related compound epoxysorbicillinol (**40**) (Figure 47); this assignment was based on the *Exciton Chirality Method*.[191] To obtain an independent, unequivocal answer on the absolute stereostructure of the newly isolated hydroxy-derivative **14**, quantum chemical calculations of its CD spectra were performed.

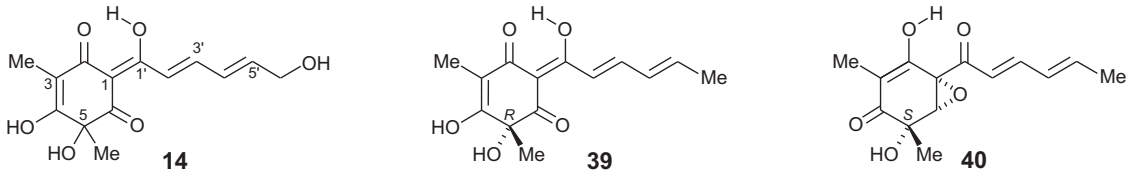

Figure 47. Structures of hydroxyoxosorbicillinol (**14**), oxosorbicillinol (**39**), and epoxysorbicillinol (**40**).

Starting with the *R*-enantiomer of **14**, the rotations of all hydroxy groups were calculated by using the AM1 approach. The semiempirical calculations showed a strong hydrogen bond between the hydroxyl at C-1′ and the carbonyl at C-2, whereas the other hydroxy functions adopted three (for OH-5, OH-6′) and two (for OH-4) possible orientations. After optimization of the 18 structures thus obtained, only six conformers with an energy difference less than 3 kcal·mol^{-1} as compared to the global minimum were found. Final RI-BLYP/SVP optimization revealed that the two hydroxy groups at C-4 and C-5 prefer an orientation with hydrogen bond formation ($H_{OH\text{-}4}\cdots O_{OH\text{-}5}$ and $H_{OH\text{-}5}\cdots O_{CO\text{-}6}$), whereas the other possibilities (viz. with one H···O bond or without hydrogen bonds) resulted in an increase of energy by ca. 6 kcal·mol^{1}. Thus, only three conformers differing in the orientation of OH-6′ (Figure 48) remained for further excited-state computations. It is remarkable that the two conformers with hydrogen atom of OH-6′ oriented towards the conjugated π-system of the sorbyl chain appeared energetically more favorable by more than 1 kcal·mol^{-1} hinting at a noticeable O-H···π interaction.

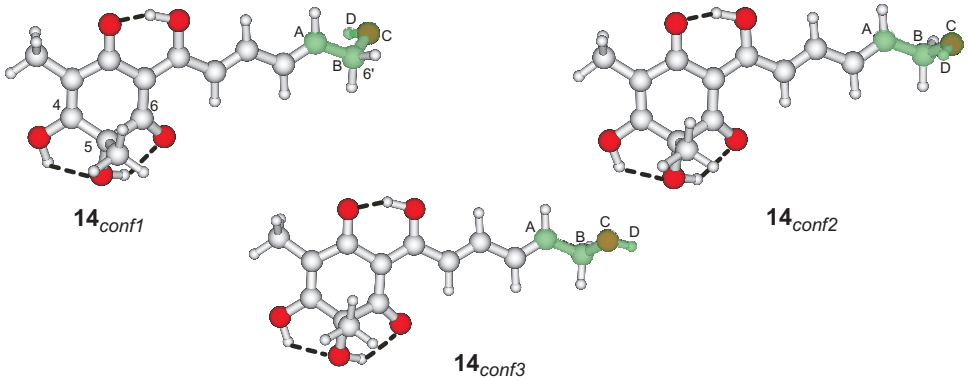

Conformer	$\Delta\Delta H_f$ [kcal·mol^{-1}]	θ_{ABCD} [°]
14$_{conf1}$	0.00	-59
14$_{conf2}$	0.014	59
14$_{conf3}$	1.55	-167

Figure 48. Three minimum conformers of **14** found during the AM1-BLYP/SVP conformational analysis.

CD calculations were performed at semiempirical (CNDO/S) and TDDFT (B3LYP/SVP) levels. The single CD spectra of the three conformers of **14** were very similar within each of the method and differed only in the respective excitation energies. Comparison of the experimental UV curve of **14** with the overall calculated ones in both cases revealed a blue shift, viz. of 12 nm for the CNDO/S predicted spectrum and of 20 nm for the B3LYP/TZVP simulated one. The accordingly shifted CD spectra of (*R*)-**14** calculated by both methods reasonably reproduced the experimental curve, particularly the first three major bands (Figure 49). On the basis of the TDDFT results, the first CD signal observed around 400 nm was attributed to the HOMO-LUMO excitation predicted at 389 nm (with a weighting factor of 0.868), and the next two bands at 330 and 290 nm were correlated with transitions calculated at 344 and 318 nm with major contributions from $HOMO_{-2}$–LUMO (0.467) and $HOMO_{-4}$–LUMO (0.492) excitations, respectively. Although the CD intensities of the two following Cotton effects below 260 nm were somewhat underestimated by both calculations, the sign of these bands in the spectrum of (*R*)-**14** was the same as in the experimental spectrum.

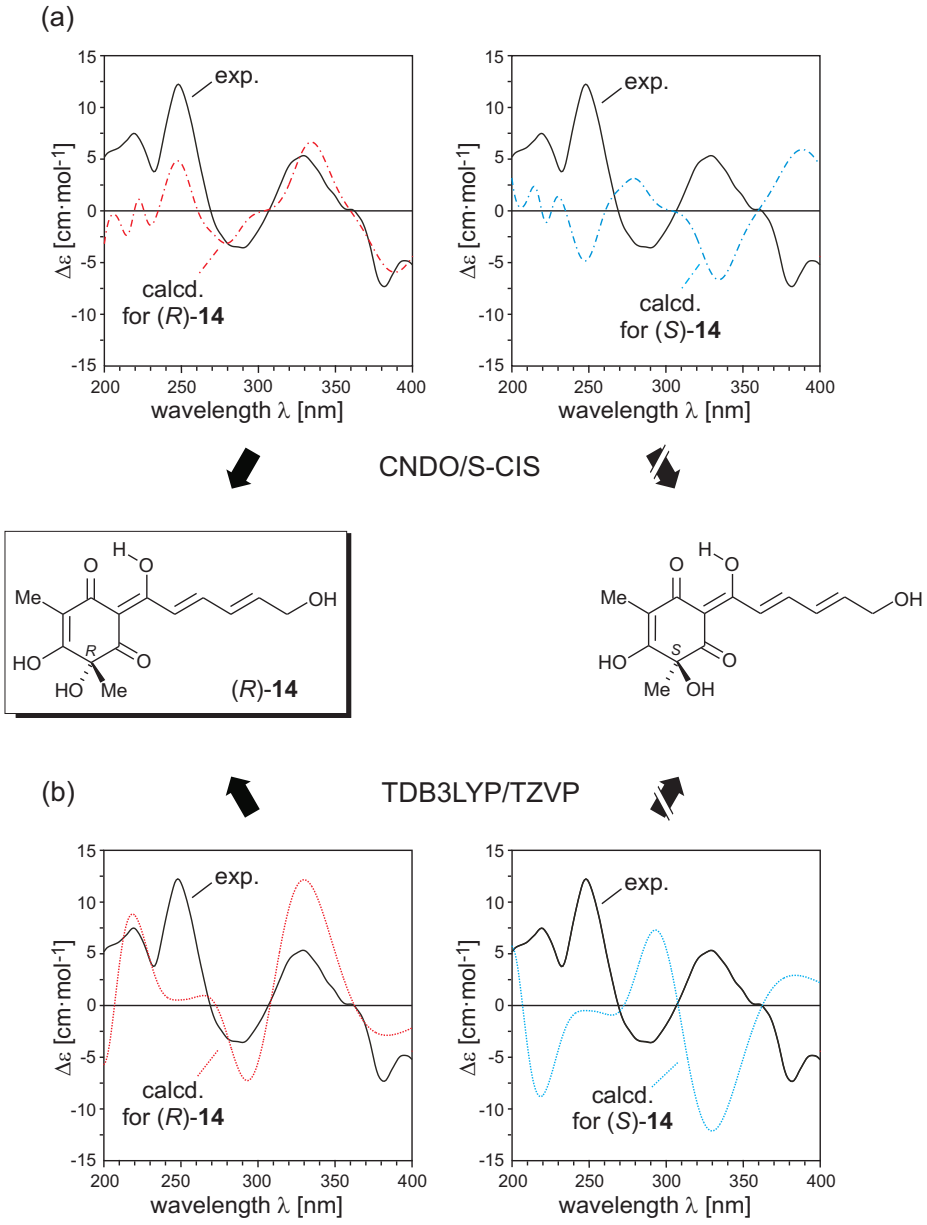

Figure 49. Comparison of the experimental CD curve of hydroxyoxosorcillinol (**14**) with the spectra theoretically predicted for (*R*)- and (*S*)-**14** by using CNDO/S (a) and TDB3LYP/TZVP (b).

Consequently, the absolute configuration of the natural hydroxyoxosorbicillinol (**14**) was unambiguously determined as *R*, which, furthermore, provided a solid confirmation of the earlier suggested configurational attbution at this center in the structurally similar compound, oxosorbicillinol **37**.

4.2.5. Resistoflavin (15)

Resistoflavin (**15**)[192] is a pentacyclic polyketide metabolite, isolated from various terrestrial and marine-derived *Streptomyces* species,[193] and possessing a marked antibacterial activity. It represents an interesting case of a non-planar, 'boat'-shaped oxofunctionalized polyketide, which is derived from an unusual 'interior', i.e., non-peripheral hydroxylation of the flat, 'discoid' polyphenol resistomycin (**41**) by means of a monooxygenase RemO, as was recently ascertained in the group of Prof. C. Hertweck (Figure 50).[39] Our task was to determine the absolute configuration of resistoflavin (**15**), and thus to establish the stereochemical course of this unprecedented enzymatic reaction.

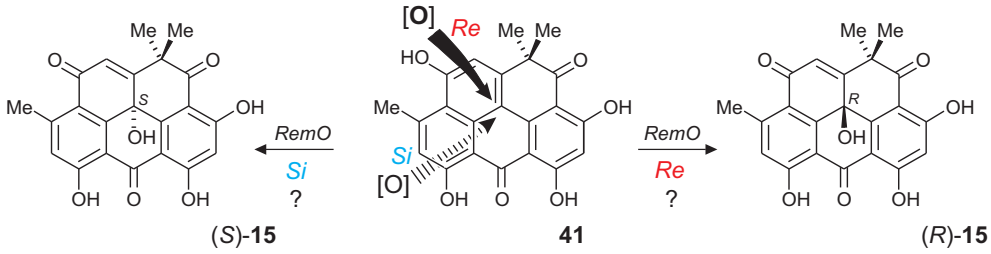

Figure 50. Structures of resistoflavin (**15**) and resistomycin (**40**), and possible stereochemical courses of the RemO-catalyzed hydroxylation of **15**.

The unique structure of resistoflavin (**15**) does not permit an empirical comparison of its CD spectrum with that of any other chiral compound of known configuration. Therefore, CD spectra for each of the two possible enantiomers of **15** were predicted by quantum chemical calculations and then compared with the experimental one. The conformational analysis was carried out for the *R*-enantiomer of **15** at both, the AM1 and the RI-BLYP/SVP levels. The AM1 based computations revealed that the three ´outer´, phenolic hydroxy functions adopt only one energetically preferable orientation, with strong hydrogen bonds ($d_{H\text{-}O}$ ca. 1.98 Å) to the adjacent respective carbonyl groups, while the interior, bisbenzylic hydroxy group was found to have three possible alignments towards the available carbonyl groups, all being at the same distance. For ring II (Figure 51, right) the AM1

calculations predicted two conformations: an energetically favored pseudo-twist-boat geometry with the keto group lying in the plane of the benzene ring V, and, in the case of the central hydroxy group being oriented towards the carbonyl function (as in *conf03*), a pseudo-boat array with the carbonyl group being directed above the plane of ring V. The four conformers thus obtained were further optimized using the density functional theory (RI-BLYP/SVP). In this case, no minimum corresponding to the pseudo-boat conformation was found, thus diminishing the number of conformers for the subsequent CD calculations to three geometries (Figure 51).

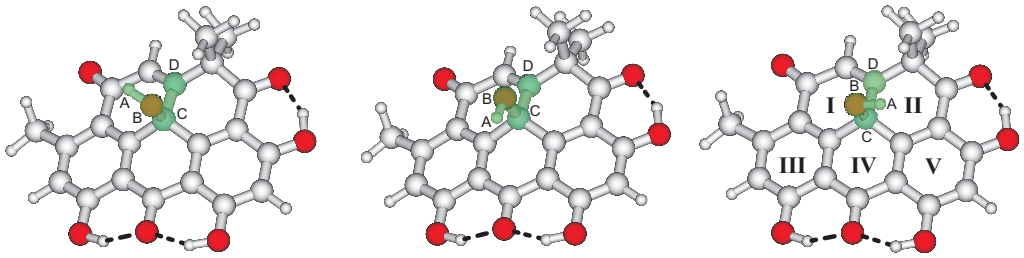

15$_{conf1}$ **15**$_{conf2}$ **15**$_{conf3}$

$\Delta\Delta H_f$ [kcal·mol^{-1}]	**15**$_{conf1}$ (θ_{ABCD})	**15**$_{conf2}$ (θ_{ABCD})	**15**$_{conf3}$ (θ_{ABCD})
AM1	0.28 (58°)	0.00 (176°)	1.76 (-71°)
RI-BLYP/SVP	0.00 (64°)	0.88 (177°)	2.85 (-92°)

Figure 51. Results of the AM1 and RI-BLYP/SVP conformational analysis of **15**; three minimum geometries of **15** differing in the orientation of the inner hydroxy group.

The CD and UV spectra of these conformers were calculated by using the semiempirical CNDO/S-CIS approach and by the TDDFT method applying the hybrid functional B3LYP and the TZVP basis set. The Boltzmann weighting of the single spectra was based on the DFT-derived energies. Comparison of the experimental UV curve of **15** with the CNDO/S calculated one revealed a red shift of 18 nm, which was subsequently applied to the theoretical CD spectra. The experimental CD curve of **15** appeared highly complex, showing seven well separated CD signals (Figure 52). Although some of the experimental features were not reproduced correctly (e.g., the bands at 400 nm and 198 nm), the overall shape of

the semiempirical CD spectrum simulated for the *R*-enantiomer of **15** greatly resembled the measured curve, while the spectrum predicted for (*S*)-**15** behaved almost oppositely (Figure 52a).

The subsequent TDDFT calculations showed that the overall B3LYP-based UV spectrum is red-shifted in comparison to the experimental one by 0.20 eV (i.e., 12 nm), with respect to the most intensive UV band.[39] In the experimental CD spectrum of **15** a broad signal above 400 nm, with a positive sign, was attributed to a HOMO-LUMO excitation predicted at λ_{calc} = 411 nm, the next negative band near 325 nm was correlated with the calculated transitions at 361, 339, 326, and 311 nm, representing mainly the excitations to the LUMO and the $LUMO_{+1}$.[39] The low–intensity CD band observed at 275 nm was assigned to the calculated one at 292 nm, although the predicted intensity was too high. This absorption predominantly arises from the excitation of the $HOMO_{-1}$ to the $LUMO_{+2}$.[39] The negative Cotton effect at 260 nm was correlated with the calculated one at 272 nm, which has a multi-configuration character. The following four experimental bands were well reproduced by the calculations, too (Figure 52b).

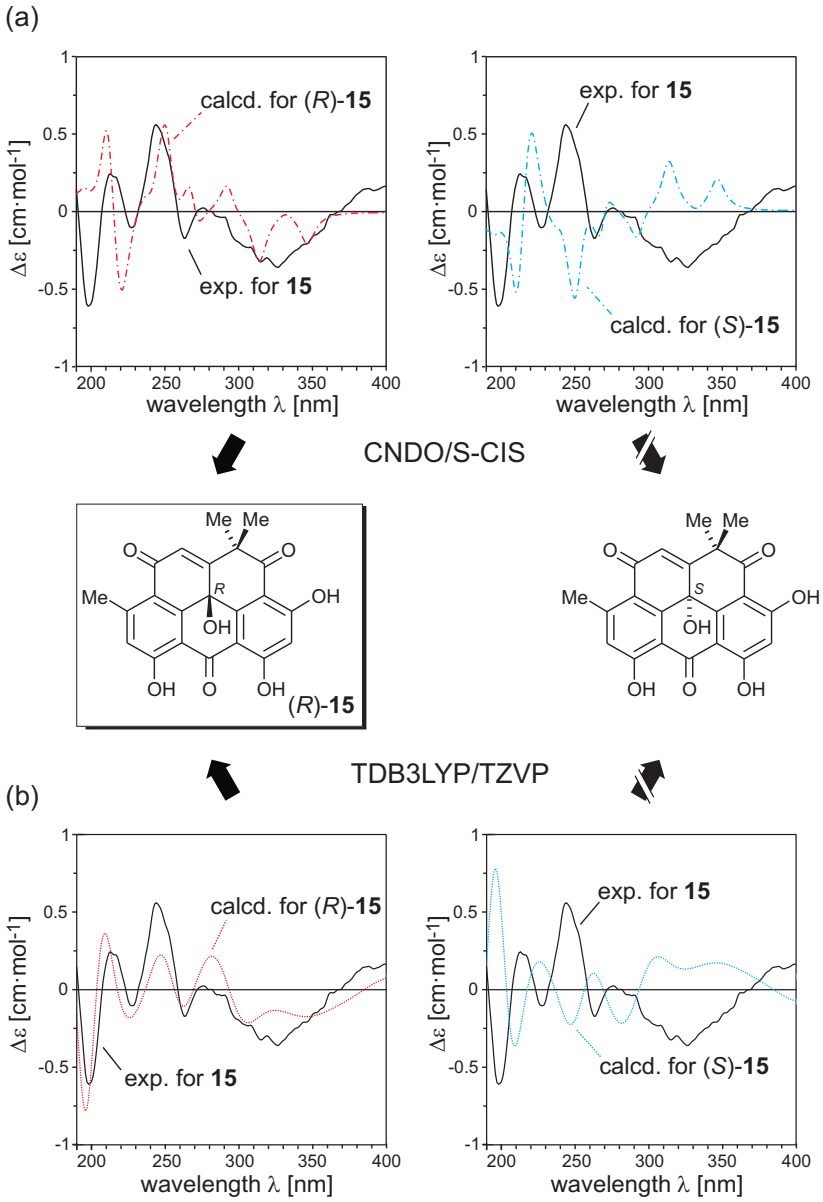

Figure 52. Comparison of the experimental CD curve of **15** with the spectra computationally predicted for (*R*)- and (*S*)-**15** by using the semiempirical CNDO/S-CIS method (a) and the TDDFT (B3LYP/TZVP) approach (b).

The B3LYP/TZVP CD spectrum calculated for (*R*)-**15**, finally, showed a very good agreement with the experimental curve, reproducing all features. Accordingly, the spectrum predicted for (*S*)-**15** displayed an opposite behavior. Thus, both, the semiempirical approach and the time-dependent DFT method, provided the CD spectra of **15** with nearly the same accuracy, permitting unambiguous assignment of the absolute configuration of naturally occurring resistoflavin as (–)-(*R*)-**15**, thus

evidencing that the RemO-catalyzed hydroxylation takes place from the *Re*-face of **41** with loss of aromaticity and planarity of ring I.

4.3. Cases where TDDFT and DFT/MRCI methods are superior to semiempirical approaches

4.3.1. TaClo (16)

TaClo (**16**) and its *N*-methylated derivative, are highly halogenated tetrahydro-β-carbolines and act as potent dopaminergic neurotoxins,[194] similar to MPTP (1-methyl-4-phenyl-1,2,3,6-tetrahydropyridine), which is known to cause Parkinson's disease in humans, monkeys and mice.[195] A particular danger of TaClo (**16**) is that, in contrast to the unnatural compound MPTP, it might readily be formed in the human organism, by spontaneous reaction of biogenic tryptamine with the therapeutically administrated hypnotic agent chloral.[196] These two substances actually gave the name for **16**, which consists of "Ta" from tryptamine and "Clo" from chloral. From the stereochemical point of view, TaClo (**16**) is a chiral compound, the two enantiomers of which were attributed in the past by CNDO calculations.[197] Although the obtained CD spectra permitted attribution of the absolute configuration of TaClo, based on the fit of the curves in the region of 200–250 nm, the first experimental band around 280 nm was yet not reproduced by these calculations. Therefore, it was of high interest whether more accurate calculations, viz. by using the semiempirical MNDO-based OM2 approach or the TDDFT method, could correctly simulate the experimental CD curve of **16**.

The renewed calculations were performed for the *R*-enantiomer of **16**. The molecule contains only one flexible part, viz. the tetrahydropyrido moiety (ring **A**, Figure 53), which may adopt four possible orientations giving two conformers with the nitrogen atom below the plane of the indole ring and the amino hydrogen in equatorial or axial positions, and two respective structures with the nitrogen above

the plane (Figure 53). According to the AM1 optimization, conformer **16**$_{conf4}$ 'up ax' is the energetically more favorable one.

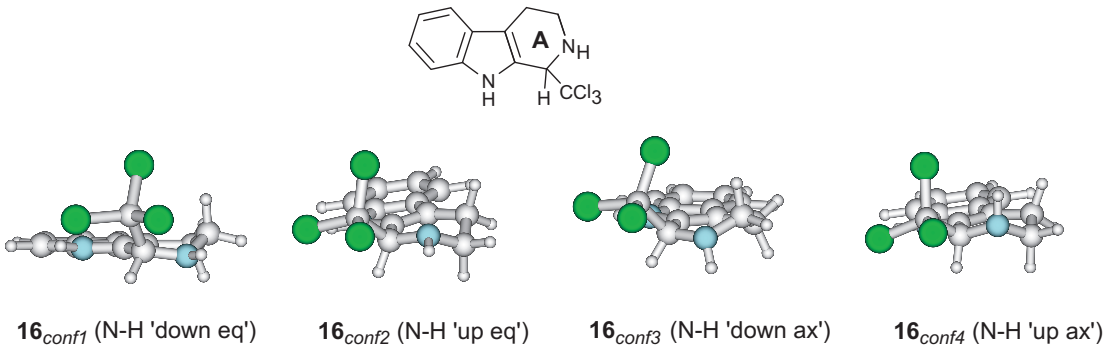

16$_{conf1}$ (N-H 'down eq') **16**$_{conf2}$ (N-H 'up eq') **16**$_{conf3}$ (N-H 'down ax') **16**$_{conf4}$ (N-H 'up ax')

$\Delta\Delta H_f$ [kcal·mol^{-1}]	**16**$_{conf1}$	**16**$_{conf2}$	**16**$_{conf3}$	**16**$_{conf4}$
AM1	1.53	3.74	0.84	0.00
RI-BLYP/SVP	0.00	1.27	1.60	2.23

Figure 53. Four conformers of TaClo (**16**) and their relative energies calculated at the AM1 and RI-BLYP/SVP levels.

As mentioned above, halogen atoms are not included in the parameter set of some semiempirical spectroscopy-oriented methods, like CNDO/S and OM2. Therefore, for the semiempirical excited-state energy computations presented here, the chlorine atoms of each conformer of **16** were replaced by hydrogens. The overall CNDO/S spectrum of (*R*)-**16** thus calculated for the AM1 optimized structures indeed matched very well the experimental curve of the first eluting enantiomer of **16**, requiring only a small blue-shift of 3 nm. A particularly good agreement was observed below 260 nm, whereas in the region of higher wavelengths only a poor matching was found (Figure 54a).[40] By contrast, the OM2-CIS calculations reproduced the first positive Cotton effect, although with too low intensity (Figure 54b). In this case, a red shift of 23 nm was necessary. Unfortunately, an additional consideration of the double excitations (OM2-SDCI) did not improve the resulting spectrum, providing even less accurate transition energy values.

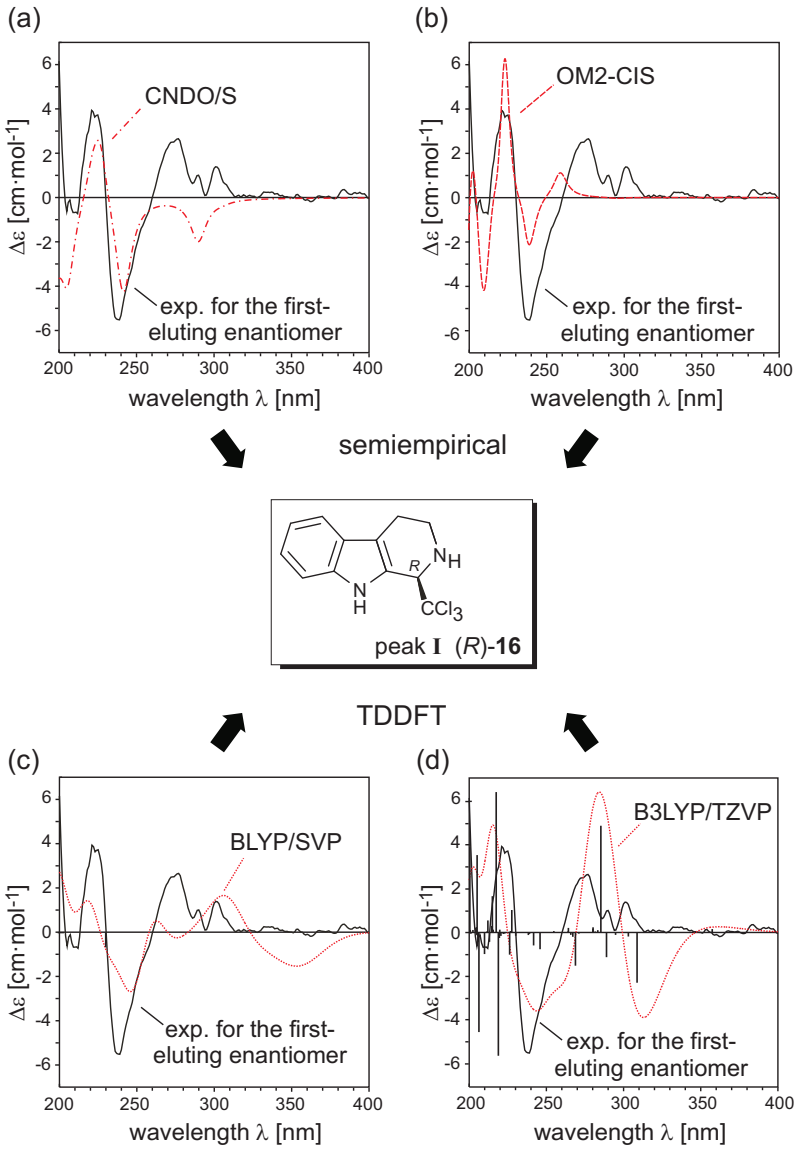

Figure 54. The results of the semiempirical [CNDO/S (a), OM2 (b)] and the time-dependent DFT calculations [BLYP/SVP (c), B3LYP/TZVP (d)] of (*R*)-TaClo (**16**).

For the time-dependent DFT calculations, the initial four structures were further optimized at the RI-BLYP/SVP level. This led to significant changes in the relative energies of the conformers as compared to the AM1 results (Figure 53), revealing conformer **16**$_{conf1}$, with the nitrogen below the β-carboline ring plane and hydrogen in the equatorial position, to be the global minimum. The same basic framework was found in the crystals of *N*-formyl-TaClo,[40] which thus proved the reliability of the DFT optimization of **16**. For the CD computations, two TDDFT methods, viz. BLYP/SVP and B3LYP/TZVP, were applied, treating the lowest 25 and 30 excited

states, respectively. In contrast to the semiempirical methods, the TDDFT calculations permitted the consideration of halogen atoms, and hence four conformers of TaClo (**16**) were calculated without any changes in the structures. While B3LYP/TZVP method predicted the excitation energies very accurately and no UV correction was required, the BLYP/SVP approach provided substantially underestimated energies, so that the resulting spectrum had to be blue-shifted by ca. 44 nm. Each of the TDDFT based CD spectrum of (*R*)-**16** reasonably reproduced all experimental CD features of the first eluting enantiomer of TaClo, including the positive band at 280 nm. According to the molecular orbital analysis of the B3LYP results, this band predominantly arises from a π–(π^* + σ^*) transition (with a weighting factor of 0.726) occurring from the HOMO orbital, which is almost completely localized at the indole ring of **16**, to the $LUMO_{+1}$. The latter one represents a combination of the π^* orbital of the β-carboline ring and σ^* orbitals of the CCl_3 unit (Figure 55). This might be a reason why semiempirical methods did not reproduce this region correctly, as chlorine atoms were not taken into consideration. The OM2-calculated transition at 265 nm with a positive rotatory strength thus should not be attributed to the experimentally observed first positive Cotton effect. Remarkably, both TDDFT calculations predicted an additional negative CD band above 310 nm, which is not present or can at least not to be seen in the experimental spectrum of TaClo (**16**). This CD signal corresponds to the intramolecular charge-transfer transition (with a weight of 0.986), appearing from the π-type $HOMO_{-1}$ orbital at the indole ring to the lowest unoccupied σ^* MO (LUMO), totally localized at the CCl_3 group (Figure 55). Evidently, an impact of this transition is overestimated by TDDFT methods, which might be attributed to the known problem of poor description of the charge-transfer transitions and of RYDBERG excited states within the currently applied exchange-correlation DFT functionals.[132]

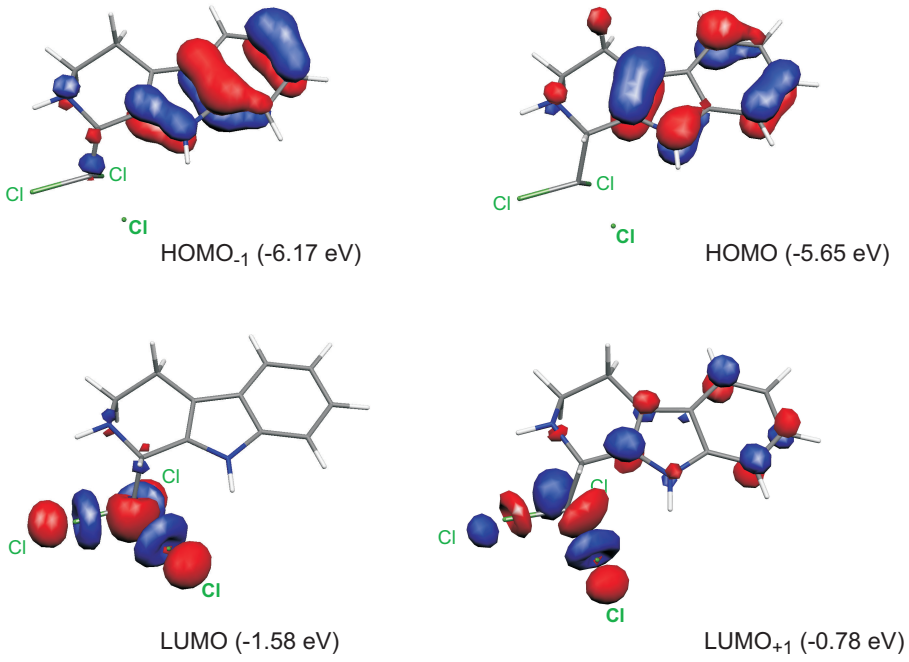

Figure 55. Two highest occupied molecular orbitals ($HOMO_{-1}$ and HOMO) and two lowest unoccupied MOs (LUMO and $LUMO_{+1}$) of TaClo (**16**).

4.3.2. Gephyromycin (17)

While in the previous example semiempirical methods correctly reproduced at least the major part of the CD spectrum and were able to provide information about the stereostructure of the compound, the investigation of the absolute configuration of the novel highly oxygenated angucyclinone gephyromycin (**17**) by these approaches was more difficult. Gephyromycin (**17**), isolated by G. Lang in cooperation with Prof. Fiedler (Tübingen) from the *Streptomyces* strain NTK 14, is the first angucyclinone that possesses an intramolecular ether bridge (Figure 56).[41] Its unique constitution and the relative configuration were unambiguously determined by G. Lang by extensive NMR measurements and further corroborated by an X-ray structure analysis (Figure 56).[41] The only item that remained unknown thus was the absolute configuration, which could be either (3*S*, 4a*S*, 6a*S*, 12a*R*, 12b*R*)-**17** or, fully opposite, (3*R*, 4a*R*, 6a*R*, 12a*S*, 12b*S*)-**17** (Figure 56, right). Prediction of the CD spectra

for both possible enantiomers and their comparison with the experimental curve of **17** was expected to give an answer.

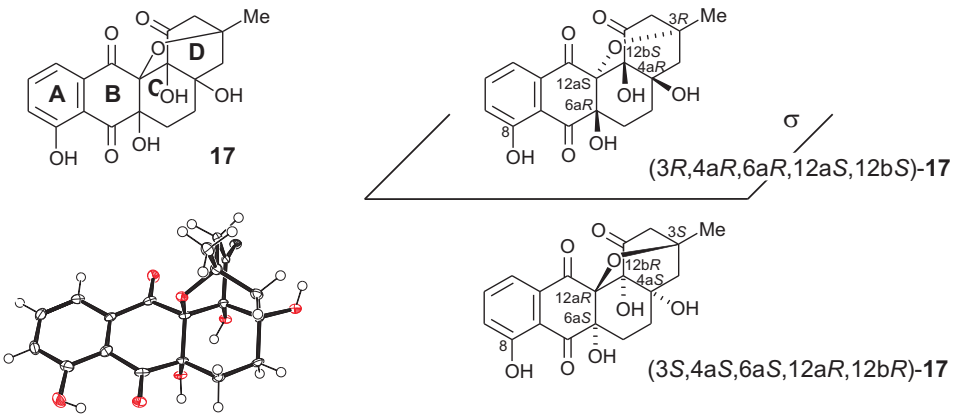

Figure 56. Gephyromycin (**17**): constitution and relative configuration from an X-ray structure analysis (left bottom), and its two possible absolute stereostructures, "*R,R,R,S,S*"-**17** (right top) and "*S,S,S,R,R*"-**17** (right bottom).

Conformational analysis of gephyromycin (**17**) was arbitrarily carried out for the "*S,S,S,R,R*"-enantiomer. The structure of the bridged tetracyclic framework of **17** appeared very rigid, and thus only the flexibility of the hydroxy functions had to be considered. The saturated six-membered ring **C** (Figure 56) acquired exclusively a chair conformation, which was also verified by the NMR data. AM1 calculations of the reaction coordinates for the rotations of all OH groups showed that the two hydroxyls at C-8 and C-4a adopt only one orientation, generating hydrogen bonds to the oxygen atoms of the keto group at C-7 ($d_{O\text{-}H}$ 1.99 Å) and the hydroxy function at C-12b ($d_{O\text{-}H}$ 2.4 Å), respectively (Figure 57). The hydroxy group at C-6a showed two possible orientations, one with the hydrogen bond to OH-12b ($d_{O\text{-}H}$ 2.12 Å) and the other with the hydrogen atom directed towards the conjugated π-system (O-H···π interaction). The remaining hydroxyl at C-12b also revealed two alignments: the first one with the hydrogen oriented towards two carbonyl groups at C-1 and C-12 and located exactly between them ($H_{OH\text{-}12b}\cdots O_{C\text{-}1}$ 2.4 Å; $H_{OH\text{-}12b}\cdots O_{C\text{-}12}$ 2.3 Å), and the second one with formation of a hydrogen bond to OH-6a ($d_{O\text{-}H}$ 2.08 Å) (as in Figure 57). The

behavior of these two hydroxyls, OH-6a and OH-12b, appeared interdependent, thus providing only two conformers (Figure 57) for further CD computations.

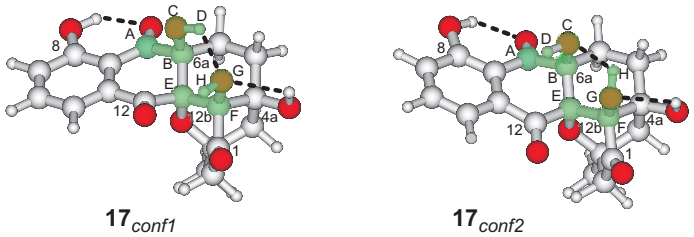

17$_{conf1}$ **17**$_{conf2}$

Conformer	$\Delta\Delta H_f$ [kcal·mol^{-1}]	θ_{ABCD} [°]	θ_{EFGH} [°]
17$_{conf1}$	0.00	-173	62
17$_{conf2}$	5.14	80	-70

Figure 57. Two AM1-based conformers of **17** differing in the orientations of the hydroxy functions at C-6a and C-12b.

The semiempirical CD calculations were performed at both, the CNDO/S and the OM2 levels. While the resulting OM2 CD spectrum predicted for the "*S,S,S,R,R*"-enantiomer of **17** moderately resembled the shape of the experimental curve of **17**, except for the lack of a broad negative band around 350 nm and a wrong sign of the band at 235 nm, CNDO/S calculations provided entirely wrong spectra (Figure 58). The fact that the OM2 method gave better results hinted at a strong n-π* character of the CD spectrum of **17**, as these transitions are rather poorly described within the CNDO approach and have been reasonably improved in the MNDO-based methods.[198] But in any case, an unequivocal configurational assignment of **17** based on the semiempirical calculations seemed impossible or insecure (Figure 58).

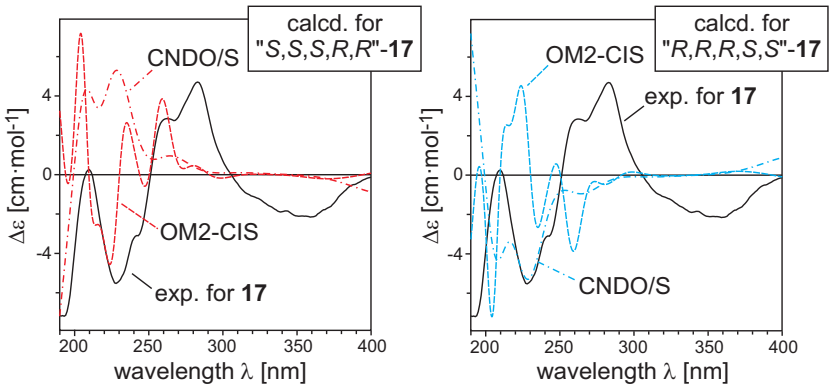

Figure 58. Results of the CNDO/S and OM2-CIS calculations for the two possible enantiomers of **17**, (3*S*, 4a*S*, 6a*S*, 12a*R*, 12b*R*)-**17** and (3*R*, 4a*R*, 6a*R*, 12a*S*, 12b*S*)-**17**.

Initially assuming that a reason for this might be a too high rigidity predicted for the set of hydroxy functions of **17** by the AM1 calculations, two other derivatives, possessing a higher flexibility around the C-OR bonds, were analyzed. These are the tetra-*O*-methylated and tetra-*O*-acetylated compounds, **17a** and **17b** (Figure 59, middle), which provided 16 and 11 conformations, respectively. As the CD spectrum of "*S,S,S,R,R*"-**17** calculated by the OM2 method showed a better agreement with the experimental curve as compared to the respective CNDO-based one, the CD calculations of both derivatives, **17a** and **17b**, were performed only at the OM2 level. Unfortunately, it appeared difficult to synthesize the fully *O*-methylated or *O*-acetylated compounds, also because of the small quantities of **17** available, and therefore the theoretical CD spectra of two enantiomers of **17a** and **17b** were directly compared with the experimental curve of the authentic gephyromycin (**17**). The UV shifts of 13 and 20 nm in the direction of higher wavelengths were applied for **17b** and **17a**, respectively. Now, the resulting overall CD spectra predicted for the "*S,S,S,R,R*"-enantiomer of **17a** and **17b** showed a reasonable agreement with the experimental CD curve of natural gephyromycin (**17**), while the ones simulated for "*R,R,R,S,S*"-**17** clearly behaved oppositely (Figure 59), thus providing a first hint at the configurational attribution of gephyromycin (**17**) as 3*S*, 4a*S*, 6a*S*, 12a*R*, 12b*R*.[41]

Another reason for the poor quality of the prediction of the CD spectrum of **17** by the semiempirical CNDO and in part the OM2 method might be an inaccurate

treatment of the molecular orbitals of such a highly constrained 2-oxa[2.2.2]bicyclooctane system in combination with an extremely high number of oxygen-containing functions in **17**, which are furthermore involved in hydrogen bond formation. Due to the increased computational resources in our group, it became possible to investigate this molecule with more exact DFT methods.

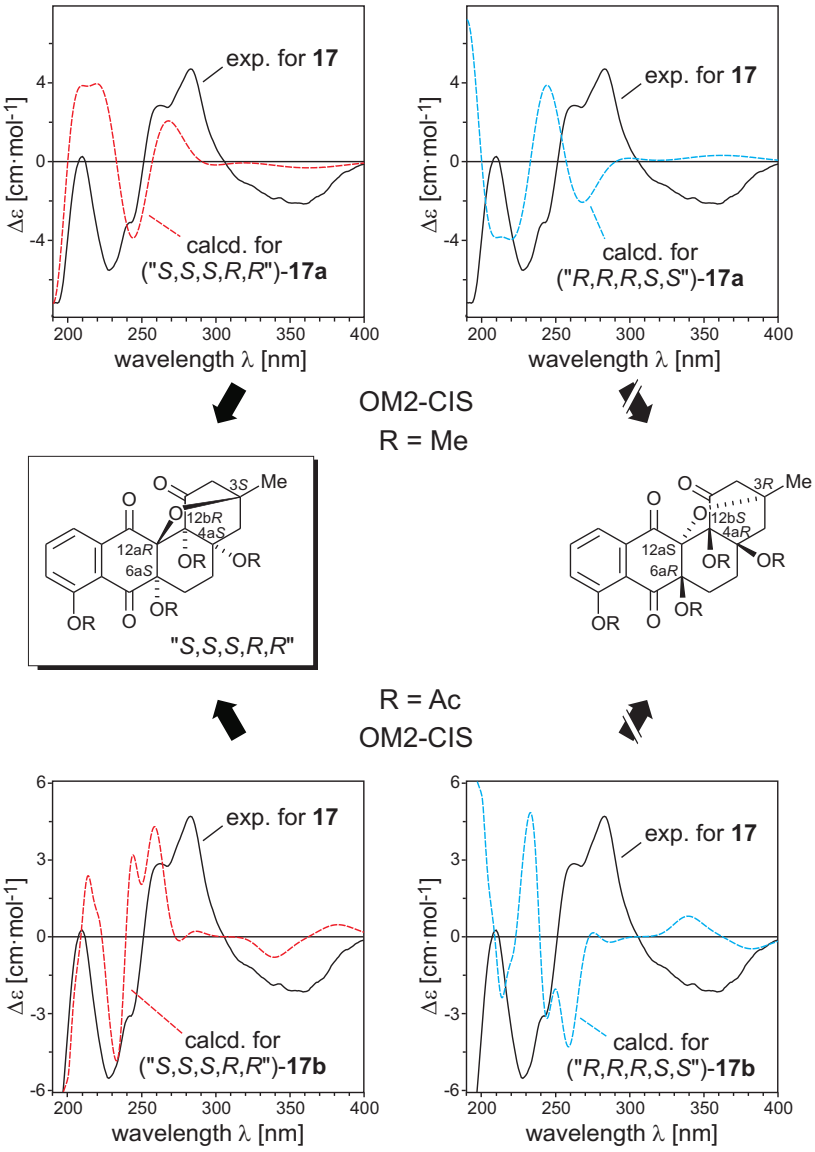

Figure 59. Comparison of the experimental CD curve of **17** with the CD spectra predicted (OM2-CIS) for the two possible enantiomers of its per-*O*-methylated and per-*O*-acetylated derivatives, **17a** and **17b**, respectively.

For the TDDFT excited-state energy calculations, the two initial AM1-based conformers of **17** were further optimized at the higher RI-BLYP/SVP level. This resulted in a small change in the structure of the global minimum conformer **17**$_{conf1}$, revealing the hydroxy group at C-12b to adopt preferably an orientation with hydrogen bond formation to the carbonyl function at C-1 ($d_{O\text{-}H}$ 1.98 Å). Furthermore, the energy difference between the two minima of **17** increased to up to 9 kcal·mol^{-1}, which made an impact of the second conformer **17**$_{conf2}$ in the overall CD spectrum of **17** almost negligible, so that only the global minimum structure was used for the CD computations.

The CD and UV spectra of gephyromycin (**17**) were now calculated by using the hybrid functional B3LYP and the TZVP basis set, considering the 30 lowest-energy excitations. Comparison of the calculated and the measured UV spectra revealed a blue shift of 16 nm. As seen in Figure 60, the accordingly UV-corrected CD spectrum predicted for "*S*,*S*,*S*,*R*,*R*"-**17** perfectly reproduced the experimental CD curve of **17**, including the broad low-intensity band with a negative CE at about 350 nm, thus firmly corroborating the above configurational attribution of gephyromycin (**17**).

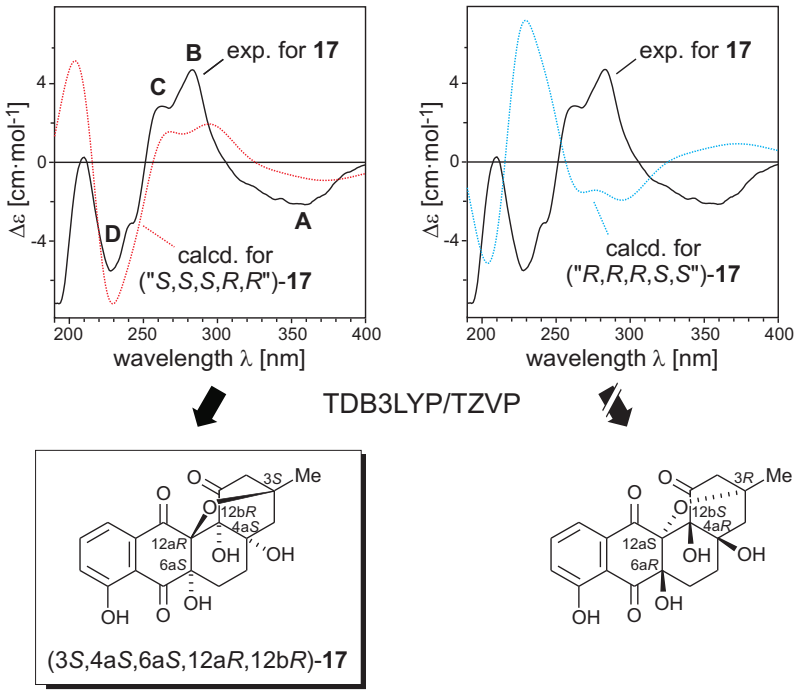

Figure 60. Determination of the absolute configuration of gephyromycin (**17**) by TDB3LYP/TZVP calculations.

A detailed analysis of the electronic excitations exhibiting large rotatory strength values showed that all bands of the CD spectrum of **17** indeed have a substantial n-π* character (Table 4 and Figure 61). Only one excitation with a large negative rotatory strength calculated at 285 nm, which corresponds to the minimum observed at 270 nm, arises from π–π*-type transitions. The most relevant occupied molecular orbitals 90 ($HOMO_{-8}$), 92 ($HOMO_{-6}$), 96 ($HOMO_{-2}$), and 97 ($HOMO_{-1}$) possess complex shapes, representing actually a conjugation of n-orbitals of the oxygen atoms of the carbonyl, the hydroxyl, and the ether groups, with σ-type orbitals of the saturated rings B, C and D, while in the case of the orbitals 94 ($HOMO_{-4}$) and 95 ($HOMO_{-3}$), a π-type orbital of ring A interacts with n MOs. The lowest unoccupied molecular orbitals 99 (LUMO) and 100 ($LUMO_{+1}$) are π* orbitals of the aromatic ring A combined with π* MOs of the carbonyl functions at C-7 and C-12, whereas the virtual orbital 101 ($LUMO_{+2}$) is an exclusively π* orbital of the keto group at C-1. These three LUMOs, 99–101, appeared adequate for an assignment of the entire CD spectrum of **17**.

Table 4. Identification of the most important excitations of gephyromycin (**17**) as calculated by the TDB3LYP/TZVP method.

Exp.	ΔE [nm]	*f*	$R \cdot 10^{-40}$ [erg·cm3]	Transition	Type of transition[a]	Weight
A	387	1×10^{-4}	-7.5	97-99	$n_{CO,COC,OH,}+\sigma_{B,C,D}-\pi^*_{A,CO}$	0.859
B	308	2×10^{-3}	12.9	95-99	$\pi_A+n_{CO,COC,OH}-\pi^*_{A,CO}$	0.267
				96-99	$n_{CO,OH}+\sigma_{B,C,D}-\pi^*_{A,CO}$	0.239
				97-100	$n_{CO,COC,OH,}+\sigma_{B,C,D}-\pi^*_{A,CO}$	0.210
	285	0.027	-32.1	94-99	$\pi_A+n_{CO,OH}-\pi^*_{A,CO}$	0.301
				98-100	$\pi_A-\pi^*_{A,CO}$	0.220
				93-99		0.170
C	276	5×10^{-3}	47.3	96-101	$n_{CO,OH}+\sigma_{B,C,D}-\pi^*_{CO-1}$	0.290
				96-100	$n_{CO,OH}+\sigma_{B,C,D}-\pi^*_{A,CO}$	0.243
				97-101	$n_{CO,COC,OH,}+\sigma_{B,C,D}-\pi^*_{CO-1}$	0.188
D	266	0.060	-42.6	92-99	$n_{CO,OH,COC}+\sigma_c-\pi^*_{A,CO}$	0.482
				94-99	$\pi_A+n_{CO,OH}-\pi^*_{A,CO}$	0.137
	245	7×10^{-3}	-17.7	97-101	$n_{CO,COC,OH,}+\sigma_{B,C,D}-\pi^*_{CO-1}$	0.219
				90-99	$\sigma_D+n_{OH,COC,CO}-\pi^*_{A,CO}$	0.146
				95-100	$\pi_A+n_{CO,COC,OH}-\pi^*_{A,CO}$	0.142
	240	0.114	-19.6	94-100	$\pi_A+n_{CO,OH}-\pi^*_{A,CO}$	0.437
				90-99	$\sigma_D+n_{OH,COC,CO}-\pi^*_{A,CO}$	0.178
	239	0.053	-10.8	90-99	$\sigma_D+n_{OH,COC,CO}-\pi^*_{A,CO}$	0.540
				94-100	$\pi_A+n_{CO,OH}-\pi^*_{A,CO}$	0.267

[a] π_A and $\sigma_{B,C,D}$ are π- and σ-type orbitals of rings A, B C, and D. $n_{CO,OH,COC}$ is an n-type orbital of the oxygen atom of the carbonyl (CO), the hydroxyl (OH), and the ether (COC) functions.

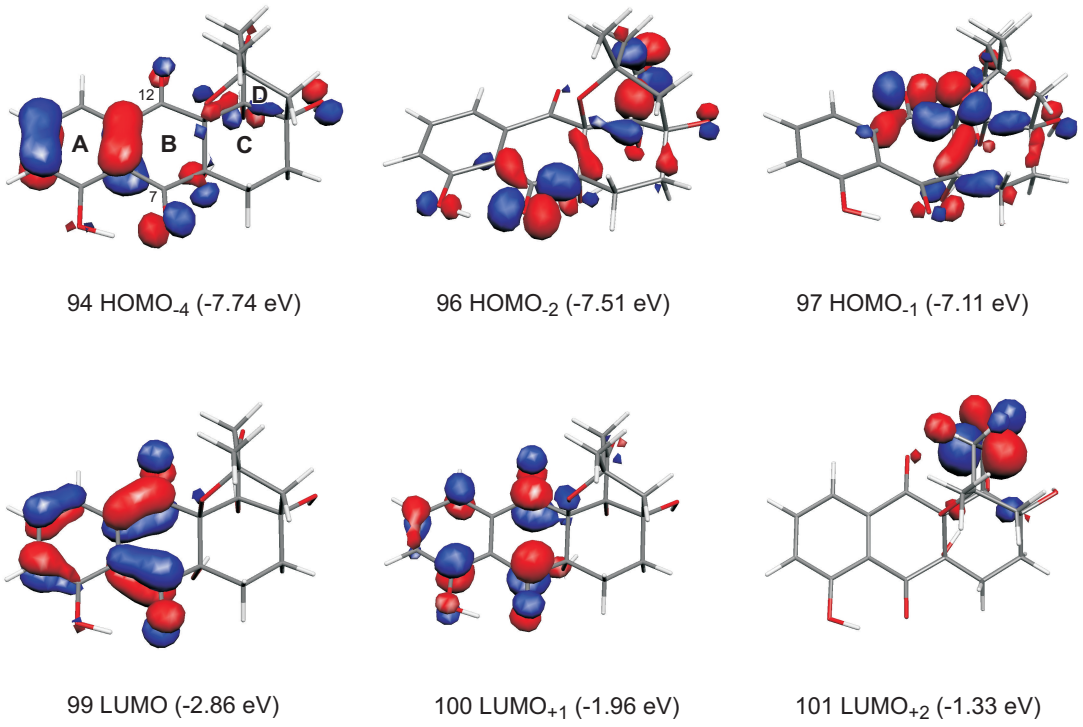

Figure 61. The most significant occupied and unoccupied molecular orbitals of gephyromycin (**17**).

It could be shown that for the description of the n–π* transitions involving such complex molecular orbitals [here the occupied (n + σ)- and (n + π)-MOs], which comprise a high number of oxygen-containing functionalities associated with strong hydrogen bonds, the higher-level DFT methods have to be preferred to the semiempirical approaches, and particularly to the CNDO/S method. A good agreement in the case of the OM2-based CD spectra of the derivatives **17a** and **17b**, in which hydrogen bonds formation was excluded, might be probably attributed to a fortunately better treatment of the respective molecular orbitals, which provided the improved results.

4.3.3. Neoechinulin A (18)

The diketopiperazine alkaloid neoechinulin A (**18**) (Figure 62) is another remarkable fungal compound for which attribution of the absolute stereostructure

could be achieved only by using TDDFT method, while semiempirical calculations provided fairly equivocal results. Neoechinulin A (**18**) together with its closest analog, neoechinulin B (**42**), has been isolated from various *Aspergillus*[199] and *Eurotium*[200] species, and has recently been identified in our group by B. Ullmann in the fungal strain R04-3-14, available from the marine sponge *Axinella damicornis*. High interest in these known natural products was stimulated by their promising biological activities, such as UV-A protective,[201] antioxidant,[202] and also neuroprotective properties,[203] which have been thoroughly investigated for neoechinulin A (**18**), but still remained unexplored for neoechinulin B (**42**). On the other hand, we were interested in the stereostructure of the diketopiperazine unit of neoechinulin A (**18**), which had previously only been assumed to be *S*-configured on the basis of feeding experiments,[204] but had not yet been confirmed by any other methods. The *Z*-configuration of the C-8-C-9 double bond of **18** had been deduced from various NMR experiments[205] and unambiguously corroborated by an X-ray structure analysis[206] (Figure 62). In view of a too small quantity of neoechinulin A available, the chemical degradation to L- or D-alanine ester appeared difficult, and therefore quantum chemical CD calculations seemed to be the most appropriate method for the determination of the absolute configuration of **18**.

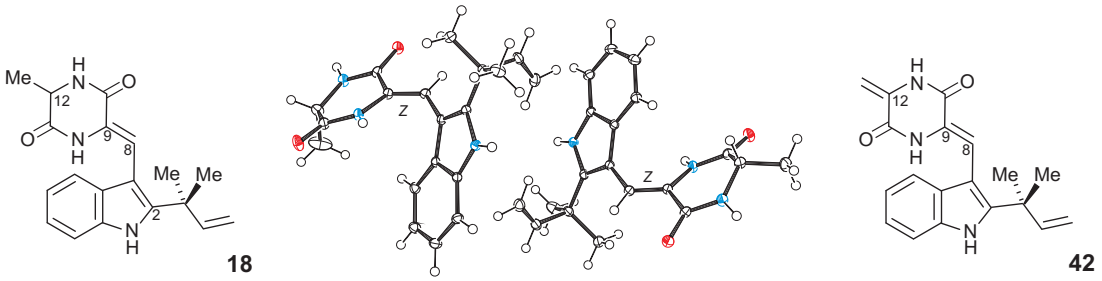

Figure 62. Neoechinulins A (**18**) and B (**42**), and an ORTEP plot of the crystal structure of **18,** demonstrating the Z-configuration at its C-8–C-9 double bond.

Investigations on the conformational behavior of neoechinulin A (**18**) were performed for the *S*-enantiomer by using the semiempirical AM1 approach. The structure of **18** revealed two flexible parts, viz. the isoprenyl group at C-2, which was

characterized by the dihedral angles θ_{ABCD} and θ_{EFGH} (Table 5, top), and the diketopiperazine ring ("ring" in Table 5), which was oriented above or below the plane of the indole ring of **18**. The latter structural feature was also found by the X-ray analysis of neoechinulin A,[206] which showed the presence of two independent molecules (with the diketopiperazine unit above and below the indole ring, Figure 62) in an asymmetric unit of **18**. AM1 calculations thus resulted in 12 conformers being in the range of 3 kcal·mol^{-1} above the global minimum, **18**$_{conf1}$ (Table 5), which was stabilized by an intramolecular N-H···π interaction between the amine proton of the indole unit and the π system of the isoprenyl double bond of **18**.

Table 5. Identification of the reaction coordinates analyzed for neoechinulin A (**18**); the AM1-BLYP/SVP-BLYP/TZVP optimized conformers of **18**, with their relative energies and characteristic dihedral angles, as well as the global minimum conformer.

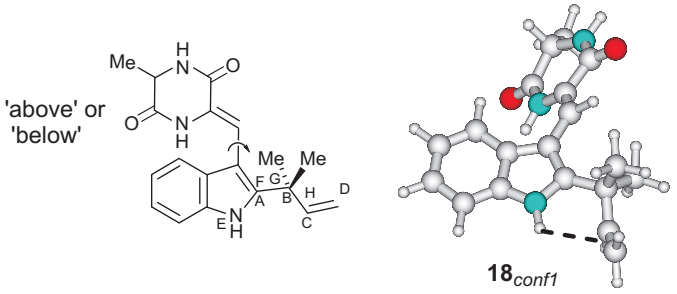

18$_{conf1}$

Conformer[a]	$\Delta\Delta H_f$ [kcal·mol^{-1}]			"ring"	θ_{ABCD} [°]		θ_{EFGH} [°]	
	AM1	BLYP			AM1	DFT[b]	AM1	DFT[b]
		SVP	TZVP					
18$_{conf1}$	0.00	0.00	0.00	below	-112	-113	16	25
18$_{conf2}$	0.03	0.28	0.13	above	112	113	-16	-23
18$_{conf3}$	0.22	0.14	0.26	below	101	115	8	-40
18$_{conf4}$	0.24	0.40	0.37	above	-101	-115	-8	38
18$_{conf5}$	0.65	0.68	0.65	above	172	124	121	119
18$_{conf6}$	0.64	1.20	1.04	above	-64	-15	122	116
18$_{conf7}$	0.95	1.16	1.38	below	172	127	139	130
18$_{conf8}$	0.71	1.76	1.79	below	-106	-119	136	124
18$_{conf9}$	0.81	1.96	1.80	above	-127	-120	109	109
18$_{conf10}$	0.19	2.20	2.15	above	-62	-64	-12	-12

Conformer[a]	$\Delta\Delta H_f$ [kcal·mol^{-1}]			"ring"	θ_{ABCD} [°]		θ_{EFGH} [°]	
	AM1	BLYP			AM1	DFT[b]	AM1	DFT[b]
		SVP	TZVP					
18$_{conf11}$[c]	0.34	as **18**$_{conf5}$						
18$_{conf12}$[c]	0.52	as **18**$_{conf3}$						
18$_{conf13}$[c]	1.03	as **18**$_{conf7}$						

[a] Numbering of the conformers corresponds to the BLYP/TZVP energies. [b] These are the BLYP/SVP calculated dihedral angles. [c] DFT optimization of these conformers leads to already present structures.

The semiempirical CNDO/S excited-state energy calculations of 13 AM1-simulated structures gave, however, unclear results. As seen in Figure 63, the overall shape of the averaged CD spectrum[c] predicted for the *S*-enantiomer of **18** largely resembled the measured curve of (–)-neoechinulin A (**18**), giving a preference for the *S*-configuration. However, the first CD band calculated at 233 nm with a negative sign had no correspondence to the experimental features and, furthermore, the next two positive and one negative bands were substantially shifted as compared to the respective experimental Cotton effects (Figure 63a), so that the definite CD-peaks attribution and, consequently, the configurational determination, appeared difficult. The CD spectrum of (*S*)-**18** calculated by the OM2 method[a] showed an even worse agreement with the measured curve, predicting the wrong sign for the CD signal at 215 nm.

[c] According to the UV correction, the CNDO/S and OM2 calculated CD spectra of **18** were red-shifted by 15 and 35 nm, respectively.

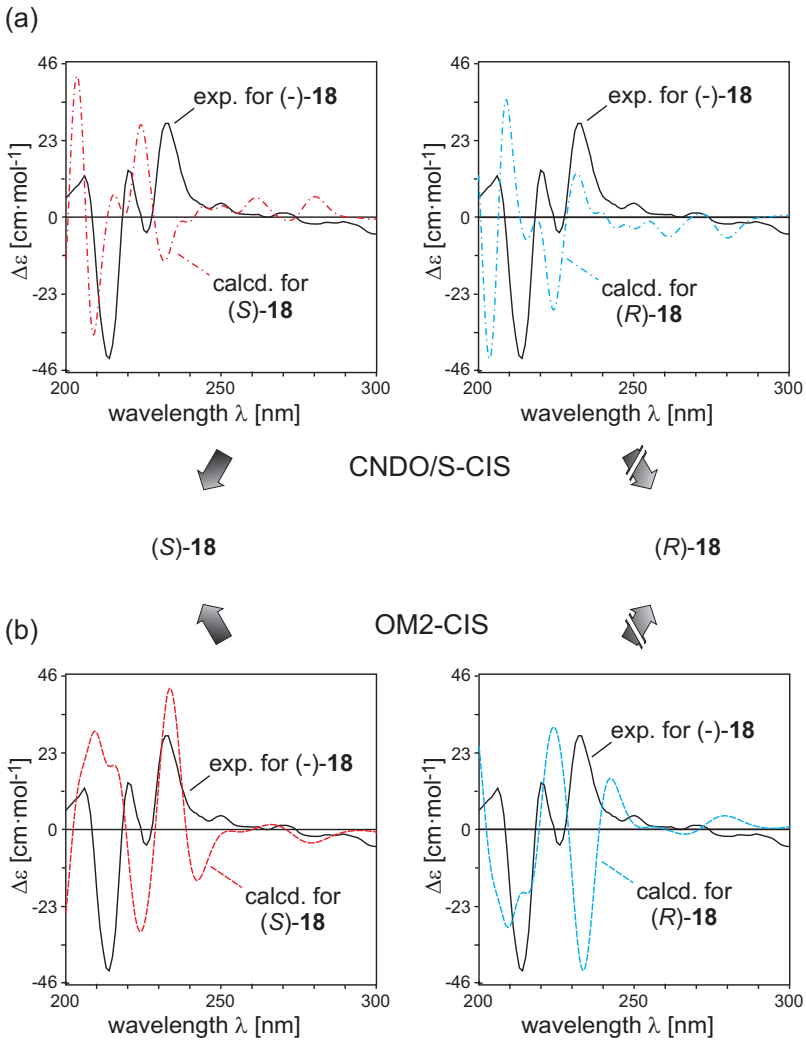

Figure 63. Comparison of the measured CD curve of (–)-**18** with the CNDO/S- (a) and OM2-CIS-based (b) CD spectra calculated for (*S*)-**18** and (*R*)-**18**.

The problems in the prediction of the CD spectrum of **18** by semiempirical methods might probably be related to the particular structure of neoechinulin A (**18**), viz. to the presence of two sets of helical conformers (with the diketopiperazine ring "above" and "below", Figure 64, left). These conformers, although possessing the same absolute configuration at the stereogenic center and, thus, being diastereomers, still adopt near-enantiomeric orientations of the chromophores, thus providing virtually opposite CD spectra (Figure 64, right). Since the theoretical overall CD curve is substantially determined by the conformer distribution and, hence, is highly sensitive to the accuracy of the calculated relative energies of the conformers, a more

exact method for the structure and energy optimization was required. For this purpose the DFT approach employing the BLYP functional in conjugation with two different basis sets, viz. SVP and TZVP, was applied.

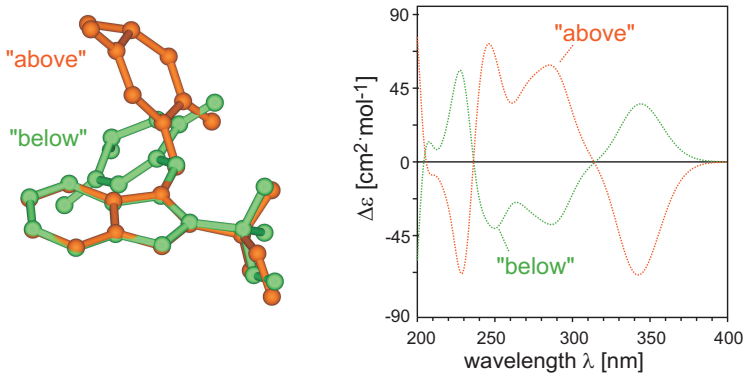

Figure 64. The two conformers of neoechinulin A (**18**) being of the same absolute configuration but possessing pseudo-enantiomeric chromophoric frameworks (on the left), which provided mirror-image like CD spectra (on the right).

The BLYP/SVP optimization reduced the number of the conformers to ten and, furthermore, gave substantially different relative energies as compared to the AM1 results (Table 6). The subsequent application of the larger TZVP atomic basis set resulted in very similar energies, and no changes in the structures of the conformers were identified. The repeated semiempirical CD calculations on the DFT-optimized structures provided slightly better results, which, however, were not sufficient for an unambiguous configurational attribution. This evidenced that the errors did not only originate from the optimization step, but also from the inexact semiempirical treatment of the excited states. Therefore, CD spectra of **18** were calculated using the TDB3LYP/TZVP method, taking into account the 40 lowest excitations. According to the UV correction, the resulting spectra required shifts of 15 nm to higher wavelengths region. Analysis of the electronic excitations corresponding to the experimental features **A**–**D** (Figure 65 and Table 6) showed that the first positive Cotton effect **A** at 235 nm arises from the π-π^*-type transitions occurring from the occupied molecular orbitals 84–86 to the virtual MOs 88 and 91, which are mostly

located at the indole ring and at the C-8-C-9 double bond. The second positive band **C** at 220 nm can be attributed to the n–π* and π–π* transitions preferentially appearing within the diketopiperazine ring, whereas the strong negative band **D** comprises many excitations, of which most have a π–π* (indole ring) character (Table 6).

Table 6. Characterization of the TDB3LYP/TZVP calculated electronic excitations of neoechinulin A (**18**) corresponding to the experimental features **A**–**D**.

Peak	ΔE [nm]	*f*	$R \cdot 10^{-40}$ [erg·cm3]	Transition	Type of transition	Weight
A	233	0.118	53.4	84-88	$\pi_{indole,C=C}-\pi^*_{indole}$	0.719
	229	0.284	48.0	86-91	$\pi_{indole,C=C}-\pi^*_{indole}$	0.375
				85-88	$\pi_{indole}-\pi^*_{indole}$	0.166
				84-91	$\pi_{indole,C=C}-\pi^*_{indole}$	0.111
B	213	0.058	-11.2	84-90	$\pi_{indole,C=C}-\pi^*_{diketopiperazine}$	0.615
C	209	9×10^{-3}	5.0	83-88	$n_{CO}+\pi_{CONH}-\pi^*_{indole}$	0.660
	203	0.021	16.8	86-95	$\pi_{indole,C=C}-\sigma^*_{indole}$	0.422
				85-91	$\pi_{indole}-\pi^*_{indole}$	0.119
	202	0.011	8.7	83-90	$n_{CO}+\pi_{CONH}-\pi^*_{diketopiperazine}$	0.362
				82-90	$n_{CO}-\pi^*_{diketopiperazine}$	0.316
D	198	0.059	-16.5	85-92	$\pi_{indole}-\sigma^*_{indole}$	0.232
				81-88	$\pi_{CONH}+n_{CO}-\pi^*_{indole}$	0.138
				82-90	$n_{CO}-\pi^*_{Diketopiperazine}$	0.126
				85-91	$\pi_{indole}-\pi^*_{indole}$	0.123
	196	0.061	-37.9	85-91	$\pi_{indole}-\pi^*_{indole}$	0.258
				82-90	$n_{CO}-\pi^*_{Diketopiperazine}$	0.137
	195	0.398	-75.6	84-91	$\pi_{indole,C=C}-\pi^*_{indole}$	0.486

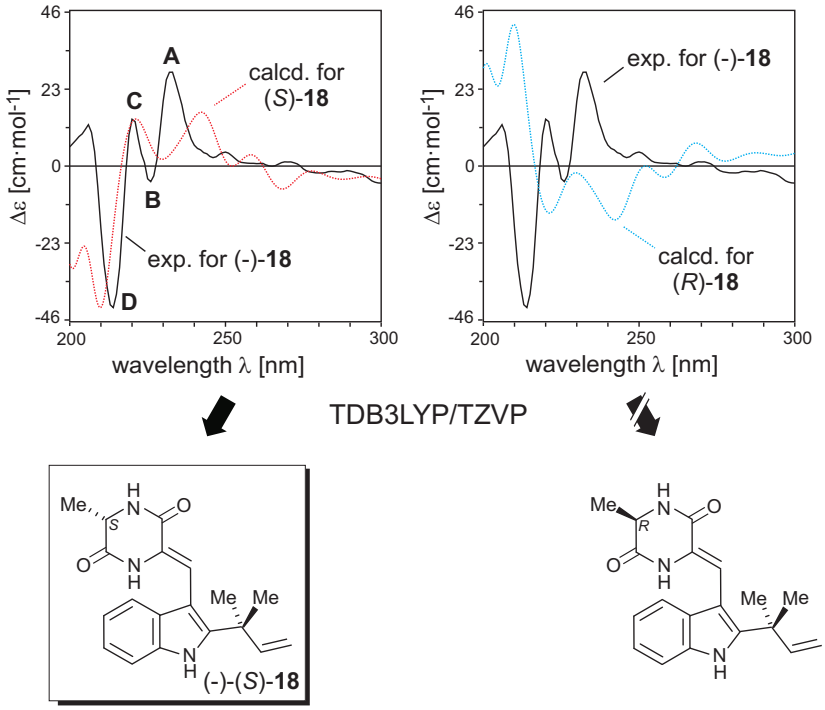

Figure 65. Elucidation of the absolute configuration of (–)-neoechinulin A (**18**) by comparison of its experimental CD spectrum with the TDB3LYP/TZVP predicted curves.

Finally, the TDDFT-based CD curve calculated for (*S*)-**18** properly reproduced the experimental CD spectrum of (–)-neoechinulin A (**18**), whereas the one predicted for (*R*)-**18** showed an opposite behavior. Consequently, the absolute configuration of the naturally predominant enantiomer of neoechinulin A, (–)-**18**, was unambiguously determined to be *S*. As short time after these results were obtained, a Japanese group (Prof. Kobayashi, Tokyo) reported on the first enantio-selective total synthesis of (-)-neoechinulin A,[207] which additionally confirmed the quantum chemically achieved configurational attribution.

4.3.4. Knipholone (19)

Knipholone (**19**) is the first isolated and structurally characterized representative of the young class of naturally occurring 4-phenylanthraquinones. It was discovered by Dagne and Steglich in 1984 in the Ethiopian torch lily *Kniphofia foliosa*,[208] and later in two *Bulbine* species.[209] Phenylanthraquinones, and particularly knipholone (**19**),

are remarkable due to their various pharmacological activities, such as antimalarial[210] and antitumoral,[211] along with an inhibition of leukotriene formation.[212] The constitution of **19** was derived from spectroscopic investigations and from reductive degradation to the known products, chrysophanol (**43**) and 4,6-dihydroxy-2-methoxyacetophenone (**44**) (Scheme 2a).[208] The absolute configuration at the rotationally hindered biaryl axis of knipholone (**19**) was investigated by quantum chemical CD calculations in 1999[213] and 2001.[214] The first CD studies were based on the BOLTZMANN procedure employing the semiempirical PM3 approach for the conformational optimization, and the CNDO/S method for the calculations of the CD spectra. Within the second approach,[214] the conformational behavior of **19** was investigated by MD simulations with the MM3 force field. In this case, the CD computations were likewise performed at the CNDO/S level. In both cases, the main (dextrorotatory) atropo-enantiomer of **19** was deduced to have the *M*-configuration (Scheme 2b).

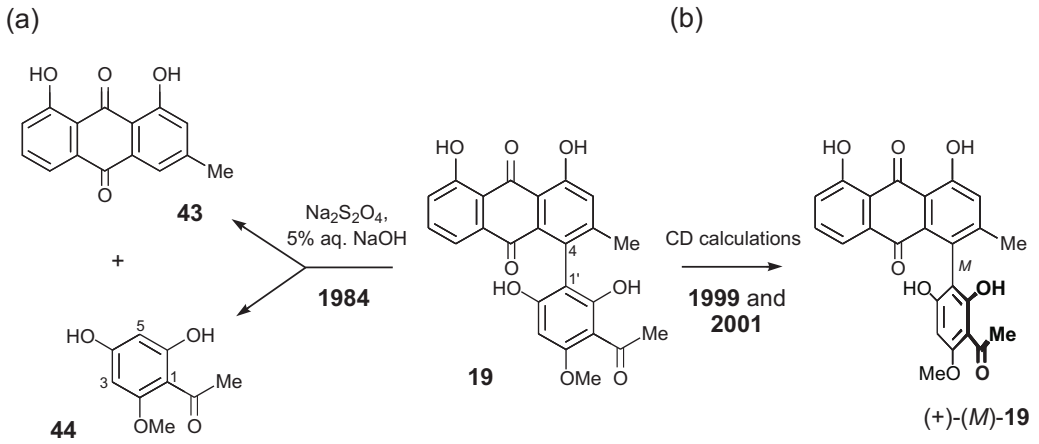

Scheme 2. Structure of knipholone (**19**) as determined by reductive cleavage of the biaryl axis (a), and its absolute axial configuration deduced from the earlier CD calculations.

In view of this stereochemical assignment, the result of the first, atropo-enantioselective total synthesis of knipholone (**19**) and other related phenylanthraquinones,[214,215] following the lactone concept,[172] was unexpected.

Going into details, the key step of this synthesis was the enantioselective ring cleavage reaction of the configurationally unstable biaryl lactone **45** by using the CBS system (oxazaborolidine **46** · BH_3) (Scheme 3a). Previous experience with quite a broad variety of different model biaryl lactones of type **A** (Scheme 3b) and the application of this method to a series of most diverse natural biaryls[216] have evidenced that the cleavage of any lactone **A** with the *S*-enantiomer of the CBS catalyst [(S)-**46**] should lead to a product **B**, i.e., with the phenolic OH group down (Scheme 3b, top). Consequently, the use of (*R*)-**46** should give *ent*-**B**, with the OH group up (Scheme 3b, bottom).

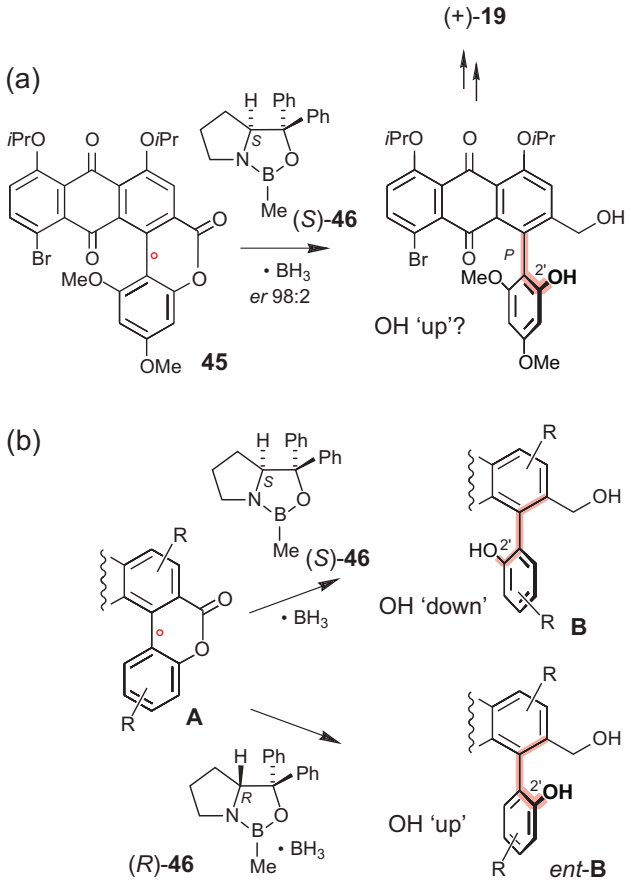

Scheme 3. The initially assumed stereochemical course of the atroposelective lactone-ring opening of the 'knipholone lactone' **45** with the (*S*)-CBS reagent [(S)-**46**] as the key step in the first total synthesis of (+)-knipholone (**19**) (a), and 'usual' stereochemical course of such reaction with other biaryl lactones (b).

Therefore, for the synthesis of the naturally predominant, dextrorotatory form of knipholone, (+)-**19**, with its assumed *M*-configuration, i.e., with 2′-OH up, the *R*-enantiomer of **46** was initially used. However, this resulted in the 'wrong' laevorotatory enantiomer of **19**, so that (*S*)-**46** had to be taken to reach the natural product. In the course of the intensive investigations of the lactone cleavage reactions for the preparation of many different axially chiral biaryls, it was noticed that the synthesis of knipholone (**19**) is actually the only exception to the otherwise fully reproducible stereochemical course of such reactions. This not understandable inconsistency gave rise to the first doubts about the correctness of the configurational assignment of **19**. A second hint was the newly measured CD spectra of **19** recently obtained from diverse sources, including cleavage products of novel-type dimeric phenylanthraquinones. These CD spectra were found to be partially different from the previously reported ones, i.e., from the one that had been the basis for the configurational assignment in 1999. Therefore, these two facts, viz. the seemingly inconsistent lactone cleavage direction and the new CD measurements, together with the more accurate computational methods available meanwhile, warranted a systematic re-investigation of the absolute configuration of knipholone (**19**).[38]

The renewed investigations of the absolute configuration of **19** were again based on CD computations, but now using more advanced methods, viz. the TDDFT[29] and DFT/MRCI[30] approaches. In analogy to the previous theoretical work, a comprehensive conformational analysis of the (*M*)-atropo-enantiomer of **19** was performed at the semiempirical PM3 level. During this procedure all flexible parts of the molecule, namely the anthraquinone ring, the acetyl function at C-3′, the methoxy substituent at C-4′, and the two hydroxy groups at C-2′ and C-6′ were analyzed, resulting in the same twelve conformers as had been reported by J. Kraus.[213,217] The remarkable features of the PM3-based optimization were the pronounced 'concave' and 'convex' curvatures of the anthraquinone ring of **19** (Figure 66a) and the twisted orientations of the acetyl group at C-3′ with respect to

the phenyl ring (Figure 66b), attaining even a perpendicular position if no hydrogen bonding to the acetyl oxygen occurred.

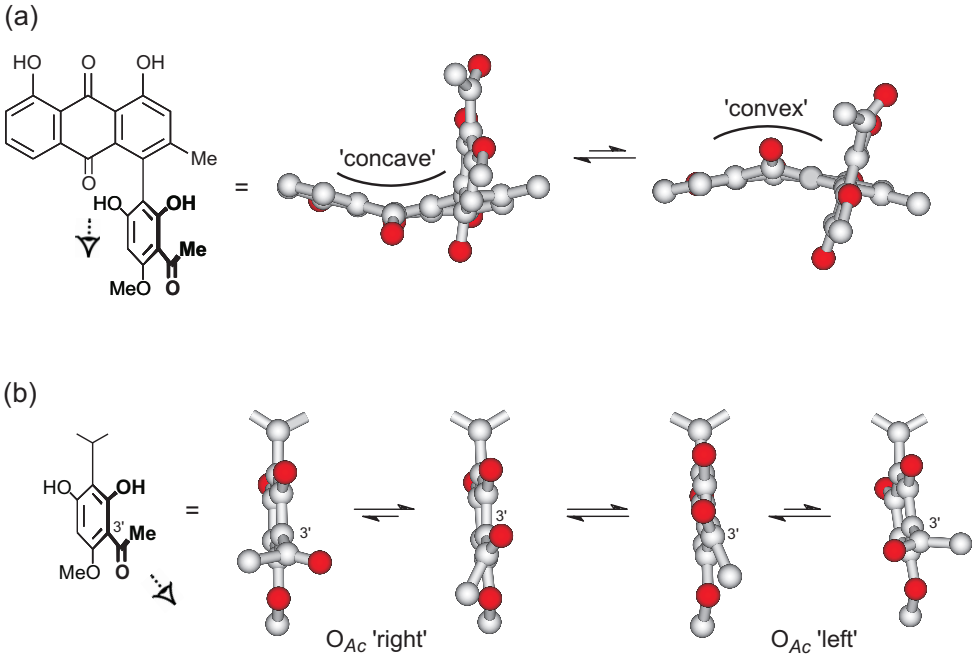

Figure 66. Some conformational features of the PM3-optimized knipholone (**19**): 'concave' and 'convex' curvatures of the anthraquinone ring (a), and twisting of the acetyl group relative to the phenyl plane (b).

Further optimizations of these structures by the DFT-based RI-BLYP/SVP method revealed only two relevant conformers within an energetic cut-off of 3 kcal·mol^{-1}. These two minima differed in the dihedral angle θ_{ABCD} at the biaryl axis (Figure 67), which adopted a value of –109° in the global minimum conformer and –79° in the second minimum structure. The global minimum was stabilized by formation of a strong hydrogen bond ($d_{O\text{-}H}$ 1.70 Å) between the hydroxy function at C-6′ and the carbonyl at C-10 (Figure 67, left). The respective conformers with the OH-6′ group down were found to be much higher in energy (more than 5 kcal·mol^{-1}) and therefore were not taken into consideration.

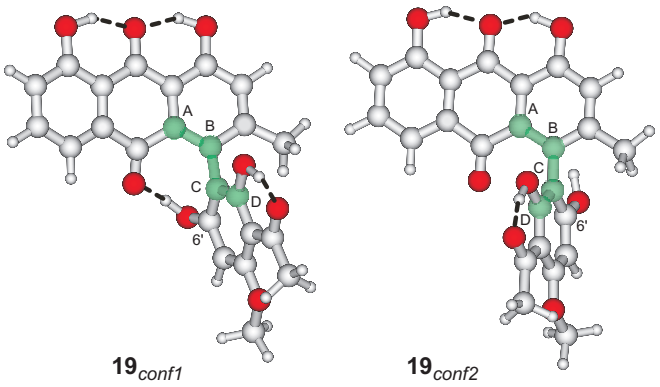

19$_{conf1}$ **19**$_{conf2}$

$\Delta\Delta H_f$ [kcal·mol^{-1}]	**19**$_{conf1}$ (θ_{ABCD})	**19**$_{conf2}$ (θ_{ABCD})
BLYP/SVP	0.00 (-109°)	1.31 (-79°)
BLYP/TZVP	0.00 (-104°)	0.39 (-94°)
B3LYP/TZVP	0.00 (-104°)	0.16 (-92°)
f_i^{B3LYP}	0.57	0.43

Figure 67. Two minimum structures of the *M*-enantiomer of knipholone, (*M*)-**19**, differing in the dihedral angle at the biaryl axis; the relative energies of these two conformers as calculated by the BLYP/SVP, BLYP/TZVP, and B3LYP/TZVP methods, and the weighting factors for the B3LYP optimized structures.

In contrast to the semiempirical results, the DFT-optimized conformers of **19** showed neither 'concave' nor 'convex' curvatures of the anthraquinone ring, but rather exhibited an almost planar orientation, yet with a small degree of distortion due to the presence of the hydrogen bond in the presumable global minimum structure. In the second conformer of **19** the anthraquinone ring was even fully planar. Furthermore, again different from the semiempirical calculations, the acetyl group at C-3' revealed only one energetically preferred orientation, viz. lying in the phenyl plane, with formation of a strong hydrogen bond to the hydroxy function at C-2'. These conformational arrays constitute an important issue, since the geometries of the chromophoric frameworks, i.e., the anthraquinone portion and the acetophenone ring, and their orientations appear critical for the quality of the subsequently calculated excited-state wavefunctions, and hence for the resulting accuracy of the final CD spectrum. Therefore, these two minima were further optimized by applying a better method without the RI approximation and by using a

significantly enlarged basis set, namely B3LYP/TZVP. As a result, no significant changes in the geometries of the conformers were observed, but the difference between the BLYP/SVP- and B3LYP/TZVP-based relative energies of the two conformers was found to be rather large, more than 1 kcal·mol^{-1} (Figure 67). The optimization at the BLYP/TZVP level reduced the relative-energy difference to 0.39 kcal·mol^{-1}, which was nearer to the B3LYP-based results, thus evidencing that in this case the basis set used has a stronger influence on the energy difference than the functional.

The excited-state energy calculations were performed with the TDDFT method by using the B3LYP functional and the TZVP basis set, and by the DFT/MRCI approach with the standard BHLYP hybrid functional and the SVP atomic-orbitals basis. The TDDFT-based CD spectra of the two conformers of **19** were very similar. Therefore, the more costly DFT/MRCI calculations were carried out only for the global minimum structure, and by applying a configuration selection cut-off of 0.8 E_h.[15] The single CD and UV spectra calculated by the TDDFT approach for the individual conformers of **19** were added up according to their B3LYP/TZVP energies following the Boltzmann statistics. The resulting theoretical CD and UV spectra were compared with the newly measured curves of (+)-knipholone [(**+**)-**19**] (Figure 68).

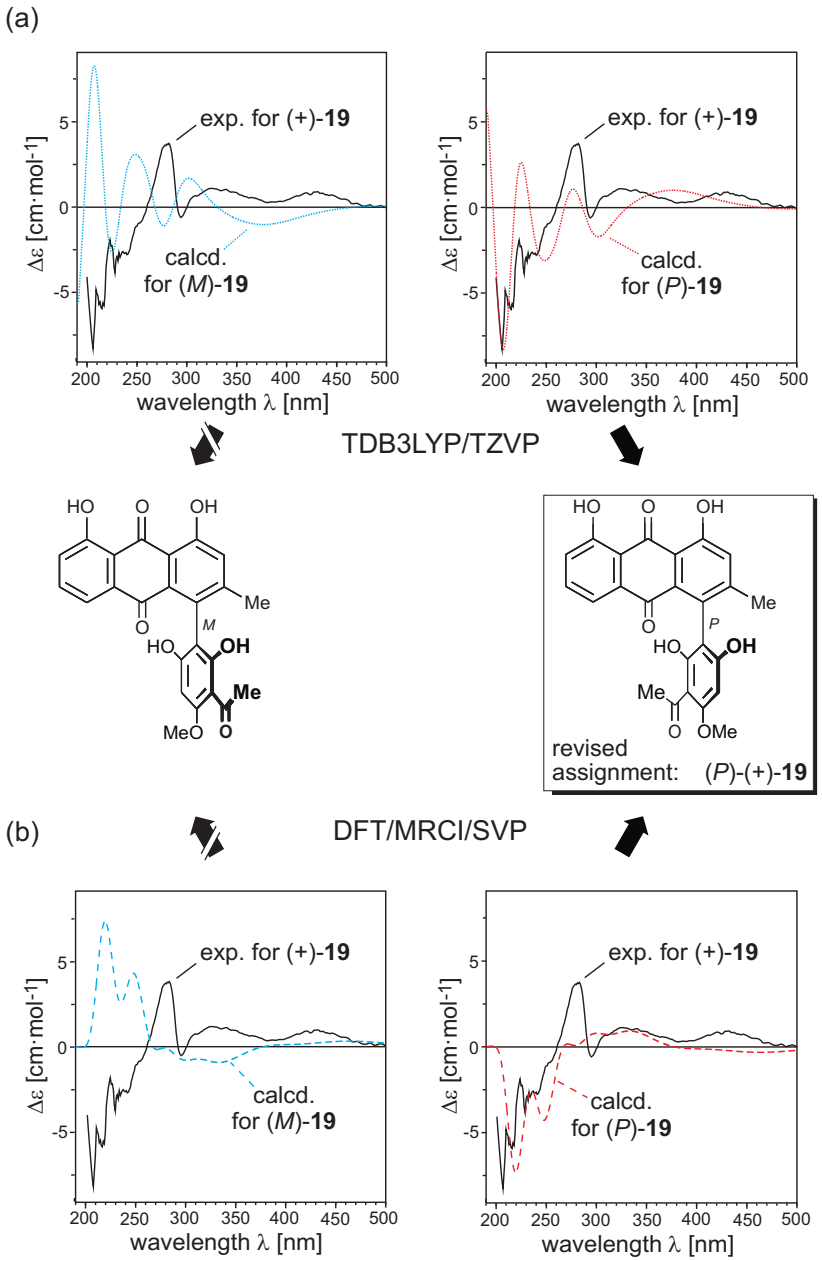

Figure 68. Results of the TDB3LYP/TZVP (a) and DFT/MRCI/SVP (b) CD calculations for (*M*)-**19** and (*P*)-**19**, and their comparison with the experimental CD spectrum of (+)-**19** measured in methanol.

The comparison of the measured UV curve of **19** with the TDDFT-based spectrum revealed that the calculated excitation energies were overestimated by approximately 0.2–0.3 eV (corresponding to 10 nm) with respect to the first three experimental UV bands.[38] Therefore, the corresponding CD spectra predicted for (*M*)- and (*P*)-**19** were red-shifted by 10 nm in comparison to the experimental CD

curve of (+)-**19**, according to the UV correction.[14] The CD spectrum calculated for (*M*)-**19** showed an unambiguously opposite behavior as compared to the measured CD curve, whereas the spectrum predicted for the *P*-enantiomer matched the experimental one of (+)-**19** very well, including the broad low-intensity bands around 350 and 430 nm (Figure 68a), thus clearly indicating that (+)-**19** is *P*-configured, and not *M* as had initially been assigned![213,214]

The same results were obtained from the DFT/MRCI calculations. In this case, however, the UV correction revealed[38] that the calculated CD spectra of **19** can be compared with the experimental data without any shift (Figure 68b). Despite the underestimated intensity of the third positive CD band at 270 nm, the CD spectrum of (*P*)-**19** reproduced the experimental spectrum with a reasonable accuracy, permitting to confirm the above revised absolute axial configuration of (+)-knipholone, (+)-**19**, as *P*.

The most probable reason for the former erroneous configurational assignment is the treatment of the molecule merely at a semiempirical level for both steps, the optimization and the CD computations, or, in the case of the MD simulations, by simply using empirical force field calculations for the conformational search. This assumption was indirectly confirmed by the fact that even optimization of the minimum structures at the RI-BLYP/SVP level for the ensuing CD calculations provided ambiguous results regarding the required UV correction[38] (not shown here). Evidently that for calculating such molecules with structurally challenging chromophores (here the anthraquinone and acetophenone portions), great caution is needed when using only semiempirical methods.

4.3.5. Knipholone anthrone (20)

Knipholone anthrone (**20**), which is the reduced analog of knipholone (**19**), is likewise a natural product displaying significant antimalarial[210] and antioxidant[218] activities. It was isolated by Dagne and Yenesew in 1993 from the stems of *Kniphofia foliosa*.[219] In analogy to the parent compound **19**, the absolute axial configuration of

knipholone anthrone (**20**) was independently determined by semiempirical CD calculations,[213,214] attributing the dextrorotatory atropo-enantiomer of **20** to possess the *M*-configuration [(+)-(*M*)-**20**]. The direct comparison of the experimental CD spectra of these two, although closely related compounds, was not possible due to the different type of the 'upper' chromophores, viz. the anthrone system in **20** vs the anthraquinone ring in knipholone (**19**).

After having evidenced the apparently wrong initial attribution of the absolute configuration of knipholone (**19**) and with its now successful and unequivocal revision, it became necessary to re-investigate the absolute stereostructure of its anthrone (**20**). This was particularly important also in view of the newly measured CD curve of knipholone anthrone (**20**). The recent CD measurements of several freshly prepared samples of **20**, isolated from various sources and prepared in different solvents, resulted always in the same CD pattern, which, however, revealed two additional intense CD signals above 280 nm, which were not to be seen in the old spectrum of **20**. These spectral differences may certainly be ascribed to a partial decomposition of the chemically less stable compound knipholone anthrone (**20**) (Figure 69).

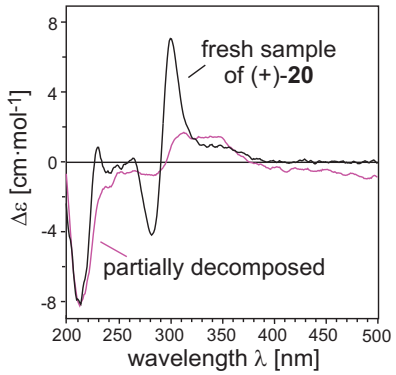

Figure 69. Comparison of the CD spectra of freshly dissolved knipholone anthrone (+)-(**20**) and of the partially decomposed sample of **20**, the latter one resembling the old CD spectrum used for the configurational assignment in 1999.[213]

The re-measured spectrum of **20**, itself, seemed to be indicative of the wrong initial assignment of the absolute configuration of knipholone anthrone (**20**). The CD

couplet with the first positive Cotton effect (CE) at 300 nm and the second negative one at 280 nm of almost identical intensities (Figure 69) resembled a classical exciton couplet arising from the interaction between the acetophenone[220] and anthrone[221,222] chromophores. According to the *Exciton Chirality Method*,[84] this CD split should indicate a 'positive chirality', which would correspond to a *P*-configuration of **20**, whereas *M*-configured knipholone anthrone [as assumed for (+)-**20**] would be expected to be a case of a 'negative chirality' (Figure 70).

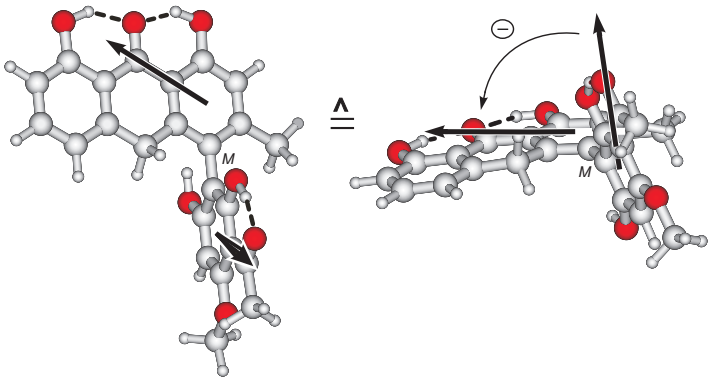

Figure 70. Expected negative Cotton effect for (*M*)-knipholone anthrone (**20**) with its 'negative chirality', following the *Exciton Chirality Method*.

To finally clarify the configurational assignment at the biaryl axis of knipholone anthrone (**20**), higher-level theoretical CD investigations were again undertaken. Starting with the *M*-enantiomer of **20**, all flexible parts of the molecule, viz. the biaryl axis, the acetyl group, and the two hydroxy functions at C-2' and C-6', were investigated at the AM1 level. According to earlier semiempirical calculations,[213] the anthrone ring of **20** showed only a planar orientation (i.e., without curvatures). The AM1-based conformational search revealed eight conformers, which were further submitted to the BLYP/SVP optimization. As a result, two minimum conformers with a different orientation at the biaryl axis were found (Figure 71). The calculations showed that for the hydroxy group at C-6' the 'up' orientation is the more favorable one (analogous to **19**), while the conformers with OH-6' down were by ca. 4 kcal·mol^{-1} higher in energy. The subsequent B3LYP/TZVP optimization of

two minimum structures revealed only one conformer to be stable, namely the one with the dihedral angle θ_{ABCD} of -80° (**20**$_{conf01}$) at the biaryl axis.

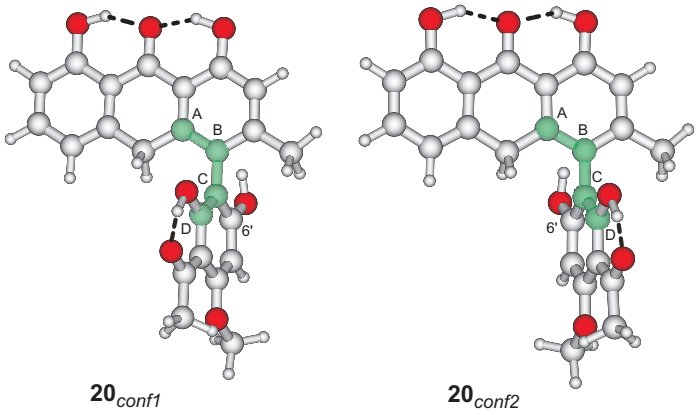

20$_{conf1}$ **20**$_{conf2}$

$\Delta\Delta H_f$ [kcal·mol^{-1}]	**20**$_{conf1}$ (θ_{ABCD})	**20**$_{conf2}$ (θ_{ABCD})
BLYP/SVP	0.00 (-76°)	0.26 (-103°)
B3LYP/TZVP	0.00 (-80°)	turned to **20**$_{conf1}$

Figure 71. Two BLYP/SVP calculated minimum conformers of knipholone anthrone [(*M*)-**20**], which finally conversed to one global minimum, viz. **20**$_{conf01}$, after optimization at the B3LYP/TZVP level.

The CD and UV spectra of **20** were calculated by using the same approaches as for compound **19**, i.e., the TDB3LYP/TZVP method and the DFT/MRCI (BHLYP/SVP) approach. The comparison of the experimental UV curve of **20** with the theoretical ones, predicted by both methods, showed that the excitations corresponding to the first three experimental bands were overestimated in energy by 0.3–0.4 eV (i.e., by ca. 15 nm), so that the calculated UV spectra had to be shifted to higher wavelengths by 15 nm.[38] The same wavelength shift was applied to the theoretical CD spectra of **20**, which were then compared with the newly-measured CD curve of (+)-knipholone anthrone [(+)-**20**] (Figure 72).

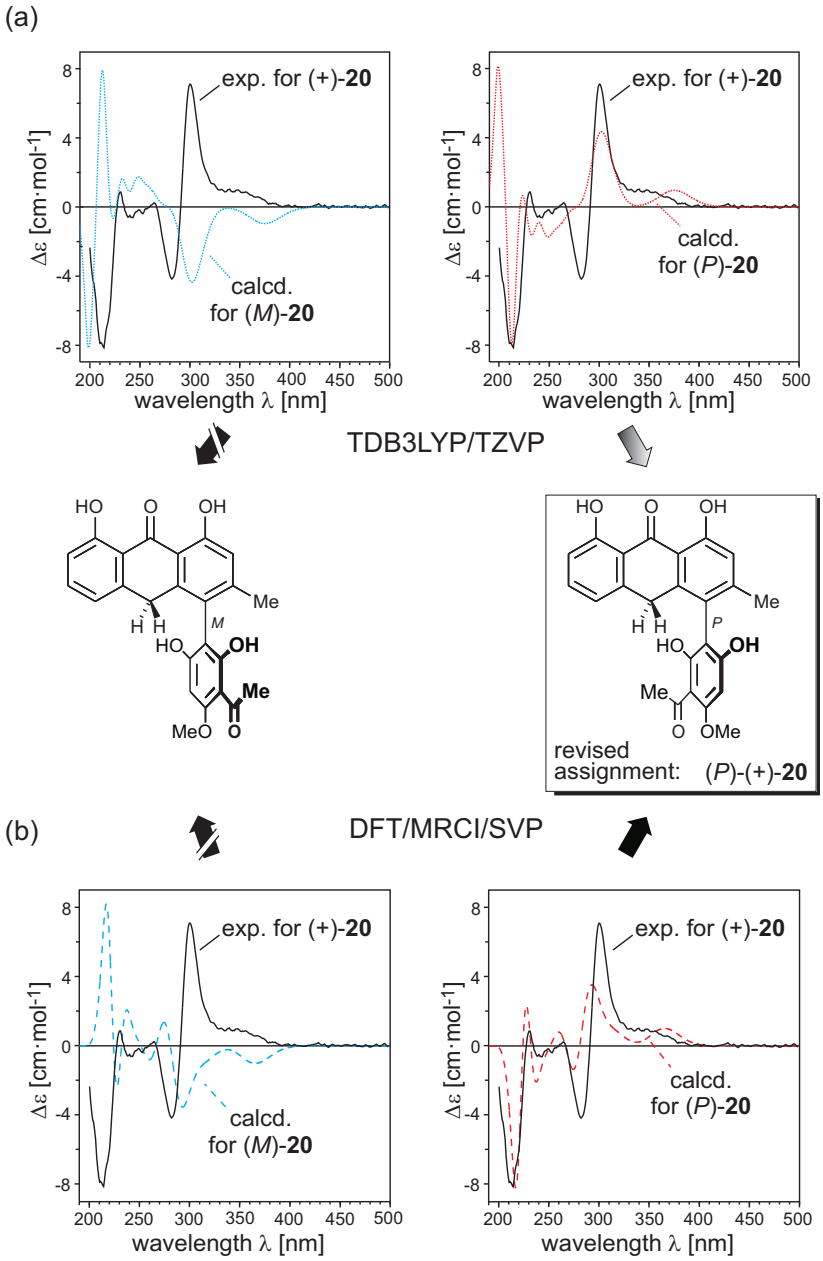

Figure 72. Revised assignment of the absolute axial configuration of (+)-knipholone anthrone (**20**) by the TDB3LYP/TZVP (a) and the DFT/MRCI/SVP (b) calculations performed on the *M*-enantiomer of **20**.

As seen from Figure 72, the first two CD bands predicted for the *M*-enantiomer of knipholone anthrone (**20**), by both methods, showed negative Cotton effects, whereas in the experimental spectrum they had a positive sign, indicating the opposite absolute configuration of (+)-**20**, i.e., *P*. While the TDDFT calculations were not able to entirely simulate the positive exciton couplet around 300 nm, the

DFT/MRCI/SVP-based CD spectrum of (*P*)-**20** fully reproduced all features of the experimental CD curve of (+)-**20**, including the CD split (Figure 72b). The new experimental spectra of pure (+)-**20** and the high-level calculations clearly indicated that the absolute configuration of (+)-**20** must be revised to be *P*, and not *M* as had been assumed earlier.[213,214] This result is thus in agreement with the prediction made by the *Exciton Chirality Method* described above.

Besides the renewed quantum chemical CD investigations of the absolute configuration of both, knipholone (**19**) and knipholone anthrone (**20**), further experimental attempts were undertaken for an additional evidence of the new configurational assignment. Since CD calculations proved the homochiral behavior for these compounds, i.e., that the dextrorotatory forms of **19** and **20** should have the same absolute *P*-configuration, at first their stereochemical interconversion had to be investigated. For this purpose, the reduction of (*P*)-**19** to (*P*)-**20** and, *vice versa*, the oxidation of (*P*)-**20** to (*P*)-**19** were thoroughly analyzed by chromatography on a chiral phase with online CD coupling (LC-CD), unambiguously proving the stereochemical identity of (+)-(*P*)-knipholone (**19**) and (+)-(*P*)-knipholone anthrone (**20**). These experiments were performed in our group by Dr. J. Muttanyatta-Comar. The next proof of the revised configurational assignment was expected from crystallization experiments. Unfortunately, all attempts to crystallize appropriate derivatives of knipholone (**19**) equipped with chiral auxiliaries or with 'heavy' atoms failed to give crystals of suited quality for an X-ray structure analysis. Therefore, another strategy has been sought. Thus, an additional confirmation of the new absolute configuration of (+)-knipholone, i.e., (+)-(*P*)-**19**, was achieved by performing the stereochemically unequivocal transformation of the phenylanthraquinone **19** into the 'leuco' phenylanthracene derivative **13** (by M. Knauer),[38] whose absolute configuration was independently determined by quantum chemical CD calculations (see Chapter 4.2.3).[38]

4.4. Challenging cases for the prediction of molecular CD

4.4.1. Joziknipholones A (21) and B (22)

Due to their remarkable antimalarial activities, axially chiral phenylanthraquinones, such as knipholone (**19**),[208,209,210] knipholone anthrone (**20**),[210,219] 4′-*O*-demethylknipholone,[214] bulbine-knipholone,[223] 4′-*O*-demethyl-knipholone-4′-*β*-D-glucopyranoside,[224] and isoknipholone,[42] constitute a group of promising bioactive compounds towards the fight against malaria. Tropical malaria is the most dangerous infectious disease, which takes lives of about two million people worldwide each year. Therefore, the search for new, more efficient antimalarial agents is one of the first-priority goals in our group.

Recently, two novel representatives of this class were isolated by Dr. Yenesew and co-workers in Kenya from the roots of the African plant *Bulbine frutescens*. These are the first phenylanthraquinone dimers, named joziknipholone A (**21**) and B (**22**)[42] [from the Swahili word *jozi* (= pair)], exhibiting good antiplasmodial activities and low cytotoxicities, which makes them promising candidates for antimalarial drugs. The constitutions of both compounds, which were found to be diastereomers, were initially derived from NMR experiments carried out by the African group, and then further elaborated and approved in our group by Dr. Joan Muttanyatta-Comar.[42]

The extensive 1D- and 2D- NMR measurements (including NOESY, COSY, ROESY, HSQC, and HMBC), together with high-resolution mass spectrometric and UV studies, showed that these compounds are ‘mixed’ knipholone-knipholone anthrone dimers, with an sp^2-sp^3 axis between C-7 and C-10′ (Figure 73a). Thus, joziknipholones A (**21**) and B (**22**) possess both types of chirality: axial, due to the rotationally hindered biaryl axes of the knipholone and knipholone anthrone portions, and central, due to the 7,10′-linkage. The specific NMR data, such as the NOESY correlations from H-10′ to H-6, the upfield shift of H-5‴, together with the deshielded signal of the acetyl group at C-3‴ (Figure 73b), which are characteristic

for both, **21** and **22**, gave first hints at the configuration in the 'northern' part of the molecules, viz. at the biaryl axis of the knipholone anthrone moiety relative to the stereogenic center, leaving either 4′*M*,10′*R* (i.e., **A**, Figure 73b) or its enantiomorphous version, 4′*P*,10′*S* (*ent*-**A**) as possible partial structures.

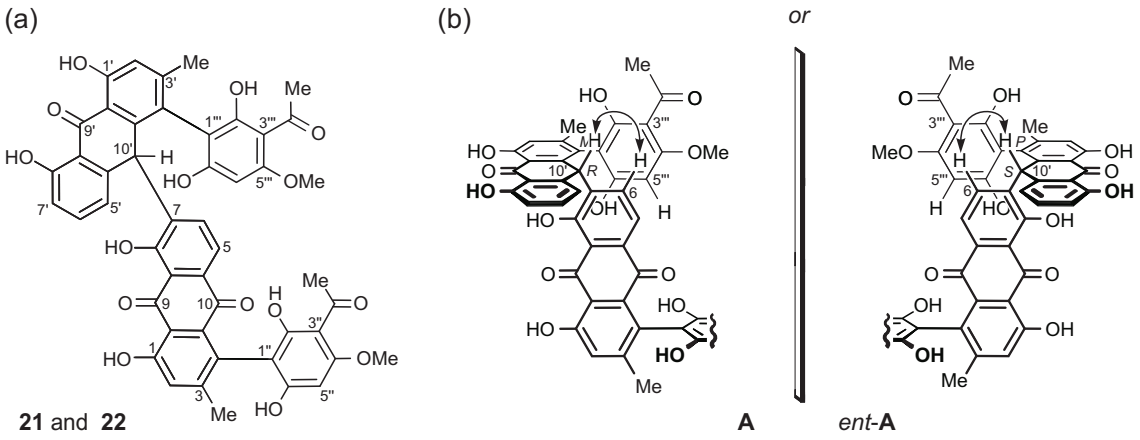

Figure 73. Constitution of joziknipholones A (**21**) and B (**22**) (a) and two enantiomorphous partial structures, **A** and *ent*-**A**, representing the relative configuration in the 'northern' moiety of the molecules (b).

The absolute configuration at the 'southern' biaryl axis, viz. at the knipholone moiety, was initially determined for joziknipholone A (**21**) by the reductive cleavage of the central C-7–C-10′ bond. HPLC-CD analysis of the obtained products revealed the resulting knipholone (**19**) to be *P*-configured, as based on the comparison with the CD curves of the authentic **19** and the recently re-calculated spectra. These first experiments did not give, however, an answer about the configuration of the knipholone anthrone portion. Therefore, quantum chemical CD calculations appeared to be the method of choice.

Based on the above mentioned NMR features and on the results of the cleavage reaction, only two diastereomeric structures of **21** seemed possible, viz. (4*P*,4′*M*,10′*R*)-**21** or (4*P*,4′*P*,10′*S*)-**21** (Figure 74). Thus, the CD spectrum was independently calculated for each stereostructure. Despite their diastereomeric nature, these two structures possess pseudo-enantiomeric frameworks concerning

the main anthraquinone/anthrone chromophore (Figure 73 and 74) and should, therefore, provide nearly opposite CD spectra.

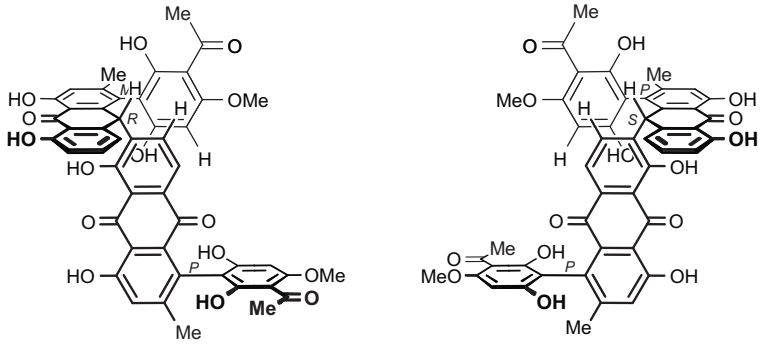

Figure 74. Two possible full absolute stereostructures for joziknipholone A (**21**), (4*P*,4′*M*,10′*R*)-**21** and (4*P*,4′*P*,10′*S*)-**21**, possessing pseudo-enantiomeric main chromophores.

The calculations started with the 4*P*,4′*P*,10′*S*-diastereomer of **21**. The conformational behavior of **21** was investigated at the AM1 level, taking into account the conformational features of the monomeric portions, knipholone (**19**) and knipholone anthrone (**20**) (Chapters 4.3.4 and 4.3.5). Since semiempirical methods had failed in the prediction of the CD spectra of **19** and **20** (Chapters 4.3.4 and 4.3.5), the AM1 predicted conformers of **21** were directly submitted to a RI-BLYP/SVP optimization. In analogy to the monomers, knipholone (**19**) and knipholone anthrone (**20**), the DFT calculations of joziknipholone (**21**) showed the formation of strong hydrogen bonds in the anthraquinone and anthrone portions, and in the acetylphloroglucinol units. The orientations around the biaryl axes were found to be almost identical to those of the global minima of the monomers, viz. with dihedral angles of –109° (for the knipholone portion) and –79° (for the knipholone anthrone moiety). Screening of the reaction coordinate for the rotation around the central C-7–C-10′ bond of **21** revealed two minimum structures, one with a *syn*-orientation of the protons at C-6 and C-10′ (Figure 75, right) and the other one with an *anti*-arrangement (Figure 75, left). The BLYP/SVP calculations of these two minima in gas

phase and in CH_2Cl_2[d] revealed the *anti*-conformer to be energetically more favorable by 1.64 and 0.98 kcal·mol^{-1}, respectively.

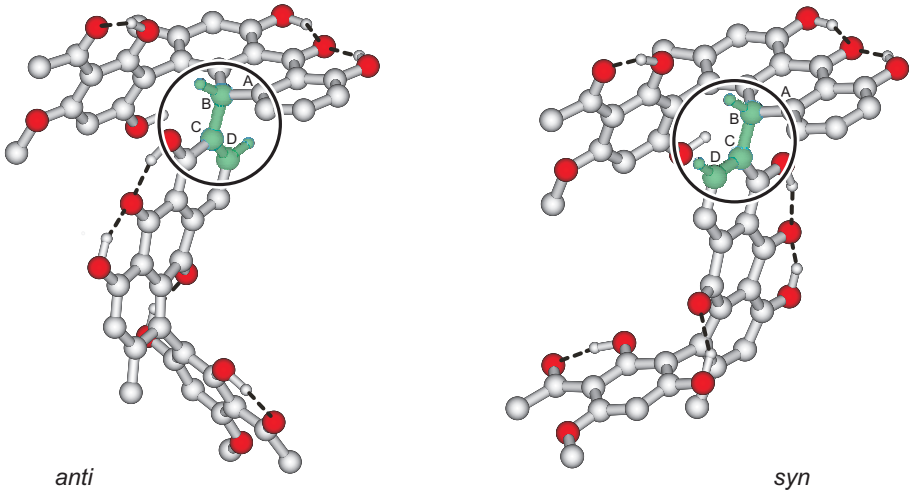

anti *syn*

$\Delta\Delta H_f$ [kcal·mol^{-1}] BLYP/SVP	*anti* (θ_{ABCD})	*syn* (θ_{ABCD})
gas	0.00 (-48°)	1.64 (-131°)
CH_2Cl_2	0.00	0.98

Figure 75. Two minimum conformers established for **21**.

To investigate the conformational stability of the central C-7–C-10′ bond of **21**, the rotational barrier was theoretically estimated by calculating that of **47** as a simplified model (Figure 76), in which the acetylphloroglucinol unit and the methyl substituent of the knipholone portion of **21** were omitted to reduce the size of the computed molecule, without changing the most important 'core geometry' around the central C-7–C-10′ bond. The transition state structures of **47** were located and optimized using the STQN[225] method at the BLYP/3-21G[226] level. To get more accurate results, the rotational barriers were calculated by taking into account zero-point vibrational energies of the minimum conformers and transition states, which

[d] This was the single-point BLYP/SVP calculation by applying a polarizable continuum (PCM) model as implemented in GAUSSIAN 03.

were furthermore scaled by a factor of 0.9945 as recommended for BLYP/3-21G calculations.[227]

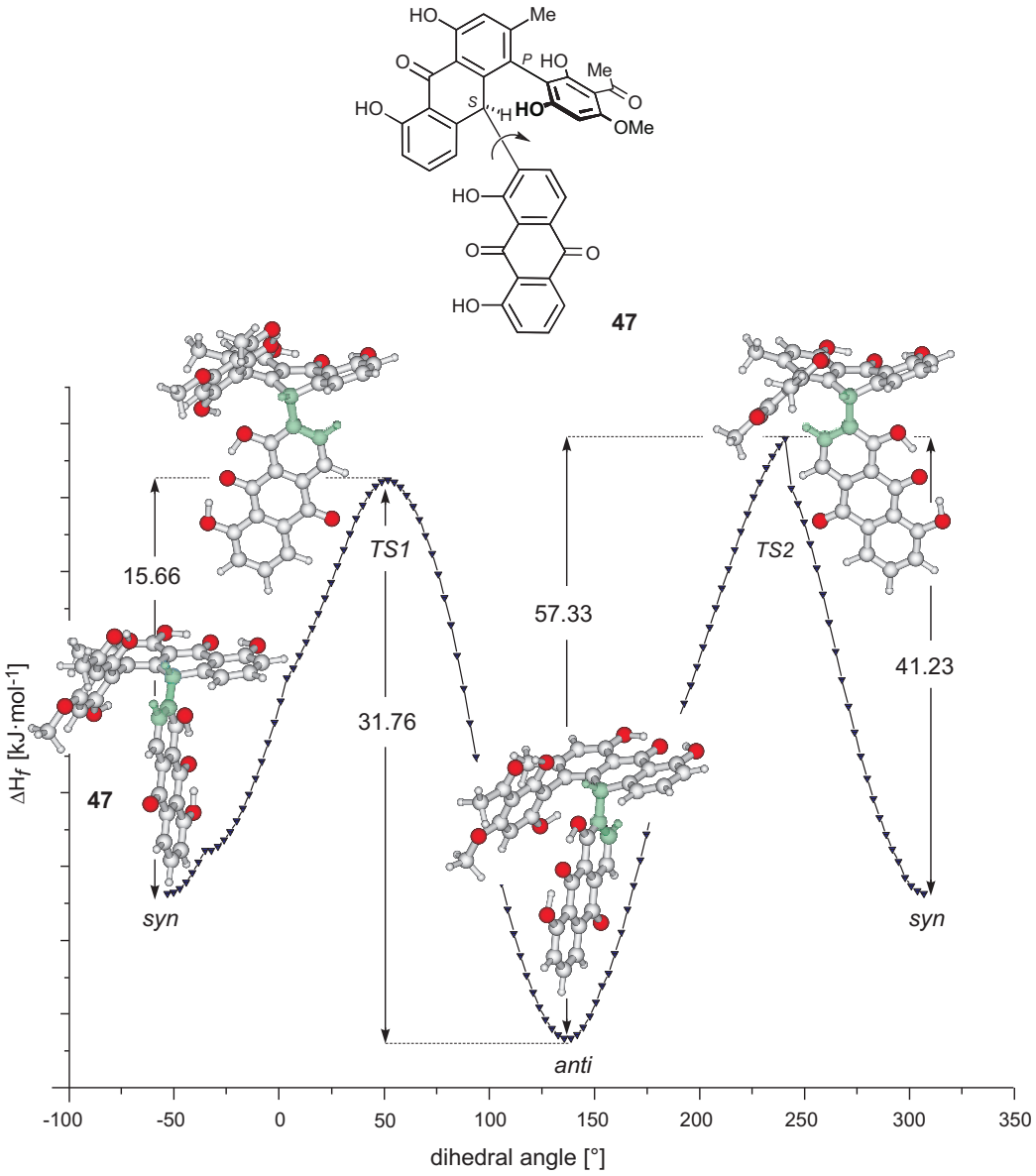

Figure 76. Diagram showing the rotational barriers at the central sp^2-sp^3 axis calculated for **47** as a simplified model compound. The reaction coordinate was calculated by the AM1 method, while the presented rotational barrier energy values were obtained from the BLYP/3-21G calculations.

The obtained low rotational barrier values (Figure 76) revealed that the central bond of **21** should rotate rather freely, proving that the two global minimum structures, *syn* and *anti*, should both be present in solution and should have a substantial impact on the resulting circular dichroism. Therefore, CD calculations,

based on the TDDFT method, were performed for both basic conformers of **21**. An application of the more accurate hybrid functional B3LYP, or of the DFT/MRCI method, which had shown good results in the case of knipholone (**19**) and knipholone anthrone (**20**) (Chapters 4.3.4 and 4.3.5), was not possible for the dimer, because of the large size of the molecule and the resulting too high computational costs, so that the calculations were done by using the RI-BLYP/TZVP method. The calculated single spectra were added up according to the Boltzmann statistics giving the overall CD curve predicted for (4*P*,4′*P*,10′*S*)-**21**. In the case of the other possible candidate, 4*P*,4′*M*,10′*R*-**21**, analogous conformers, *syn* and *anti*, were found, and the CD spectrum was obtained as described above. Comparison of the experimental CD curve of **21** with the theoretically predicted ones showed that the first positive band (at 310 nm) in the measured spectrum was reproduced by the curve calculated for the 4*P*,4′*P*,10′*S*-diastereomer, whereas the one predicted for (4*P*,4′*M*,10′*R*)-**21** displayed negative peaks in this region (Figure 77). The spectral region from 200 to 285 nm was very similar in both theoretical spectra, and hence could not be used for comparison with the experimental curve. However, although the TDDFT-based calculations could not provide an unambiguous full configurational assignment of **21**, due to the large size of the molecule, they still gave a preference for 4*P*,4′*P*,10′*S* rather than for 4*P*,4′*M*,10′*R*. Thus, for an additional confirmation of the absolute configuration of **21**, further experimental work was necessary.

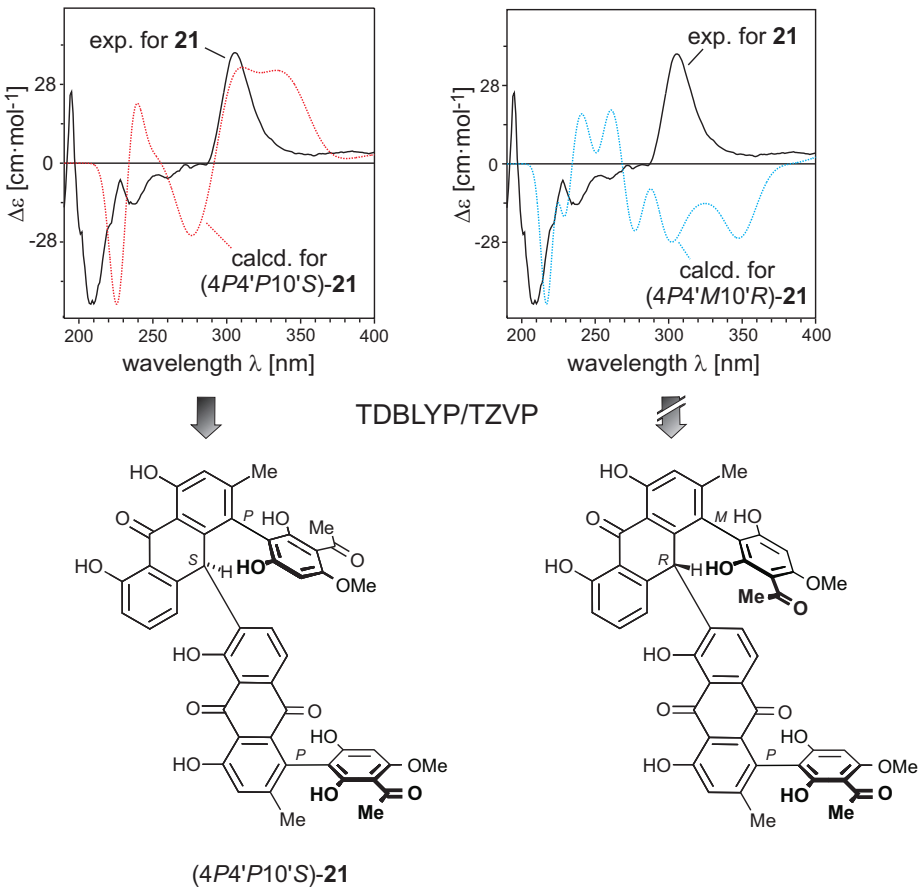

Figure 77. Comparison of the experimental CD spectrum of **21** with the spectra calculated for the two possible stereoisomers, (4*P*,4′*P*,10′*S*)-**21** and (4*P*,4′*M*,10′*R*)-**21**.

Fortunately, Dr. J. Muttanyatta-Comar in our group succeeded in optimizing the degradation cleavage protocol, which allowed her to obtain both monomeric portions, knipholone (**19**) and knipholone anthrone (**20**). Analytical separation and offline CD measurements of these products with subsequent comparison with the CD curves of the authentic samples and with the newly calculated CD spectra of **19** and **20** unambiguously revealed both, knipholone and knipholone anthrone to be *P*-configured, thus proving the above assignment that **21** should have the 4*P*,4′*P*,10′*S*-configuration.

As to the second phenylanthraquinone dimer, joziknipholone B (**22**), the cleavage of its central C-7–C-10′ bond resulted in the *P*-configured knipholone anthrone, as in **21**, while the formed knipholone was found to have the *M*-configuration. Since NMR data, including NOESY correlations, of the two dimers, **21** and **22**, were almost

identical, the *P*-configuration in the anthrone moiety of **22** directly indicated the *S*-configuration at the stereogenic center, thus deducing joziknipholone B (**22**) to have the 4*M*,4′*P*,10′*S*-stereostructure (Figure 78, right). Its CD spectrum was obtained by simple reflection at the wavelength axis (Δε = 0) of the curve predicted for (4*P*,4′*M*,10′*R*)-**21**.

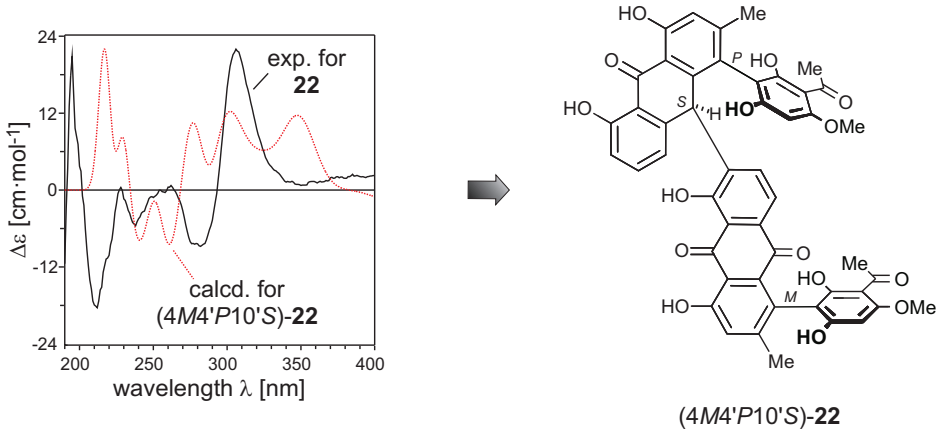

Figure 78. Comparison of the experimental CD curve of joziknipholone B (**22**) with the spectrum predicted for (4*M*4′*P*10′*S*)-**22**.

The theoretical spectrum thus produced for the 4*M*,4′*P*,10′*S*-diastereomer was compared with the experimental curve of **22**, again indicating that for the attribution of the absolute configuration of such a type of molecules, i.e., of molecules possessing both, axial and central elements of chirality and having anthrone, anthraquinone and/or acetophenone chromophores, higher-level methods are required (e.g., the TDDFT method with the hybrid functionals, like B3LYP or BHLYP, or the DFT/MRCI technique).

4.4.2. Petrosifungin A (23)

In all above-described cases, the determination of the absolute stereostructure of a chiral compound basically consisted of the task of distinguishing between two enantiomers. This task profits from the fact that the chiroptical properties of enantiomers, and particularly circular dichroism, have – by definition – opposite sign

over the entire spectral region. The last examples, joziknipholones A (**21**) and B (**22**), although being diastereomers, chiroptically still behave like (pseudo)enantiomers, due to the mirror-image like spatial arrays of their main chromophores (Figure 74, Chapter 4.4.1). In the case of the biaryls **5** and **7**, which possess both types of stereogenic elements, a rotationally hindered axis and a chiral center, the CD spectrum appeared sensitive only to the configuration at the biaryl linkage, and not at the center. This again became a problem of differentiation between two enantiomers rather than between atropo-diastereomers. A different situation occurred for petrosifungin A (**23**), the compound completing the main chapter of this thesis. A remarkable structural feature of this natural product is the presence of a large number of stereogenic centers. Their absolute, and even their relative configurations were all unknown. Therefore, in order to determine the full stereostructure of **23**, including the absolute configurations, various diastereomeric structures had to be considered.

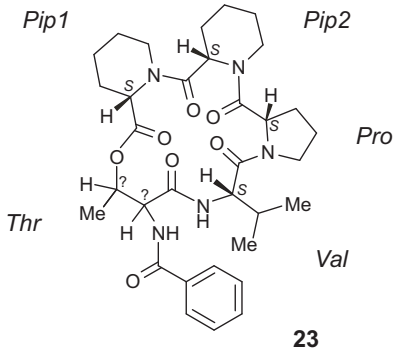

Figure 79. Structure of petrosifungin A (**23**).

Petrosifungin A (**23**) is a cyclodepsipeptide isolated in our group by G. Lang from a strain of *Penicillium brevicompacum* derived from the Mediterranean sponge *Petrosia ficiformis*.[228] The molecule **23** comprises four amino acids, viz. threonine (*Thr*), valine (*Val*), proline (*Pro*), and pipecolinic acid (*Pip*) (Figure 79). The absolute configurations of the valine, proline, and pipecolinic acid units were determined to be L by acid hydrolysis followed by derivatization with a chiral reagent GITC (2,3,4,6-tetra-*O*-

acetyl-β-D-glucopyranosyl isothiocyanate) and subsequent comparative HPLC analysis.[228] The corresponding GITC derivatives of the four possible threonine stereoisomers could not be resolved by HPLC, and hence could not be compared with the available reference compounds. Therefore, to assign the absolute configurations of two stereogenic centers of the threonine moiety of **23**, the CD spectra of the four possible remaining diastereomers of petrosifungin A (Figure 80) were predicted by quantum chemical calculations. Furthermore, it was of interest whether an alteration of the absolute configuration of the threonine moiety will – or will not - influence the CD spectrum of such a multicentered system, in which all chiral centers are in a direct vicinity to the chromophoric groups.

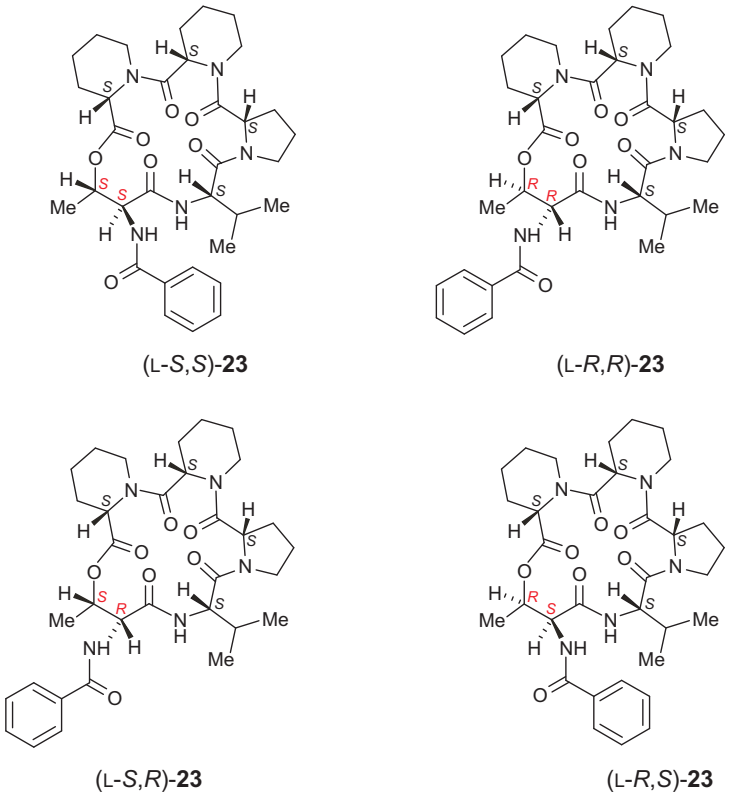

Figure 80. The four possible diastereomeric structures of petrosifungin A (**23**): (L-*S*,*S*)-, (L-*R*,*R*)-, (L-*S*,*R*)-, and (L-*R*,*S*)-**23**, where L indicates four *S*-configured centers of *Pip*, *Val*, and *Pro* components.

Taking into account the high flexibility of petrosifungin A (**23**), the conformational behavior of each of its diastereomers was simulated by the molecular

dynamics approach at 700 K by the use of the TRIPOS force field. The single CD spectra of the structures thus obtained were calculated at the CNDO/S level and then arithmetically averaged to provide the overall CD curves for (L-*S*,*S*)-, (L-*R*,*R*)-, (L-*S*,*R*)-, and (L-*R*,*S*)-**23**. The experimental CD spectrum of (–)-**23** exhibited a pronounced couplet with a negative COTTON effect at 220 nm and a positive one at 180 nm (Figure 81, left). As seen in Figure 81 (right), the resulting overall CNDO/S–based CD spectra of the four possible diastereomers of **23** were very similar to each other and differed only slightly in the intensities, so that no definite configurational distinction was possible, and thus no attribution. Therefore, further experimental work was necessary.

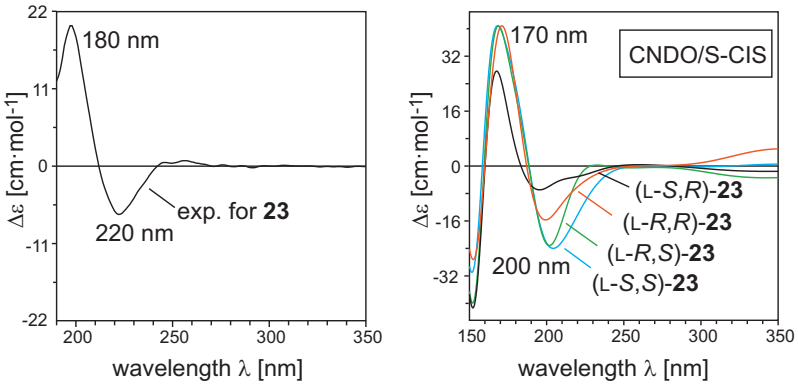

Figure 81. The experimental CD spectrum of (–)-**23** (left), and the CNDO/S-based CD spectra calculated for the four possible diastereomers of **23**.

A search for alternative chiral derivatizating agents revealed that N^{α}-(2,4-dinitro-5-fluorophenyl)-L-alaninamide (FDAA or Marfey's reagent) gives well-separated threonine derivatives. Their comparative HPLC analysis indicated that the α–position of the *Thr* moiety is L-configured while the second chiral center has the *R*-configuration. Consequently, the naturally occurring petrosifungin A (–)-**23** possesses the [S_{Pip},S_{Pip},S_{Pro},S_{Val},$(R,S)_{Thr}$]- or the (L-*R*,*S*)-configuration (Figure 80, right bottom).

Within CD investigations, an optimal differentiation is attained only in the case of the enantiomers, as their CD spectra are perfect contraries over the entire

spectral region. The distinction between diastereomers is generally more complicated and depends on contributions of the particular stereogenic elements on the appearance of the overall CD spectrum. Thus, for axially chiral biaryls possessing one or more additional stereogenic centers (like **5** and **7**), the CD spectrum is largely determined by the effect of axial chirality (due to the biaryl chromophore) and not by the configuration of stereogenic centers. Consequently, only the axial configuration can be assigned (i.e., one can distinguish between atropo-diastereomers), irrespective of the absolute configuration at the stereogenic centers, which has to be determined by other methods. In very few cases the situation is opposite, in that the chiroptical properties of the stereogenic centers dominate the axis.[229] Finally, the most difficult situation occurs when all stereogenic elements equally contribute to the overall CD spectrum (as seemingly in **23**).[230] In such cases, higher-level calculations or/and additional experimental evidences are necessary.

Chapter 5

Circular dichroism in the solid state

As in all of the cases described above (Chapter 4), experimental CD spectra, which serve as a basis for comparison with the theoretically predicted curves, are usually measured in solution. Therefore, the calculation of the CD spectra requires the consideration of all possible conformational species that occur in solution, and hence do contribute to the molecular CD, a task, which may become very difficult in the case of highly flexible compounds. Recently, the method of determining the absolute configuration by CD calculations has been extended to the crystalline state.[43,44] Evidently, the conformational 'freezing' of a chiral compound in the crystal should substantially facilitate theoretical CD study due to the fact that the structure of the conformer in the crystal can be easily determined by the X-ray diffraction method – provided that crystals of sufficient quality can be obtained. Thus, solid-state CD spectroscopy in combination with quantum chemical CD computations might provide an attractive additional tool for the attribution of the absolute configuration of chiral compounds. To examine this novel methodology and to check the possibility of its improvement, viz. by taking into account surrounding effects

caused by the densely 'packed' molecules in the crystal, a well-known natural product, dioncophylline A (**24**), was chosen as a model compound.[45]

5.1 Dioncophyline A (24) – a rewarding model compound

Dioncophylline A (**24**)[90,231,232] is a naphthylisoquinoline alkaloid possessing both, central and axial chirality. Its full absolute stereostructure, (1*R*,3*R*,7*P*)-**24** (Figure 82a), was established in our group by using a broad variety of most different analytical, chemical, X-ray crystallographic, and computational methods, namely by NMR,[90,233] oxidative degradation,[57a] by stereoselective total synthesis,[234 by X-ray structure analyses both, in the absence or presence of heavy atoms,[235,236] and by circular dichroism spectroscopy (after dehydrogenation) with application of the *Exciton Chirality Method*,[90] and by semiempirical CD calculations (of the authentic alkaloid) based on the molecular dynamics (MD) approach.[142] Although the unambiguously determined absolute stereostructure is given, this compound still exemplifies an extraordinary model for stereochemical investigations due to its biaryl axis. Despite its stable configuration (*P*), its conformational orientation is flexible and, then, has a drastic influence on the CD spectrum. Thus, partial rotation around this axis by varying the dihedral angle ABCD ($30° < \theta_{ABCD} < 135°$, Figure 82a) – yet without changing its *P*-configuration – followed by CNDO/S-based CD calculations of the single rotamers thus obtained revealed a far-reaching change in the CD behavior of dioncophylline A (**24**). Under these conditions, even mirror-image like, fully opposite CD spectra were obtained for different conformers, although all possessing the same absolute configurations at the axis and the centers (Figure 82b). The semiempirical AM1-based screening of the reaction coordinate for the rotation around the axis of **24** (Figure 82c) showed two energetically nearly identical ($\Delta\Delta E$ 0.2 kcal·mol^{-1}) – and thus similarly populated – minimum conformers with dihedral angles θ_{ABCD} of 106° and

78°,[e] whose CD spectra were found to be nearly opposite to each other (Figure 82e). Further optimization of these two minima at the DFT level (BLYP/6-31G**) gave, on the other hand, only one minimum structure with an angle of 105°, proving the second conformer with θ_{ABCD} of 78° to be unstable, which might thus be considered as an artifact of the AM1 calculations. Still, in agreement with the semiempirical calculations, the respective energy profile predicted by DFT (Figure 82f) indicated a substantial rotational flexibility at the axis of **24**, resulting in very similar energies within a quite broad range of dihedral angles. This had the consequence that the resulting overall theoretical CD curve of **24**, which was substantially determined by the conformer distribution, should thus strongly depend on the accuracy of the method used for the conformational analysis and for the calculation of the energies of the respective minimum conformers.

[e] Similar conformers, with the respective angles of 110° and 85°, were also found in the crystals of dioncophylline A (**24**) obtained by crystallization from acetone with traces of TFA (trifluoroacetic acid), presumably remained from the preparative HPLC column.

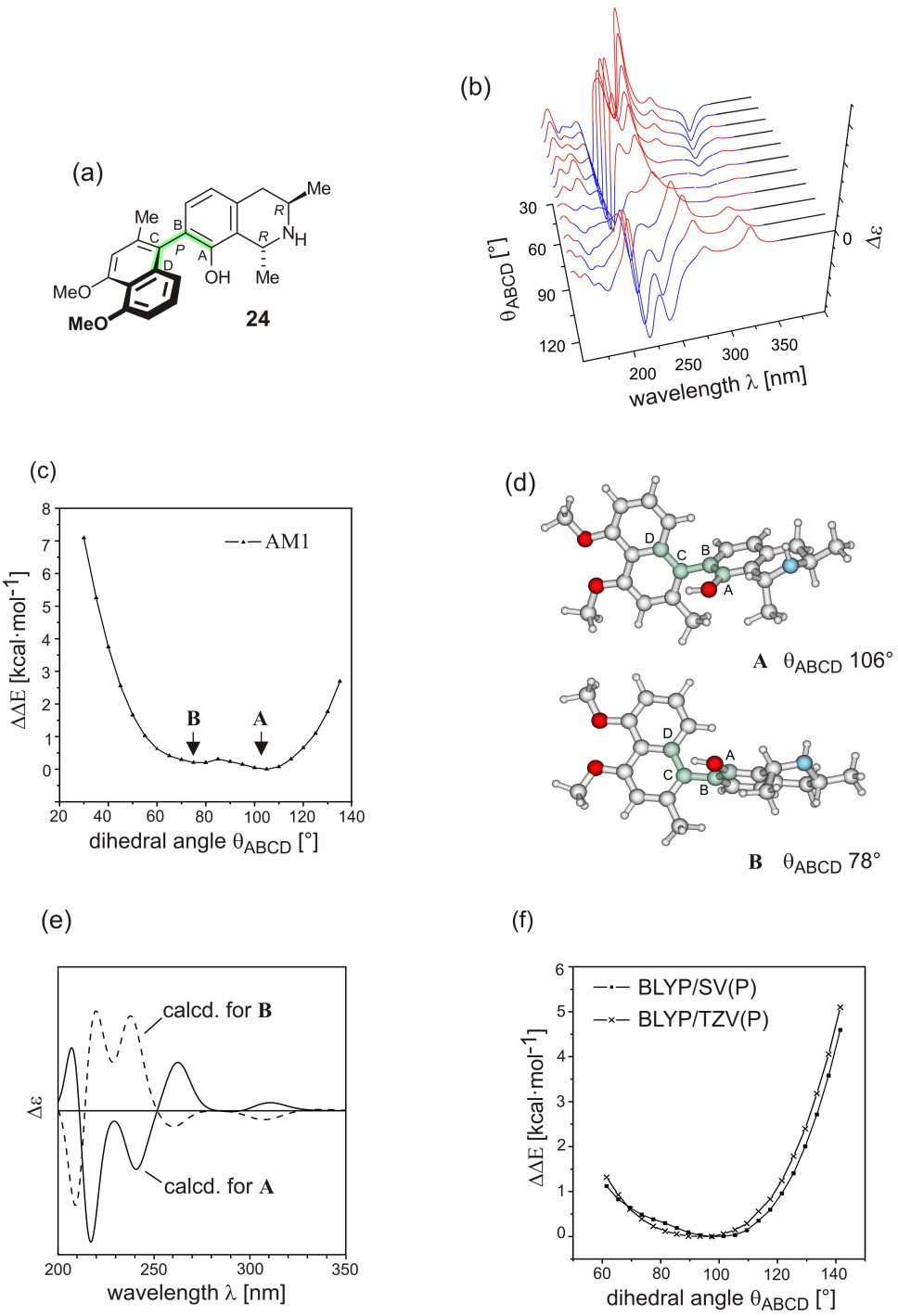

Figure 82. Dioncophylline A (**24**) with its absolute stereostructure (a), a series of CNDO/S calculated CD spectra (red and blue areas correspond to positive and negative Δε values, respectively) of its rotamers (b), and reaction coordinate (AM1) for the partial (twisting) rotation around the biaryl axis (c) revealing two minimum conformers **A** and **B** (d), whose CD spectra were found to be almost mirror-image like (e); the energy profiles for the axial rotation calculated at the DFT level (f).

In the crystals, by contrast, as obtained from dichloromethane/ethanol, dioncophylline A (**24**) was found to adopt only one conformation, viz. with a dihedral angle θ_{ABCD} = 115° (Figure 83),[235] which does not correspond to any of the two preferential angles predicted at the AM1 level to occur in solution (106° and 78°), but should, due to the rigid structure, permit an unequivocal prediction of the CD spectrum. Thus, dioncophylline A (**24**) seemed to be an ideal model for stereochemical solid-state CD investigations.

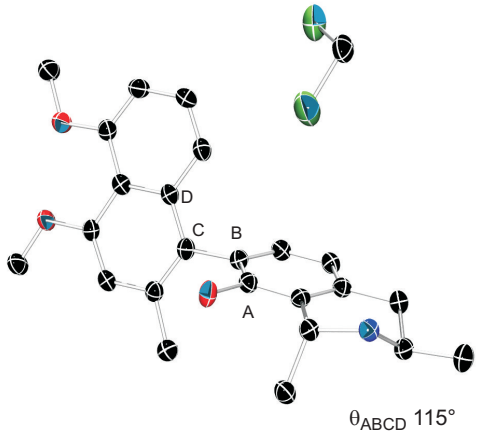

Figure 83. Single conformer of dioncophylline A (**24**) as found in the crystal (likewise present in the crystal: a molecule of CH_2Cl_2).[235]

5.2 CD computations of the monomer

Solid-state CD measurements on dioncophylline A (**24**) were carried out on the Universal Chiroptical Spectrophotometer (UCS-1), designed and constructed by Kuroda et al.[101] The instrument is able to measure all the polarization phenomena, i.e., linear birefringence (LB), linear dichroism (LD), circular birefringence (CB), and CD, simultaneously. Furthermore, it permits to obtain artifact-free CD spectra, avoiding any macroscopic anisotropies typical of the solid-state samples such as LD and LB.

The solid-state CD spectrum of **24** obtained by the KBr matrix method is shown in Figure 84. It comprises two peaks with positive Cotton effects at 280 and 245 nm, separated by a low-intensity negative band at 260 nm and followed by a broad,

strongly negative signal at 227 nm. Similar transmittance CD and absorption spectra were obtained for both, the solid (KBr disk) and the solution (EtOH) states (Figure 84), thus indicating related conformational patterns in the solid (as a KBr pellet) and in solution.

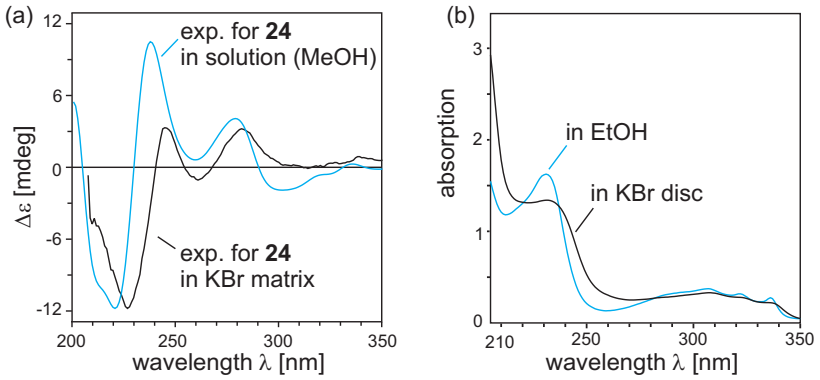

Figure 84. The experimental CD (a) and UV (b) spectra of **24** as measured in ethanol solution, and in the solid state as a KBr pellet.

Based on the X-ray derived coordinates of the single conformer of (1*R*,3*R*,7*P*)-**24** found in the crystal, CD calculations were performed by using three different approaches: the semiempirical CNDO/S-CIS method, which had previously shown good results for a large variety of axially chiral biaryls,[13,24c,33,34,237] and the more accurate TDDFT (B3LYP/TZVP) and DFT/MRCI (BHLYP/SVP)[f] techniques. For the latter two approaches, the initial X-ray based geometry was additionally re-optimized by DFT at the B3LYP/TZVP level with regard to all bond lengths of **24** while preserving the whole set of valence and dihedral angles and hence saving the overall conformation. This optimization led to an increase of the bond lengths between the heavy atoms by 0.3–0.5%, and by 10–15% for the bonds involving hydrogen atoms.

To compare the experimental solid-state CD curve of dioncophylline A (**24**) with the theoretical spectra, the latter ones were shifted in accordance with the UV correction by 6 nm (blue shift, CNDO/S-CIS), 8 nm (red shift, TDDFT), and 15 nm

[f] As in the previous cases of using the DFT/MRCI method, a configuration selection cut-off of $0.8E_h$[14] was applied for **24**, too.

(red shift, DFT/MRCI) to compensate an error in the prediction of the energies of the excited states. The first positive band observed experimentally at 280 nm was predicted by each theoretical method with a too low intensity. The best overall match between theory and experiment was achieved in the case of the DFT/MRCI methodology (Figure 85c), whereas TDDFT calculations revealed the first positive and second negative signals to be substantially shifted to the region of shorter wavelengths (Figure 85b). The repeated TDB3LYP computations on the original structure obtained from X-ray diffraction analysis did not yield any substantial improvement in the spectrum. Nevertheless, the overall agreement between the experimental (KBr) based curve of **24** and all simulated spectra permitted an unambiguous attribution of the axial configuration of dioncophylline A (**24**) as *P*, which again, independently, confirmed the previous assignments.[90,142,234,236]

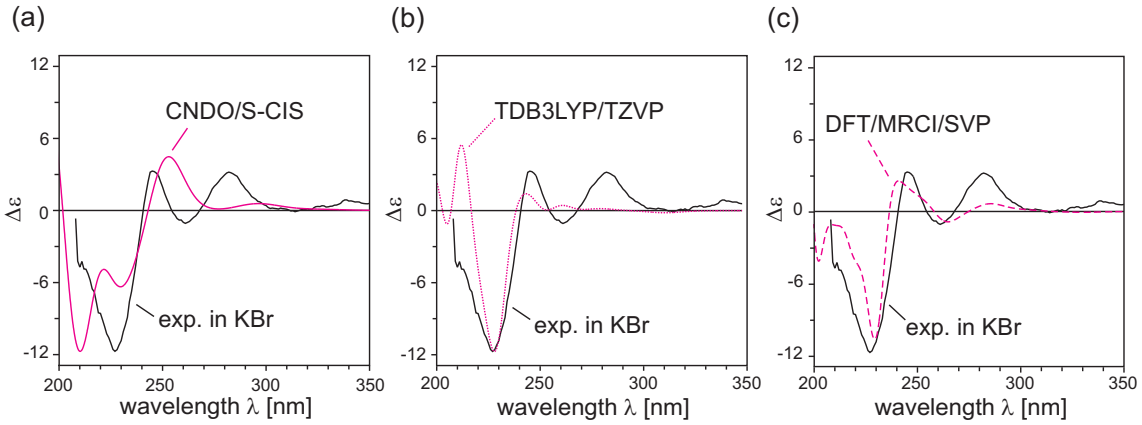

Figure 85. Comparison of the experimental KBr-based CD curve of dioncophylline A (**24**) with the spectra calculated for a single molecule of (*P*)-**24** by using CNDO/S-CIS (a), TDB3LYP/TZVP (b), and DFT/MRCI/SVP (c).

Thus, the combination of solid-state CD spectroscopy and CD computations of a single X-ray derived molecule proved its applicability for the attribution of the absolute (this time, axial) configuration. However, it was still of interest how the closest neighbors of any molecule of dioncophylline A (**24**) in the crystal affect its CD behavior, and whether the quantum chemical treatment of larger systems, e.g., of the dyads of **24** or of a 'one-piece' cluster with several molecules, can improve the

quality of the above-presented results. In the case of dioncophylline A (**24**), neighboring effects seemed to be of particular importance, since this relatively large molecule, comprising two electronically different, almost orthogonally oriented chromophores, should 'see' its different closest neighbors in the crystal in different ways. In other words, depending on the direction in the crystal structure, the one or the other chromophoric units of two individual molecules (isoquinoline to isoquinoline, naphthalene to naphthalene, or isoquinoline to naphthalene) will be oriented at different distances and angles, thus providing a set of diverse intermolecular interactions that may influence the CD behavior of **24**, possibly even substantially. To investigate this effect, CD calculations were performed for all imaginable dyads, each comprising one 'central' molecule of **24** and its neighbor from the nearest surroundings.

5.3 Consideration of dyads – neighboring effect

The unit cell of dioncophylline A (**24**) contains four molecules, which were named **I**, **II**, **III**, and **IV**, as shown in Figure 86a. The molecules formally generated by the translation along the principal axes x, y, and z were given the respective indexes **x**, **y**, and **z**. It was shown that each of the molecules of **24** in the crystal has the same molecular environment. For the investigation of the neighboring effect, one molecule with all its neighbors can therefore be chosen randomly. Thus, CD computations were performed on all possible dyads, which always consisted of the molecule **Ix** as the center (Figure 86b, pink) and, in turn, all its neighboring molecules, viz. **Ix-I**, **Ix-Iz, Ix-Ixz, Ix-II, Ix-IIx, Ix-IIz**, **Ix-IIxz**, **Ix-III**, **Ix-IIIx**, **Ix-IIIy**, **Ix-IIIxy**, **Ix-IVy**, **Ix-IVxy**, **Ix-IVyz**, **Ix-IVxyz** (Figure 86b). The coordinates of each of the dyads were obtained as a result of constructing the desired fragment of the crystal structure of **24** and subsequent cancelling all atoms of the other molecules, while leaving those of the two molecules of interest.[238] For reasons of computational economy, the CD spectra were now calculated only by using the computationally inexpensive CNDO/S-CIS method, which had also shown a good agreement concerning the predicted

wavelengths and the relative intensities for the 'monomer' of **24**. In order to simplify a comparative analysis of the obtained CD curves, they were grouped in accordance to the same molecular number given and, additionally, compared with the CD spectrum of the single conformer found in the crystal ('monomer'). Despite the fact that some of the dyads appeared geometrically identical and hence provided the same CD spectra, they are still presented for the sake of completeness.

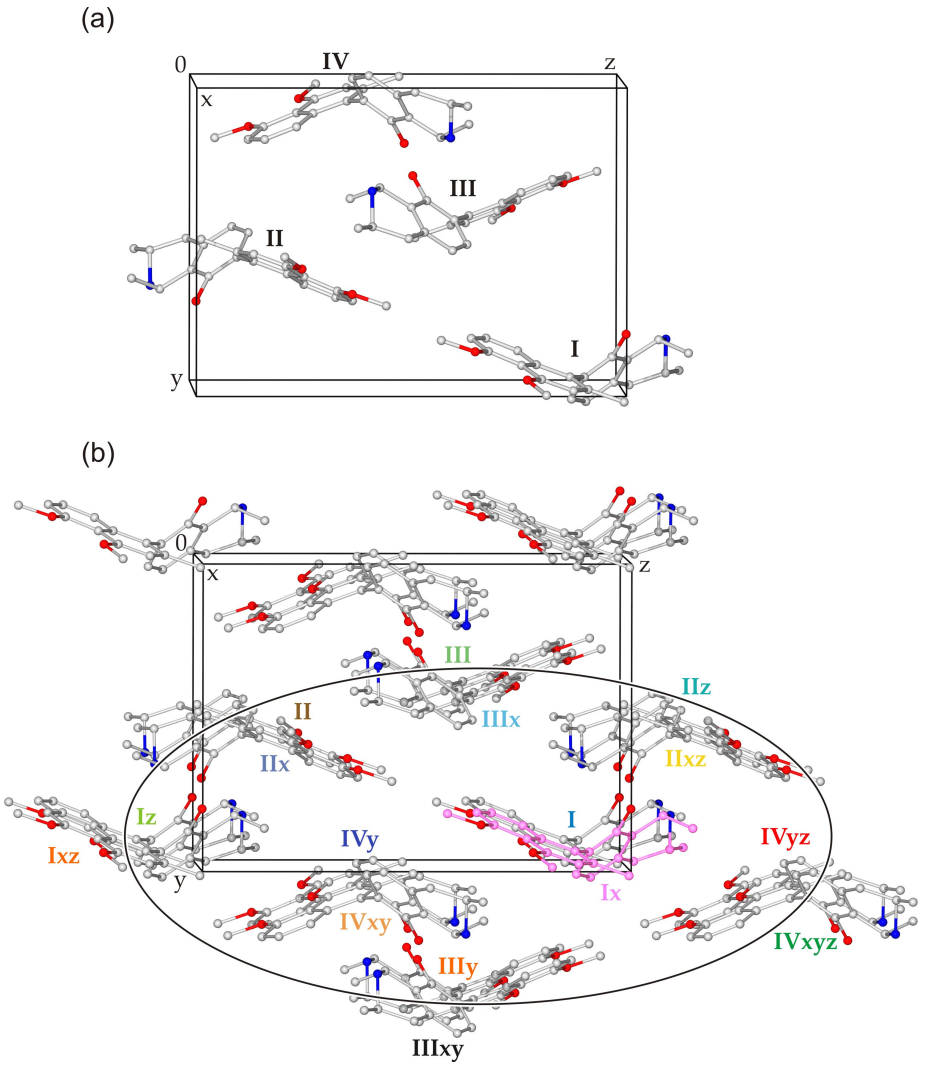

Figure 86. A simplified representation of the unit cell of dioncophylline A (**24**), containing four molecules labeled as **I**, **II**, **III**, and **IV** (a), and a fragment of the crystal lattice of **24** demonstrating the 'central' molecule **Ix** (pink) and all its neighbors taken into account (b). For reasons of clarity, solvent molecules and all hydrogen atoms of **24** were omitted.

The comparison of the CD curves calculated for the dyads with the neighbors of type I (i.e., the dyads **Ix** + **I**, **Ix** + **Iz**, **Ix** + **Ixz**, Figure 87, left) and the spectrum predicted for the single conformer showed that this type of neighborhood does not influence the CD behavior (Figure 87, right), clearly indicating a negligible intermolecular interaction, which can be explained in the case of the molecules **Iz** and **Ixz** with a too large spatial distance from **Ix** and, in the case of molecule **I**, with the parallel orientation of the molecular chromophores of **I** and **Ix**, which prevents them from interaction.

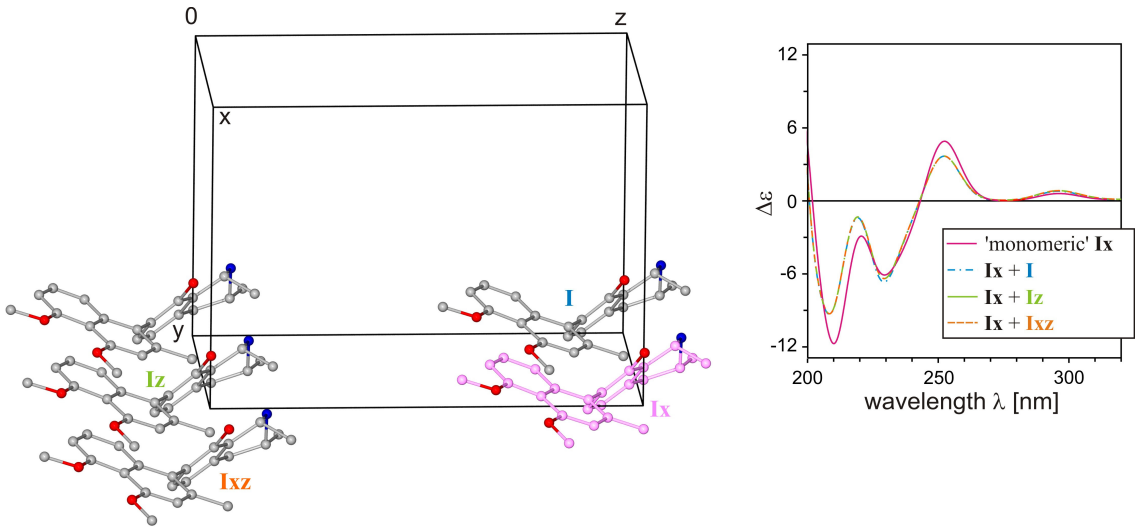

Figure 87. Plot of the 'central' molecule **Ix** with the neighbors of type I (viz. **I**, **Iz**, and **Ixz**) and CD spectra of the corresponding dyads.

From the CD plot for the neighbors of type II (Figure 88, right) it can be seen that taking molecule **II** as the neighbor (i.e., the dyad **Ix** + **II**) gave the same CD spectrum as taking the molecule **IIx** (i.e., the dyad **Ix** + **IIx**). Moreover, the CD behavior of these dyads did not differ substantially from that of the CD of the monomer. This observation can be interpreted by the weak interaction of the almost parallel-arranged naphthalene chromophores of **Ix** and **II**, and of **Ix** and **IIx** (Figure 88, left). In the cases of the dyads with the molecules **IIz** and **IIxz** (i.e., the dyads **Ix** + **IIz** and **Ix** + **IIxz**), their CD spectra were also identical to each other, but differed from the CD curves of the first pairs of dyads and from the CD of the monomer in

the intensities being switched for the negative peak at 230 nm. This revealed a noticeable interdependency between the overlaying naphthalene and isoquinoline moieties, viz. the isoquinoline part of **Ix** with the naphthalene portion of **IIz**, and the naphthalene unit of **Ix** with the isoquinoline half of **IIxz** (Figure 88, left).

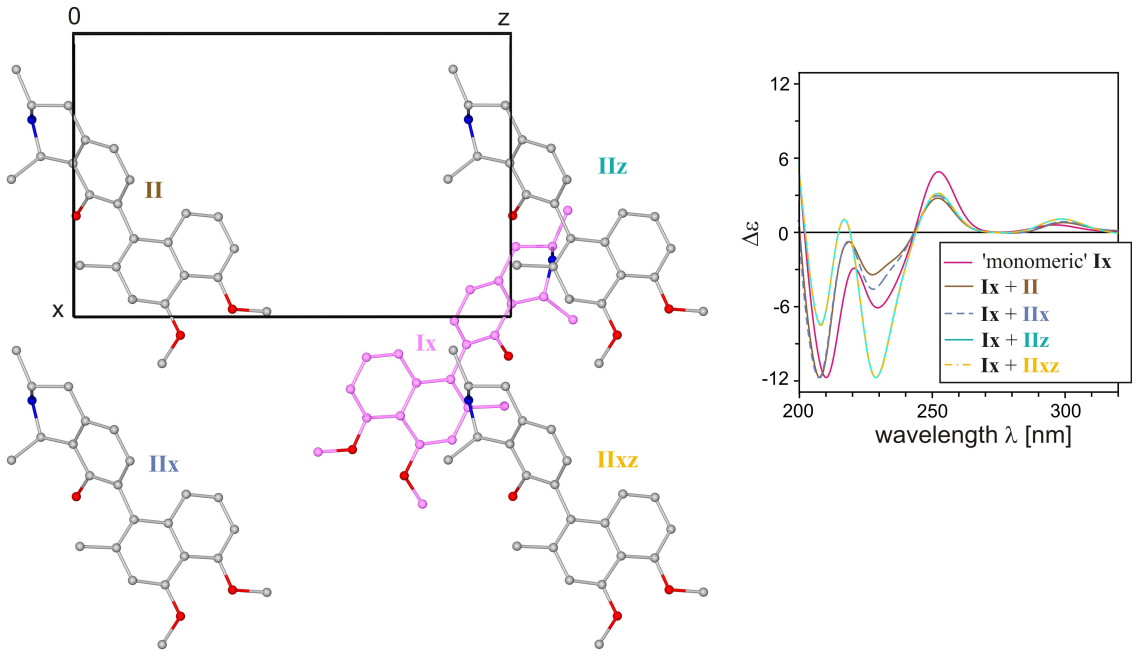

Figure 88. Plot of the neighbors of type II (viz. **II**, **IIx**, **IIz**, and **IIxz**) in the xz plane of the unit cell of **24** and CD spectra of the corresponding dyads.

The neighbors of type III are located above the molecule **Ix**, as **III** and **IIIx**, and below, as **IIIy** and **IIIxy** (Figure 89, left). In this case, the dyad with the molecule **III** as the neighbor (i.e., the dyad **Ix** + **III**) was identical to the one with the molecule **IIIy** (i.e., the dyad **Ix** + **IIIy**) and hence, they resulted in the same CD spectrum. Consequently, the neighbors **IIIx** and **IIIxy** (i.e., the dyads **Ix** + **IIIx** and **Ix** + **IIIxy**) exhibited an equal CD behavior as well, so that the below-lying neighbors, **IIIy** and **IIIxy** (i.e., the dyads **Ix** + **IIIy** and **Ix** + **IIIxy**), did not cause any changes in the CD behavior in comparison to the respective molecules of type III lying above. On the other hand, the CD curves for the dyads including the molecules **III** and **IIIx** strongly differed from each other; some signals even possessed opposite signs, and furthermore they were distinct from the CD spectrum of the monomer (Figure 89, right). This might be due to the presence of different types of interactions, namely a

naphthalene-naphthalene one in the case of the overlaying naphthalene portions of **IIIx** or **IIIxy** and that of the molecule **Ix** (naphthalene centroid – naphthalene centroid, ca. 7.0 Å, and the closest interatomic distance, ca. 5.4 Å), and an isoquinoline-naphthalene one for the isoquinoline half of the molecule **III** or **IIIy** and the naphthalene part of **Ix** (centroid – centroid, ca. 8.0 Å, and the closest interatomic distance, ca. 3.7 Å), and *vice versa*, for the isoquinoline moiety of **Ix** and the naphthalene parts of **III** or **IIIy** (centroid – centroid, ca. 8.0 Å).

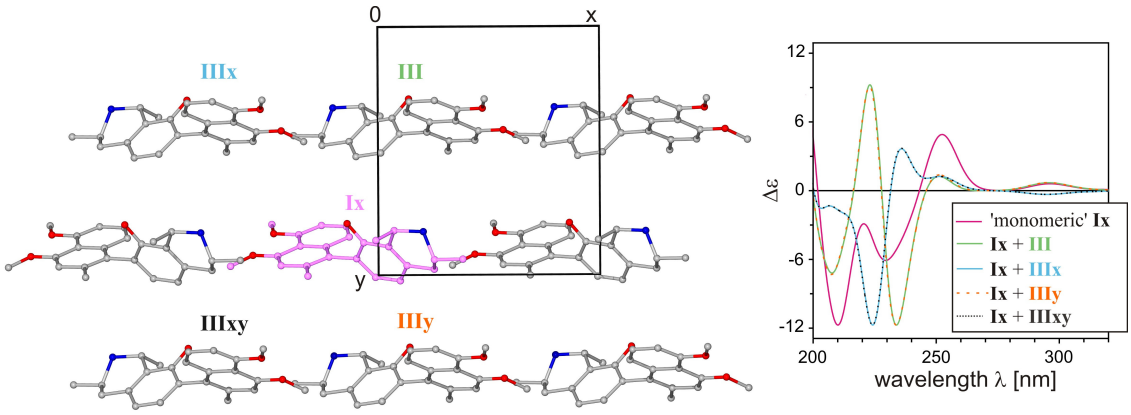

Figure 89. Neighbors of type III (viz. **III**, **IIIx**, **IIIy**, and **IIIxy**) as depicted in the xy plane of the unit cell of **24** and comparison of the respective CD spectra.

In the cases of the neighbors of type IV, which are located on the right (**IVyz**, **IVxyz**) and on the left (**IVy**, **IVxy**) side of the molecule **Ix** (Figure 90, left), the following situation occurred: Considering the molecules **IVy** and **IVyz** as the neighbors (i.e., the dyads **Ix** + **IVy** and **Ix** + **IVyz**) resulted in identical CD spectra, which were furthermore similar to the spectrum of the monomer (Figure 90, right), thus clearly indicating marginal interactions between these molecules and **Ix**. Furthermore, **IVxy** and **IVxyz**, each in combination with **Ix**, likewise gave geometrically the same dyads (i.e., the dyads **Ix** + **IVxy** and **Ix** + **IVxyz**), whose CD spectra revealed a substantially different behavior as compared to the spectra of the first pairs of dyads and that of the monomer of **1** (Figure 90, right), viz. showing the signals at 300 and 230 nm to be of opposite signs. As evidenced in Figure 90 (left),

this behavior can be explained by remarkably strong intermolecular naphthalene-isoquinoline interactions: naphthalene (**Ix**) – isoquinoline (**IVxy**) and isoquinoline (**Ix**) – naphthalene (**IVxyz**) with a centroid – centroid distance of ca. 5.4 Å).

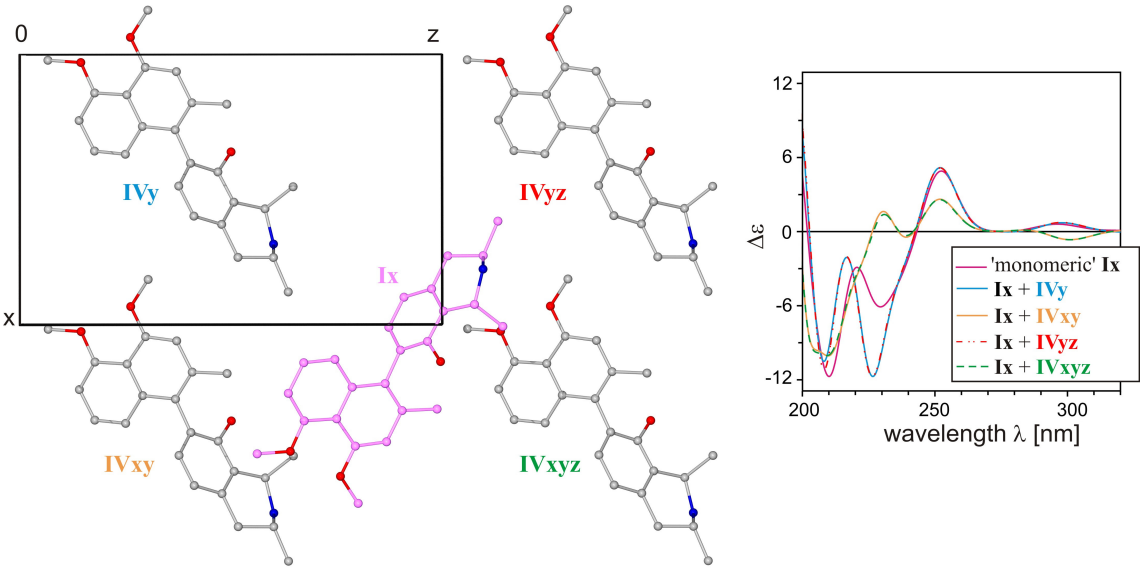

Figure 90. Plot of the neighbors of type IV (namely **IVy**, **IVxy**, **IVyz**, and **IVxyz**) in the xz plane of the unit cell of **24** and comparison of the CD spectra of the corresponding dyads.

Thus, the calculations described above have proven that the surrounding effects should indeed have a certain influence on the CD behavior of dioncophylline A (**24**) in the solid state: For one molecule of **24** (here presented for **Ix**), four of the neighboring molecules – **IIz** (same effect as **IIxz**), **III** (same effect as **IIIy**), **IIIx** (same effect as **IIIxy**), and **IVxy** (same effect as **IVxyz**) – have a substantial impact, while the other neighbors – **I**, **Iz**, **Ixz**, **II** (analogous to **IIx**), **IVy** (analogous to **IVyz**) – possess little or no influence.

The spectrum resulting from the arithmetical average over the CD curves of all dyads considered, did however, not show any substantial change in comparison to the spectrum of the 'monomeric' **24** (Figure 91). Thus, no improvements as compared to the aforementioned results (Section 5.2) were achieved. Calculations of the larger aggregate,[45,239] viz. a one-piece fragment from the crystal, including 16 molecules of

dioncophylline A (**24**) (these were the molecules shown in Figure 86b, except for the molecules **IIz**, **IIIy**, **IIIxy**, **IVxy**, and **IVxyz**) provided a better agreement to the experimental curve, namely, the higher intensity for the peak at about 280 nm (Figure 91b). Consequently, these results showed that there is indeed an effect on the CD spectrum from the crystalline structure, but this effect is negligible and, therefore, the consideration of only one molecule of dioncophylline A (**24**) is sufficient for an assignment of its absolute axial configuration by means of solid-state CD spectroscopy.

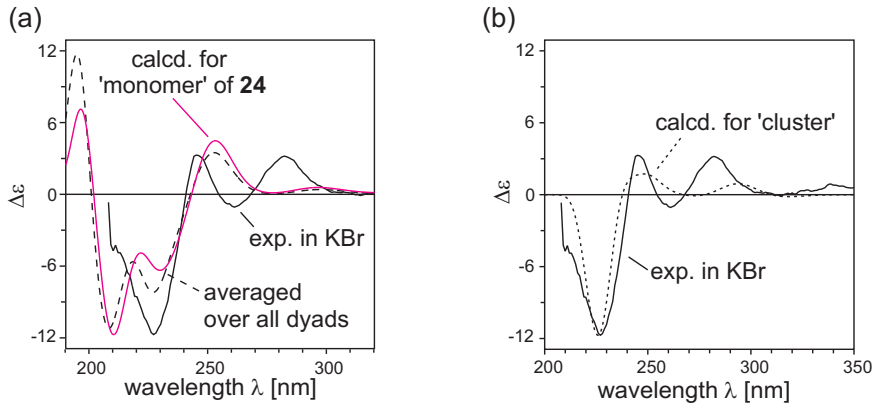

Figure 91. (a) Comparison of the experimental solid-state (KBr matrix) CD spectrum of dioncophylline A (**24**) with the curve predicted (CNDO/S) for its single molecule, and with the spectrum obtained as an average over all calculated dyads, and also (b) with the curve calculated (ZINDO/S) for the cluster of 16 molecules[239] from the crystal of **24**.

The effect of neighboring molecules on the solid-state CD spectrum has already been investigated by Antus and Kurtán for naphthylethylidene acetals of glycosides by using an approximate method.[240] The present work, with its in-depth, systematic study of the possible surrounding effects, should further contribute to the problem of intrinsic solid-state CD effects, and the results found so far should give a higher security for the configurational assignment by the solid-state CD method, as first reported by Krohn.[43]

Chapter 6

Summary

Quantum chemical calculation of circular dichroism (CD) spectra in combination with experimental CD studies is one of the most powerful analytical tools for the elucidation of the three-dimensional structure of a chiral molecule. The rapidly developing computer technologies and a broad diversity of quantum chemical methods available now permit to study virtually any molecule by selecting the most appropriate method in each particular case, with regard to the desired accuracy, time consumption, and required computer resources. Further prospects of this method are associated with solid-state CD spectroscopy, which deals with a conformationally 'frozen' molecule, thus opening the way for the configurational attribution of chiral compounds with high conformational flexibility.

In the course of this work, the absolute configurations of various chiral compounds were determined by using several methods of different theoretical background: the semiempirical CIS methods (viz. CNDO/S and OM2) and *ab initio* approaches based on the time-dependent DFT theory (TDDFT) and on the 'hybrid' multireference CI procedure (DFT/MRCI). Since CD is highly sensitive to the conformational behavior of the molecule, particular attention was paid to the search

of the most relevant structures (by using the BOLTZMANN approach and the MD method) and to the prediction of their energies. The investigated molecules were divided into four groups in dependence on the method used for their configurational attribution.

1. At first, the application of the simplest approach, CNDO/S-CIS, in combination with the BOLTZMANN method or MD simulations, was demonstrated (Figure 92).

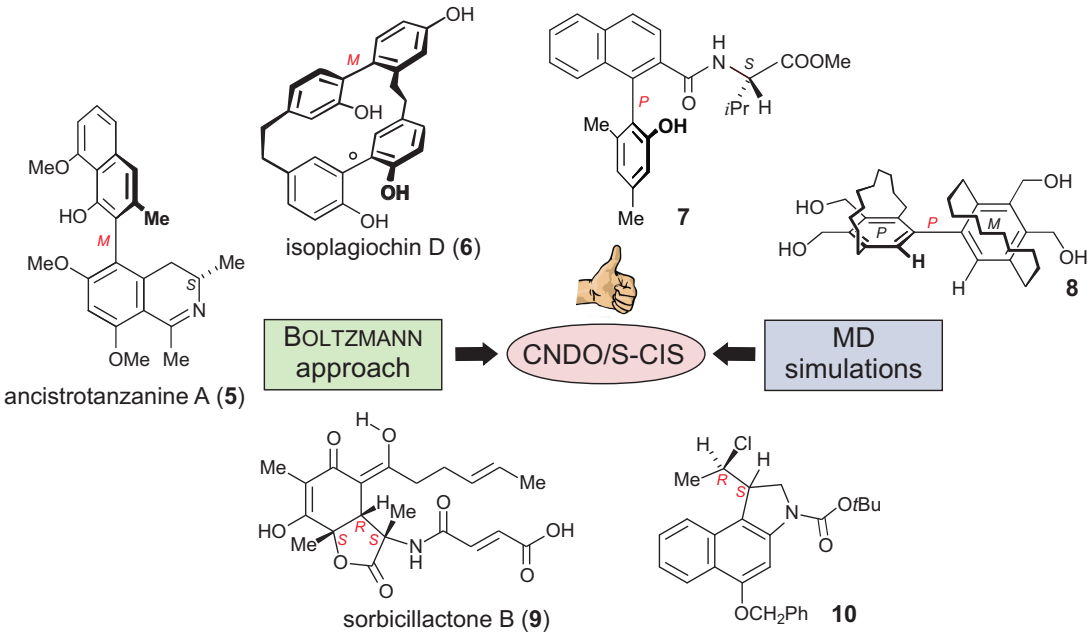

Figure 92. Compounds whose absolute configurations were established by the semiempirical CNDO/S-CIS approach.

The combination MD - CNDO/S-CIS provided excellent results for the biaryls **5** and **6**, and also for the highly flexible sorbicillactone B (**9**) and the benz[e]indole **10**. In the case of the bi[10]paracyclophane **8**, however, MD simulations generated inaccurate geometries, which resulted in a wrong configurational attribution. Using the more tedious but more accurate BOLTZMANN method solved the problem. Therefore, for all following projects, the force-field calculations - if performed – were, in each case, accompanied by the BOLTZMANN method. The excited-states CNDO/S calculations provided reasonably good results for all of these compounds regarding the CD peaks pattern and the excitation energies. For compounds **5**, **6**, **7**, and **8**, which have in common a biaryl system as the main chromophore, the excitation

energies were only slightly underestimated. In the cases of sorbicillactone B (**9**) and the benz[e]indole **10**, however, which possess different chromophoric frameworks, somewhat higher energies were obtained. The good overall agreements between the experimental CD curves of all of these compounds and the respective CNDO/S-based spectra provided the unambiguous configurational attributions, so that higher-level CD calculations seemed to be unnecessary.

2. In the next chapter all those compounds were collected for which both, semiempirical and TDDFT methods resulted in almost the same accuracy (Figure 93).

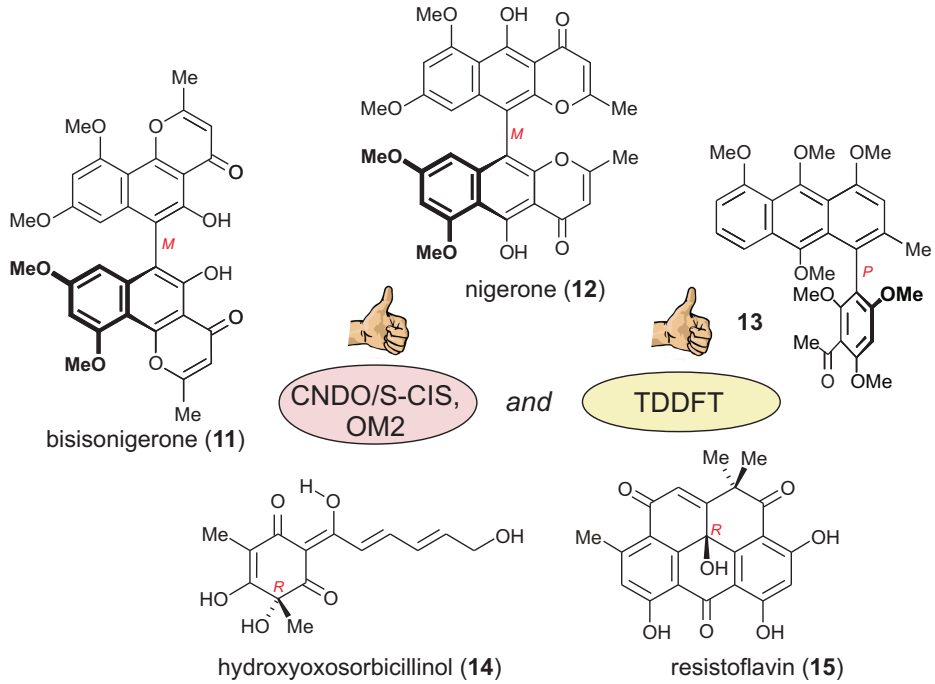

Figure 93. Compounds whose absolute configurations were determined by both, semiempirical and TDDFT approaches, giving almost the same accuracy.

Once again, CNDO/S calculations proved to be particularly successful for biarylic molecules (here, **11**, **12**, and **13**), giving only minor errors in the excitation energies. The semiempirical OM2 approach, as applied to bisisonigerone (**11**) and nigerone (**12**), appeared less powerful and provided too high excitation energies. The TDDFT calculations predicted the excited-states energies of **12**, **13**, and **15** very accurately, whereas for compounds **11** and **14** the results were slightly worse. The CD intensities of molecules **11**, **13**, and **14** were equally well reproduced by both methods, CNDO/S

and TDB3LYP, while for nigerone (**12**) and resistoflavin (**15**) the TDDFT-based spectra were somewhat closer to the respective experimental curves than the CNDO/S predicted ones.

3. The third part of the thesis concerned molecules for which only higher-level methods were able to reproduce the experimental CD spectra correctly, thus delivering the unambiguous configurational attribution (Figure 94).

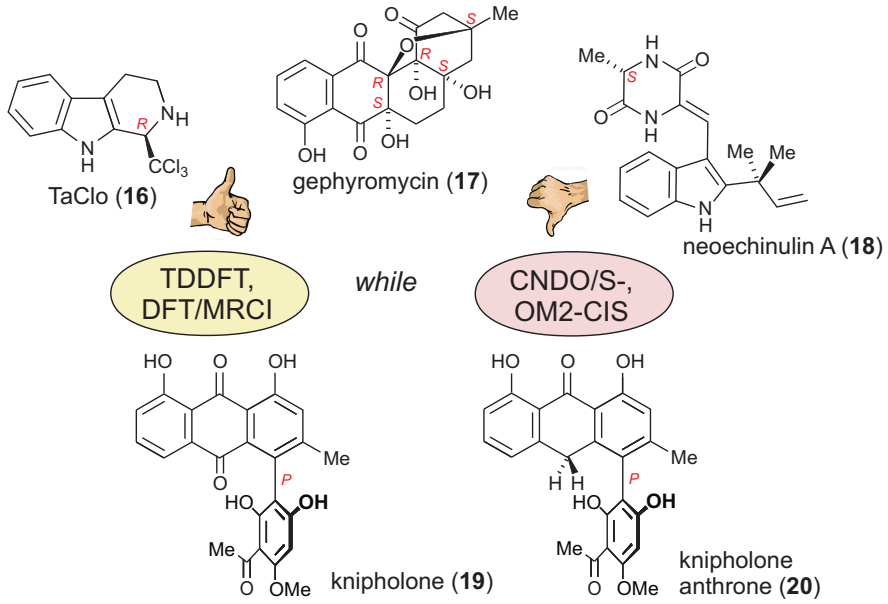

Figure 94. Benefits of the TDDFT and DFT/MRCI methods.

Analysis of these compounds revealed that semiempirical methods provided very poor results or even totally failed in the following cases: 1. Halogen-containing molecules if their CD spectra are largely determined by excitations involving halogen atoms (as in **16**); 2. Systems with excitations having a substantial n-π^* character (as in **17** and **18**), although the OM2 method showed somewhat better results than the CNDO/S approach in these cases; 3. Highly constrained structures with a large number of heteroatoms and hydrogen bonds (as in **17**). Furthermore, the examples of molecules **18**, **19**, and **20**, having structurally challenging chromophores, demonstrated a great importance of the structure-optimization step, which may drastically change the final result. Thus, a wrong configurational attribution had earlier been obtained for knipholone (**19**) and knipholone anthrone (**20**), which were

investigated only at a semiempirical level. Only now, within this thesis, the use of advanced methods (viz. DFT, TDB3LYP/TZVP, and DFT/MRCI/SVP) in combination with the experimental studies afforded correct absolute configurations of **19** and **20**.

4. The fourth part of this work dealt with two problematic cases of theoretical CD predictions (Figure 95).

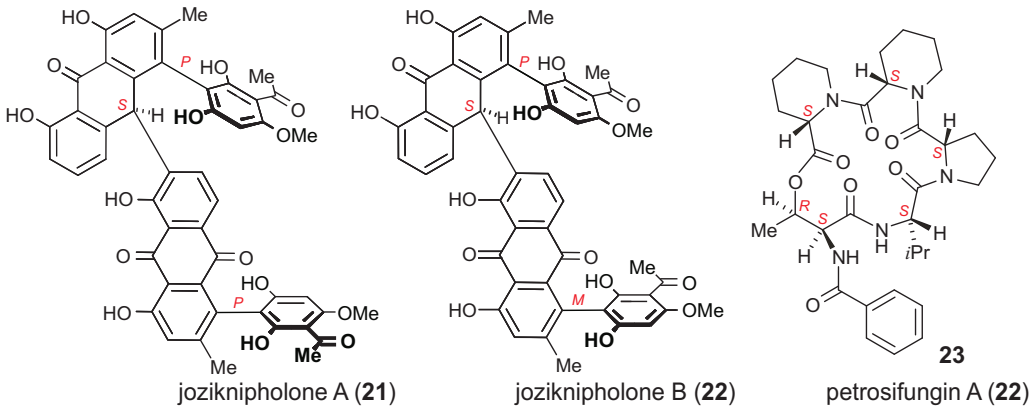

Figure 95. Challenging cases for the assignment of the absolute configurations.

Because of the large size of the molecules, CD calculations for the diastereomeric phenylanthraquinone dimers, joziknipholones A (**21**) and B (**22**), could only be done at the relatively low TDBLYP/TZVP level, which appeared inadequate for the fully correct reproduction of their experimental CD spectra. The solid configurational attribution of **21** and **22** could be then achieved only from the experimental work. Along with the CD calculations, compound **21** was investigated with regard to the rotation around its central sp^2-sp^3, configurationally nearly stable, axis.

In the case of cyclodepsipeptide petrosifungin A (**23**), possessing six stereogenic centers, several diastereomeric structures had to be considered. Because of the high flexibility, the diastereomers were investigated at a semiempirical level, which, however, resulted in virtually the same CD spectra, so that an unequivocal configurational distinction and attribution was not possible. A reliable discrimination between the diastereomers seems to be a common problem for CD calculations. This applies particularly to the molecules in which all stereogenic elements equally or similarly contribute to the overall CD spectrum appearance. In such cases, a higher-

level treatment (like TDB3LYP or DFT/MRCI) is required, whereas, in cases of highly flexible (as **23**) or very large molecules (as e.g., **21**), a combination of theoretical and experimental investigations is preferable.

5. Another project of this PhD work concerned a recently introduced method of determining the absolute stereostructures by a combination of solid-state CD spectroscopy and CD calculations. This approach was now successfully applied to the conformationally flexible naphthylisoquinoline alkaloid, dioncophylline A (**24**) (Figure 96), whose CD spectrum is known to be highly sensitive to the orientation at the biaryl axis.

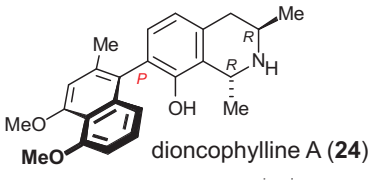

Figure 96. Dioncophylline A (**24**) as a model compound for solid-state CD investigations.

At first, CD calculations were performed for the single conformer of **24** found in the crystal by using three different methods, which showed very similar results and permitted the configurational assignment of dioncophylline A (**24**). Additionally, an influence of the neighboring molecules in the crystal on the CD behavior of **24** was examined by considering a set of dyads as well as a 16-molecule fragment of the crystal structure of **24**, which should cover the synergetic effects of the crystal and result in an improved CD spectrum. Such investigations were performed for the first time in this work, proving that there is indeed an effect of the crystalline structure on the CD spectrum of **24**. Although in this particular case only a small improvement could be achieved, this analysis seems to give a higher security for the configurational assignment with the novel solid-state CD method.

A whole range of chiral compounds described in this dissertation permitted, thus, to conclude that in most cases quantum chemical CD calculations do provide a high efficiency and reliability in solution of stereochemical problems. A particular success was provided by the TDB3LYP/TZVP method, which resulted in high accuracies at moderate computational costs. Nevertheless, it is fair to note that the

computationally cheap semiempirical methods do generally show good results for simple biaryl chromophores, and hence, they are still useful for calculating large systems with axial chirality. For cases where also the TDB3LYP/TZVP method is not accurate enough, other, more advanced density functionals (such as BHLYP) together with more extended basis sets, or the DFT/MRCI approach may become a beneficial alternative.

Outlook

The outlook for CD calculations is associated with the development of novel, more exact density functionals such as the double-hybrid B2PLYP or local-hybrid functionals, which should describe the excited states with a higher quality.

New methods, like dispersion-corrected DFT, should increase the accuracy of the conformational analysis.

The excited-states calculations should benefit from the application of multireference methods (like DFT/MRCI and MRMP2), which become feasible for larger molecules.

The inclusion of solvent effects by using, for example, COSMO calculations should also become increasingly commonly used within CD calculations.

For the crystalline compounds, particularly if they possess a high conformational flexibility in solution, the novel solid-state CD method should be considered as an important tool for the determination of absolute stereostructures.

Chapter 7

Zusammenfassung

Quantenchemische Rechnungen des Circular-Dichroismus (CD) in Kombination mit experimentellen CD-Studien sind eines der besten analytischen Werkzeuge zur Aufklärung der absoluten Stereostruktur. Die ständige Entwicklung der Computertechnologie und eine breite Vielfalt vorhandener quantenchemischen Methoden erlauben nun Untersuchungen an praktisch jedem molekularen System. Dafür muss man in jedem einzelnen Fall die am besten geeignete Methode, hinsichtlich der gewünschten Genauigkeit, des Zeitaufwands und der vorhandenen Computer-Ressourcen finden. Weitere aussichtsreiche Perspektive dieser Methode ergibt sich die Festkörper-CD-Spektroskopie, denn damit kann man konformativ "eingefrorene" Moleküle vermessen. So öffnet sich der Weg für die Konfigurationsaufklärung chiraler Verbindungen mit hoher molekularer Flexibilität.

Im Laufe dieser Arbeit wurden die absoluten Konfigurationen einer Reihe von chiralen Verbindungen unter Verwendung von verschiedenen theoretischen Methoden aufgeklärt. Dafür wurden die semiempirische CIS-Methoden (nämlich, CNDO/S und OM2) und höherwertige *Ab-initio*-Ansätze (TDDFT und DFT/MRCI) benutzt. Der Circular-Dichroismus ist stark abhängig vom konformativen Verhalten

des Moleküls. Besondere Aufmerksamkeit lag daher auf der Durchsuchung der relevantesten Strukturen (die BOLTZMANN- und MD-Ansätze) und auf der Vorhersage ihrer Energien. Alle untersuchten Verbindungen wurden in vier Gruppen unterteilt in Abhängigkeit von der benutzten Methode für ihre vollständige Konfigurations-zuordnung.

1. Zuerst wurde die Anwendung des einfachsten CNDO/S-CIS-Ansatzes in Kombination mit der BOLTZMANN- oder der MD-Methode gezeigt (Abb. 92).

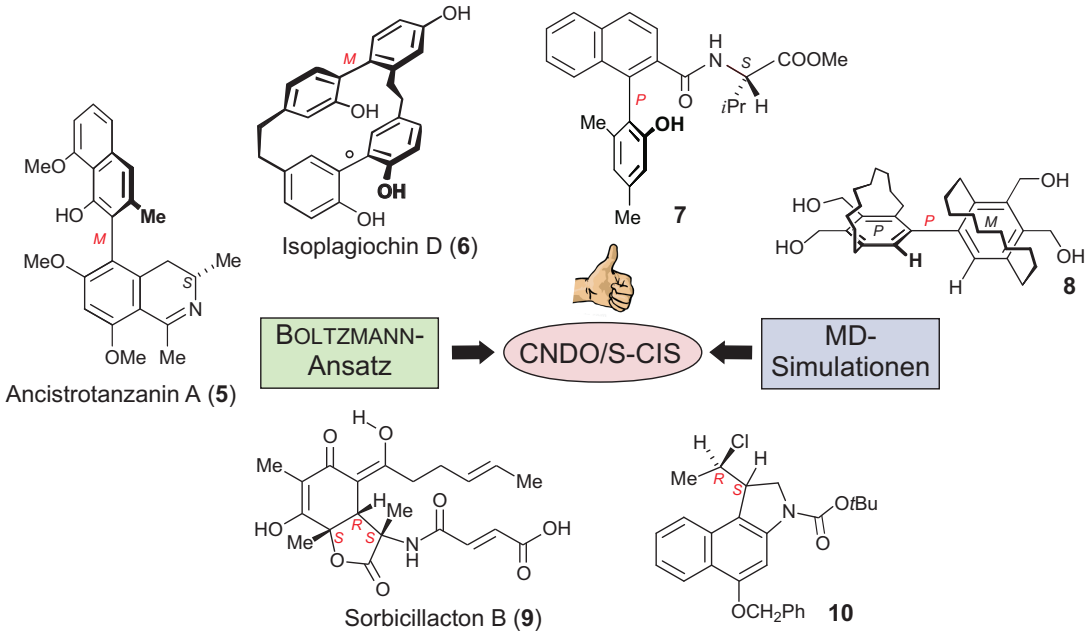

Abb. 92. Substanzen, deren absolute Konfigurationen durch semiempirische CNDO/S-CIS-Rechnungen zugewiesen wurden.

Die Kombination MD - CNDO/S-CIS lieferte sehr gute Ergebnisse für die Biaryle **5** und **6** sowie für die sehr flexiblen Moleküle Sorbicillacton B (**9**) und Benz[e]indol **10**. Im Fall des Bi[10]paracyclophans **8** jedoch ergaben die MD-simulierten Strukturen die falsche Konfiguration. Mit Hilfe der aufwendigeren, aber genaueren BOLTZMANN-Methode konnte dieses Problem gelöst werden. Deshalb wurden für alle folgenden Projekte die Ergebnisse des MD-Ansatzes immer zusätzlich mit der BOLTZMANN-Methode bestätigt. Die CNDO/S-Berechnungen der angeregten Zustände lieferten für alle diese Verbindungen oft gute Ergebnisse, sowohl in Bezug auf die CD-Peaks als auch für die Anregungsenergien. Für die Verbindungen **5**, **6**, **7**

und **8**, die im Prinzip alle ein Biaryl-System als Hauptchromophor haben, wurden die Anregungsenergien nur leicht unterschätzt. In den Fällen des Sorbicillactons B (**9**) und des Benz[e]indols **10**, die deutlich unterschiedliche Chromophore besitzen, wurden hingegen etwas höheren Energien erhalten. Die generell gute Übereinstimmung zwischen den experimentellen CD-Kurven aller Substanzen und den jeweiligen CNDO/S-Spektren erlaubte eine Zuordnung der eindeutige Absolutkonfiguration, so dass weitere, zeitaufwendigere CD-Rechnungen unnötig erschienen.

2. Im nächsten Kapitel wurden Verbindungen behandelt, für die sowohl semiempirische als auch TDDFT-Rechnungen in fast der gleichen Genauigkeit resultierten (Abb. 93).

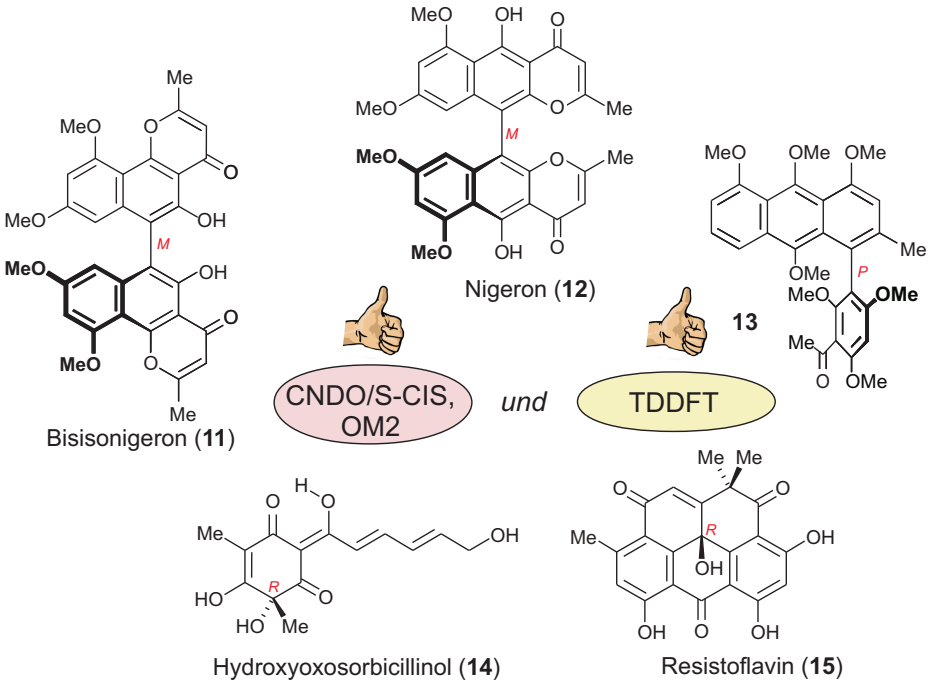

Abb. 93. Verbindungen, deren absolute Konfigurationen durch semiempirische CNDO/S-CIS- und TDDFT-Ansätze mit fast der gleichen Genauigkeit zugewiesen wurden.

Die CNDO/S-Rechnungen erwiesen sich wieder als besonders erfolgreich für Biaryl-Moleküle (hier **11**, **12** und **13**), für die es nur kleine Fehler bei den Anregungsenergien gab. Der semiempirische OM2-Ansatz schien weniger genau zu sein und lieferte zu hohe Energien für Bisisonigeron (**11**) und Nigeron (**12**). Die

TDDFT-Rechnungen ergaben eine sehr exakte Beschreibung der angeregten Zustände von **12**, **13** und **15**, während die Ergebnisse für die Verbindungen **11** und **14** etwas schlechter waren. Die CD-Intensitäten der Moleküle **11**, **13** und **14** wurden durch beide Methoden, CNDO/S und TDB3LYP, reproduziert, während im Fall von Nigeron (**12**) und Resistoflavin (**15**) die TDDFT-Spektren etwas näher an den jeweiligen experimentellen Kurven lagen als die CNDO/S-vorhergesagten Spektren.

3. Der dritte Teil der Dissertation befasste sich mit Molekülen, für die nur die high-level-Methoden die experimentellen CD-Spektren korrekt reproduzierten und damit eine eindeutige Konfigurationszuordnung ermöglichten (Abb. 94).

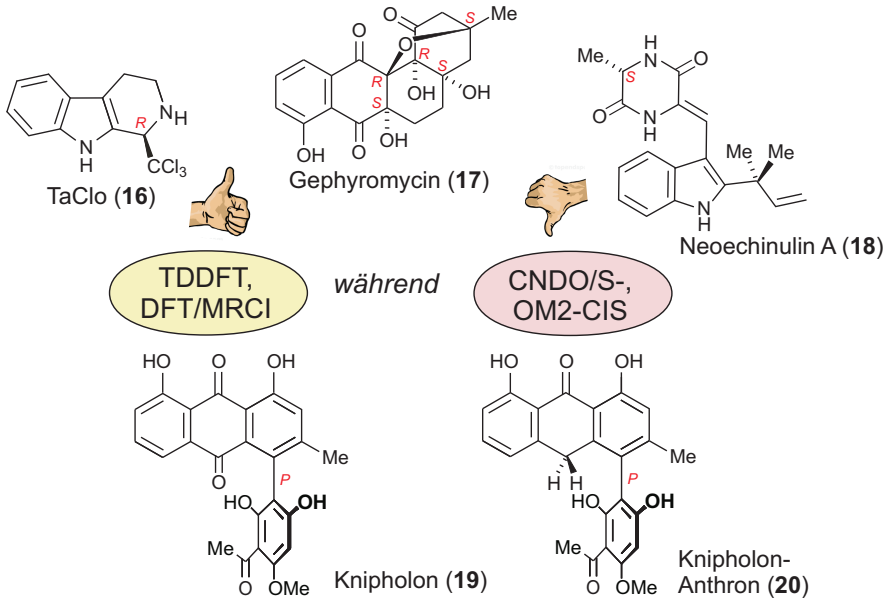

Abb. 94. Vorteil der benefit-Methoden.

Die Untersuchungen zeigten, dass semiempirische Methoden schlechte Ergebnisse liefern oder sogar vollständig ungeeignet sind in den folgenden Fällen: 1. Halogen enthaltende Substanzen, vor allem wenn ihre CD-Spektren größtenteils durch Anregungen aus den Halogenatome entstehen (wie in **16**); 2. Systeme mit Anregungen, die einem hohen n-π*-Charakter besitzen (wie in **17** und **18**), auch wenn die OM2-Methode hier etwas bessere Ergebnisse als der CNDO/S-Ansatz gezeigt hat; 3. Sehr gespannte Strukturen mit einer großen Anzahl von Heteroatomen und Wasserstoff-Brücken (wie in **17**). Außerdem zeigten Beispiele wie die Moleküle

18, **19** und **20**, mit schwierigen Chromophoren, die hohe Bedeutung, verläßliche Struktur-Optimierungen durchzuführen, da diese Ergebnisse zu drastischen Änderungen bei der CD-Berechnung führen können. So waren auch die Konfigurationen von Knipholon (**19**) und Knipholon-Anthron (**20**) falsch zugewiesen worden, da sie zunächst nur auf semiempirischem Niveau untersucht worden waren. Erst jetzt, im Rahmen dieser Arbeit, konnte durch die Verwendung aktueller Methoden auf höchstem Niveau (nämlich DFT, TDB3LYP/TZVP und DFT/MRCI/SVP) in Kombination mit den experimentellen Untersuchungen die korrekte absolute Konfigurationen von **19** und **20** bestimmt werden.

4. Im vierten Teil dieser Arbeit wurden zwei problematischere Fälle zur theoretischen Vorhersage von CD-Spektren diskutiert (Abb. 95).

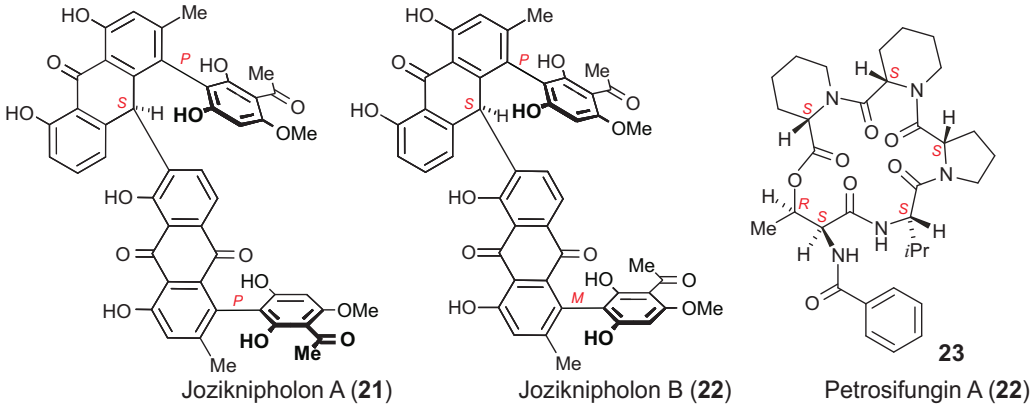

Abb. 95. Problematische Fälle bei der Bestimmung der absoluten Konfigurationen.

Der erste betraf die diastereomeren Phenylanthrachinon-Dimere Joziknipholon A (**21**) und B (**22**) (Abb. 95). Aufgrund der Größe dieser Moleküle konnten nur relativ einfache TDBLYP/TZVP-Rechnungen durchgeführt werden. Die resultierenden CD-Spektren ermöglichten aber keine sichere Konfigurations-zuordnung. Dies wurde erst durch zusätzliche experimentelle Arbeit erreicht. Zusammen mit den CD-Rechnungen für **21** wurde außerdem die Rotation um die zentrale sp^2-sp^3 Achse untersucht, die konfigurativ stabil zu sein scheinte.

Im Fall des Cyclodepsipeptids Petrosifungin A (**23**), das sechs Stereozentren besitzt, sollten mehrere diastereomere Strukturen betrachtet werden. Aufgrund der hohen Flexibilität wurden alle mögliche Diastereomere nur auf semiempirischem

Niveau untersucht. Dies führte jedoch zu nahezu identischen CD-Spektren, so dass eine definitive Konfigurationsunterscheidung und Zuordnung nicht möglich war. Eine zuverlässige Unterscheidung zwischen Diastereomeren scheint ein generelles Problem für CD-Rechnungen zu sein. Das gilt besonders, wenn alle stereogene Elemente die gleiche oder ähnliche Beiträge zum Gesamt-CD-Spektrum liefern. Dies erfordert im Allgemeinen eine Behandlung auf höheren Niveaus (z.B. TDB3LYP oder DFT/MRCI), wohingegen in Fällen hochflexibler (wie z.B. **23**) oder sehr großer Moleküle (wie **21**), eine Kombination von theoretischen und experimentellen Untersuchungen vorzuziehen ist.

5. Ein weiteres Projekt dieser Doktorarbeit befasste sich mit einer erst kürzlich eingeführte Methode zur Konfigurationsbestimmung, der Festkörper-CD-Spektroskopie in Kombination mit CD-Rechnungen. Dieser Ansatz wurde nun erfolgreich für das flexible Naphthylisochinolin-Alkaloid Dioncophyllin A (**24**) angewendet (Abb. 96), dessen CD-Spektrum sich als sehr empfindlich gegenüber der Orientierung an der Biaryl-Achse gezeigt hat.

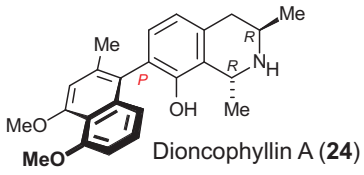

Abb. 96. Dioncophyllin A (**24**) als Modell-Substanz für Festkörper-CD-Untersuchungen.

Zuerst wurde das einzelne Konformer, das aus der Kristallstruktur von **24** ermittelt wurde, mit drei verschiedenen Methoden betrachtet. Alle Rechnungen zeigten sehr ähnliche Ergebnisse und erlaubten eine sichere Zuordnung der absoluten axialen Konfiguration von Dioncophyllin A (**24**). Als nächstes wurde ein Einfluss der benachbarten Moleküle im Kristall auf das CD-Verhalten von **24** untersucht. Dafür wurde eine Reihe von Dyaden sowie ein 16-Molekül-Fragment der Kristallstruktur von **24** berücksichtigt, in dem man offensichtlich zu synergistischen Effekten des Kristalls und damit zu Verbesserung des CD-Spektrums kommen kann. Sollche Studien wurden zum ersten Mal durchgeführt, und es konnte tatsächlich

gezeigt werden, dass Effekte im Kristall vorhanden sind. Obwohl dadurch im Fall von **24** nur eine kleine Verbesserung erreicht werden konnte, bietet diese Analyse im Allgemeinen eine höhere Sicherheit für die Zuordnung der Absolutkonfigurations mit dem neuartigen Festkörper-CD-Ansatz.

Die gesamte Reihe der chiralen Verbindungen, die in dieser Doktorarbeit beschrieben sind, zeigt, dass quantenchemische CD-Rechnungen in den meisten Fällen in der Lage sind, stereochemische Probleme mit hoher Effizienz und ausreichender Zuverlässigkeit zu lösen. Besonders erfolgreich dabei war der TDB3LYP/TZVP-Ansatz, der sehr hohe Genauigkeiten bei mäßigem Rechenaufwand ermöglicht. Trotzdem muss man bemerken, dass die schnelleren semiempirischen Rechnungen üblicherweise gute Ergebnisse für einfache Biaryl-Chromophore zeigen und dass sie deshalb immer noch wertvoll sind, um große Systeme mit axialer Chiralität zu berechnen. In Fällen, in denen auch die TDB3LYP/TZVP-Methode nicht ausreichend ist, sind verbesserte Dichtefunktionale (wie BHLYP) zusammen mit einem erweiterten Basissatz oder der DFT/MRCI-Ansatz mögliche Alternativen.

Ausblick

Die Zukunft von CD-Rechnungen steht in einer engen Verbindung mit der Entwicklung neuer Funktionale, wie z.B. des Doppelhybridfunktionals B2PLYP oder lokal hybridisierter Funktionale, die die angeregten Zustände mit höherer Genauigkeit berechnen sollten.

Auch neue Methoden, wie z.B. die Dispersions-korrigierte DFT, sollten vor allem bei der Konformationsanalyse noch exaktere Ergebnisse liefern.

Die Berechnung von angeregten Zuständen sollten vom Einsatz von Multi-Reference-Verfahren (wie DFT/MRCI und MRMP2) profitieren, die nun auch für größere Moleküle realisierbar sind.

Gerade für geladene Moleküle ist die Berücksichtigung von Lösungsmitteleffekten (wie z.B. mit der COSMO-Methode) äußerst wichtig und sollte bei den Berechnungen öfter in Betracht gezogen werden.

Für konformativ hoch-flexible Moleküle, die in kristalliner Form vorliegen, ist Festkörper-CD eine interessante Alternative zur Aufklärung der Absolutkonfiguration.

List of Abbreviations

ACM	Adiabatic Connection Method
AM1	Austin Model 1
A(M)O	Atomic (Molecular) Orbital
B	Becke's Exchange Functional
BH	Becke's Half-and-Half Exchange Functional
BM	BOLTZMANN Method
B2PLYP	Double-Hybrid Density Functional
B3	Becke's Three-Parameter Exchange Functional
calcd.	Calculated
CB	Circular Birefringence
(E)(V)CD	(Electronic) (Vibrational) Circular Dichroism
CE	COTTON Effekt
CI	Configuration Interaction
CID	CI with Doubles
CIS	CI with Singles
CISD	CI with Singles and Doubles
CISDT	CI with Singles, Doubles, and Triples
CISDTQ	CI with Singles, Doubles, Triples, and Quadrupoles
CNDO/S	Complete Neglect of Differential Overlap for Spectroscopy
Conf	Conformer
COSY	Correlation Spectroscopy (an NMR Technique)
CSF	Configuration State Function
DRCD	Diffuse-Reflectance Circular Dichroism
Epl	Elliptically Polarized Light
exp.	Experimental
FF	Force Field
GGA	Generalized Gradient Approximation

HF	Hartree Fock
HMBC	Heteronuclear Multiple Bond Correlation (an NMR Technique)
HOMO	Highest Occupied Molecular Orbital
HPLC	High Performance Liquid Chromatochraphy
HSQC	Heteronuclear Single-Quantum Correlation
INDO/S	Intermediate Neglect of Differential Overlap for Spectroscopy
LB	Linear Birefringence
lCpl	Left Circularly Polarized Light
LD	Linear Dichroism
LDA	Local Density Approximation
Lpl	Linearly Polarized Light
LSDA	Local Spin Density Approximation
LUMO	Lowest Unoccupied Molecular Orbital
LYP	Lee-Yang-Parr's Correlation Functional
MD	Molecular Dynamics
MM3	Molecular Mechanics (Force Field) 3
MNDO	Modified Neglect of Differential Overlap
MR	Multireference
NMR	Nuclear Magnetic Resonance
NOESY	Nuclear Overhauser Effect Spectroscopy (an NMR Technique)
OM2	Orthogonalization Model 2
ORD	Optical Rotatory Dispersion
PCM	Polarizable Continuum Model
PM3	Parametric Method 3
rCpl	Right Circularly polarized light
RI	Resolution of Identity
ROA	RAMAN Optical Activity
ROESY	Rotational Frame Overhauser Effect Spectroscopy (an NMR Technique)

STQN	Synchronous Transit-Guided Quasi-Newton method
SVP	Split-Valence Polarized basis set
(TD)DFT	(Time Dependent) Density Functional Theory
TS	Transition State
TZVP	Triple-Zeta Valence Polarized Basis Set
UCS	Universal Chiroptical Spectrophotometer
UV/Vis	Ultraviolet/Visible

Literature and Notices

[1] L. Kelvin; *Baltimore Lectures on Molecular Dynamics and the Wave Theory of Light*; Cambridge University Press, London, **1904**.

[2] For a classical historical overview, see: T. M. Lowry; *Optical Rotatory Power*; Longsmans, London, **1935**. Reprinted in Dover, New York, **1964**.

[3] R. S. Cahn, C. K. Ingold, V. Prelog; Specification of Molecular Chirality; *Angew. Chem.* **1966**, *78*, 413–477; *Angew. Chem. Int. Ed.* **1966**, *5*, 385–415.

[4] V. Prelog, G, Helmchen; Basic Principles for the CIP-System and Proposals for a Revision; *Angew. Chem.* **1982**, *94*, 614–631; *Angew. Chem. Int Ed.* **1982**, *21*, 567–583.

[5] E. Brenna, C. Fuganti, S. Serra; Enantioselective Perception of Chiral Odorants; *Tetrahedron: Asymmetry* **2003**, *14*, 1–42.

[6] M. Nozaki, N. Suzuki, S. Oshikubo; *Flavour Science: Recent Developments*; The Royal Society of Chemistry, Cambridge, **1996**.

[7] J. Solms; The Taste of Amino Acids, Peptides, and Proteins; *J. Agric. Food Chem.* **1969**, *17*, 686–688.

[8] a) G. Haniotakis, W. Francke, K. Mori, H. Redlich, V. Schurig; Sex-Specific Activity of (*R*)-(–)- and (*S*)-(+)-1,7-dioxaspirol[5.5]undecane, the Major Pheromone of Dacus oleae; *J. Chem. Ecol.* **1986**, *12*, 1559–1568. b) K. Mori; Chirality and Insect Pheromones; *Chirality* **1998**, *10*, 578–586.

[9] A. Mack, J. O. Salazar; Eszopiclone: a Novel Cyclopyrrolone with Potential Benefit in both Transient and Chronic Insomnia; *Formulary* **2003**, *38*, 582–593.

[10] T. D. Crawford; *Ab initio* Calculation of Molecular Chiroptical Properties; *Theor. Chem. Acc.* **2006**, *115*, 227–245.

[11] a) P. L. Polavarapu; Optical Rotation: Recent Advances in Determining the Absolute Configuration; *Chirality* **2002**, *14*, 768–781. b) A. Lattanzi, R. G. Viglione, A. Scettri, R. Zanasi; TDDFT Response Theory Calculation of Optical Rotation as a Method for the Assignment of Absolute Configuration of Camphor-Derived Furyl Hydroperoxide and Alcohol; *J. Phys. Chem. A* **2004**, *108*, 10749–10753.

[12] a) S. Grimme, A. Banlmann, G. Haufe; Ab Initio Calculations for the Optical Rotations of Conformationally Flexible Molecules: A Case Study on Six-, Seven-, and Eight-Membered Fluorinated Cycloalkanol Esters; *Chirality* **2002**, *14*, 793–797. b) P. L. Polavarapu, J. He, J. Crassous, K. Ruud; Absolute Configuration of C_{76} from Optical Rotatory Dispersion; *ChemPhysChem* **2005**, *6*, 2535–2540.

[13] G. Bringmann, K.-P. Gulden, H. Busse, J. Fleischhauer, B. Kramer, E. Zobel; The Calculation of CD Spectra for the Elucidation of the Absolute Configuration of Chiral Biaryls; *Planta Med.* **1992**, *58* (Suppl. 1), 705.

[14] G. Bringmann, S. Busemann; Quantumchemical Calculation of CD Spectra: The Absolute Configuration of Biologically Active Natural Products; in: *Natural Product Analysis* (Eds.: P. Schreier, M. Herderich, H. U. Humpf, W. Schwab), Vieweg, Wiesbaden, **1998**, pp. 195–212.

[15] C. Diedrich, S. Grimme; Systematic Investigation of Modern Quantum Chemical Methods to Predict Electronic Circular Dichroism Spectra; *J. Phys. Chem. A* **2003**, *107*, 2524–2539.

[16] P. J. Stephens, D. M. McCann, F. J. Devlin, A. B. Smith III; Determination of the Absolute Configurations of Natural Products via Density Functional Theory Calculations of Optical Rotation, Electronic Circular Dichroism, and Vibrational Circular Dichroism: The Cytotoxic Sesquiterpene Natural Products

Quadrone, Suberosenone, Suberosanone, and Suberosenol A Acetate; *J. Nat. Prod.* **2006**, *69*, 1055–1064.

[17] G. Bringmann, T. A. M. Gulder, M. Reichert, T. Gulder; The Online Assignment of the Absolute Configuration of Natural Products: HPLC-CD in Combination with Quantum Chemical CD Calculations; *Chirality* **2008**, *20*, 628–642.

[18] G. Bringmann, T. Bruhn, K. Maksimenka, Y. Hemberger; The Assignment of Absolute Stereostructures by Quantum Chemical Circular Dichroism Calculations; *Eur. J. Org. Chem.* **2009**, *17*, 2717–2727.

[19] a) T. B. Freedman, X. Cao, R. K. Dukor, L. A. Nafie; Absolute Configuration of Chiral Molecules in the Solution State Using Vibrational Circular Dichroism; *Chirality* **2003**, *15*, 743–758. b) F. J. Devlin, P. J. Stephens, J. R. Cheeseman, M. J. Frisch; Prediction of VCD Spectra Using Density Functional Theory: Camphor and Fenchone; *J. Am. Chem. Soc.* **1996**, *118*, 6327–6328.

[20] a) G. Maas; Determination of Absolute and Relative Configuration by X-ray and Neutron Diffraction Methods; in: *Methods of Organic Chemistry* (Eds.: G. Helmchen, R. Hoffmann, J. Mulzer, E. Schaumann), E21 ed., Thieme Verlag, Stuttgart, **1996**, pp. 379–397. b) S. H. Wilen, J. Z. Qi, P. G. Williard; Resolution, Asymmetric Transformation, and Configuration of Tröger's Base. Application of Tröger's Base as a Chiral Solvating Agent; *J. Org. Chem.* **1991**, *56*, 485–487.

[21] P. Welzer; Determination of Absolute and Relative Configuration using chemical methods; in: *Methods of Organic Chemistry* (Eds.: G. Helmchen, R. Hoffmann, J. Mulzer, E. Schaumann), E21 ed., Georg Thieme Verlag, Stuttgart, **1996**, pp. 399–497.

[22] a) J. A. Dale, H. S. Mosher; Nuclear Magnetic Resonance Enantiomer Reagents; *J. Am. Chem. Soc.* **1973**, *95*, 512–519. b) S. Yamaguchi; Nuclear Magnetic

Resonance Analysis Using Chiral Derivatives; in: *Assymmetric synthesis* (Ed.: J. D. Morrison), Academic Press, New York, **1983**, pp. 1–125.

[23] G. Bringmann, R. God, M. Schäffer; An Improved Degradation Procedure for Determination of the Absolute Configuration in Chiral Isoquinoline and β-Carboline Derivatives; *Phytochemistry* **1996**, *43*, 1393–1403.

[24] a) G. Bringmann, M. Stahl, K.-P. Gulden; Circular Dichroism of Naphthyldihydroisoquinoline Alkaloids: Determination of the Axial Configuration of Yaoundamine A; *Tetrahedron* **1997**, *53*, 2817–2822. b) M. Dreyer, B. W. Nugroho, F. I. Bohnenstengel, R. Ebel, V. Wray, L. Witte, G. Bringmann, J. Mühlbacher, M. Herold, P. D. Hung, L. C. Kiet, P. Proksch; New Insecticidal Rocaglamide Derivatives and Related Compounds for *Aglaia oligophylla*; *J. Nat. Prod.* **2001**, *64*, 415–420. c) G. Bringmann, J. Mühlbacher, M. Reichert, M. Dreyer, J. Kolz, A. Speicher; Stereochemistry of Isoplagiochin C, A Macrocyclic Bisbibenzyl from Liverworts; *J. Am. Chem. Soc.* **2004**, *126*, 9283–9290. d) G. Bringmann, T. Gulder, M. Reichert, F. Meyer; Ancisheynine, the First *N,C*-Coupled Naphthylisoquinoline Alkaloid: Total Synthesis and Stereochemical Analysis; *Org. Lett.* **2006**, *8*, 1037–1040.

[25] a) G. Bringmann, M. Reichert, Y. Hemberger; The Absolute Configuration of Streptonigrin; *Tetrahedron* **2008**, *64*, 515–521. b) G. Bringmann, D. C. G. Götz, T. A. M. Gulder, T. H. Gehrke, T. Bruhn, T, Kupfer, K. Radacki, H. Braunschweig, A. Heckmann, C. Lambert; Axially Chiral ß,ß′-Bisporphyrins: Synthesis and Configurational Stability Tuned by the Central Metals; *J. Am. Chem. Soc.* **2008**, *130*, 17812–17825. c) G. Bringmann, S. Rüdenauer, T. Bruhn, L. Benson; Total Synthesis of the Antimalarial Naphthylisoquinoline Alkaloid 5-Epi-4′-O-demethylancistrobertsonine C by Asymmetric Suzuki Cross Coupling Reaction; *Tetrahedron* **2008**, *64*, 5563–5568. d) Z. Yunt, K. Reinhardt, A. Li, M. Engeser, H.-M. Dahse, M. Gütschow, T. Bruhn, G. Bringmann, J. Piel; Cleavage of Four Carbon-Carbon Bonds during Biosynthesis of the

Griseorhodin A Spiroketal Pharmacophore; *J. Am. Chem. Soc.* **2009**, *131*, 2297–2305. e) J. Bunzen, T. Bruhn, G. Bringmann, A. Lützen; Synthesis and Helicate Formation of a New Family of BINOL-Based Bis(bipyridine) Ligands; *J. Am. Chem. Soc.* **2009**, *131*, 3621–3630.

[26] a) M. Xu, T. Bruhn, B. Hertlein, R. Brun, A. Stich, J. Wu, G. Bringmann; Shuangancistrotectorines A-E, Dimeric Naphthylisoquinoline Alkaloids with Three Chiral Biaryl Axes, from the Chinese Plant *Ancistrocladus tectorius*; *Chem. Eur. J.* **2010**, *16*, 4206–4216. b) D. C. G. Götz, T. Bruhn, O. Senge, G. Bringmann; Synthesis and Stereochemical Characterization of Highly Unsymmetric *β*,meso-Linked Porphyrin Arrays; *J. Org. Chem.* **2009**, *74*, 8005–8020.

[27] a) J. Del Bene, H. H. Jaffé; Use of the CNDO Method in Spectroscopy I: Benzene, Pyridine, and the Diazines; *J. Phys. Chem.* **1968**, *48*, 1807–1813. b) J. Del Bene, H. H. Jaffé; Use of the CNDO Method in Spectroscopy II: Five-Membered Rings; *J. Phys. Chem.* **1968**, *48*, 4050–4055. c) R. L. Ellis, G. Kuehnlenz, H. H. Jaffé; Use of the CNDO Method in Spectroscopy VI: Further n-π* Transitions; *Theor. Chim. Acta* **1972**, *26*, 131–140.

[28] a) W. Weber, W. Thiel; Orthogonalization Corrections for Semiempirical Methods; *Theor. Chem. Acc.* **2000**, *103*, 495–506. b) E. K. U. Gross, J. F. Dobson, M. Petersilka; Density Functional Theory of Time-Dependent Phenomena; *Top. Curr. Chem.* **1996**, *181*, 80–172.

[29] a) E. K. U. Gross, W. Kohn; Time-Dependent Density Functional Theory; *Adv. Quantum Chem***. 1990**, *21*, 255–291. b) M. E. Casida; in *Recent Advances in Density Functional Methods* (Ed.: D. P. Chong), World Scientific, Singapore, **1995**, pp. 155–192. c) E. K. U. Gross, J. F. Dobson, M. Petersilka; in *Topics in Current Chemistry* (Ed.: R. F. Nalewajski), Springer-Verlag, Heidelberg, **1996**, pp. 81-171.

[30] S. Grimme, M. Waletzke; A Combination of Kohn-Sham Density Functional Theory and Multi-Reference Configuration Interaction Methods; *J. Chem. Phys.* **1999**, *111*, 5645–5655.

[31] G. Bringmann, M. Dreyer, J. H. Faber, P. W. Dalsgaard, D. Stærk, J. Jaroszewski, H. Ndangalasi, F. Mbago, R. Brun, M. Reichert, K. Maksimenka, S. Brøgger Christensen; Ancistrotanzanine A, the First 5,3'-Coupled Naphthylisoquinoline Alkaloid, and Two Further, 5,8'-Linked Related Compounds from the Newly Described Plant Species *Ancistrocladus tanzaniensis*; *J. Nat. Prod.* **2003**, *66*, 1159–1165.

[32] J. M. Scher, J. Zapp, H. Becker, N. Kather; J. Kolz, A. Speicher, M. Dreyer, K. Maksimenka, G. Bringmann; Optically Active Bisbibenzyls from *Bazzania trilobata*: Isolation and Stereochemical Analysis by Chromatographic, Chiroptical, and Computational methods; *Tetrahedron* **2004**, *60*, 9877–9881.

[33] G. Bringmann, H. Scharl, K. Maksimenka, K. Radacki, H. Braunschweig, P. Wich, C. Schmuck; Atropodiastereoselective Cleavage of Configurationally Unstable Biaryl Lactones with Amino Esters; *Eur. J. Org. Chem.* **2006**, 4349–4361.

[34] G. Bringmann, T. A. M. Gulder, K. Maksimenka, D. Kuckling, W. Tochtermann; A Borderline Case Between *meso* and Stable C_1: an Axially Chiral, yet Configurationally Semi-stable Biphenyl with Two Oppositely Configured [10]Paracyclophane Portions; *Tetrahedron* **2005**, *61*, 7241–7246.

[35] G. Bringmann, G. Lang, T. A. M. Gulder, H. Tsuruta, J. Mühlbacher, K. Maksimenka, S. Steffens, K. Schaumann, R. Stöhr, J. Wiese, J. F. Imhoff, S. Perovic-Ottstadt, O. Boreiko, W. E. G. Müller; The First Sorbicillinoid Alkaloids, the Antileukemic Sorbicillactones A and B, from a Sponge-Derived *Penicillium chrysogenum* Strain; *Tetrahedron* **2005**, *61*, 7252–7265.

[36] L. F. Tietze, F. Major, I. Schuberth, D. A. Spiegl, B. Krewer, K. Maksimenka, G. Bringmann, J. Magull; Selective Treatment of Cancer: Synthesis, Biological Evaluation and Structural Elucidation of Novel Analogues of the Antibiotic CC-1065 and the Duocarmycins; *Chem. Eur. J.* **2007**, *13*, 4396–4409.

[37] M. C. Kozlowski, E. C. Dugan, E. S. DiVirgilio, K. Maksimenka, G. Bringmann; Asymmetric Total Synthesis of Nigerone and *ent*-Nigerone: Enantioselective Oxidative Biaryl Coupling of Highly Hindered Naphthols; *Adv. Synth. Catal.* **2007**, *349*, 583–594.

[38] G. Bringmann, K. Maksimenka, J. Mutanyatta-Comar, M. Knauer, T. Bruhn; The Absolute Axial Configurations of Knipholone and Knipholone Anthrone by TDDFT and DFT/MRCI CD Calculations: a Revision; *Tetrahedron* **2007**, *63*, 9810–9824.

[39] K. Ishida, K. Maksimenka, K. Fritzsche, K. Scherlach, G. Bringmann, C. Hertweck; The Boat-Shaped Polyketide Resistoflavin Results from *Re*-Facial Central Hydroxylation of the Discoid Metabolite Resistomycin; *J. Am. Chem. Soc.* **2006**, *128*, 14619–14624.

[40] G. Bringmann, D. Feineis, R. God, K. Maksimenka, J. Mühlbacher, K. Messer, M. Münchbach, K.-P. Gulden, E.-M. Peters, K. Peters; Resolution and Chiroptical Properties of the Neurotoxin 1-Trichloromethyl-1,2,3,4-tetrahydro-ß-carboline (TaClo) and Related Compounds: Quantum Chemical CD Calculations and X-ray Diffraction Analysis; *Tetrahedron* **2004**, *60*, 8143–8151.

[41] G. Bringmann, G. Lang, K. Maksimenka, A. Hamm, T. A. M. Gulder, A. Dieter, A. T. Bull, J. E. M. Stach, N. Kocher, W. E. G. Müller, H.-P. Fiedler; Gephyromycin, the First Bridged Angucyclinone, from *Streptomyces griseus* Strain NTK 14; *Phytochemistry* **2005**, *66*, 1366–1373.

[42] G. Bringmann, J. Mutanyatta-Comar, K. Maksimenka, J. M. Wanjohi, M. Heydenreich, R. Brun, W. E. G. Müller, M. G. Peter, J. O. Midiwo, A. Yenesew;

Joziknipholones A and B: the First Dimeric Phenylanthraquinones, from the Roots of *Bulbine frutescens*; *Chem. Eur. J.* **2008**, *14*, 1420–1429.

[43] a) H. Hussain, K. Krohn, U. Flörke, B. Schulz, S. Dräger, G. Pescitelli, S. Antus, T. Kurtán; Absolute Configurations of Globosuxanthone A and Secondary Metabolites from *Microdiplodia* sp. – A Novel Solid-State CD/TDDFT Approach; *Eur. J. Org. Chem.* **2007**, 292–295. b) K. Krohn, Z. Ullah, H. Hussain, U. Flörke, B. Schulz, S. Dräger, G. Pescitelli, P. Salvadori, S. Antus, T. Kurtán; Massarilactones E-G, New Metabolites from the Endophytic Fungus *Coniothyrium* sp., Associated with the Plant *Artimisia maritima*; *Chirality* **2007**, *19*, 464–470.

[44] a) M. Kwit, N. D. Sharma, D. R. Boyd, J. Gawronski; Absolute Configuration of Conformationally Flexible cis-Dihydrodiol Metabolites by the Method of Confrontation of Experimental and Calculated Electronic CD Spectra and Optical Rotations; *Chem. Eur. J.* **2007**, *13*, 5812–5821. b) W. Zhang, K. Krohn, U. Zia, U. Flörke, G. Pescitelli, L. Di Bari, S. Antus, T. Kurtán, J. Rheinheimer, S. Dräger, B. Schulz; New Mono- and Dimeric Members of the Secalonic Acid Family: Blennolides A–G Isolated from the Fungus Blennoria sp.; *Chem. Eur. J.* **2008**, *14*, 4913–4923. c) T. Kurtán, G. Pescitelli, P. Salvadori, A. Kenez, S. Antus, L. Szilagyi, T.-Z. Illyes, I. Szabo; Circular Dichroism of Diglycosyl Dichalcogenides in Solution and Solid State; *Chirality* **2008**, *20*, 379–385.

[45] G. Bringmann, K. Maksimenka, T. Bruhn, M. Reichert, T. Harada, R. Kuroda; Quantum Chemical CD Calculations of Dioncophylline A in the Crystalline State; *Tetrahedron* **2009**, *65*, 5720–5728.

[46] J. M. Bijvoet, A. F. Peerdeman, A. J. van Bommel; Determination of the Absolute Configuration of Optically Active Compounds by Means of X-Rays; *Nature* **1951**, *168*, 271–272.

[47] a) G. Bringmann, W. Saeb, K. Peters, E.-M. Peters; The Absolute Stereostructure of Dioncophylline A by Anomalous X-ray Dispersion of a 5-Bromo Derivative; *Phytochemistry* **1997**, *45*, 1283–1285. b) S. T. Deyrup, D. C. Swenson, J. B. Gloer, D. T. Wicklow; Caryophyllene Sesquiterpenoids from a Fungicolous Isolate of *Pestalotiopsis disseminata*; *J. Nat. Prod.* **2006**, *69*, 608–611. c) Y. F. Hallock, K. P. Manfredi, J. W. Blunt, J. H. Cardellina II, M. Schäffer, K.-P. Gulden, G. Bringmann, A. Y. Lee, J. Clardy, G. François, M. R. Boyd; Korupensamines A–D, Novel Antimalarial Alkaloids from *Ancistrocladus korupensis*; *J. Org. Chem.* **1994**, *59*, 6349–6355.

[48] H. D. Flack; On Enantiomorph-Polarity Estimation; *Acta Cryst.* **1983**, *A39*, 876-881.

[49] R. Kowalczyk, J. Skarzewski; *O*-Methylatrolactic Acid as a New Reagent for Determination of the Enantiomeric Purity and Absolute Configuration of Chiral Alcohols and Amines; *Tetrahedron: Asymmetry* **2006**, *17*, 1370–1379.

[50] D. Enders, C. R. Thomas, J. Runsink; 5-Amino-4-aryl-2,2-dimethyl-1,3-dioxans: Application as Chiral NMR Shift Reagents and Derivatizing Agents for Acidic Compounds; *Tetrahedron: Asymmetry* **1999**, *10*, 323–326.

[51] a) C. J. Welch; The Measurement of Enantiopurity Using Phosphorus-NMR; *Tetrahedron: Asymmetry* **1991**, *2*, 1127–1132. b) A.-S. Chauvin, G. Bernardinelli, A. Alexakis; Determination of the Absolute Configuration of Chiral Cyclic Alcohols Using Diamine Derivatizing Agents by ^{31}P NMR Spectroscopy; *Tetrahedron: Asymmetry* **2006**, *17*, 2203–2209.

[52] a) W. H. Pirkle, D. L. Sikkenga, M. S. Pavlin; Nuclear Magnetic Resonance Determination of Enantiomeric Composition and Absolute Configuration of γ-Lactones Using Chiral 2,2,2-Trifluoro-1-(9-anthryl)ethanol; *J. Org. Chem.* **1977**, *42*, 384–387. b) M. S. C. Pedras, M. Hossain, M. G. Sarwar, S. Montaut; Determination of the Enantiomeric Purity of the *Phytoalexins spirobrassinins* by

^{1}H NMR Using Chiral Solvation; *Bioorg. Med. Chem. Lett.* **2004**, *14*, 5469–5471. c) S. Higashibayashi, Y. Kishi; Assignment of the Relative and Absolute Configurations of Acyclic Secondary 1,2-Diols; *Tetrahedron* **2004**, *60*, 11977–11982.

[53] D. Neuhaus, M. P. Williamson; *The Nuclear Overhauser Effect in Structural and Conformational Analysis*; 2nd ed., Wiley-VCH, New York, **2000**.

[54] a) G. Bringmann, R. Zagst, H. Reuscher, L. Aké Assi; Ancistrobrevine B, the First Naphthylisoquinoline Alkaloid with a 5,8′-Coupling Site, and Related Compounds from *Ancistrocladus abbreviatus*; *Phytochemistry* **1992**, *31*, 4011-4014. b) G. Bringmann, D. Koppler, D. Scheutzow, A. Porzel; Determination of Configuration at the Biaryl Axes of Naphthylisoquinoline Alkaloids by Long-Range NOE Effects; *Magn. Reson. Chem.* **1997**, *35*, 297–301. c) G. Bringmann, I. Kajahn, M. Reichert, S. E. H. Pedersen, J. H. Faber, T. Gulder, R. Brun, S. B. Christensen, A. Ponte-Sucre, H. Moll, G. Heubl, V. Mudogo; Ancistrocladinium A and B, the First *N*,*C*-Coupled Naphthyldihydro-isoquinoline Alkaloids, from a Congolese *Ancistrocladus* Species; *J. Org. Chem.* **2006**, *71*, 9348–9356.

[55] H. Duddeck, W. Dietrich, G. Tóth; *Structure Elucidation by Modern NMR*; 3rd ed., Springer, New York, **1998**.

[56] a) G. Bringmann, G. Lang, M. Michel, M. Heubes; Stereochemical Assignment of the Fungal Metabolite Xestodecalactone A by Total Synthesis; *Tetrahedron Lett.* **2004**, *45*, 2829–2831. b) G. Bringmann, D. Menche; Stereoselective Total Synthesis of Axially Chiral Natural Products via Biaryl Lactones; *Acc. Chem. Res.* **2001**, *34*, 615–624. c) D. R. Williams, D. C. Kammler, A. F. Donnell, W. R. F. Goundry; Total Synthesis of (+)-Apiosporamide: Assignment of Relative and Absolute Configuration; *Angew. Chem.* **2005**, *117*, 6873–6876; *Angew. Chem. Int. Ed.* **2005**, *44*, 6715–6718. d) K. N. Fleming, R. E. Taylor; Total Synthesis and

Stereochemical Assignment of Myriaporones 1, 3, and 4; *Angew. Chem.* ***2004***, *116*, 1760–1762; *Angew. Chem. Int. Ed.* **2004**, *43*, 1728–1730.

[57] a) G. Bringmann, T. Geuder, M. Rübenacker, R. Zagst; A Facile Degradation Procedure for Determination of Absolute Configuration in 1,3-Dimethyltetra- and Dihydroisoquinolines; *Phytochemistry* **1991**, *30*, 2067–2070. b) G. Bringmann, R. God, M. Schäffer; An Improved Degradation Procedure for Determination of the Absolute Configuration in Chiral Isoquinoline and β-Carboline Derivatives; *Phytochemistry* **1996**, *43*, 1393–1403. c) H. A. Bates, J. J. Magrath, A. Kaushal; A Direct Method for Assignment of Absolute Configurations in Crown Gall Metabolites: the Structure of Nopaline; *J. Nat. Prod.* **1985**, *48*, 598–601. d) T. Someno, S. Kunimoto, H. Nakamura, H. Naganawa, D. Ikeda; Absolute Configuration of Kigamicins A, C and D; *J. Antibiot.* **2005**, *58*, 56–60.

[58] D. H. Whiffen; Optical Rotation and Geometrical Structure*; Chem. Ind.* **1956**, 964–968.

[59] J. H. Brewster; A Useful Model of Optical Activity. I. Open Chain Compounds; *J. Am. Chem. Soc.* **1959**, *81*, 5475–5483.

[60] a) P. L. Polavarapu, D. K. Chakraborty; Absolute Stereochemistry of Chiral Molecules from Ab Initio Theoretical and Experimental Molecular Optical Rotations; *J. Am. Chem. Soc.* **1998**, *120*, 6160–6164. b) R. K. Kondru, P. Wipf, D. N. Beratan; Theory-Assisted Determination of Absolute Stereochemistry for Complex Natural Products via Computation of Molar Rotation Angles; *J. Am. Chem. Soc.* **1998**, *120*, 2204–2205.

[61] a) H. Musso, W. Steckelberg; (–)-(*S*)-2,2′-Diamino-4,4′-dimethoxy-6,6′-dimethyl-biphenyl – Zur Konfigurationsbestimmung optisch aktiver 2,2′-Diamino-biphenyle mittels Rotationsdispersion und Circulardichroismus; *Liebigs Ann. Chem.* **1966**, *693*, 187–196. b) L. A. Mitscher, Y. H. Park, D. Clark, J.

L. Beal; Antimicrobial Agents from Higher Plants. Antimicrobial Isoflavanoids and Related Substances from *Glycyrrhiza glabra* L. var. *typica*; *J. Nat. Prod.* **1980**, *2*, 259–269.

[62] R. de L. Kronig; The Theory of Dispersion of X-Rays; *J. Opt. Soc. Am.* **1926**, *12*, 547–557.

[63] E. L. Eliel, S. H. Wilen, L. N. Mander; *Stereochemistry of Organic Compounds*; John Wiley & Sons, Inc., New York, **1994**.

[64] a) C. Minghua, N. Ruilin, L. Zhongrong, Z. Jun; Isospiropachysine, a Steroidal Alkaloid from *Pachysandra axillaris*; *Phytochemistry* **1990**, *29*, 3927–3930. b) G. Bringmann, C. Güntner, S. Busemann, M. Schäffer, J. D. Olowokudejo, B. I. Alo; Ancistroguineines A and B as well as Ancistrotectorine-Naphthylisoquinoline Alkaloids from *Ancistrocladus guineënsis*; *Phytochemistry* **1998**, *47*, 37–43. c) G. Bringmann, M. Dreyer, M. Michel, F. Tayman, R. Brun; Ancistroheynine B and Two Further 7,3′-Coupled Naphthylisoquinoline Alkaloids from *Ancistrocladus heyneanus*; *Phytochemistry* **2004**, *65*, 2903–2907.

[65] a) G. Bringmann, M. Dreyer, H. Rischer, K. Wolf, H. A. Hadi, R. Brun, H. Meimberg, G. Heubl; Ancistrobenomine A, the First Naphthylisoquinoline Oxygenated at Me-3, and Related 5,1′-Coupled Alkaloids, from the 'New' Plant Species *Ancistrocladus benomensis*; *J. Nat. Prod.* **2004**, *67*, 2058–2062. b) M. Dreyer; Isolierung, Charakterisierung und stereochemische Analyse von Naphthylisochinolin-Alkaloiden und anderen Naturstoffen; Dissertation, Universität Würzburg, **2004**.

[66] J. P. Foucher, J. L. Pousset, A. Cavé, R. R. Paris; Alkaloids of *Ancistrocladus congolensis*; *Plantes Méd. Phytothér.* **1975**, *9*, 26 –31.

[67] J. Fleischhauer, A. Koslowski, B. Kramer, E. Zobel, G. Bringmann, K.-P. Gulden, T. Ortmann, B. Peter; Messung und Berechnung der CD-Spektren der

Biaryl-Alkaloide Ancistrocladein und Dioncophyllein A; *Z. Naturforsch.* **1993**, *48b*, 140–148.

[68] G. Bringmann, J. Mühlbacher, K. Messer, M. Dreyer, R. Ebel, B.W. Nugroho, V. Wray, P. Proksch; Cyclorocaglamide, the First Bridged Cyclopentatetrahydrobenzofuran, and a Related "Open Chain" Rocaglamide Derivative from *Aglaia oligophylla*; *J. Nat. Prod.* **2003**, *66*, 80–85.

[69] J. Mühlbacher; Molecular Modelling und Chiralität: Aufklärung der absoluten Konfiguration von Natur- und Wirkstoffen mit ungewöhnlichem Circular-Dichroismus; Dissertation, Universität Würzburg, **2003**.

[70] a) P. Crabbé; *ORD and CD in Chemistry and Biochemistry: An Introduction*; Academic, New York, **1972**. b) G. Snatzke, F. Snatzke; *Chiroptische Methoden*; in: Analytiker-Taschenbuch (Eds.: H. Kienitz, R. Bock, W. Fresenius, W. Huber, G. Tölg), Springer, Berlin, **1980**, p. 217.

[71] a) L. Verbit; The Benzene Ring as an Optically Active Chromophore; *J. Am. Chem. Soc.* **1965**, *87*, 1617–1619. b) H. E. Smith, L. P. Fontana; A Sector Rule for the Circular Dichroism of the Benzene Chromophore; *J. Org. Chem.* **1991**, *56*, 432–435.

[72] E. Charney; *The Molecular Basis of Optical Activity. Optical Rotatory Dispertion and Circular Dichroism*; Wiley, New York, **1979**.

[73] P. Crabbé, E. Velarde, H. W. Anderson, S. D. Clark, W. R. Moore, A. F. Drake, S. F. Mason; Optical Activity and Absolute Configuration of Chiral Allenes; *J. Chem. Soc., Chem. Commun.* **1971**, 1261–1264.

[74] I. Listowsky, G. Avigad, S. Englard; Conformational Equilibria and Stereochemical Relations among Carboxylic Acids; *J. Org. Chem.* **1970**, *35*, 1080–1085.

[75] H. E. Smith; The Salicylidenamino Chirality Rule: a Method for the Establishment of the Absolute Configurations of Chiral Primary Amines by Circular Dichroism; *Chem. Rev.* **1983**, *83*, 359–377.

[76] N. Harada, M. Ohashi; K. Nakanishi; The Benzoate Sector Rule, a Method for Determining the Absolute Configurations of Cyclic Secondary Alcohols; *J. Am. Chem. Soc.* **1968**, *90*, 7349–7351.

[77] W. Moffitt, R. B. Woodward, A. Moscowitz, W. Klyne, C. Djerassi; Structure and the Optical Rotatory Dispersion of Saturated Ketones; *J. Am. Chem. Soc.* **1961**, *83*, 4013–4018.

[78] D. A. Lightner; The Octan Rule; in: *Circular Dichroism – Principles and Applications* (Eds.: N. Berova, K. Nakanishi, R. W. Woody), 2nd ed., Wiley-VCH, New York, **2000**, pp. 261–303.

[79] a) L. A. Gorthey, M. Vairamani, C. Djerassi; Optical Rotatory Dispersion Studies. 138. Synthesis and Conformational Analysis of β-Heteroatom-substituted Cyclohexanones; *J. Org. Chem.* **1985**, 50, 4173–4182. b) S. L. Rodgers, N. Kalyanam, D. A. Lightner; Contrasting Circular Dichroism n-π* Cotton Effects of (1*R*,5*S*,6*S*)-6(*endo*)-Methylbicyclo[3.2.1]octan-8-one and (1*S*,2*S*,4*R*)-2(*endo*)-Methylbicyclo[2.2.1]heptan-7-one; *J. Chem. Soc., Chem. Commun.* **1982**, 1040–1042.

[80] T. D. Bouman, D. A. Lightner; The Octant Rule – 5: On the Nature of the Third Nodal Surface. An Understanding of "Anti-Octant" and Front Octant Effects by a CNDO/S Study of Rotatory Strengths of the Carbonyl n-π* Transition; *J. Am. Chem. Soc.* **1976**, *98*, 3145–3154.

[81] A. Moscowitz, K. Mislow, M. A. W. Glass, C. Djerassi; Optical Rotatory Dispersion Associated with Dissymmetric Non-conjugated Chromophores. An Extension of the Octant Rule; *J. Am. Chem. Soc.* **1962**, *84*, 1945–1955.

[82] U. Weiss, H. Ziffer, E. Charney; Optical Activity of Non-planar Conjugated Dienes – I: Homoannular Cisoid Dienes; *Tetrahedron* **1965**, *21*, 3105–3120.

[83] L. A. Neubert, M. Carmack; Circular Dichroism of Disulfides with Dihedral Angles of 0, 30, and 60 deg. in the 400–185 nm Spectral Region; *J. Am. Chem. Soc.* **1974**, *96*, 943–945.

[84] a) N. Harada, K. Nakanishi; A Method for Determining the Chiralities of Optically Active Glycols; *J. Am. Chem. Soc.* **1969**, *91*, 3989–3991. b) N. Harada, K. Nakanishi; The Exciton Chirality Method and Its Application to Configurational and Conformational Studies of Natural Products; *Acc. Chem. Res.* **1972**, *5*, 257-263.

[85] W. Kuhn; The Physical Significance of Optical Rotatory Power; *Trans. Faraday Soc.* **1930**, *26*, 293–308.

[86] a) W. Moffitt; Optical Rotatory Dispersion of Helical Polymers; *J. Chem. Phys.* **1956**, *25*, 467–478. b) W. Moffitt, D. D. Fitts, J. G. Kirkwood; Critique of the Theory of Optical Activity of Helical Polymers; *Proc. Natl. Acad. Sci.* **1957**, *43*, 723–730.

[87] J. G. Kirkwood; On the Theory of Optical Rotatory Power; *J. Chem. Phys.* **1937**, *5*, 479–491.

[88] a) A. S. Davydov; Theory of Absorption Spectra of Molecular Crystals; *Zhur. Eksptl. I Teoret. Fiz.* **1948**, *18*, 210–218. b) A. S. Davydov; Theory of the Absorption Spectrum of Biphenyl; *Zhur. Eksptl. Teoret. Fiz.* **1948**, *18*, 201–209.

[89] N. Harada, S.-M. L. Chen, K. Nakanishi; Quantitative Definition of Exciton Chirality and the Distant Effect in the Exciton Chirality Method; *J. Am. Chem. Soc.* **1975**, *97*, 5345–5352.

[90] G. Bringmann, M. Rübenacker, J. R. Jansen, D. Scheutzow, L. Aké Assi; On the Structure of the Dioncophyllaceae Alkaloids Dioncophylline A

("Triphyophylline") and "*O*-Methyl-Triphyophylline"; *Tetrahedron Lett.* **1990**, *31*, 639–642.

[91] T. Hattori, K. Sakurai, N. Koike, S. Miyano, H. Goto, F. Ishiya, N. Harada; Is the CD Exciton Chirality Method Applicable to Chiral 1,1'-Biphenanthryl Compounds?; *J. Am. Chem. Soc.* **1998**, *120*, 9086–9087.

[92] T. Furo, T. Mori, T. Wada, Y. Inoue; Absolute Configuration of Chiral [2.2]Paracyclophanes with Intramolecular Charge-Transfer Interaction. Failure of the Exciton Chirality Method and Use of the Sector Rule Applied to the Cotton Effect of the CT Transition; *J. Am. Chem. Soc.* **2005**, *127*, 8242–8243.

[93] A. Rodger, B. Nordén; *Circular Dichroism & Linear Dichroism*; Oxford Univ. Press, Oxford, **1997**.

[94] a) C. A. Parish, J.-G. Dong, W. G. Bornmann, J. Chang, K. Nakanishi, N. Berova; Circular Dichroism Studies of Bisindole *Vinca* Alkaloids; *Tetrahedron* **1998**, *54*, 15739–15758. b) K. Vandyck, B. Matthys, J. Van der Eycken; Synthesis and Absolute Configuration of (1*S*,8*S*)-As-hydrindacene-1,8-diol as Determined by the Circular Dichroism Exciton Chirality Method; *Tetrahedron Lett.* **2004**, *46*, 75–78. c) C. L. Cardoso, V. S. Bolzani, D. H. S. Silva, H. Ishii, N. Berova, K. Nakanishi; The Absolute Configuration of 1-(3',4'-Dihydroxy-cinnamoyl)cyclopentane-2,3-diol from the Amazonian Tree *Chimarrhis turbinate*; *J. Nat. Prod.* **2006**, *69*, 1046–1050.

[95] a) J. Poirson, M. Vallet, F. Bretenaker, A. Le Floch, J.-Y. Thépot; Resonant Cavity Gas-Phase Polarimeter; *Anal. Chem.* **1998**, *70*, 4636–4639. b) T. Müller, K. B. Wiberg, P. H. Vaccaro; Cavity Ring-Down Polarimetry (CRDP): A New Scheme for Probing Circular Birefringence and Circular Dichroism in the Gas Phase; *J. Phys. Chem. A* **2000**, *104*, 5959–5968.

[96] R. Kuroda, T. Honma; CD Spectra of Solid-State Samples; *Chirality* **2000**, *12*, 269–277.

[97] R. Kuroda; Solid-State CD: Application to Inorganic and Organic Chemistry; in: *Circular Dichroism – Principles and Applications* (Eds.: N. Berova, K. Nakanishi, R. W. Woody), 2nd ed., Wiley-VCH, New York, **2000**, pp. 159–184.

[98] B. Elsässer, K. Krohn, U. Flörke, N. Root, H.-J. Aust, S. Draeger, B. Schulz, S. Antus, T. Kurtán; X-ray Structure Determination, Absolute Configuration and Biological Activity of Phomoxanthone A; *Eur. J. Org. Chem.* **2005**, 4563–4570.

[99] T. Asahi, H. Utsumi, Y. Itagaki, I. Kagomiya, J. Kobayashi; Optical Activity of Crystalline Glutamic Acids; *Acta Cryst.* **1996**, *A52*, 766–769.

[100] J. Kobayashi, Y. Uesu; A New Optical Method and Apparatus 'HAUP' for Measuring Simultaneously Optical Activity and Birefringence of Crystals. I. Principles and Construction; *J. Appl. Cryst.* **1983**, *16*, 204–211.

[101] R. Kuroda, T. Harada, Y. Shindo; A Solid-State Dedicated Circular Dichroism Spectrophotometer: Development and Application; *Rev. Sci. Instrum.* **2001**, *72*, 3802–3810.

[102] N. Asano, T. Harada, T. Sato, N. Tajima, R. Kuroda; Supramolecular Chirality Measured by Diffuse Reflectance Circular Dichroism Spectroscopy; *Chem. Commun.* **2009**, 899–901.

[103] a) I. Bilotti, P. Biscarini, E. Castiglioni, F. Ferranti, R. Kuroda; Reflectance Circular Dichroism of Solid-State Chiral Coordination Compounds; *Chirality* **2002**, *14*, 750–756. b) T. Harada, H. Hayakawa, R. Kuroda; Vertical-type Chiroptical Spectrophotometer (I): Instrumentation and Application to Diffuse Reflectance Circular Dichroism Measurement; *Rev. Sci. Instrum.* **2008**, *79*, 073103–073109. c) T. Harada, Y. Miyoshi, R. Kuroda; High Performance Diffuse Reflectance Circular Dichroism Spectrophotometer; *Rev. Sci. Instrum.* **2009**, *80*, 046101–046104.

[104] We sincerely thank to Prof. Reiko Kuroda (University of Tokio) for measuring the solid-state CD spectra for us.

[105] a) G. Holzwarth, E. C. Hsu, H. S. Mosher, T. R. Faulkner, A. Moscowitz; Infrared Circular Dichroism of Carbon-Hydrogen and Carbon-Deuterium Stretching Modes. Observations; *J. Am. Chem. Soc.* **1974**, *96*, 251–252. b) T. R. Faulkner, A. Moscowitz, G. Holzwarth, E. C. Hsu, H. S. Mosher; Infrared Circular Dichroism of Carbon-Hydrogen and Carbon-Deuterium Stretching Modes. Calculations; *J. Am. Chem. Soc.* **1974**, *96*, 252–253.

[106] a) L. D. Barron, M. P. Bogaard, A. D. Buckingham; Raman Scattering of Circularly Polarized Light by Optically Active Molecules; *J. Am. Chem. Soc.* **1973**, *95*, 603–605. b) W. Hug, S. Kint, G. F. Bailey, J. R. Scherer; Raman Circular Intensity Differential Spectroscopy. Spectra of (–)-α-Pinene and (+)-α -Phenylethylamine; *J. Am. Chem. Soc.* **1975**, *97*, 5589–5590.

[107] a) L. A. Nafie; Infrared and Raman Vibrational Optical Activity: Theoretical and Experimental Aspects; *Annu. Rev. Phys. Chem.* **1997**, *48*, 357–386. b) G. Zuber, W. Hug; Computational Interpretation of Vibrational Optical Activity: The ROA Spectra of (4*S*)-4-Methylisochromane and the (4*S*)-Isomers of Galaxolide®; *Helv. Chim. Acta* **2004**, *87*, 2208–2234. c) T. B. Freedman, X. Cao, L. M. Phillips, P. T. W. Cheng, R. Dalterio, Y.-Z. Shu, H. Zhang, N. Zhao, R. B. Shukla, A. Tymiak, S. K. Gozo, L. A. Nafie, J. Z. Gougoutas; Determination of the Absolute Configuration and Solution Conformation of a Novel Disubstituted Pyrrolidine Acid A by Vibrational Circular Dichroism; *Chirality* **2006**, *18*, 746–753.

[108] L. D. Barron, J. R. Escribano; Stokes–antiStokes Asymmetry in Natural Raman Optical Activity; *Chem. Phys.* **1985**, *98*, 437–446.

[109] G.-S. Yu, T. B. Freedman, L. A. Nafie; Dual Circular Polarization Raman Optical Activity of Related Terpene Molecules: Comparison of Backscattering DCP_I and Right-Angle ICP Spectra; *J. Raman Spectrosc.* **1995**, *26*, 733–743.

[110] J. A. Schellman; Circular Dichroism and Optical Rotation; *Chem. Rev.* **1975**, *75*, 323–331.

[111] L. Rosenfeld; Quantenmechanische Theorie der natürlichen optischen Aktivität von Flüssigkeiten und Gasen; *Z. Phys.* **1928**, *52*, 161–174.

[112] E. U. Condon, W. Altar, H. Eyring; One-Electron Rotatory Power; *J. Chem. Phys.* **1937**, *5*, 753–775.

[113] A. Moscowitz; Action of Light and Organic Crystals; in: *Modern Quantum Chemistry* (Ed.: O. Sinanoglu), Academic Press, New York, **1965**, pp. 1-4.

[114] R. A. Harris; Oscillator Strengths and Rotational Strengths in Hartree-Fock Theory; *J. Chem. Phys.* **1969**, *50*, 3947–3951.

[115] W. Moffitt; Optical Rotatory Dispersion of Helical Polymers; *J. Chem. Phys.* **1956**, *25*, 467–478.

[116] H. A. Bethe, E. E. Salpeter; *Quantum Mechanics of One- and Two-Electron Systems*; Springer, Berlin, **1957**.

[117] R. Ahlrichs, M. Bär, H.-P. Baron, R. Bauerschmitt, S. Böcker, P. Deglmann, M. Ehrig, K. Eichkorn, S. Elliott, F. Furche, F. Haase, M. Häser, H. Horn, C. Hättig, C. Huber, U. Huniar, M. Kattannek, A. Köhn, C. Kölmel, M. Kollwitz, K. May, C. Ochsenfeld, H. Öhm, H. Patzelt, O. Rubner, A. Schäfer, U. Schneider, M. Sierka, O. Treutler, B. Unterreiner, M. V. Arnim, F. Weigend, P. Weis, H. Weiss, TURBOMOLE, Version 5.6, Universität Karlsruhe, Kaiserstraße 12, 76131 Karlsruhe, Deutschland, **2002**.

[118] a) M. J. Frisch, G. W. Trucks, H. B. Schlegel, G. E. Scuseria, M. A. Robb, J. R. Cheeseman, V. G. Zakrzewski, J. A. Montgomery, Jr., R. E. Stratmann, J. C. Burant, S. Dapprich, J. M. Millam, A. D. Daniels, K. N. Kudin, M. C. Strain, O. Farkas, J. Tomasi, V. Barone, M. Cossi, R. Cammi, B. Mennucci, C. Pomelli, C. Adamo, S. Clifford, J. Ochterski, G. A. Petersson, P. Y. Ayala, Q. Cui, K. Morokuma, D. K. Malick, A. D. Rabuck, K. Raghavachari, J. B. Foresman, J.

Cioslowski, J. V. Ortiz, A. G. Baboul, B. B. Stefanov, G. Liu, A. Liashenko, P. Piskorz, I. Komaromi, R. Gomperts, R. L. Martin, D. J. Fox, T. Keith, M. A. Al-Laham, C. Y. Peng, A. Nanayakkara, C. Gonzalez, M. Challacombe, P. M. W. Gill, B. Johnson, W. Chen, M. W. Wong, J. L. Andres, C. Gonzalez, M. Head-Gordon, E. S. Replogle, J. A. Pople, GAUSSIAN 98, Revision A.7, Gaussian, Inc., Carnegie Office Park, Pittsburgh, PA 15106, USA, **1998**. b) M. J. Frisch, G. W. Trucks, H. B. Schlegel, G. E. Scuseria, M. A. Robb, J. R. Cheeseman, J. A. Montgomery, Jr., T. Vreven, K. N. Kudin, J. C. Burant, J. M. Millam, S. S. Iyengar, J. Tomasi, V. Barone, B. Mennucci, M. Cossi, G. Scalmani, N. Rega, G. A. Petersson, H. Nakatsuji, M. Hada, M. Ehara, K. Toyota, R. Fukuda, J. Hasegawa, M. Ishida, T. Nakajima, Y. Honda, O. Kitao, H. Nakai, M. Klene, X. Li, J. E. Knox, H. P. Hratchian, J. B. Cross, C. Adamo, J. Jaramillo, R. Gomperts, R. E. Stratmann, O. Yazyev, A. J. Austin, R. Cammi, C. Pomelli, J. W. Ochterski, P. Y. Ayala, K. Morokuma, G. A. Voth, P. Salvador, J. J. Dannenberg, V. G. Zakrzewski, S. Dapprich, A. D. Daniels, M. C. Strain, O. Farkas, D. K. Malick, A. D. Rabuck, K. Raghavachari, J. B. Foresman, J. V. Ortiz, Q. Cui, A. G. Baboul, S. Clifford, J. Cioslowski, B. B. Stefanov, G. Liu, A. Liashenko, P. Piskorz, I. Komaromi, R. L. Martin, D. J. Fox, T. Keith, M. A. Al-Laham, C. Y. Peng, A. Nanayakkara, M. Challacombe, P. M. W. Gill, B. Johnson, W. Chen, M. W. Wong, C. Gonzalez, J. A. Pople, GAUSSIAN 03, Revision B.04, Gaussian, Inc., Carnegie Office Park, Pittsburgh, PA 15106, USA, **2003**.

[119] a) D. R. Hartree; The Wave Mechanics of an Atom with a Non-Coulomb Central Field I: Theory and Methods; *Proc. Camb. Phil. Soc.* **1928**, *24*, 89–110. b) D. R. Hartree; The Wave Mechanics of an Atom with a Non-Coulomb Central Field II: Some Results and Discussion; *Proc. Camb. Phil. Soc.* **1928**, *24*, 111–132. c) D. R. Hartree; The Wave Mechanics of an Atom with a Non-Coulomb

Central Field III: Term Values and Intensities in Series in Optical Spectra; *Proc. Camb. Phil. Soc.* **1928**, *24*, 426–437.

[120] J. B. Foreman, M. Head-Gordon, J. A. Pople, M. J. Frisch; Toward a Systematic Molecular Orbital Theory for Excited States; *J. Phys. Chem.* **1992**, *96*, 135-149.

[121] J. E. Ridley, M. C. Zerner; An Intermediate Neglect of Differential Overlap Technique for Spectroscopy: Pyrrole and the Azines; *Theor. Chim. Acta* **1973**, *32*, 111–134.

[122] R. G. Parr, W. Yang; *Density Functional Theory of Atoms and Molecules*; Oxford Univ. Press, New York, **1989**.

[123] P. Hohenberg, W. Kohn; Inhomogeneous Electron Gas; *Phys. Rev.* **1964**, *136*, B864–B871.

[124] W. Kohn, L. J. Sham; Self-Consistent Equations Including Exchange and Correlation Effects; *Phys. Rev.* **1965**, *140*, A1133–A1138.

[125] J. Harris; Adiabatic-Connection Approach to Kohn-Sham Theory; *Phys. Rev. A* **1984**, *29*, 1648–1659.

[126] a) A. D. Becke; Density-Functional Thermochemistry III: The Role of Exact Exchange; *J. Chem. Phys.* **1993**, *98*, 5648–5652. b) C. Lee, W. Yang, R. G. Parr; Development of the Colle-Salvetti Correlation-Energy Formula into a Functional of the Electron Density; *Phys. Rev. B* **1988**, *37*, 785–789.

[127] A. D. Becke; A New Mixing of Hartree–Fock and Local Density-functional Theories; *J. Chem. Phys.* **1993**, *98*, 1372–1377.

[128] E. Runge, E. K. U. Gross; Density-Functional Theory for Time-Dependent Systems; *Phys. Rev. Lett.* **1984**, *59*, 997–1000.

[129] J. Autschbach, T. Ziegler, S. J. A. van Gisbergen, E. J. Baerends; Circular Dichroism Spectra of Organic Molecules; *J. Chem. Phys.* **2002**, *116*, 6930–6940.

[130] C. Neiss, P. Saalfrank, M. Parac, S. Grimme; Quantum Chemical Calculation of Excited States of Flavin-Related Molecules; *J. Phys. Chem. A* **2003**, *107*, 140–147.

[131] Y. Wang, G. Raabe, C. Repges, J. Fleischhauer; Time-dependent Density Functional Theory Calculations on the Chiroptical Properties of Rubroflavin: Determination of its Absolute Configuration by Comparison of Measured and Calculated CD Spectra; *Int. J. Quantum Chem.* **2003**, *93*, 265–270.

[132] a) D. J. Tozer, R. D. Amos, N. C. Handy, B. O. Roos, L. Serrano-Andres; Does Density Functional Theory Contribute to the Understanding of Excited States of Unsaturated Organic Compounds?; *Mol. Phys.* **1999**, *97*, 859–868; b) A. Dreuw, J. L. Weisman, M. Head-Gordon; Long-range Charge-transfer Excited States in Time-dependent Density Functional Theory Require Non-local Exchange; *J. Chem. Phys.* **2003**, *119*, 2943–2946.

[133] E. Casida, C. Jamorski, K. C. Casida, D. R. Salahub; Molecular Excitation Energies to High-lying Bound States from Time-dependent Density-functional Response Theory: Characterization and Correction of the Time-dependent Local Density Approximation Ionization Threshold; *J. Chem. Phys.* **1998**, *108*, 4439–4449.

[134] R. van Leeuwen, E. J. Baerends; Exchange-correlation Potential with Correct Asymptotic Behavior; *Phys. Rev. A* **1994**, *49*, 2421–2431.

[135] Y. Zhao, D. G. Truhlar; Density Functional for Spectroscopy: No Long-Range Self-Interaction Error, Good Performance for Rydberg and Charge-Transfer States, and Better Performance on Average than B3LYP for Ground States; *J. Phys. Chem. A* **2006**, *110,* 13126–13130.

[136] S. Grimme, F. Neese; Double-hybrid Density Functional Theory for Excited Electronic States of Molecules; *J. Chem. Phys.* **2007**, *127*, 154116-1–154116-18.

[137] A. B. J. Parusel, S. Grimme; DFT/MRCI Calculations on the Excites States of Porphyrin, Hydroporphyrins, Tetrazaporphyrins and Metalloporphyrins; *J. Porphyrins Phthalocyanins* **2001**, *5*, 225-232.

[138] C. M. Marian, N. Gilka; Performance of the Density Functional Theory/Multireference Configuration Interaction Method on Electronic Excitation of Extended π-Systems; *J. Chem. Theory Comput.* **2008**, 4, 1501–1515.

[139] O. Vahtras, J. Almlöf, M. W. Feyereisen; Integral Approximations for LCAO-SCF Calculations; *Chem. Phys. Lett.* **1993**, *213*, 514–518.

[140] J.-G. Dong, J. Guo, I. Akritopoulou-Zanze, A. Kawamura, K. Nakanishi, N. Berova; Theoretical and Experimental CD of Conformationally Flexible Complex Molecules - Application to Ouabain Pentanaphthoate and Analogs; *Chirality* **1999**, *11*, 707–721.

[141] N. Berova, L. D. Bari, G. Pescitelli; Application of Electronic Circular Dichroism in Configurational and Conformational Analysis of Organic Compounds; *Chem. Soc. Rev.* **2007**, *36*, 914–931.

[142] G. Bringmann, J. Mühlbacher, C. Repges, J. Fleischhauer; MD-Based CD Calculations on the Absolute Axial Configuration of the Naphthylisoquinoline Alkaloid Dioncophylline A; *J. Comput. Chem.* **2001**, *22*, 1273–1278.

[143] B. Bulheller; Quanten-chemische Berechnungen zur Strukturaufklärung von chiralen Naturstoffen mittels Circular-Dichroismus; Diplomarbeit, Universität Würzburg **2005**.

[144] Pre-optimization of the starting geometries is usually performed by using TRIPOS force-field as implemented in the SYBYL program package.[145]

[145] SYBYL, Tripos, Inc., 1699 South Hanley Road, St. Louis, MO 63144, USA.

[146] M. J. S. Dewar, E. G. Zoebisch, E. F. Healy, J. J. P. Stewart; AM1: A New General Purpose Quantum Mechanical Molecular Model; *J. Am. Chem. Soc.* **1985**, *107*, 3902–3909.

[147] a) J. J. P. Stewart; Optimization of Parameters for Semiempirical Methods I: Method; *J. Comput. Chem.* **1989**, *10*, 209–220. b) J. J. P. Stewart; Optimization of Parameters for Semiempirical Methods II: Applications; *J. Comput. Chem.* **1989**, *10*, 221–264.

[148] a) A. D. Becke; Density-Functional Exchange-Energy Approximation with Correct Asymptotic Behavior; *Phys. Rev. A* **1988**, *38*, 3098–3100.

[149] a) N. L. Allinger, Y. H. Yuh, J.-H. Lii; Molecular Mechanics: The MM3 Force Field for Hydrocarbons 1; *J. Am. Chem. Soc.* **1989**, *111*, 8551–8566. b) J.-H. Lii, N. L. Allinger; Molecular Mechanics: The MM3 Force Field for Hydrocarbons 2. Vibrational Frequencies and Thermodynamics; *J. Am. Chem. Soc.* **1989**, *111*, 8566–8575. c) J.-H. Lii, N. L. Allinger; Molecular Mechanics: The MM3 Force Field for Hydrocarbons 3. The van der Waals' Potentials and Crystal Data for Aliphatic and Aromatic Hydrocarbons; *J. Am. Chem. Soc.* **1989**, *111*, 8576–8582. d) W. Cui, F. Li, N. L. Allinger; Simulation of Conformational Dynamics with the MM3 Force Field: The Pseudorotation of Cyclopentane; *J. Am. Chem. Soc.* **1993**, *115*, 2943–2951.

[150] J. W. Downing, BDZDO/MCDSPD, Department of Chemistry and Biochemistry, University of Colorado, Boulder, BO 80309, USA.

[151] W. Thiel, MNDO99, Version 6.0, Max-Planck-Institut für Kohlenforschung, Kaiser-Wilhelm-Platz 1, 45470 Mülheim, Deutschland, **2001**.

[152] A. Schäfer, C. Huber, R. Ahlrichs; Fully Optimized Contracted Gaussian Basis Sets of Triple Zeta Valence Quality for Atoms Li to Kr; *J. Chem. Phys.* **1994**, *100*, 5829–5835.

[153] A. Schäfer, H. Horn, R. Ahlrichs; Fully Optimized Contracted Gaussian Basis Sets for Atoms Li to Kr; *J. Chem. Phys.* **1992**, *97*, 2571–2577.

[154] T. Bruhn, K. Maksimenka, G. Bringmann; SpecDis, Version 1.31, Universität Würzburg, Germany, **2008**.

[155] a) G. François, G. Bringmann, J. D. Phillipson, L. Aké Assi, C. Dochez, M. Rübenacker, C. Schneider, M. Wéry, D. C. Warhurst, G. C. Kirby; Activity of Extracts and Naphthylisoquinoline Alkaloids from *Triphyophyllum peltatum*, *Ancistrocladus abbreviatus* and *A. barteri* against *Plasmodium falciparum in vitro*; *Phytochemistry* **1994**, *35*, 1461–1464. b) G. François, G. Bringmann, C. Dochez, C. Schneider, G. Timperman, L. Aké Assi; Activities of Extracts and Naphthylisoquinoline Alkaloids from *Triphyophyllum peltatum*, *Ancistrocladus abbreviatus* and *Ancistrocladus barteri* against *Plasmodium berghei* (Anka strain) in vitro; *J. Ethnopharmacol.* **1995**, *46*, 115–120. c) G. François, G. Timperman, W. Eling, L. Aké Assi, J. Holenz, G. Bringmann; Naphthylisoquinoline Alkaloids against Malaria: Evaluation of the Curative Potential of Dioncophylline C and Dioncopeltine A against *Plasmodium berghei* in vivo; *Antimicrob. Agents Chemother.* **1997**, *41*, 2533–2539.

[156] a) G. Bringmann, A. Hamm, C. Günther, M. Michel, R. Brun, V. Mudogo; Ancistroealaines A and B, Two New Bioactive Naphthylisoquinolines, and Related Naphthoic Acids from *Ancistrocladus ealaensis*; *J. Nat. Prod.* **2000**, *63*, 1465-1470. b) G. Bringmann, K. Messer, R. Brun, V. Mudogo; Ancistrocongolines A–D, New Naphthylisoquinoline Alkaloids from *Ancistrocladus congolensis*; *J. Nat. Prod.* **2002**, *65*, 1096–1101.

[157] a) G. Bringmann, V. Hoerr, U. Holzgrabe, A. Stich; Antitrypanosomal Naphthylisoquinoline Alkaloids and Related Compounds; *Pharmazie* **2003**, *58*, 343-346. b) A. Ponte-Sucre, J. H. Faber, T. Gulder, I. Kajahn, S. E. H. Pedersen, M. Schultheis, G. Bringmann, H. Moll; Activity of Naphthylisoquinoline

Alkaloids and Synthetic Analogs against *Leishmania major*; *Antimicrob. Agents Chemother.* **2007**, *51*, 188–194.

[158] a) G. Bringmann, J. Holenz, L. Aké Assi, C. X. Zhao, K. Hostettmann; Molluscicidal Activity of Naphthylisoquinoline Alkaloids from *Triphyopyllum* and *Ancistrocladus* Species; *Planta Med.* **1996**, *62*, 556–557. b) G. Bringmann, J. Holenz, L. Aké Assi, K. Hostettmann; Molluscicidal Activity (*Biomphalaria glabrata*) of Dioncophylline A. Structure-Activity Investigations; *Planta Med.* **1998**, *64*, 485-486.

[159] a) C. Rummey; 3D-QSAR-Untersuchungen an antimalaria-aktiven Naphthylisochinolin-Alkaloiden; Dissertation, Universität Würzburg, **2002**. b) M. Kuroda, Y. Mimaki, H. Sakagami, Y. Sashida; Bulbinelonesides A-E, Phenylanthraquinone Glycosides from the Roots of *Bulbinella floribunda ; J. Nat. Prod.* **2003**, 66, 894–897.

[160] M. Cheek, C. Frimodt-Møller, V. Hørlyck; A New Submontane Species of *Ancistrocladus* from Tanzania; *Kew Bull.* **2000**, *55*, 207–212.

[161] M. Reichert; Konfigurationsaufklärung chiraler Naturstoffe durch quantenchemische CD-Rechnungen; Diplomarbeit, Universität Würzburg **2003**.

[162] a) T. Hashimoto, S. Kanayama, Y. Kan, M. Tori, Y. Asakawa; Isoplagiochins C and D, New Type of Macrocyclic Bis(bibenzyls), Having Two Biphenyl Linkages from the Liverwort *Plagiochila fruticosa*; *Chem. Lett.* **1996**, 741–742. b) H. Anton, L. Kraut, R. Mues, I. Z. M. Morales; Phenanthrenes and Bibenzyls from a *Plagiochila* species; *Phytochemistry* **1997**, *46*, 1069–1075.

[163] T. Hashimoto, H. Irita, S. Takaoka, M. Tanaka, Y. Asakawa; New Chlorinated Cyclic Bis(bibenzyls) from the Liverworts *Herbertus sakuraii* and *Mastigophora diclados*; *Tetrahedron* **2000**, *56*, 3153–3159.

[164] a) D. H. Williams, B. Bardsley; The Vancomycin Group of Antibiotics and the Fight against Resistant Bacteria; *Angew. Chem.* **1999**, *111*, 1264–1286; *Angew. Chem. Int. Ed.* **1999**, *38*, 1172–1193.

[165] H. E. Blackwell, Y. Zhao; Chemical Genetic Approaches to Plant Biology; *Plant Physiology* **2003**, *133*, 448–455.

[166] G. Bringmann, C. Günther, M. Ochse, O. Schupp, S. Tasler; Biaryls in Nature: A Multi-Facetted Class of Stereochemically, Biosynthetically, and Pharmacologically Intriguing Secondary Metabolites; in: *Progress in the Chemistry of Organic Natural Products* (Eds.: W. Herz, H. Falk, G. W. Kirby, R. E. Moore), vol. 82, Springer, Wien, **2001**, pp. 1–249.

[167] a) K. N. Baker, A. V. Fratini, T. Resch, H. C. Knachel, W.W. Adams, E.P. Socci, B.L. Farmer; Crystal Structures, Phase Transitions and Energy Calculations of Poly(*p*-phenylene) Oligomers; *Polymer* **1993**, *34*, 1571–1587; b) A. J. Heeger; Semiconducting and Metallic Polymers: The Fourth Generation of Polymeric Materials; *Phys. Chem. B* **2001**, *105*, 8475–8491.

[168] K. Yamamuro, S. Ono, I. Tabushi; New Liquid Crystals Having 4,4'-Biphenanthryl Core; *Tetrahedron Lett.* **1988**, *29*, 1797–1798.

[169] a) D. J. Cram; The Design of Molecular Hosts, Guests, and Their Complexes; *Angew. Chem.* **1988**, *100*, 1041–1052; *Angew. Chem. Int. Ed.* **1988**, *27*, 1009–1020; b) E. Weber; Molecular Recognition: Designed Crystalline Inclusion Complexes of Carboxylic Hosts; *J. Mol. Graphics* **1989**, *7*, 12–27.

[170] a) R. Noyori, H. Takaya; BINAP: An Efficient Chiral Element for Asymmetric Catalysis; *Acc. Chem. Res.* **1990**, *23*, 345–350; b) H. Sasaki, R. Irie, T. Hamada, K. Suzuki, T. Katsuki; Highly Enantioselective Epoxidation of Conjugated *cis* Olefins; *Tetrahedron* **1994**, *50*, 11827–11838; c) G. Bringmann, M. Breuning; Novel Concepts in Directed Biaryl Synthesis. 66. Enantioselective Addition of Diethylzinc to Aldehydes Using Novel Axially Chiral 2-(Aminomethyl)-1-(2-

Hydroxyphenyl)-Naphthalene Catalysts; *Tetrahedron: Asymmetry* **1998**, *9*, 667–679.

[171] G. Bringmann, A. J. Price Mortimer, P. A. Keller, M. J. Gresser, J. Garner, M. Breuning; Atroposelective Synthesis of Axially Chiral Biaryl Compounds; *Angew. Chem.* **2005**, *117*, 5518–5563; *Angew. Chem. Int. Ed.* **2005**, *44*, 5384–5427.

[172] a) G. Bringmann, M. Breuning, S. Tasler; The Lactone Concept. An Efficient Pathway to Axially Chiral Natural Products and Useful Reagents; *Synthesis* **1999**, 525–558. b) G. Bringmann, S. Tasler, R.-M. Pfeifer, M. Breuning; The Directed Synthesis of Axially Chiral Ligands, Reagents, Catalysts, and Natural Products through the 'Lactone Methodology'; *J. Organomet. Chem.* **2002**, *661*, 49–65.

[173] W. Tochtermann, D. Kuckling, C. Meints, J. Kraus, G. Bringmann; Bridged Bioxepines and Bi[10]Paracyclophanes - Synthesis and Absolute Configuration of a Bi[10]Paracyclophane with Two Chiral Planes and One Chiral Axis; *Tetrahedron* **2003**, *59*, 7791–7801.

[174] S. F. Mason, R. H. Seal, D. R. Roberts; Optical Activity in the Biaryl Series; *Tetrahedron* **1974**, *30*, 1671–1682.

[175] L. F. Tietze, T. Feuerstein; Highly Selective Compounds for the Antibody-Directed Enzyme Prodrug Therapy of Cancer; *Aust. J. Chem.* **2003**, *56*, 841–854.

[176] L. F. Tietze, R. Hannemann, W. Buhr, M. Lögers, P. Menningen, M. Lieb, D. Starck, T. Grote, A. Döring, I. Schuberth; Prodrugs of the Cytostatic CC-1065 That Can Be Activated in a Tumor-Selective Manner; *Angew. Chem.* **1996**, *108*, 2840–2842; *Angew. Chem. Int. Ed.* **1996**, *35*, 2674–2677.

[177] L. F. Tietze, T. Herzig, A. Fecher, F. Haunert, I. Schuberth; Highly Selective Glycosylated Prodrugs of Cytostatic CC-1065 Analogues for Antibody-Directed Enzyme Tumor Therapy; *ChemBioChem* **2001**, *2*, 758–765.

[178] X. Li, J. Yang, M. C. Kozlowski; Enantioselective Oxidative Biaryl Coupling Reactions Catalyzed by 1,5-Diazadecalin Metal Complexes; *Org. Lett.* **2001**, *3*, 1137–1140.

[179] B. W. Bycroft, T. A. Dobson, J. C. Roberts; The Structure of Flavasperone ("Asperxanthone"), a Metabolite of *Aspergillus niger*; *J. Chem. Soc.* **1962**, 40–44.

[180] C. P. Gorst-Allman, P. S. Steyn, C. J. Rabie; Structural Elucidation of the Nigerones, Four New Naphthopyrones from Cultures of *Aspergillus niger*; *J. Chem. Soc., Perkin Trans. 1* **1980**, 2474–2479.

[181] K. Koyama, S. Natori, Y. Iitaka; Absolute Configurations of Chaetochromin A and Related Bis(naphtho-γ-pyrone) Mold Metabolites (Organic, Chemical); *Chem. Pharm. Bull.* **1987**, *35*, 4049–4055.

[182] A. Fleming; On the Antibacterial Action of Cultures of a Penicillium, with Special Reference to their Use in the Isolation of *B. influenza*; *Brit. J. Exp. Pathol.* **1929**, *31*, 226–236.

[183] E. P. Abraham, G. G. F. Newton; Purification and Some Properties of Cephalosporin N, a New Penicillin; *Biochem. J.* **1954**, *58*, 94–102.

[184] W. O. Godtfredsen, S. Jahnsen, H. Lorck, K. Roholt, L. Tybring; Fusidic Acid: a New Antibiotic; *Nature* **1962**, *193*, 987.

[185] R. Traber, M. M. Dreyfuss; Occurrence of Cyclosporins and Cyclosporin-like Peptolides in Fungi; *J. Ind. Microbiol.* **1996**, *17*, 397–401.

[186] N. Abe, O. Sugimoto, K. Tanji, A. Hirota; Identification of the Quinol Metabolite "Sorbicillinol", a Key Intermediate Postulated in Bisorbicillinoid Biosynthesis; *J. Am. Chem. Soc.* **2000**, *122*, 12606–12607.

[187] N. Abe, T. Murata, A. Hirota; Novel DPPH Radical Scavengers, Bisorbicillinol and Demethyltrichodimerol, form a Fungus; *Biosci. Biotechnol. Biochem.* **1998**, *62*, 661–666.

[188] R. Andrade, W. A. Ayer, P. P. Mebe; Isolation of the Metabolites and the Structure of Trichodimerol; *Can. J. Chem.* **1992**, *70*, 2526–2535.

[189] N. Abe, T. Murata, K. Yamamoto, A. Hirota; Bisorbibetanone, a Novel Oxidized Sorbicillin Dimer, with 1,1-Diphenyl-2-picrylhydrazyl Radical Scavenging Activity from a Fungus; *Tetrahedron Lett.* **1999**, *40*, 5203–5206.

[190] N. Abe, K. Yamamoto, A. Hirota; Novel Fungal Metabolites, Demethylsorbicillin and Oxosorbicillinol, Isolated from *Trichoderma* sp. USF-2690; *Biosci. Biotechnol. Biochem.* **2000**, *64*, 620–622.

[191] S. Sperry, G. J. Samuels, P. Crews; Vertinoid Polyketides from the Saltwater Culture of the Fungus *Trichoderma longibrachiatum* Separated from a *Haliclona* Marine Sponge*; J. Org. Chem.* **1998**, *63*, 10011–10014.

[192] K. Eckardt, H. Fritzsche, D. Tresselt; Zur Konstitution des Antibiotikums Resistoflavin; *Tetrahedron* **1970**, *26*, 5875–5883.

[193] a) G. Höfle, H. Wolf; Isolierung, ^{13}C-NMR-Spektren und Biogenese von Resistomycin und Resistoflavin aus *Streptomyces griseoflavus* B 71 (Actinomycetales); *Liebigs Ann. Chem.* **1983**, 835-843. b) I. Kock, R. P. Maskey, M. A. F. Biabani, E. Helmke, H. Laatsch; 1-Hydroxy-1-norresistomycin and Resistoflavin Methyl Ether: New Antibiotics from Marine-derived Streptomycetes; *J. Antibiot.* **2005**, *58*, 530–534. c) A. Gorajana, B. V. V. S. N. Kurada, S. Peela, P. Jangam, S. Vinjamuri, E. Poluri, A. Zeeck; 1-Hydroxy-1-norresistomycin, a New Cytotoxic Compound from a Marine Actinomycete, *Streptomyces chibaensis* AUBN1/7; *J. Antibiot.* **2005**, *58*, 526–529.

[194] P. Riederer, P. Foley, G. Bringmann, D. Feineis, R. Brückner, M. Gerlach; Biochemical and Pharmacological Characterization of 1-Trichloromethyl-1,2,3,4-tetrahydro-β-carboline: a Biologically Relevant Neurotoxin; *Eur. J. Pharmacol.* **2002**, *442*, 1–16.

[195] a) J. W. Langston, P. Ballard, J. W. Tetrud, I. Irwin; Chronic Parkinsonism in Humans Due to a Product of Meperidine-Analog Synthesis; *Science* **1983**, *219*, 979–980. b) R. S. Burns, C. C. Chiueh, S. P. Markey, M. H. Ebert, D. M. Jacobowitz, I. J. Kopin; A Primate Model of Parkinsonism: Selective Destruction of Dopaminergic Neurons in the Pars Compacta of the Substantia Nigra by *N*-Methyl-4-phenyl-1,2,3,6-tetrahydropyridine; *Proc. Natl. Acad. Sci. U.S.A.* **1983**, *80*, 4546–4550. c) R. E. Heikkila, A. Hess, R. C. Duvoisin; Dopaminergic Neurotoxicity of 1-Methyl-4-phenyl-1,2,5,6-tetrahydropyridine in Mice; *Science* **1984**, *224*, 1451–1453.

[196] G. Bringmann, R. God, S. Fähr, D. Feineis, K. Fornadi, F. Fornadi; Identification of the Dopaminergic Neurotoxin 1-Trichloromethyl-1,2,3,4-tetrahydro-β-carboline in Human Blood after Intake of the Hypnotic Chloral Hydrate; *Anal. Biochem.* **1999**, *270*, 167–175.

[197] G. Bringmann, R. God, D. Feineis, B. Janetzky, H. Reichmann; TaClo as a Neurotoxic Lead: Improved Synthesis, Stereochemical Analysis, and Inhibition of the Mitochondrial Respiratory Chain; *J. Neural Trans. Supp.* **1995**, *46*, 245–254.

[198] M. C. Zerner; in: *Reviews in Computational Chemistry* (Eds.: K. B. Lipkowitz, D. B. Boyd), vol. 2, VCH, Weinheim, Cambridge, New York, **1991**, pp. 313–365.

[199] a) A. Dossena, R. Marchelli, A. Pochini; New Metabolites of *Aspergillus amstelodami* Related to the Biogenesis of Neoechinulin; *J. Chem. Soc., Chem. Commun.* **1974**, 771–772. b) H. Nagasawa, A. Isogai, K. Ikeda, S. Sato, S. Murakoshi, A. Suzuki, S. Tamura; Isolation and Structure Elucidation of a New Indole Metabolite from *Aspergillus ruber*; *Agric. Biol. Chem.* **1975**, *39*, 1901–1902.

[200] L. Butinar, P. Zalar, J. C. Frisvad, N. Gunde-Cimerman; The genus *Eurotium* – Members of Indigenous Fungal Community in Hypersaline Waters of Salterns; *FEMS Microbiol. Ecol.* **2005**, *51*, 155–166.

[201] Y. Li, X. Li, S.-K. Kim, J. S. Kang, H. D. Choi, J. R. Rho, B. W. Son; Golmaenone, a New Diketopiperazine Alkaloid from the Marine-Derived Fungus *Aspergillus* sp.; *Chem. Pharm. Bull.* **2004**, *52*, 375–376.

[202] R. Yagi, M. Doi; Isolation of an Antioxidative Substance Produced by *Aspergillus repens*; *Biosci. Biotechnol. Biochem.* **1999**, *63*, 932–933.

[203] K. Maruyama, T. Ohuchi, K.Yoshida, Y. Shibata, F. Sugawara, T. Arai; Protective Properties of Neoechinulin A against SIN-1–Induced Neuronal Cell Death; *J. Biochem.* **2004**, *136*, 81–87.

[204] R. Marchelli, A. Dossena, G. Casnati; Biosynthesis of Neoechinulin by *Aspergillus amstelodami* from *cyclo*-L-[*U*-^{14}C]Alanyl-L-[5,7-$^{3}H_2$]tryptophyl; *J. Chem. Soc., Chem. Commun.* **1975**, 779–780.

[205] a) H. Nagasawa, A. Isogai, A. Suzuki, S. Tamura; ^{13}C-NMR Spectra and Stereochemistry of Isochinolins A, B and C; *Agric. Biol. Chem.* **1979**, *43*, 1759–1763. b) S. Nakatsuka, H. Miyazaki, T. Goto; Total Synthesis of (±)-Neoechinulin A, an Indole Alkaloid Containing Oxidized Diketopiperazine; *Tetrahedron Lett.* **1980**, *21*, 2817–2820.

[206] We are grateful to Dr. K. Radacki from the group of Prof. Braunschweig (University of Würzburg) for the X-ray structure analysis of neoechinulin A.

[207] T. Aoki, S. Kamisuki, M. Kimoto, K. Ohnishi, Y. Takakusagi, K. Kuramochi, Y. Takeda, A. Nakazaki, K. Kuroiwa, T. Ohuchi, F. Sugawara, T. Arai, S. Kobayashi; Total Synthesis of (–)-Neoechinulin A; *Synlett* **2006**, 0677–0680.

[208] E. Dagne, W. Steglich; Knipholone: A Unique Anthraquinone Derivative from *Kniphofia foliosa*; *Phytochemistry* **1984**, *23*, 1729–1731.

[209] L. F. Van Staden, S. E. Drewes; Knipholone from *Bulbine latifolia* and *Bulbine frutescens*; *Phytochemistry* **1994**, *35*, 685–686.

[210] G. Bringmann, D. Menche, M. Bezabih, B. M. Abegaz, R. Kaminsky; Antiplasmodial Activity of Knipholone and Related Natural Phenylanthraquinones; *Planta Med.* **1999**, *65*, 757–758.

[211] M. Kuroda, Y. Mimaki, H. Sakagami, Y. Sashida; Bulbinelonesides A-E, Phenylanthraquinone Glycosides from the Roots of *Bulbinella floribunda; J. Nat. Prod.* **2003**, *66*, 894–897.

[212] A. A. Wube, F. Bucar, K. Asres, S. Gibbons, M. Adams, B. Streit, A. Bodensieck, R. Bauer; Knipholone, a Selective Inhibitor of Leukotriene Metabolism; *Phytomedicine* **2006**, *13*, 452–456.

[213] G. Bringmann, J. Kraus, D. Menche, K. Messer; Elucidation of the Absolute Configuration of Knipholone and Knipholone Anthrone by Quantum Chemical CD Calculations; *Tetrahedron* **1999**, *55*, 7563–7572.

[214] G. Bringmann, D. Menche, J. Kraus, J. Mühlbacher, K. Peters, E.-M. Peters, R. Brun, M. Bezabih, B. M. Abegaz; Atropo-Enantioselective Total Synthesis of Knipholone and Related Antiplasmodial Phenylanthraquinones; *J. Org. Chem.* **2002**, *67*, 5595–5610.

[215] G. Bringmann, D. Menche; Novel Concepts in Directed Biaryl Synthesis. Part 93. First, Atropo-Enantioselective Total Synthesis of the Axially Chiral Phenylanthraquinone Natural Products Knipholone and 6'-O-Methylknipholone; *Angew. Chem.* **2001**, *113*, 1733–1736; *Angew. Chem. Int. Ed.* **2001**, *40*, 1687–1690.

[216] a) G. Bringmann, T. Pabst, P. Henschel, J. Kraus, K. Peters, E.-M. Peters, D. S. Rycroft, J. D. Connolly; Nondynamic and Dynamic Kinetic Resolution of Lactones with Stereogenic Centers and Axes: Stereoselective Total Synthesis of Herbertenediol and Mastigophorenes A and B; *J. Am. Chem. Soc.* **2000**, *122*,

9127–9133. b) G. Bringmann, D. Menche, J. Mühlbacher, M. Reichert, N. Saito, S. S. Pfeiffer, B. H. Lipshutz; On the Verge of Axial Chirality: Atroposelective Synthesis of the AB-Biaryl Fragment of Vancomycin; *Org. Lett.* **2002**, *4*, 2833–2836. c) G. Bringmann, W. Saeb, M. Rübenacker; Directed Joint Total Synthesis of the Three Naphthylisoquinoline Alkaloids Dioncolactone A, Dioncopeltine A, and 5'-*O*-Demethyldioncophylline A; *Tetrahedron* **1999**, *55*, 423–432. d) G. Bringmann, M. Ochse, R. Götz; First Atropo-Divergent Total Synthesis of the Antimalarial Korupensamines A and B by the "Lactone Method"; *J. Org. Chem.* **2000**, *65*, 2069–2077.

[217] J. Kraus; Quantenchemische Berechnungen zur Strukturaufklärung chiraler organischer Verbindungen und zur Simulation dynamischer Prozesse von Biarylverbindungen; Dissertation, Universität Würzburg, **2001**.

[218] S. Habtemariam, Antioxidant Activity of Knipholone Anthrone; *Food Chem.* **2007**, *102*, 1042–1047.

[219] E. Dagne, A. Yenesew; Knipholone Anthrone from *Kniphofia foliosa*; *Phytochemistry* **1993**, *34*, 1440–1441.

[220] L. Doub, J. M. Vandenbelt; The Ultraviolet Absorption Spectra of Simple Unsaturated Compounds. I. Mono and *p*-Disubstituted Benzene Derivatives; *J. Am. Chem. Soc.* **1947**, *69*, 2714–2723.

[221] R. Shimada, L. Goodman; Polarization of Aromatic Carbonyl Spectra; *J. Chem. Phys.* **1965**, *43*, 2027–2041.

[222] J. Dehler, F. Dörr, Polarization der Absorptions- und Lumeneszenzübergänge in Aromatischen Ketonen; *Tetrahedron Lett.* **1965**, *6*, 2155–2160.

[223] G. Bringmann, D. Menche, R. Brun, T. Msuta, B. M. Abegaz; Bulbine-Knipholone, a New, Axially Chiral Phenylanthraquinone from *Bulbine abyssinica* (Asphodelaceae): Isolation, Structural Elucidation, Synthesis, and Antiplasmodial Activity; *Eur. J. Org. Chem.* **2002**, 1107–1111.

[224] B. M. Abegaz, M. Bezabih, T. Msuta, R. Brun, D. Menche, J. Mühlbacher, G. Bringmann; Gaboroquinones A and B and 4'-*O*-Demethylknipholone-4'-*O*-β-D-glucopyranoside, Phenylanthraquinones from the Roots of *Bulbine frutescens* *J. Nat. Prod.* **2002**, *65*, 1117–1121.

[225] C. Peng, P. Y. Ayala, H. B. Schlegel, M. J. Frisch; Using Redundant Internal Coordinates to Optimize Equilibrium Geometries and Transition States; *J. Comp. Chem.* **1996**, *17*, 49–56.

[226] J. S. Binkley, J. A. Pople, W. J. Hehre; Small Split-Valence Basis Sets for First-Row Elements; *J. Am. Chem. Soc.* **1980**, *102*, 939–947.

[227] A. P. Scott, L. Radom; Harmonic Vibrational Frequencies: An Evaluation of Hartree-Fock, Møller-Plesset, Quadratic Configuration Interaction, Density Functional Theory, and Semiempirical Scale Factors; *J. Phys. Chem.* **1996**, *100*, 16502–16513.

[228] G. Bringmann, G. Lang, S. Steffens, K. Schaumann; Petrosifungins A and B, Novel Cyclodepsipeptides from a Sponge-Derived Strain of *Penicillium Brevicompactum*; *J. Nat. Prod.* **2004**, *67*, 311–315.

[229] F. Bracher, W. J. Eisenreich, J. Mühlbacher, M. Dreyer, G. Bringmann; Saludimerines A and B, Novel-Type Dimeric Alkaloids with Stereogenic Centers and Configurationally Semistable Biaryl Axes; *J. Org. Chem.* **2004**, *69*, 8602–8608.

[230] J. Wu, S. Zhang, T. Bruhn, Q. Xiao, H. Ding, G. Bringmann; Xylogranatins F–R: Antifeedants from the Chinese Mangrove, Xylocarpusgranatum, A New Biogenetic Pathway to Tetranortriterpenoids; *Chem. Eur. J.* **2008**, *14*, 1129–1144.

[231] Y. F. Hallock, C. B. Hughes, J. H. Cardellina, II, M. Schäffer, K.-P. Gulden, G. Bringmann and M. R. Boyd; Dioncophylline A, the Principal Cytotoxin from *Ancistrocladus letestui*; *Nat. Prod. Lett.* **1995**, *6*, 315–320.

[232] G. Bringmann, G. François, L. Aké Assi, J. Schlauer; The Alkaloids of *Triphyophyllum peltatum*; *Chimia* **1998**, *52*, 18–28.

[233] G. Bringmann, D. Koppler, D. Scheutzow, A. Porzel; Determination of Configuration at the Biaryl Axes of Naphthylisoquinoline Alkaloids by Long-range NOE Effects; *Magn. Reson. Chem.* **1997**, *35*, 297–301.

[234] G. Bringmann, J. R. Jansen, H. Reuscher, M. Rübenacker, K. Peters, H. G. Von Schnering; Acetogenic Isoquinoline Alkaloids. 17. First Total Synthesis of (-)-Dioncophylline A (Triphyophylline) and of Selected Stereoisomers: Complete (Revised) Stereostructure; *Tetrahedron Lett.* **1990**, *31*, 643–646.

[235] G. Bringmann, R. Zagst, B. Schöner, H. Busse, M. Hemmerling, C. Burschka; Structure of the Naphthyl Isoquinoline Alkaloid Dioncophylline A; *Acta Crystallogr., Sect. C: Cryst. Struct. Commun.* **1991**, *C47*, 1703–1705.

[236] G. Bringmann, W. Saeb, K. Peters, E.-M. Peters; The Absolute Stereostructure of Dioncophylline A by Anomalous X-Ray Dispersion of a 5-Bromo Derivative; *Phytochemistry* **1997**, *45*, 1283–1285.

[237] M. Müller, K. Lamottke, W. Steglich, S. Busemann, M. Reichert, G. Bringmann, P. Spiteller; Biosynthesis and Stereochemistry of Phlegmacin-Type Fungal Pigments; *Eur. J. Org. Chem.* **2004**, 4850–4855.

[238] This procedure was performed with ORTEP program: L. J. Farrugia; *ORTEP*-3 for Windows - a Version of *ORTEP*-III with a Graphical User Interface (GUI); *J. Appl. Cryst.* **1997**, *30*, 565.

[239] I gratefully acknowledge the help of Dr. T. Bruhn, who calculated the CD spectrum for the cluster from the crystal of dioncophylline A.

[240] G. Kerti, T. Kurtán, A. Borbás, Z. B. Szabó, A. Lipták, L. Szilágyi, Z. Illyés-Tünde, A. Bényei, S. Antus, M. Watanabe, E. Castiglioni, G. Pescitelli, P. Salvadori; Synthesis and Chiroptical Properties of (Naphthyl)ethylidene Ketals of Carbohydrates in Solution and Solid State; *Tetrahedron* **2008**, *64*, 1676–1688.